Breakdown and absence of quasiparticles in Kitaev's models

Dissertation
zur Erlangung des Doktorgrades
der Naturwissenschaften

vorgelegt beim Fachbereich Physik
der Johann Wolfgang Goethe-Universität
in Frankfurt am Main

von
Roman Louis Smit
aus Bad Soden am Taunus

Frankfurt, 2022
(D 30)

vom Fachbereich Physik der
Johann Wolfgang Goethe-Universität als Dissertation angenommen.

Dekan: Prof. Dr. Harald Appelshäuser

Gutachter: Prof. Dr. Peter Kopietz
Prof. Dr. Roser Valentí

Datum der Disputation:

Abstract

This thesis has two main parts.

The first part is based on our publication [1], where we use perturbation theory to calculate decay rates of magnons in the Kitaev-Heisenberg-Γ (KHΓ) model. This model describes the magnetic properties of the material α-$RuCl_3$, which is a candidate for a Kitaev spin liquid. Our motivation is to validate a previous calculation from Ref. [2]. In this thesis, we map out the classical phase diagram of the KHΓ model. We use the Holstein-Primakoff transformation and the $1/S$ expansion to describe the low temperature dynamics of the Kitaev-Heisenberg-Γ model in the experimentally relevant zigzag phase by spin waves. By parametrizing the spin waves in terms of hermitian fields, we find a special parameter region within the KHΓ model where the analytical expressions simplify. This enables us to construct the Bogoliubov transformation analytically. For a representative point in the special parameter region, we use these results to numerically calculate the magnon damping, which is to leading order caused by the decay of single magnons into two. We also calculate the dynamical structure factor of the magnons.

The second part of this thesis is based on our publication [3], where we use the functional renormalization group to analyze a discontinuous quantum phase transition towards a non-Fermi liquid phase in the Sachdev-Ye-Kitaev (SYK) model. In this thesis, we perform a disorder average over the random interactions in the SYK model. We argue that in the thermodynamic limit, the average renormalization group (RG) flow of the SYK model is identical to the RG flow of an effective disorder averaged model. Using the functional RG, we find a fixed point describing the discontinuous phase transition to the non-Fermi liquid phase at zero temperature. Surprisingly, we find a finite anomalous dimension of the fermions, which indicates critical fluctuations and is unusual for a discontinuous transition. We also determine the RG flow at zero temperature, and relate it to the phase diagram known from the literature.

Contents

Abbreviations

DFP discontinuity fixed point

FRG functional renormalization group

iDE imaginary Dyson equation

IV integer valence

KHΓ Kitaev-Heisenberg-Γ

nFL non-Fermi liquid

QSL quantum spin liquid

RG renormalization group

RVB resonating valence bond

SYK Sachdev-Ye-Kitaev

List of Figures

Chapter 1

Introduction

Quasiparticles are a central concept in condensed matter physics [4, 5, 6, 7, 8]. Collective modes in a many body system can often be characterized by quantum numbers which resemble the quantum numbers known from ordinary particles, like momentum, charge or spin. One example are the wave-like excitations in spin systems called spin waves or magnons [4, 8, 9]. Another notable example is the Fermi-liquid theory [10, 11] used to describe the electronic properties of normal metals. In this thesis, we investigate two models where the two above-mentioned scenarios break down. Both of these models are based on toy models proposed by Alexei Kitaev.

The first part of this thesis is based on our publication [1]. There, we calculate decay rates of magnons in α-$RuCl_3$, a candidate material for the realization of a spin liquid phase. We show that the decay rates are high enough to destroy the quasiparticle-character of the magnons, which was referred to as 'breakdown of magnons' in a previous publication [2].

The second part is based on our publication [3]. There, we perform a scaling analysis in a simple fermionic toy model, the Sachdev-Ye-Kitaev (SYK) model [12]. This model hosts a phase with no quasiparticle excitations at all, called the non-Fermi liquid (nFL) phase [13]. This makes it an interesting toy model for strange metals and high temperature superconductivity [14]. Here, we find an unusual result, namely that the discontinous phase transition to the nFL phase is characterized by strong critical fluctuations, a property which is normally only expected at continuous phase transitions or critical points.

The remainder of this introductory chapter is dedicated to explain the motivation and physical backgrounds of both topics. In Sec. 1.1 we introduce Kitaev's quantum spin liquid and summarize the current status of the search for experimental realizations. In Sec. 1.1.1, we explain our motivation to calculate magnon decay rates in the Kitaev-Heisenberg-Γ (KHΓ) model. In Sec. 1.2, we motivate our scaling analysis in the SYK model. This includes a short introduction to the method used for the analysis, the func-

tional renormalization group (FRG), in Sec. 1.2.1. In Sec. 1.2.2, we briefly introduce the SYK model and the discontinuous phase transition to the nFL phase. The detailed analyses of the two problems is presented in the two following chapters separately, chapter 2 is dedicated to the breakdown of magnons in the KHΓ model and chapter 3 is dedicated to the scaling analysis in the SYK model. In the Appendix, we provide a summary of the thesis in German language.

1.1 The search for Kitaev's quantum spin liquid

Generally, quantum spin liquid (QSL) states are characterized by persisting magnetic quantum fluctuations and absence of magnetic ordering down to lowest temperatures [15]. Usually, they host fractional magnetic excitations. Such a state was first proposed by Philip W. Anderson in the form of *resonating valence bond (RVB)* states [16], where localized spins pair up to form singlet states. Quantum fluctuations in the arrangement of the pairings can be described in terms of so-called *spinons*, which are magnetic excitations with spin 1/2. While many candidate materials have been proposed, it is still debated whether they host QSL states [17]. In the past, this confusion has partly been due to a lack of theoretical understanding, as no derivation of a QSL state from a microscopic model has been known since recently. A substantial advancement in the understanding of QSLs is due to Alexei Kitaev, who presented the (now termed) *Kitaev model* together with its exact solution and showed that this model has a QSL ground state [18]. This ground state is very distinct from the RVB state proposed by Anderson. The fractional excitations are described by anyonic Majorana modes, as opposed to the spinons found in RVB states. These exotic quasiparticles are of particular interest because they can be used for fault-tolerant topological quantum computing [19, 20]. We introduce the Kitaev model in more detail in Sec. 2.1.

A physical realization of this exotic state, termed *Kitaev QSL*, would surely be of interest, but there is a problem: the couplings between the localized spins in the Kitaev model are rather artificial and other more common couplings are usually dominant in real materials. A possible solution was proposed with the *Khaliullin mechanism* [21], where strong spin orbit coupling leads to the formation of a spin-orbit triplet state. The crystal field of the neighboring atoms can then lead to an energy splitting which reduces the triplet to an effective *pseudo spin* 1/2. Due to a specific geometric alignment of the unit cells, the interactions between neighboring pseudo spins are of the type described by the Kitaev model and can get comparable in magnitude to the more common magnetic interactions like the Heisenberg interaction. In subsequent years, many candidate materials were proposed (see Ref. [22] for a review), one of which is α-$RuCl_3$. This

material is an ordered magnet at low temperatures [23] and as such, cannot be a realization of a Kitaev QSL. There is a debate whether a Kitaev QSL can be induced by destroying the magnetic order by an external magnetic field [22, 24, 25, 26, 27, 28]. Interestingly, it has been argued that even in the absence of an external field, the observed inelastic neutron scattering spectra are best explained by fractional magnetic excitations as described by the Kitaev model [29, 30]. While the Kitaev ground state is destroyed by non-Kitaev couplings between the pseudo spins, the fractional excitations supposedly do survive. This would allow neutron scattering within a broad energy range and could explain the scattering continuum observed in α-$RuCl_3$.

1.1.1 Magnon decay in the Kitaev-Heisenberg-Γ model

As an alternative to the interpretation as a QSL, the authors of Ref. [2] argue that the broad neutron scattering continua in α-$RuCl_3$ could be explained by other mechanisms. Usually, one expects that the excitation spectrum of an ordered magnet is described by spin-waves [4, 8, 9], which are well defined quasi-particles with spin 1, called magnons. One would expect that these magnetic excitations lead to sharp peaks in neutron scattering experiments. However, the magnetic couplings and the special crystal structure in α-$RuCl_3$ allow scattering channels from the one-magnon to the two-magnon states, which leads to a short magnon lifetime, diminishing their quasiparticle character. The authors of Ref. [2] call this the 'breakdown of magnons'. In the extreme, a consequence would be an incoherent magnon spectrum which would result in a broad neutron scattering spectrum. The authors state that the broad magnon spectrum may result either from the absence of magnetic quasi-particles altogether, or from other types of non-magnonic quasi-particles. Leaving open the possibility for fractional excitations, the mechanism presented in Ref. [2] may be seen as a more general approach to a description of the broad neutron scattering spectra in α-$RuCl_3$. To substantiate their claim, the authors describe the material by the KHΓ model, which is an extension of the Kitaev model that we introduce in Sec. 2.2. They first estimate the coupling parameters of the model by comparing experimental data from inelastic neutron scattering with results they produced by exact diagonalization of the Hamiltonian [31]. They proceed to approximate the leading anharmonic coupling, which is the three legged vertex describing the decay of one magnon into two magnons, by a single constant number. With this approximation, they calculate the damping of the spin waves. This way, they reach considerable agreement with experiments as well as with the exact diagonalization results. In order to validate this interpretation of the scattering continuum in terms of the breakdown of magnons, it is important to check whether the approximation of the interaction vertex, which is in general momentum and channel-dependent, as one single number is justi-

fied. The authors did this only indirectly by testing the approximation on a different, simpler spin model where a more detailed calculation had already been published [32].

The work presented in this thesis was originally intended as an extension of the analysis in Ref. [2]. Our goal was to validate these results by a more detailed calculation. However, this turned out to be a complicated task due to the complexity of the Hamiltonian. While trying to tackle this problem, we were able to identify a special region in the parameter space of the KHΓ model, where the problem simplifies and a more detailed analysis is possible. The authors of Ref. [2] then repeated their calculation for a set of parameters which lies within this special region, allowing a comparison with our more detailed calculation. While this set of parameters probably has no immediate physical relevance, it was now possible to validate the cruder approximation. We note that the method described in this thesis is quite general and can in principle be used to identify similar special regions in other bosonic systems as well.

1.2 Quantum phase transition in the SYK model

Physics in the vicinity of a continuous phase transition is characterized by critical fluctuations on all length scales [33]. A discontinuous phase transition on the other hand is characterized by a state of phase separation, with two or more sharply distinguished non-critical phases of matter. In this work, we study a discontinuous quantum phase transition in the SYK model and surprisingly find evidence for the presence of critical fluctuations.

We begin this section with a summary of the FRG, which is the method we use for our analysis. Thereafter we briefly introduce the SYK model and the discontinuous phase transition we want to investigate.

1.2.1 Functional renormalization group

We recapitulate that the renormalization group (RG) as developed by Kadanoff [34] and Wilson [35, 36, 37] is based on coarse-graining the dynamic degrees of freedom of a physical theory. This is typically achieved by successively integrating out modes with high energies, large momenta, or small length scales and termed *mode elimination*. The coupling constants of the resulting effective theory will in general depend on the degree of coarse-graining, leading to the RG flow in the abstract space of the coupling constants. Due to the mode elimination procedure, the degree of coarse-graining - and hence the RG flow - is determined by a flowing energy, momentum or length scale. As a result, macroscopic properties of a physical system, which are governed by the coarse grained degrees of freedom, can be inferred from the RG flow of its microscopic theory. The most interesting features of the RG flow are usually the *fixed points* in the space of coupling constants.

There, the couplings between the degrees of freedom stay fixed relative to the flowing scale, i.e. a model with those couplings is scale invariant. It turns out that the phenomenology of physical systems near a critical point or near a phase transition can be explained by the RG flow near a critical fixed point which attracts most couplings and repels at least one. In particular, the critical exponents of a continuous phase transition can be found from an analysis of the RG flow near a critical fixed point and the scaling hypothesis [34, 38] can be proved. Moreover, the reason for the universality of the critical exponents across large groups of different physical systems can be explained [33, 39]: the RG flow is typically characterized by a small number of fixed points. But this means that the low energy or large scale behavior of the whole coupling space is determined by only few fixed points. This leads to qualitatively identical macroscopic behavior in large groups of models, which can be grouped into universality classes.

To find the RG flow of the SYK model, we will utilize the *functional renormalization group* (FRG) [39, 40, 41, 42]. The FRG is a formulation of the RG in terms of functional differential equations. The coarse-graining procedure is implemented by artificially introducing an explicit scale dependence to the free propagator,

$$G^0_{\alpha\beta}(\boldsymbol{k},\omega) \to G^0_{\Lambda,\alpha\beta}(\boldsymbol{k},\omega)\,. \tag{1.1}$$

Here, we denote the energy, momentum, or length scale by Λ. The scale dependence is usually chosen such that the propagator is suppressed in the infrared regime: if Λ is a length scale, then the propagator should vanish for lengths much larger than Λ and if Λ is an energy or momentum scale, then the propagator should vanish for frequencies or momenta much smaller than Λ. In the opposite ultraviolet regime, the propagator is unchanged, and between the ultraviolet and the infrared regime, the Λ-dependence can in principle be chosen arbitrarily. This procedure adds an artificial scale dependence to all correlation functions of the theory, which will then 'flow' with the scale Λ.

Here, we use the FRG in the form presented in Ref. [39]. The central quantities are the *irreducible vertices* with n external legs, written as

$$\Gamma^{(n)}_{\Lambda,\alpha_1\ldots\alpha_n}(\boldsymbol{k_1}\omega_1,\ldots,\boldsymbol{k_n}\omega_n)\,. \tag{1.2}$$

These irreducible vertices are precisely the vertices appearing in the tree expansion of Feynman diagrams, and can hence be physically interpreted as effective n-particle interactions.

For formal convenience, a generating functional $\mathit{\Gamma}_\Lambda[\boldsymbol{\phi}]$ is defined such that it generates the irreducible vertices by the functional derivatives

$$\Gamma^{(n)}_{\Lambda,\alpha_1\ldots\alpha_n}(\boldsymbol{k_1}\omega_1,\ldots,\boldsymbol{k_n}\omega_n) = \frac{\delta^n\,\mathit{\Gamma}_\Lambda[\boldsymbol{\phi}]}{\delta\phi_{\alpha_1}(\boldsymbol{k_1}\omega_1)\ldots\delta\phi_{\alpha_n}(\boldsymbol{k_n}\omega_n)}\bigg|_{\boldsymbol{\phi}=0}\,. \tag{1.3}$$

Here, the components ϕ_α of the vector $\boldsymbol{\phi}$ are sources of the generating functional. Formally, the generating functional of the irreducible vertices is the Legendre transform of the generating functional for the connected Green's functions with respect to the source fields. The irreducible vertices are thus closely related to the correlation functions of the fields, and the sources ϕ_α are the expectation values of the original fields [5, 39].

The generating functional $\Gamma_\Lambda[\boldsymbol{\phi}]$ can be differentiated with respect to the scale Λ, which leads to a linear differential equation for $\Gamma_\Lambda[\boldsymbol{\phi}]$. This formally exact flow equation is commonly known as the *Wetterich equation*. The Wetterich equation can be functionally expanded into a power series in the sources ϕ_α, leading to an infinitely large system of coupled differential equations for the irreducible vertices $\Gamma_\Lambda^{(n)}$. This system of flow equations is referred to as the *vertex expansion* and can typically only be solved approximately.

The connection to the Wilsonian RG is established by the insight that the infrared regime of the irreducible vertices coincides with the bare vertices of a Wilsonian action where the ultraviolet regime has already been integrated out [43]. Consequently, the infrared part of the flowing irreducible vertices can directly by identified with the flowing coupling constants in a corresponding Wilsonian RG.

1.2.2 Phase transition in the SYK model

The SYK model was introduced by Alexei Kitaev during a lecture [12]. He states that it is a simplification of a random Heisenberg model examined earlier by Sachdev and Ye [44], where Kitaev replaced the spin degrees of freedom by Majorana modes. In this form, the SYK model served as a simple, exactly solvable toy model for the gauge-gravity duality. For a given quantum field theory, this duality describes a one-to-one mapping to an equivalent gravitational theory. It was soon realized that a complex fermionic variant of the SYK model could be a valuable toy model in condensed matter physics. We will define the Hamiltonian of this model later in Sec. 3.1.

The SYK model is exactly solvable in the sense that a simple equation for the self energy of the fermions can be derived in the thermodynamic limit, which can be solved analytically in the zero temperature limit and numerically for finite temperatures [14, 45, 46]. The explicit form of the solution at low temperatures depends on the chemical potential μ. For large $|\mu|$ one finds an integer valence (IV) state where the self energy vanishes and, depending on the sign of μ, all modes are either uniformly occupied or uniformly unoccupied. For smaller $|\mu|$, one finds a scale invariant solution with anomalous dimension $\eta = 1/2$, i.e. the single-mode Green's function obeys a power law, $G(\tau) \propto \tau^{-1/2}$. Moreover, the characteristic time scale of correlations and of thermodynamic equilibration is then given by the Planckian

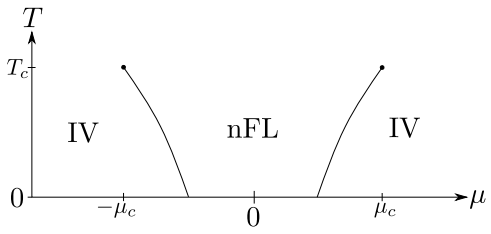

Figure 1.1: Phase diagram of the SYK model. μ is the chemical potential and T is the temperature. The discontinuous phase transitions between the nFL and the IV phases have critical endpoints at $T = T_c$, $\mu = \pm\mu_c$.

time scale $\hbar\omega/k_BT$, which is strong evidence for the lack of quasiparticle excitations [47]. It is the lack of quasiparticles which gives this phase the name nFL. Because the absence of quasiparticles is also a key property of strange metals [13], the SYK model and modifications thereof are seen as valuable toy models for strange metals and high temperature superconductivity [14].

The subject of our interest is the phase transition separating the IV and the nFL phases. It was shown that this is a discontinuous phase transition with a disconitnuity in the fermionic occupation number [46, 48]. The phase transitions have critical endpoints at some critical temperature T_c and chemical potential $\pm\mu_c$ as shown in Fig.1.1. Interestingly, the critical exponents at the critical endpoint are asymmetrical, i.e. they depend on the direction from which the critical point is approached. According to the authors of Ref. [46], an RG picture of the phase transition is problematic because of this asymmetry. In our work, we use the FRG to show that at least at zero temperature, an RG description of the phase transition is possible. Surprisingly, we find that the anomalous dimension at the phase transition is finite. This indicates strongly correlated critical fluctuations, an unexpected feature which at first sight seems to be incompatible with a discontinuous phase transition. Although the interpretation is not completely clear to us, we will discuss possible implications of this unusual result at the end of chapter 3.

Chapter 2

Breakdown of magnons in the Kitaev-Heisenberg-Γ model

Spin waves [4, 9, 8] are low energy excitations of ordered magnets in terms of well defined bosonic quasi particles, called magnons.

Here, we consider the KHΓ model, which is believed to describe a novel class of magnetic insulators [2, 49, 50, 51]. In the literature, it has been argued that materials described by this model might exhibit fractional magnetic excitations which are suitable for quantum computations [29, 30]. However, this claim has been questioned in Ref. [2] on the basis of spin wave theory. In their spin-wave calculation, the authors approximated the interaction between magnons as a momentum- and branch-independent constant. In this work, we try to supplement the analysis of Ref. [2] with yet another, more detailed approach to spin wave theory in the KHΓ-model.

A perturbative analysis of spin waves in the KHΓ-model is a challenging endeavor. Due to the presence of scattering from single- to two-magnon states, umklapp processes become important. Additionally, in the zigzag phase which we study, the magnetic unit cell consist of four atoms, leading to four magnon branches. As a consequence, eight-dimensional matrices and tensors are needed to describe the Hamiltonian. This is probably at the brink of what can be done analytically. In the approach presented here, we use a *hermitian field parametrization* [52, 53, 54, 55] of the spin waves to identify a previously unknown special region in the parameter space of the KHΓ-model, where the spin-wave theory simplifies. This allows us to caclulate the damping of the magnons within that special parameter region to leading order in perturbation theory without any further approximations of the magnonic interactions. Unfortunately, this special parameter region does not include the parameters used in Ref. [2]. Nevertheless, the authors of Ref. [2] were able to produce results for parameters which do fall into this

special region, making a principle validation of their approximation possible.

This chapter is closely oriented on our publication [1] and has the following structure. We start by introducing the Kitaev model in Sec. 2.1 and then the KHΓ model in Sec. 2.2. In Sec. 2.3, we define the lattice vectors that we will use throughout this chapter. We then proceed by exploring the classical phase diagram in Sec. 2.4, which we need for the spin wave expansion that is to follow in Sec. 2.5. Thereafter in Sec. 2.6, we diagonalize the quadratic part of the spin wave Hamiltonian using the hermitian field parametrization. This allows us to identify the special region in parameter space where the diagonalization matrices simplify. Using the analytical results for the diagonalization matrices, we give expressions for the transformed three-legged magnonic interaction vertices in terms of products of analytic matrices. Because these expressions get very long if multiplied out, we resort to numerical methods from that point on. Unfortunately, the special region we found does not overlap with the parameters found in Ref. [2]. Nevertheless, a principal validation of the approximation scheme used in Ref. [2] is possible. Therefore, we choose a representative point within the special parameter region and calculate the damping of the magnons at zero temperature in Sec. 2.7. We also calculate the dynamical structure factor in Sec. 2.8. Finally, we give a short discussion of physical and technical aspects of the results in Sec. 2.9.

2.1 The Kitaev model

The Kitaev model is defined on a honeycomb lattice with magnetic spins $S = 1/2$ located at the lattice sites. The spins interact with their nearest neighbors via an Ising interaction. Depending on the spatial orientation of the lattice bond, different components of the spin vectors couple. To make this bond-dependence more precise, consider a honeycomb lattice lying in the [111]-plane of a laboratory basis $\{\hat{\boldsymbol{x}}, \hat{\boldsymbol{y}}, \hat{\boldsymbol{z}}\}$ and aligned as shown in Fig. 2.1. The bonds between nearest neighbor sites can have three different orientations. We call those bonds that are perpendicular to the $\hat{\boldsymbol{x}}$ direction x-bonds, those that are perpendicular to the $\hat{\boldsymbol{y}}$ direction y-bonds, and those that are perpendicular to the $\hat{\boldsymbol{z}}$ direction z-bonds. The Hamiltonian for the Kitaev model can then be written as

$$H_{\text{Kitaev}} = K_x \sum_{\langle ij\rangle_x} S_i^x S_j^x + K_y \sum_{\langle ij\rangle_y} S_i^y S_j^y + K_z \sum_{\langle ij\rangle_z} S_i^z S_j^z \,, \tag{2.1}$$

where S_i^x, S_i^y, S_i^z are the vector components of the spin operator at lattice site i. The expression $\langle ij\rangle_x$ denotes the set of nearest neighbor pairs i, j separated by an x-bond, and similarly for $\langle ij\rangle_y$ and $\langle ij\rangle_z$.

In his original paper [18], Kitaev shows how to solve this model analytically. The solution is based on the decomposition of the spins into

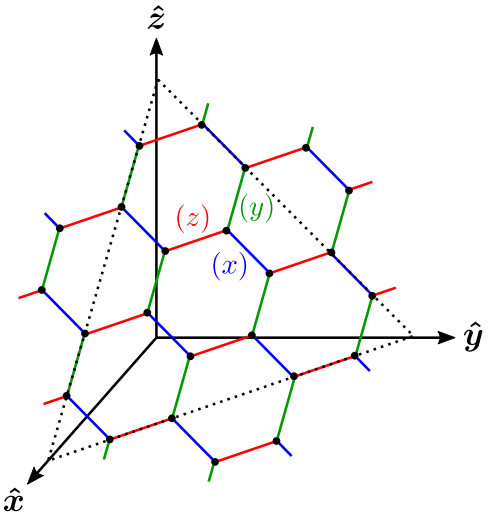

Figure 2.1: A honeycomb lattice lying in a [111]-plane of a laboratory basis $\{\hat{\boldsymbol{x}}, \hat{\boldsymbol{y}}, \hat{\boldsymbol{z}}\}$. The blue x-bonds are perpendicular to the $\hat{\boldsymbol{x}}$-direction, as are the green y-bonds to the $\hat{\boldsymbol{y}}$-direction and the red z-bonds to the $\hat{\boldsymbol{z}}$-direction

Majorana modes. These exotic particle-like objects were first introduced by Ettore Majorana with the intent to describe neutrinos [56]. Majorana modes obey fermionic anti-commutation relations and are their own antiparticles [57, 58, 59], i.e. their creation and annihilation operators fulfill the relation

$$(c^\dagger)^2 = c^2 = 0\,. \tag{2.2}$$

The algebra of the components S^x, S^y, S^z of a spin 1/2 operator can be expressed in terms of four Majorana operators [18]. This leads to an artificial enlargement of the two dimensional Hilbert space of the spin to the four dimensional Hilbert space of the four Majorana modes. Then, the exact solution of the Kitaev model can be found by associating one of the four Majorana modes with the lattice site and the three remaining modes with each adjacent lattice bond. We illustrate this in Fig. 2.2. Because two Majorana operators can be linearly combined to constitute one fermionic creation or annihilation operator [57, 58, 59], pairing the bond-associated Majorana modes of neighboring lattice sites with one another leads to one fermion associated with each lattice bond. These bond fermions can in turn be combined to constitute two types of fields, plaquette fluxes and a $\mathbb{Z}_2$ gauge field.

The plaquette fluxes are defined by the product of the six ordinary fermions associated with the bonds around a closed hexagonal loop (a plaquette) of the honeycomb lattice. These operators commute with the Hamiltonian and have eigenvalues ± 1. This allows for an interpretation as conserved fluxes through the plaquettes and the Hamiltonian can be sectioned into flux sectors. The plaquette fluxes do not capture all degrees of freedom described by the bond fermions, as can be seen by counting the dimensions in Hilbert space. Left over is one $\mathbb{Z}_2$ gauge field per lattice site, which results from the artificial enlargement of the Hilbert space due to the intro-

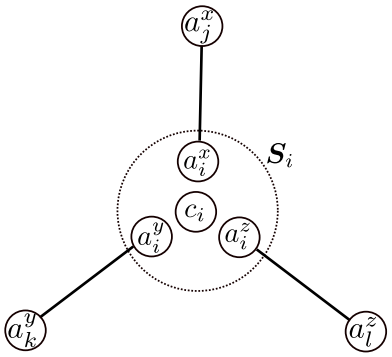

Figure 2.2: The algebra of the spin operator $\boldsymbol{S}_i$ can be expressed in terms of four Majorana modes. Identifying one Majorana mode, c_i, with the lattice site, and the remaining three, $a_i^{x,y,z}$ with the adjacent x-, y- and z-bonds, the Kitaev Hamiltonian (2.1) can be diagonalized analytically.

duction of the Majorana modes. Calculation of physical quantities requires a projection to the physical Hilbert space or, equivalently, fixing a gauge.

The dynamics within the conserved plaquette-flux sectors is described by the remaining unpaired Majorana modes at each lattice site. Depending on the relative strengths of the coupling constants K_x, K_y, K_z, the spectrum of the Majorana modes is either gapped or gapless. If one of the couplings is much larger than the others, the Majorana modes are gapped and exhibit Abelian anyonic statistics, i.e. permutation of two Majorana modes leads to a phase factor $e^{i\phi}$ which is distinct from the bosonic/ fermionic ± 1 [60]. If none of the couplings is dominant a gapless spectrum results. In this case, the low energy physics is restricted to the ground state sector of the plaquette fluxes, where all fluxes are aligned. The low energy dynamics is then fully determined by the dynamics of the Majorana modes. In the presence of an external magnetic field, the Majorana modes obey non-Abelian anyonic statistics, i.e. a permutation of two Majorana modes leads to a change of the quantum mechanical state, which can be interpreted as an operator-valued phase factor [60]. Such non-Abelian anyons are of particular practical interest since they obey so-called braiding rules which could be used to perform topological quantum computations [18, 19, 20].

2.2 The Kitaev-Heisenberg-Γ model

α-$RuCl_3$ and related materials are best described by a localized spin Hamiltonian on a honeycomb lattice [2, 49, 50, 51]. The most important couplings are a Kitaev interaction as given in Eq. (2.1), a Heisenberg interaction between nearest and third-nearest neighbors, and a symmetric off-diagonal exchange interaction. The Hamiltonian is thus given by

$$H = H_{\text{Kitaev}} + H_{\text{Heisenberg}} + H_{\Gamma} \,, \tag{2.3}$$

which constitutes the KHΓ model. The Kitaev part of the Hamiltonian is the Hamiltonian of the Kitaev model introduced in Eq. (2.1) with equal couplings $K_x = K_y = K_z = K$, i.e.

$$H_{\text{Kitaev}} = K \sum_{\alpha} \sum_{\langle ij \rangle_\alpha} S_i^\alpha S_j^\alpha \ , \tag{2.4}$$

where α enumerates the bond types x, y, z and $\langle ij \rangle_\alpha$ enumerates nearest neighbors connected by an α-bond. The Heisenberg part can be written as

$$H_{\text{Heisenberg}} = J \sum_{\langle ij \rangle} \boldsymbol{S_i} \cdot \boldsymbol{S_j} + J_3 \sum_{\langle\langle\langle ij \rangle\rangle\rangle} \boldsymbol{S_i} \cdot \boldsymbol{S_j} \ , \tag{2.5}$$

where J couples all pairs of nearest neighbors while J_3 couples all pairs of third nearest neighbors, i.e. opposite corners of the hexagons, denoted by $\langle\langle\langle ij \rangle\rangle\rangle$. The off-diagonal part H_Γ of the Hamiltonian couples different spin components of nearest neighbors. Along an x-bond, the S^y component of one spin is coupled to the S^z component of its neighbor, and equivalent couplings are realized for the y- and z-bonds. This can be written as

$$H_\Gamma = \sum_{\alpha\beta\gamma} \Gamma^\alpha_{\beta\gamma} \sum_{\langle ij \rangle_\alpha} S_i^\beta S_j^\gamma \ , \tag{2.6}$$

where α, β, γ each enumerate the bond types x, y, z. $\Gamma^\alpha_{\beta\gamma}$ is a fully symmetric tensor whose components are non-zero only in the case when all indices are distinct, i.e. $\Gamma^x_{yz} = \Gamma^x_{zy} = \Gamma^y_{zx} = \Gamma^y_{xz} = \Gamma^z_{xy} = \Gamma^z_{yx} \equiv \Gamma$.

2.3 Definition of lattice vectors

We choose a laboratory basis $\{\hat{\boldsymbol{x}}, \hat{\boldsymbol{y}}, \hat{\boldsymbol{z}}\}$ such that the honeycomb lattice lies in the [111]-plane as shown in Fig. 2.1. Then, we define sublattices and lattice vectors as shown in Fig. 2.3. The honeycomb lattice is a hexagonal Bravais lattice with two sites in each unit cell and hence can be divided into two sublattices which we name A and B. The sublattice vectors pointing from a site on sublattice A to its nearest neighbors (which lie on sublattice B) are given by

$$\boldsymbol{d}_x = \frac{d}{\sqrt{2}} (-\hat{\boldsymbol{y}} + \hat{\boldsymbol{z}}) \ , \tag{2.7a}$$

$$\boldsymbol{d}_y = \frac{d}{\sqrt{2}} (\hat{\boldsymbol{x}} - \hat{\boldsymbol{z}}) \ , \tag{2.7b}$$

$$\boldsymbol{d}_z = \frac{d}{\sqrt{2}} (-\hat{\boldsymbol{x}} + \hat{\boldsymbol{y}}) \ , \tag{2.7c}$$

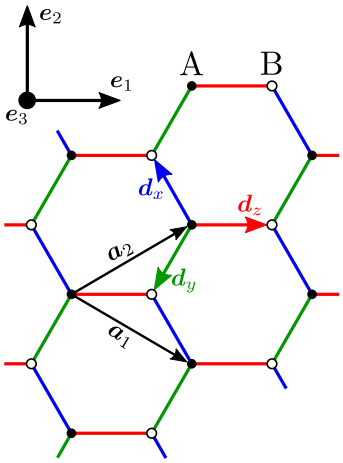

Figure 2.3: Definition of the sublattices A and B, the lattice vectors $\boldsymbol{a}_1$ and $\boldsymbol{a}_2$, the sublattice vectors $\boldsymbol{d}_x$, $\boldsymbol{d}_y$, $\boldsymbol{d}_z$ corresponding to the bond types x, y, z, and the planar basis $\{\boldsymbol{e}_1, \boldsymbol{e}_2, \boldsymbol{e}_3\}$ where $\boldsymbol{e}_3$ points towards the reader.

where d is the nearest neighbor distance and the sublattice vectors are named in correspondence to the bond types x, y, z. The lattice vectors

$$\boldsymbol{a}_1 = -\boldsymbol{d}_x + \boldsymbol{d}_z \,, \tag{2.8a}$$
$$\boldsymbol{a}_2 = -\boldsymbol{d}_y + \boldsymbol{d}_z \,, \tag{2.8b}$$

can serve as a basis for the Bravais lattice. We also define a planar basis $\{\boldsymbol{e}_1, \boldsymbol{e}_2, \boldsymbol{e}_3\}$ where $\boldsymbol{e}_1$ and $\boldsymbol{e}_2$ lie in the lattice plane and $\boldsymbol{e}_3$ is orthogonal to the lattice. In terms of the laboratory basis, the planar basis is given by

$$\boldsymbol{e}_1 = \frac{1}{\sqrt{2}} (-\hat{\boldsymbol{x}} + \hat{\boldsymbol{y}}) \,, \tag{2.9a}$$
$$\boldsymbol{e}_2 = \frac{1}{\sqrt{6}} (-\hat{\boldsymbol{x}} - \hat{\boldsymbol{y}} + 2\hat{\boldsymbol{z}}) \,, \tag{2.9b}$$
$$\boldsymbol{e}_3 = \frac{1}{\sqrt{3}} (\hat{\boldsymbol{x}} + \hat{\boldsymbol{y}} + \hat{\boldsymbol{z}}) \,. \tag{2.9c}$$

2.4 Classical ground states

The classical ground state is the spin configuration which minimizes the Hamiltonian when the spin operators are replaced by classical spin vectors. For the minimization procedure, it is convenient to rewrite the nearest and third-nearest neighbor sums in the Hamiltonian (2.3) in terms of the sublattice vectors $\boldsymbol{d}_x$, $\boldsymbol{d}_y$, $\boldsymbol{d}_z$ defined in Eq. (2.7). The Heisenberg part (2.5) can be written as

$$H_{\text{Heisenberg}} = J \sum_{i \in \text{A}} \sum_{\alpha} \boldsymbol{S}_i \cdot \boldsymbol{S}_{i+\alpha} + J_3 \sum_{i \in \text{A}} \sum_{\alpha} \boldsymbol{S}_i \cdot \boldsymbol{S}_{i-2\alpha} \,, \tag{2.10}$$

where $i \in \mathrm{A}$ iterates over all sites on sublattice A and α takes the values x, y, z. The index $(i+\alpha)$ denotes the lattice site at $\boldsymbol{R}_i + \boldsymbol{d}_\alpha$, and the index $(i-2\alpha)$ denotes the lattice site at $\boldsymbol{R}_i - 2\boldsymbol{d}_\alpha$. Note that these lattice sites belong to sublattice B. For later convenience, we rewrite the dot product between the spin vectors in the Hamiltonian (2.10) in tensor notation,

$$H_{\text{Heisenberg}} = \sum_{i\in\mathrm{A}} \sum_{\alpha\beta\gamma} S_i^\beta \left(J\,\delta_{\beta,\gamma}\right) S_{i+\alpha}^\gamma + \sum_{i\in\mathrm{A}} \sum_{\alpha\beta\gamma} S_i^\beta \left(J_3\,\delta_{\beta,\gamma}\right) S_{i-2\alpha}^\gamma \,. \tag{2.11}$$

Similarly, the Kitaev term (2.4) and the off diagonal term (2.6) of the Hamiltonian can be written in tensor notation as

$$H_{\text{Kitaev}} = \sum_{i\in\mathrm{A}} \sum_{\alpha\beta\gamma} S_i^\beta \left(K\,\delta_{\alpha,\beta}\,\delta_{\beta,\gamma}\right) S_{i+\alpha}^\gamma \,, \tag{2.12}$$

$$H_\Gamma = \sum_{i\in\mathrm{A}} \sum_{\alpha\beta\gamma} S_i^\beta\, \Gamma_{\beta\gamma}^\alpha\, S_{i+\alpha}^\gamma \,. \tag{2.13}$$

All three parts of the Hamiltonian are now expressed in the same format, and the whole Hamiltonian can be written as

$$H = \sum_{i\in\mathrm{A}} \sum_{\alpha\beta\gamma} S_i^\beta \left(W_{\beta\gamma}^\alpha\, S_{i+\alpha}^\gamma + J_3\,\delta_{\beta,\gamma}\, S_{i-2\alpha}^\gamma\right) \,, \tag{2.14}$$

where we defined the nearest-neighbor interaction tensor

$$W_{\beta\gamma}^\alpha = J\,\delta_{\beta,\gamma} + K\,\delta_{\alpha,\beta}\,\delta_{\beta,\gamma} + \Gamma_{\beta\gamma}^\alpha \,. \tag{2.15}$$

This can be written in matrix notation as

$$H = \sum_{i\in\mathrm{A}} \sum_{\alpha} \boldsymbol{S}_i \cdot \left(\boldsymbol{W}^\alpha\, \boldsymbol{S}_{i+\alpha} + J_3\, \boldsymbol{S}_{i-2\alpha}\right) \,, \tag{2.16}$$

with the bond-dependent nearest-neighbor interaction matrices

$$\boldsymbol{W}^x = \begin{pmatrix} J+K & 0 & 0 \\ 0 & J & \Gamma \\ 0 & \Gamma & J \end{pmatrix} \,, \quad \boldsymbol{W}^y = \begin{pmatrix} J & 0 & \Gamma \\ 0 & J+K & 0 \\ \Gamma & 0 & J \end{pmatrix} \,, \quad \boldsymbol{W}^z = \begin{pmatrix} J & \Gamma & 0 \\ \Gamma & J & 0 \\ 0 & 0 & J+K \end{pmatrix} \,, \tag{2.17}$$

as expressed in the laboratory basis $\{\hat{\boldsymbol{x}}, \hat{\boldsymbol{y}}, \hat{\boldsymbol{z}}\}$.

Classically, the spins $\boldsymbol{S}_i$ are vectors of fixed length S, i.e. they are fully determined by their polar and azimuthal angles θ_i and φ_i. To find the minimum of the Hamiltonian (2.16), we require that the drivatives with respect to θ_i and φ_i vanish at every lattice site. We begin by minimizing the spins on sublattice A,

$$0 \overset{!}{=} \frac{\partial H}{\partial(\theta_i, \varphi_i)} = \frac{\partial \boldsymbol{S}_i}{\partial(\theta_i, \varphi_i)} \cdot \sum_\alpha \left(\boldsymbol{W}^\alpha\, \boldsymbol{S}_{i+\alpha} + J_3\, \boldsymbol{S}_{i-2\alpha}\right) \quad \text{for all } i \in \mathrm{A} \,. \tag{2.18}$$

We notice that all spins appearing in the second term of the dot product are on sublattice B. The derivatives $\partial \boldsymbol{S}_i / \partial(\theta_i, \varphi_i)$ span the plane of vectors

perpendicular to $\boldsymbol{S}_i$. The vanishing dot product in Eq. (2.18) thus implies that any vector in this plane must be perpendicular to the second term of the dot product (or that the second term vanishes by itself). This in turn means that the spin $\boldsymbol{S}_i$ must be parallel to the second term of the dot product,

$$\boldsymbol{S}_i \propto \sum_\alpha \left(\boldsymbol{W}^\alpha \boldsymbol{S}_{i+\alpha} + J_3 \boldsymbol{S}_{i-2\alpha}\right) \quad \text{for all } i \in \mathrm{A}\,. \tag{2.19}$$

Normalization to length S leads to

$$\boldsymbol{S}_i = \pm S \frac{\sum_\alpha \left(\boldsymbol{W}^\alpha \boldsymbol{S}_{i+\alpha} + J_3 \boldsymbol{S}_{i-2\alpha}\right)}{\left|\sum_\alpha \left(\boldsymbol{W}^\alpha \boldsymbol{S}_{i+\alpha} + J_3 \boldsymbol{S}_{i-2\alpha}\right)\right|} \quad \text{for all } i \in \mathrm{A}\,. \tag{2.20}$$

Substituting this back into the Hamiltonian (2.16) leads to a an expression for the ground state energy that depends only on the spins on sublattice B,

$$E_0 = \pm S \sum_{i\in\mathrm{A}} \frac{\left[\sum_\alpha \left(\boldsymbol{W}^\alpha \boldsymbol{S}_{i+\alpha} + J_3 \boldsymbol{S}_{i-2\alpha}\right)\right]^2}{\left|\sum_\alpha \left(\boldsymbol{W}^\alpha \boldsymbol{S}_{i+\alpha} + J_3 \boldsymbol{S}_{i-2\alpha}\right)\right|}\,. \tag{2.21}$$

Noting that the energy is minimized by the minus sign then leads to

$$E_0 = -S \sum_{i\in\mathrm{A}} \left|\sum_\alpha \left(\boldsymbol{W}^\alpha \boldsymbol{S}_{i+\alpha} + J_3 \boldsymbol{S}_{i-2\alpha}\right)\right|\,, \tag{2.22}$$

The minus sign implies for the spin orientations (2.20) on sublattice A that

$$\boldsymbol{S}_i = -S \frac{\sum_\alpha \left(\boldsymbol{W}^\alpha \boldsymbol{S}_{i+\alpha} + J_3 \boldsymbol{S}_{i-2\alpha}\right)}{\left|\sum_\alpha \left(\boldsymbol{W}^\alpha \boldsymbol{S}_{i+\alpha} + J_3 \boldsymbol{S}_{i-2\alpha}\right)\right|} \quad \text{for all } i \in \mathrm{A}\,. \tag{2.23}$$

In this expression, the spins on sublattice B are coupled because they appear in different combinations within the absolute value. This makes a further minimization challenging. Luckily, we can use results from the literature to simplify the problem. The phase diagram at $J_3 = 0$ is mapped in Ref. [49] using a combination of the Luttinger-Tisza method [61] and exact diagonalization. The supplementary material of Ref. [2] generalizes the results to $J_3 \neq 0$. Six qualitatively distinct phases are identified in the classical regime: the ferromagnetic and the antiferromagnetic phase, the zigzag and the stripy phase, the 120° phase, and the incommensurate spiral phase. For the spin-wave expansion in Sec. 2.5, we need to know the absolute orientations of the spins in the respective ground states. To find those, we use the relative orientations of the spins to one another as characterized by the phases identified in the aforementioned literature and complete the minimization of the ground state energy (2.22).

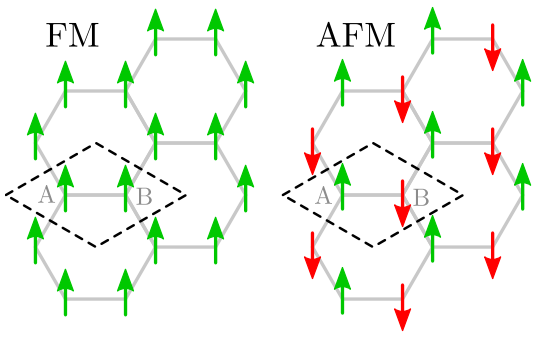

Figure 2.4: Relative alignments of the spins in the classical ferromagnetic (FM) and antiferromagnetic (AFM) ground states. The magnetic unit cell (dashed line) is the same as the unit cell of the Honeycomb lattice.

2.4.1 Ferro- and Antiferromagnetic phases

In the ferro- and antiferromagnetic phases, all spins on the same sublattice are aligned in the same direction $\boldsymbol{S}_\mathrm{A}$ resp. $\boldsymbol{S}_\mathrm{B}$, as shown in Fig. 2.4. The expression (2.22) for the ground state energy can thus be simplified to

$$\begin{aligned} E_0^{\mathrm{FM/AFM}} &= -S \sum_{i\in\mathrm{A}} \left| \sum_\alpha \left(\boldsymbol{W}^\alpha + J_3\right) \boldsymbol{S}_\mathrm{B} \right| \\ &= -\frac{N}{2} S \left| \sum_\alpha \left(\boldsymbol{W}^\alpha + J_3\right) \boldsymbol{S}_\mathrm{B} \right| , \end{aligned}$$

where N is the number of lattice sites of the Honeycomb lattice. $E_0^{\mathrm{FM/AFM}}$ is minimized if $\boldsymbol{S}_\mathrm{B}$ is the eigenvector of the interaction matrix

$$\sum_\alpha \left(\boldsymbol{W}^\alpha + J_3\right) = \begin{pmatrix} 3J+3J_3+K & \Gamma & \Gamma \\ \Gamma & 3J+3J_3+K & \Gamma \\ \Gamma & \Gamma & 3J+3J_3+K \end{pmatrix} , \tag{2.24}$$

with the largest absolute eigenvalue $\lambda_\mathrm{max}^{\mathrm{FM/AFM}}$, so that

$$E_0^{\mathrm{FM/AFM}} = -\frac{N}{2} S^2 \left| \lambda_\mathrm{max}^{\mathrm{FM/AFM}} \right| . \tag{2.25}$$

The eigenvalues and eigenvectors of the interaction matrix are

$$\lambda_1 = 3J + 3J_3 + K - \Gamma \; ; \qquad \boldsymbol{v}_1 = \frac{1}{\sqrt{2}} \begin{pmatrix} -1 \\ 1 \\ 0 \end{pmatrix} = \boldsymbol{e}_1 , \tag{2.26a}$$

$$\lambda_2 = \lambda_1 \; ; \qquad \boldsymbol{v}_2 = \frac{1}{\sqrt{6}} \begin{pmatrix} -1 \\ -1 \\ 2 \end{pmatrix} = \boldsymbol{e}_2 , \tag{2.26b}$$

$$\lambda_3 = 3J + 3J_3 + K + 2\Gamma \; ; \qquad \boldsymbol{v}_3 = \frac{1}{\sqrt{3}} \begin{pmatrix} 1 \\ 1 \\ 1 \end{pmatrix} = \boldsymbol{e}_3 . \tag{2.26c}$$

If $\lambda_1 = \lambda_2$ minimizes the ground state energy, the classical ground state is degenerate and $\boldsymbol{S}_\mathrm{B}$ lies in the lattice plane with otherwise arbitrary orientation. If λ_3 minimizes the ground state energy, the magnetization is

perpendicular to the lattice plane. The magnetization on sublattice A is determined by Eq. (2.23), which leads to

$$\boldsymbol{S}_\mathrm{A} = -S\frac{\sum_\alpha (\boldsymbol{W}^\alpha + J_3)\,\boldsymbol{S}_\mathrm{B}}{|\sum_\alpha (\boldsymbol{W}^\alpha + J_3)\,\boldsymbol{S}_\mathrm{B}|} = -\frac{\lambda_\mathrm{max}^\mathrm{FM/AFM}}{|\lambda_\mathrm{max}^\mathrm{FM/AFM}|}\boldsymbol{S}_\mathrm{B}\ . \tag{2.27}$$

If λ_max is positive, $\boldsymbol{S}_\mathrm{A} = -\boldsymbol{S}_\mathrm{B}$ and the antiferromagnetic phase is realized. For negative λ_max, the ferromagnetic phase with $\boldsymbol{S}_\mathrm{A} = \boldsymbol{S}_\mathrm{B}$ is realized.

2.4.2 Stripy and zigzag phase

The stripy and zigzag phases are sketched in Fig. 2.5. Their names refer to the stripe and zigzag patterns formed by spins with the same orientation. The zigzag phase is of our prime interest, as this is the phase realized by α-$RuCl_3$ at low temperature [29]. Both phases can be characterized (up to a 120° rotation) by the relations

$$\boldsymbol{S}_{i+\boldsymbol{a}_1} = \boldsymbol{S}_{i+\boldsymbol{a}_2} = -\boldsymbol{S}_i \tag{2.28}$$

for any lattice site i. As a result, the magnetic ground state has a lower symmetry than the honeycomb lattice and the lattice is subdivided into four sublattices a, b, c, and d as shown in Fig. 2.5.

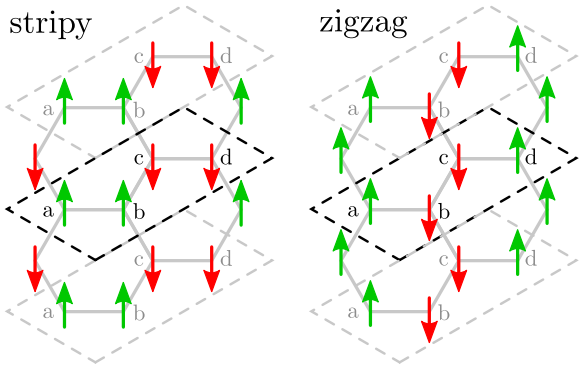

Figure 2.5: Relative alignments of the spins in the classical stripy and zigzag ground states. The magnetic unit cell (dashed black line) is twice as large as the unit cell of the honeycomb lattice. The lattice is accordingly subdivided into four sublattices a, b, c and d.

We use the relations (2.28) between the spin alignments to express the spins $\boldsymbol{S}_{i+x}$ and $\boldsymbol{S}_{i+y}$ appearing in the ground state energy (2.22) relative to the spin $\boldsymbol{S}_{i+z}$. For any point i on sublattice a or c, these relations are

$$\boldsymbol{S}_{i+x} = \boldsymbol{S}_{i+y} = -\boldsymbol{S}_{i+z}\ , \tag{2.29a}$$

$$\boldsymbol{S}_{i-2x} = \boldsymbol{S}_{i-2y} = \boldsymbol{S}_{i-2z} = \boldsymbol{S}_{i+z}\ , \tag{2.29b}$$

which leads to the ground state energy

$$\begin{aligned} E_0^\mathrm{stripy/zigzag} &= -S\sum_{i\in\mathrm{A}} |(-\boldsymbol{W}^x - \boldsymbol{W}^y + \boldsymbol{W}^z + 3J_3)\,\boldsymbol{S}_{i+z}| \\ &= -\frac{N}{2}S\,|(-\boldsymbol{W}^x - \boldsymbol{W}^y + \boldsymbol{W}^z + 3J_3)\,\boldsymbol{S}_\mathrm{b}|\ . \end{aligned} \tag{2.30}$$

In the second line we eliminated the sum by noting that $\boldsymbol{S}_{i+z}$ is either on sublattice b or d (because i is on sublattice a or c) and $\boldsymbol{S}_\mathrm{b} = -\boldsymbol{S}_\mathrm{d}$ according to the relations (2.28). Similar to the treatment before, this is minimized if $\boldsymbol{S}_\mathrm{b}$ is the eigenvector of the interaction matrix

$$(-\boldsymbol{W}^x - \boldsymbol{W}^y + \boldsymbol{W}^z + 3J_3) = \begin{pmatrix} -J+3J_3-K & \Gamma & -\Gamma \\ \Gamma & -J+3J_3-K & -\Gamma \\ -\Gamma & -\Gamma & -J+3J_3+K \end{pmatrix} \tag{2.31}$$

which has the largest absolute eigenvalue $\lambda_\mathrm{max}^\mathrm{stripy/zigzag}$, so that

$$E_0^\mathrm{stripy/zigzag} = -\frac{N}{2} S^2 \left|\lambda_\mathrm{max}^\mathrm{stripy/zigzag}\right| \tag{2.32}$$

is minimized. The eigenvalues and eigenvectors of the interaction matrix are

$$\lambda_4 = -J + 3J_3 - K - \Gamma \; ; \qquad \boldsymbol{v}_4 = \frac{1}{\sqrt{2}} \begin{pmatrix} -1 \\ 1 \\ 0 \end{pmatrix} = \boldsymbol{e}_1 \; , \tag{2.33a}$$

$$\lambda_5 = -J + 3J_3 + \frac{\Gamma}{2} - \frac{R}{2} \; ; \qquad \boldsymbol{v}_5 = \frac{1}{\sqrt{2+r^2}} \begin{pmatrix} 1 \\ 1 \\ r \end{pmatrix} \; , \tag{2.33b}$$

$$\lambda_6 = -J + 3J_3 + \frac{\Gamma}{2}\Gamma + \frac{R}{2} \; ; \qquad \boldsymbol{v}_6 = \frac{\mathrm{sign}(s)}{\sqrt{2+s^2}} \begin{pmatrix} 1 \\ 1 \\ s \end{pmatrix} \; , \tag{2.33c}$$

where we defined

$$R = \sqrt{4K^2 - 4K\Gamma + 9\Gamma^2} = \sqrt{(2K-\Gamma)^2 + 8\Gamma^2} \tag{2.34}$$

and

$$r = \frac{2K + 3\Gamma - R}{2K - 3\Gamma + R} \; , \tag{2.35a}$$

$$s = \frac{2K + 3\Gamma - R}{2K - 3\Gamma - R} = -\frac{2}{r} \; . \tag{2.35b}$$

The sign function in the definition of the eigenvector $\boldsymbol{v}_6$ in Eq. (2.33c) ensures that the eigenvectors form a right handed basis, which will be convenient later for the spin wave expansion. Similar to the ferro- and antiferromagnetic phases, the sign of the eigenvalue determines whether the stripy or the zigzag phase is realized: substituting the relations between the spin alignments (2.29) on sublattice B into the expression (2.23) for the spins on sublattice A results in

$$\begin{aligned} \boldsymbol{S}_i &= -S \frac{(-\boldsymbol{W}^x - \boldsymbol{W}^y + \boldsymbol{W}^z + 3J_3)\, \boldsymbol{S}_{i+z}}{|(-\boldsymbol{W}^x - \boldsymbol{W}^y + \boldsymbol{W}^z + 3J_3)\, \boldsymbol{S}_{i+z}|} \\ &= -\frac{\lambda_\mathrm{max}^\mathrm{stripy/zigzag}}{\left|\lambda_\mathrm{max}^\mathrm{stripy/zigzag}\right|} \boldsymbol{S}_{i+z} \qquad \text{for all } i \in \mathrm{A} \; . \end{aligned} \tag{2.36}$$

We see that spins connected by a z-bond are parallel (stripy phase) if the eigenvalue is negative and antiparallel (zigzag phase) if the eigenvalue is positive.

2.4.3 120° phase

The 120° phase can be characterized by the relations

$$\boldsymbol{S}_{j+\boldsymbol{a}_1} = \boldsymbol{R}_{120}\boldsymbol{S}_j, \tag{2.37a}$$
$$\boldsymbol{S}_{j+\boldsymbol{a}_2} = \boldsymbol{R}_{120}^{-1}\boldsymbol{S}_j \quad \text{for } j \in \mathrm{B}, \tag{2.37b}$$

where $\boldsymbol{R}_{120}$ is a right handed rotation matrix of 120° in the lattice plane. These relations can be used to find relations between the spins appearing in the expression (2.22) for the ground state energy:

$$\boldsymbol{S}_{i+x} = \boldsymbol{S}_{i+z-\boldsymbol{a}_1} = \boldsymbol{R}_{120}^{-1}\boldsymbol{S}_{i+z}\ , \tag{2.38a}$$
$$\boldsymbol{S}_{i+y} = \boldsymbol{S}_{i+z-\boldsymbol{a}_2} = \boldsymbol{R}_{120}^{-2}\boldsymbol{S}_{i+z}\ , \tag{2.38b}$$
$$\boldsymbol{S}_{i-2x} = \boldsymbol{S}_{i+z+\boldsymbol{a}_1-\boldsymbol{a}_2} = \boldsymbol{R}_{120}^{-1}\boldsymbol{S}_{i+z}\ , \tag{2.38c}$$
$$\boldsymbol{S}_{i-2y} = \boldsymbol{S}_{i+z-\boldsymbol{a}_1+\boldsymbol{a}_2} = \boldsymbol{R}_{120}\boldsymbol{S}_{i+z}\ , \tag{2.38d}$$
$$\boldsymbol{S}_{i-2z} = \boldsymbol{S}_{i+z-\boldsymbol{a}_1-\boldsymbol{a}_2} = \boldsymbol{S}_{i+z}\ , \tag{2.38e}$$

where i lies on sublattice A. The ground state energy (2.22) can then be written as

$$\begin{aligned} E_0^{120^\circ} &= -S\sum_{i\in\mathrm{A}}\left|\left(\boldsymbol{W}_x\boldsymbol{R}_{120}^{-1} + \boldsymbol{W}_y\boldsymbol{R}_{120} + \boldsymbol{W}_z + J_3\boldsymbol{R}_{120}^{-1} + J_3\boldsymbol{R}_{120} + J_3\right)\boldsymbol{S}_{i+z}\right| \\ &\equiv -S\sum_{j\in\mathrm{B}}\left|\boldsymbol{M}_{120}\boldsymbol{S}_j\right|\ . \end{aligned} \tag{2.39}$$

In the second line we defined the interaction matrix

$$\boldsymbol{M}_{120} = \boldsymbol{W}_x\boldsymbol{R}_{120}^{-1} + \boldsymbol{W}_y\boldsymbol{R}_{120} + \boldsymbol{W}_z + J_3\boldsymbol{R}_{120}^{-1} + J_3\boldsymbol{R}_{120} + J_3\ , \tag{2.40}$$

which has the explicit form

$$\boldsymbol{M}_{120} = \begin{pmatrix} J+J_3 & 2\Gamma+J+J_3+K & J+J_3 \\ 2\Gamma+J+J_3+K & J+J_3 & J+J_3 \\ J+J_3 & J+J_3 & 2\Gamma+J+J_3+K \end{pmatrix}\ . \tag{2.41}$$

The eigenvalues and eigenvectors of $\boldsymbol{M}_{120}$ are

$$\lambda_7 = -K - 2\Gamma\ ; \qquad \boldsymbol{v}_7 = \frac{1}{\sqrt{2}}\begin{pmatrix}-1\\1\\0\end{pmatrix} = \boldsymbol{e}_1\ , \tag{2.42a}$$
$$\lambda_8 = K + 2\Gamma\ ; \qquad \boldsymbol{v}_8 = \frac{1}{\sqrt{6}}\begin{pmatrix}-1\\-1\\2\end{pmatrix} = \boldsymbol{e}_2\ , \tag{2.42b}$$
$$\lambda_9 = 3J + 3J_3 + K + 2\Gamma\ ; \qquad \boldsymbol{v}_9 = \frac{1}{\sqrt{3}}\begin{pmatrix}1\\1\\1\end{pmatrix} = \boldsymbol{e}_3\ . \tag{2.42c}$$

We first notice that $\lambda_9 = \lambda_3$ and $\boldsymbol{v}_9 = \boldsymbol{v}_3$, i.e. it is the same as in the ferro-/antiferromagnetic case. As the spin is perpendicular to the lattice, it is invariant under the 120° rotation. Hence this eigenvalue describes exactly

the ferro-/antiferromagnetic phase. The remaining two eigenvectors $\boldsymbol{v}_7$ and $\boldsymbol{v}_8$ lie in the lattice plane with pseudo degenerate eigenvalues $\lambda_7 = -\lambda_8$. Upon transformation by $\boldsymbol{M}_{120}$, any vector in the lattice plane is scaled by $|\lambda_7|$ and either mirrored on the $\boldsymbol{e}_1 \times \boldsymbol{e}_3$ plane (if $\lambda_7 > 0$ and $\lambda_8 < 0$) or mirrored on the $\boldsymbol{e}_2 \times \boldsymbol{e}_3$ plane (if $\lambda_7 < 0$ and $\lambda_8 > 0$). As a consequence, $|\boldsymbol{M}_{120}\boldsymbol{S}_j| = S|\lambda_7|$ if $\boldsymbol{S}_j$ lies arbitrarily in the lattice plane, which simplifies the ground state energy (2.39) in the 120° phase to

$$E_0^{120^\circ} = -\frac{N}{2} S^2 |\lambda_7| \, . \tag{2.43}$$

We conclude that the classical ground state is degenerate as the absolute orientation of the spins within the lattice plane is not fixed. The orientations of the spins on sublattice B relative to one another are determined by the relations (2.37). The orientation of the spins on sublattice A is defined by Eq.(2.23) which amounts to

$$\boldsymbol{S}_i = -S \frac{\boldsymbol{M}_{120}\boldsymbol{S}_{j+z}}{|\boldsymbol{M}_{120}\boldsymbol{S}_{j+z}|} \quad \text{for all } i \in \text{A} \, , \tag{2.44}$$

i.e. the spin on lattice site i on sublattice A is determined by mirroring the spin on lattice site $i + z$ either on the $\boldsymbol{e}_2 \times \boldsymbol{e}_3$ plane (if $\lambda_7 > 0$) or on the $\boldsymbol{e}_1 \times \boldsymbol{e}_3$ plane (if $\lambda_7 < 0$). The pattern that emerges for $\lambda_7 < 0$ is shown exemplarily in Fig. (2.6).

In principle one could also imagine a 'left handed' 120° phase, where $\boldsymbol{R}_{120}$ is replaced by a left handed rotation of 120°. In this case the matrix corresponding to $\boldsymbol{M}_{120}$ has the eigenvalues 0, 0, λ_3 and the nontrivial eigenvector $\boldsymbol{v}_3$. The trivial eigenvalues will never minimize the Hamiltonian, while the nontrivial one describes again the ferromagnetic/antiferromagnetic phase. Note that this asymmetry between left- and right-handed rotations does not break the mirror symmetries of the lattice. Depending on the mirror plane, either sublattices A and B are interchanged or the handedness of $\boldsymbol{d}_x, \boldsymbol{d}_y, \boldsymbol{d}_z$ is reversed, which results in a restoration of the left-/ right-handedness of the rotation matrices. The left-handed and the right-handed rotation matrices would swap their roles if we chose to express the relative spin alignments (2.37) with respect to sublattice A instead of sublattice B. Note also that the directions of the vortices appearing in Fig. 2.6 is not determined by the handedness of the rotation matrices, but by the arbitrary choice of spin orientation within the lattice plane. For instance, rotating all spins by 180° within the lattice plane reverses the direction of the vortices while conserving the ground state energy.

2.4.4 Incommensurate spiral phase

All ground state energies derived so far are in agreement with the ground states energies given in the supplemental material of Ref. [2]. Similarly to

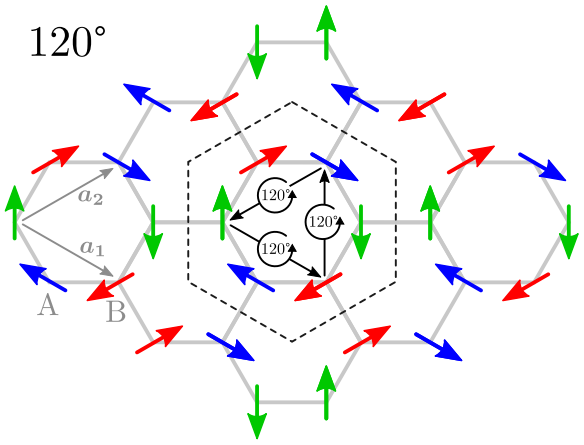

Figure 2.6: Relative alignments of the spins in the classical 120° ground state. The magnetic unit cell (dashed line) contains six lattice sites.

the 120° phase, the incommensurate spiral phase is characterized by relative rotations of the spins among each other in the lattice plane. In this case, the rotation angles are in general no rational fractions of 360°, leading to a magnetic ordering vector that is incommensurate with the honeycomb lattice. Because this complicates the minimization procedure and we are not interested in the incommensurate spiral state anyways, we content ourselves with adopting the result from Ref. [2] for the ground state energy,

$$E_0^{IS} = -\frac{N}{4} S^2 \left| K - \Gamma - \sqrt{8\Gamma^2 + K^2} \right| . \tag{2.45}$$

2.4.5 Phase diagram

To depict the phase diagram in the four dimensional space of the couplings J, K, Γ, J_3, we express all couplings in units of $\mathcal{E} \equiv \sqrt{J^2 + K^2 + \Gamma^2}$. For fixed J_3, the coupling space is then a unit sphere in the remaining three-dimensional coupling space of J, K, Γ. The phase at any point on the unit sphere is given by the corresponding minimal energy among all of the possible ground state energies given in Eqs. (2.25, 2.32, 2.43, 2.45). The resulting phase diagram for $J_3 = 0$ is shown in Fig 2.7a. Later, when we calculate the magnon damping in the zigzag phase, we will be restricted to the region in parameter space where $\Gamma = K > 0$. For vanishing third nearest neighbor interaction $J_3 = 0$ this region has no overlap with the zigzag phase. Fortunately, a positive J_3 stabilizes the zigzag phase, as is shown in Fig. 2.7b, opening a window for our later analysis of the magnon damping.

2.5 Spin wave expansion in the zigzag phase

In this section, we expand the spin-Hamiltonian (2.3) of the KHΓ model in terms of spin waves. These are magnetic excitations from the ground state which have bosonic statics. We will expand the Hamiltonian around the

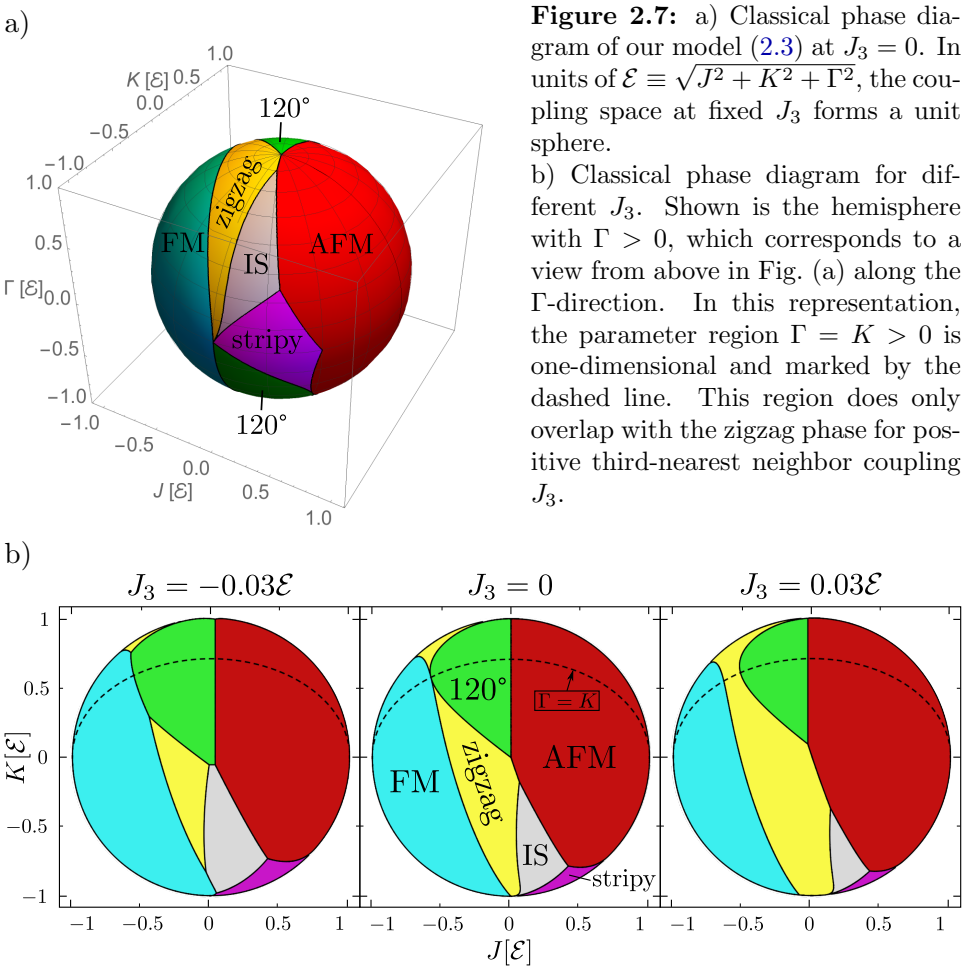

Figure 2.7: a) Classical phase diagram of our model (2.3) at $J_3 = 0$. In units of $\mathcal{E} \equiv \sqrt{J^2 + K^2 + \Gamma^2}$, the coupling space at fixed J_3 forms a unit sphere.
b) Classical phase diagram for different J_3. Shown is the hemisphere with $\Gamma > 0$, which corresponds to a view from above in Fig. (a) along the Γ-direction. In this representation, the parameter region $\Gamma = K > 0$ is one-dimensional and marked by the dashed line. This region does only overlap with the zigzag phase for positive third-nearest neighbor coupling J_3.

zigzag state, since this is the experimentally relevant phase [29]. We begin by choosing a local spin basis which is adapted to the zigzag phase in Sec. 2.5.1. Then, in Sec. 2.5.2, we apply the Holstein-Primakoff transformation [62] to the spin operators and expand the resulting bosonic Hamiltonian for low bosonic excitation numbers, a procedure often referred to as $1/S$ expansion. Finally, we perform a Fourier transformation from the real space to the crystal momentum representation in Sec. 2.5.3.

2.5.1 Local spin basis

In order to perform the spin wave expansion, we first need to choose a local right handed orthonormal basis $\{\boldsymbol{t}_i^x, \boldsymbol{t}_i^y, \boldsymbol{m}_i\}$ for each site i to express the components of the spin operators as

$$\boldsymbol{S}_i = S_i^{t_x} \boldsymbol{t}_i^x + S_i^{t_y} \boldsymbol{t}_i^y + S_i^{\parallel} \boldsymbol{m}_i \,. \tag{2.46}$$

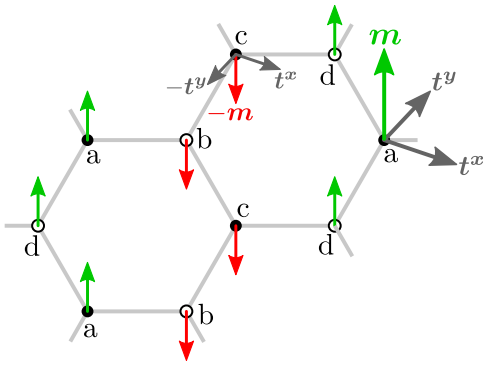

Figure 2.8: A local orthonormal right handed spin basis is chosen for each lattice site. On sublattices a and d the basis is given by $\{\boldsymbol{t}^x, \boldsymbol{t}^y, \boldsymbol{m}\}$ and on sublattices b and c by $\{\boldsymbol{t}^x, -\boldsymbol{t}^y, -\boldsymbol{m}\}$. While there is a rotational freedom in the choice of the transversal basis $\{\boldsymbol{t}^x, \boldsymbol{t}^y\}$, the third basis vector $\boldsymbol{m}$ must point along the classical magnetization in the zigzag phase.

Here, $\boldsymbol{m}_i$ must be aligned with the classical magnetization in the zigzag phase and $\boldsymbol{t}^{x,y}$ are transversal. A possible choice is

$$\boldsymbol{t}_i^x = \boldsymbol{t}^x, \quad \boldsymbol{t}_i^y = \boldsymbol{t}^y, \quad \boldsymbol{m}_i = \boldsymbol{m} \qquad \text{for } i \text{ on sublattices a, d ;} \tag{2.47a}$$

$$\boldsymbol{t}_j^x = \boldsymbol{t}^x, \quad \boldsymbol{t}_j^y = -\boldsymbol{t}^y, \quad \boldsymbol{m}_j = -\boldsymbol{m} \qquad \text{for } j \text{ on sublattices b, c ;} \tag{2.47b}$$

as shown in Fig. 2.8. We leave the explicit form of the global basis $\{\boldsymbol{t}^x, \boldsymbol{t}^y, \boldsymbol{m}\}$ open for now. The spin operators (2.46) can be expressed in terms of the ladder operators $S_i^{\pm} = S_i^{t_x} \pm i S_i^{t_y}$ as

$$\boldsymbol{S}_i = S_i^+ \boldsymbol{t}_i^- + S_i^- \boldsymbol{t}_i^+ + S_i^{\parallel} \boldsymbol{m}_i \,, \tag{2.48}$$

with the complex transversal basis vectors

$$\boldsymbol{t}_i^{\pm} = \boldsymbol{t}_i^x \pm i \boldsymbol{t}_i^y \,. \tag{2.49}$$

Using the relations of the local basis vectors (2.47) we can write

$$\boldsymbol{S}_i = \frac{1}{2}\left(S_i^+ \boldsymbol{t}^- + S_i^- \boldsymbol{t}^+\right) + S_i^{\parallel} \boldsymbol{m} \qquad \text{for } i \text{ on sublattices a, d ,} \tag{2.50a}$$

$$\boldsymbol{S}_j = \frac{1}{2}\left(S_j^+ \boldsymbol{t}^+ + S_j^- \boldsymbol{t}^-\right) - S_j^{\parallel} \boldsymbol{m} \qquad \text{for } j \text{ on sublattices b, c ,} \tag{2.50b}$$

where we defined

$$\boldsymbol{t}^{\pm} = \boldsymbol{t}^x \pm i \boldsymbol{t}^y \,. \tag{2.51}$$

Next, we want to substitute the spin operators (2.50) in the Hamiltonian (2.16) of the KHΓ model. The lattice sum in the Hamiltonian extends over the sublattice A of the honeycomb lattice. In order to account for the enlarged unit cell of the zigzag phase, we split the sum into two sums, one over sublattice a and one over sublattice c, which gives

$$\begin{aligned} H = &\sum_{i \in \mathrm{a}} \sum_{\alpha} \boldsymbol{S}_i \cdot \left(\boldsymbol{W}^{\alpha}\, \boldsymbol{S}_{i+\alpha} + J_3\, \boldsymbol{S}_{i-2\alpha}\right) \\ &+ \sum_{i \in \mathrm{c}} \sum_{\alpha} \boldsymbol{S}_i \cdot \left(\boldsymbol{W}^{\alpha}\, \boldsymbol{S}_{i+\alpha} + J_3\, \boldsymbol{S}_{i-2\alpha}\right) \,. \end{aligned} \tag{2.52}$$

Recalling that α iterates over the bonds x, y, z and $i+\alpha$ denotes the lattice site at $\boldsymbol{R}_i + \boldsymbol{d}_\alpha$, all spin operators in the Hamiltonian (2.52) can be associated with one of the sublattices a, b, c or d with the help of Fig. 2.8. The representation (2.50) of the spin operators in the global spin basis $\{\boldsymbol{t}^+, \boldsymbol{t}^-, \boldsymbol{m}\}$ can then be substituted, giving

$$\begin{aligned}
H = &\sum_{i\in\mathrm{a}} \left(\frac{1}{2}S_i^+\boldsymbol{t}^- + \frac{1}{2}S_i^-\boldsymbol{t}^+ + S_i^{\parallel}\boldsymbol{m}\right) \\
&\qquad \cdot \Bigg[\boldsymbol{W}^x\left(\frac{1}{2}S_{i+x}^+\boldsymbol{t}^- + \frac{1}{2}S_{i+x}^-\boldsymbol{t}^+ + S_{i+x}^{\parallel}\boldsymbol{m}\right) \\
&\qquad\quad + \boldsymbol{W}^y\left(\frac{1}{2}S_{i+y}^+\boldsymbol{t}^- + \frac{1}{2}S_{i+y}^-\boldsymbol{t}^+ + S_{i+x}^{\parallel}\boldsymbol{m}\right) \\
&\qquad\quad + \boldsymbol{W}^z\left(\frac{1}{2}S_{i+z}^+\boldsymbol{t}^+ + \frac{1}{2}S_{i+z}^-\boldsymbol{t}^- - S_{i+z}^{\parallel}\boldsymbol{m}\right) \\
&\qquad + J_3\sum_\alpha\left(\frac{1}{2}S_{i-2\alpha}^+\boldsymbol{t}^+ + \frac{1}{2}S_{i-2\alpha}^-\boldsymbol{t}^- - S_{i-2\alpha}^{\parallel}\boldsymbol{m}\right)\Bigg] \\
&+ \sum_{i\in\mathrm{c}}\left(\frac{1}{2}S_i^+\boldsymbol{t}^+ + \frac{1}{2}S_i^-\boldsymbol{t}^- - S_i^{\parallel}\boldsymbol{m}\right) \\
&\qquad \cdot \Bigg[\boldsymbol{W}^x\left(\frac{1}{2}S_{i+x}^+\boldsymbol{t}^+ + \frac{1}{2}S_{i+x}^-\boldsymbol{t}^- - S_{i+x}^{\parallel}\boldsymbol{m}\right) \\
&\qquad\quad + \boldsymbol{W}^y\left(\frac{1}{2}S_{i+y}^+\boldsymbol{t}^+ + \frac{1}{2}S_{i+y}^-\boldsymbol{t}^- - S_{i+x}^{\parallel}\boldsymbol{m}\right) \\
&\qquad\quad + \boldsymbol{W}^z\left(\frac{1}{2}S_{i+z}^+\boldsymbol{t}^- + \frac{1}{2}S_{i+z}^-\boldsymbol{t}^+ + S_{i+z}^{\parallel}\boldsymbol{m}\right) \\
&\qquad + J_3\sum_\alpha\left(\frac{1}{2}S_{i-2\alpha}^+\boldsymbol{t}^- + \frac{1}{2}S_{i-2\alpha}^-\boldsymbol{t}^+ + S_{i-2\alpha}^{\parallel}\boldsymbol{m}\right)\Bigg] .
\end{aligned} \tag{2.53}$$

2.5.2 Holstein-Primakoff transformation and $1/S$ expansion

Next, the local spin operators $S_i^+, S_i^-, S_i^{\parallel}$ are mapped to boson operators $b_i, b_i^\dagger$ by the Holstein-Primakoff transformation [62],

$$S_i^+ = \sqrt{2S}\left(\sqrt{1 - \frac{n_i}{2S}}\right) b_i \,, \tag{2.54a}$$

$$S_i^- = b_i^\dagger\sqrt{2S}\sqrt{1 - \frac{n_i}{2S}} \,, \tag{2.54b}$$

$$S_i^{\parallel} = S - n_i \,, \tag{2.54c}$$

where S is the total spin and $n_i = b_i^\dagger b_i$ is the occupation number operator. The Holstein-Primakoff transformation produces the correct spin-commutation relations, however the bosons can have arbitrarily high occupation number while the Hilbert space of the spins is finite. Therefore,

the mapping must be supplemented with a restriction of the bosonic occupation numbers to match the number of spin eigenstates, i.e. only such Fock states are allowed where all excitation numbers are lesser than $(2S+1)$.

In magnetically ordered phases, the Holstein-Primakoff bosons have a clear interpretation: the ground state is the eigenstate where the eigenvalue of $S_i^{\parallel}$ at each site is S. According to the transformation (2.54c) this corresponds to zero bosonic occupation. Creation of a boson at site i corresponds by Eq. (2.54a) to a reduction of the parallel spin component at site i. It becomes clear that the bosons are directly related to the magnetic excitations from the ground state.

At this point, the Holstein-Primakoff transformation may seem unnecessary, as one could describe the excitations at each site by the original spin operators just as well. The bosonic representation is however much more useful after Fourier transformation. Fourier transformed bosons are again bosons with a fixed crystal momentum, but Fourier transformed spin operators have complicated commutation relations which mix different crystal momenta, $[S^{\alpha}_{\boldsymbol{k}}, S^{\beta}_{\boldsymbol{k'}}] \propto i\epsilon_{\alpha\beta\gamma} S^{\gamma}_{\boldsymbol{k}+\boldsymbol{k'}}$.

At sufficiently low temperature, larger deviations from the ground state become rare and hence the bosonic occupation numbers n_i have small expectation values. It is then justified to expand the square roots in the Holstein-Primakoff transformation (2.54) as

$$S_i^{+} = \sqrt{2S}\left[1 - \frac{n_i}{4S} - \frac{n_i^2}{32S^2} + \mathcal{O}\left(\frac{n_i^3}{S^3}\right)\right] b_i \,, \tag{2.55a}$$

$$S_i^{-} = b_i^{\dagger}\sqrt{2S}\left[1 - \frac{n_i}{4S} - \frac{n_i^2}{32S^2} + \mathcal{O}\left(\frac{n_i^3}{S^3}\right)\right] \,, \tag{2.55b}$$

$$S_i^{\parallel} = S - n_i \,. \tag{2.55c}$$

This expansion is commonly referred to as the $1/S$ expansion, as the factor $1/S$ can be used to count the orders of the expansion. Note however that $1/S$ is not the small parameter of the expansion, as for instance $1/S = 2$ in the KHΓ model. Nevertheless, each factor of $1/S$ is accompanied by a number operator n_i. Hence, if the quantum state of the system is predominantly composed of low energy states as it is typically the case at low temperatures, the occupation numbers will be small and the expansion will be accurate.

Next, we explicitly apply the $1/S$ expansion to the Hamiltonian (2.53) order by order. We order the terms by number of bosonic operators, which corresponds to orders of $1/\sqrt{S}$. Terms with no boson operators can only result from $S_i^{\parallel}$. Collecting all pure $S_i^{\parallel}$ terms of the Hamiltonian (2.53) and substituting the expansion (2.55c) then yields the constant part of the

Hamiltonian,

$$\begin{aligned} H_0 =& \sum_{i\in \mathrm{a}} S\boldsymbol{m}\cdot(\boldsymbol{W}^x+\boldsymbol{W}^y-\boldsymbol{W}^z-3J_3)\,S\boldsymbol{m} \\ &+\sum_{i\in \mathrm{c}} (-S\boldsymbol{m})\cdot(-\boldsymbol{W}^x-\boldsymbol{W}^y+\boldsymbol{W}^z+3J_3)\,S\boldsymbol{m} \\ =& -\frac{NS^2}{2}\boldsymbol{m}\cdot(-\boldsymbol{W}^x-\boldsymbol{W}^y+\boldsymbol{W}^z+3J_3)\,\boldsymbol{m}\ . \end{aligned}$$

Referring to the discussion of the classical zigzag ground state in section 2.4, we note that this coincides with the classical ground state energy given in Eq. (2.30). Because the magnetization vector $\boldsymbol{m}$ is the eigenvector with largest positive eigenvalue $\lambda^{\mathrm{zigzag}}$, we can write

$$H_0 = -\frac{NS^2}{2}\lambda^{\mathrm{zigzag}}\ , \tag{2.56}$$

which is consistent with Eq. (2.32).

Terms with one bosonic operator can result from the combination of one $S_i^{\parallel}$ with one $S_i^{\pm}$. Collecting these terms from the full Hamiltonian (2.53) results in

$$\begin{aligned} H_1 =& \frac{S\sqrt{2S}}{2}\sum_{i\in \mathrm{a}} \boldsymbol{t}^-\cdot(\boldsymbol{W}^x+\boldsymbol{W}^y-\boldsymbol{W}^z-3J_3)\,\boldsymbol{m}\,b_i \\ &-\frac{S\sqrt{2S}}{2}\sum_{i\in \mathrm{b}} \boldsymbol{t}^-\cdot(\boldsymbol{W}^x+\boldsymbol{W}^y-\boldsymbol{W}^z-3J_3)\,\boldsymbol{m}\,b_i^\dagger \\ &-\frac{S\sqrt{2S}}{2}\sum_{i\in \mathrm{c}} \boldsymbol{t}^-\cdot(\boldsymbol{W}^x+\boldsymbol{W}^y-\boldsymbol{W}^z-3J_3)\,\boldsymbol{m}\,b_i^\dagger \\ &+\frac{S\sqrt{2S}}{2}\sum_{i\in \mathrm{d}} \boldsymbol{t}^-\cdot(\boldsymbol{W}^x+\boldsymbol{W}^y-\boldsymbol{W}^z-3J_3)\,\boldsymbol{m}\,b_i \ + \ \mathrm{h.c.} \\ =& 0\ , \end{aligned} \tag{2.57}$$

where h.c. stands for the hermitian conjugate of all preceding expressions. Note that all terms vanish because $\boldsymbol{m}$ is an eigenvector of the matrix in parenthesis and $\boldsymbol{t}^-\cdot\boldsymbol{m}=0$. This result is a necessary condition for the stability of the zigzag state: single creation and annihilation operators would act as sources and sinks for magnetic excitations and the bosonic vacuum, which is the zigzag state, would no longer be an eigenstate of the Hamiltonian.

The first nontrivial order in the $1/S$ expansion has two bosonic operators. These terms are produced by combinations of the form $S_i^{\parallel}\cdot S_j^{\parallel}$ and $S_i^{\pm}\cdot S_j^{\pm}$.

Collecting these terms from the Hamiltonian (2.53) results in

$$\begin{aligned} H_2 = -S\lambda^{\text{zigzag}} \sum_i n_i + \frac{S}{2}\Bigg\{ & W^x_{-+} \left(\sum_{i\in \text{a}} b_i b^\dagger_{i+x} + \sum_{i\in \text{c}} b^\dagger_i b_{i+x} \right) \\ & + W^y_{-+} \left(\sum_{i\in \text{a}} b_i b^\dagger_{i+y} + \sum_{i\in \text{c}} b^\dagger_i b_{i+y} \right) \\ & + W^z_{-+} \left(\sum_{i\in \text{a}} b_i b_{i+z} + \sum_{i\in \text{c}} b^\dagger_i b^\dagger_{i+z} \right) \\ & + W^x_{--} \left(\sum_{i\in \text{a}} b_i b_{i+x} + \sum_{i\in \text{c}} b^\dagger_i b^\dagger_{i+x} \right) \\ & + W^y_{--} \left(\sum_{i\in \text{a}} b_i b_{i+y} + \sum_{i\in \text{c}} b^\dagger_i b^\dagger_{i+y} \right) \\ & + W^z_{--} \left(\sum_{i\in \text{a}} b^\dagger_i b_{i+z} + \sum_{i\in \text{c}} b^\dagger_i b_{i+z} \right) \\ & + 2J_3 \sum_\alpha \left(\sum_{i\in \text{a}} b_i b_{i-2\alpha} + \sum_{i\in \text{c}} b_i b_{i-2\alpha} \right) + \text{h.c.} \Bigg\} , \end{aligned} \tag{2.58}$$

where we defined the interaction matrix elements

$$W^\alpha_{\sigma\,\sigma'} \equiv \boldsymbol{t}^\sigma \cdot \boldsymbol{W}^\alpha \, \boldsymbol{t}^{\sigma'} , \tag{2.59}$$

where the matrices $\boldsymbol{W}^\alpha$ are given in Eq. (2.17) and σ and σ' can both take the values $+$ or $-$. Note that $W^\alpha_{+-} = (W^\alpha_{-+})^*$ and $W^\alpha_{++} = (W^\alpha_{--})^*$.

Terms with three or more boson operators describe interactions and are needed to calculate the magnon lifetime. We only consider the lowest order of nontrivial interaction terms, which in our case are term with three boson operators. These terms are generated by combinations with one $S^{\|}$ and one

$S^{\pm}$. Collecting these terms gives

$$\begin{aligned} H_3 = \sqrt{\frac{S}{2}}\Bigg\{ & W^x_{m+}\left(-\sum_{i\in\mathrm{a}} n_i b^\dagger_{i+x} + \sum_{i\in\mathrm{c}} n_i b_{i+x}\right) \\ & + W^y_{m+}\left(-\sum_{i\in\mathrm{a}} n_i b^\dagger_{i+y} + \sum_{i\in\mathrm{c}} n_i b_{i+y}\right) \\ & + W^z_{m+}\left(-\sum_{i\in\mathrm{a}} n_i b_{i+z} + \sum_{i\in\mathrm{c}} n_i b^\dagger_{i+z}\right) \\ & + W^x_{-m}\left(-\sum_{i\in\mathrm{a}} b_i n_{i+x} + \sum_{i\in\mathrm{c}} b^\dagger_i n_{i+x}\right) \\ & + W^y_{-m}\left(-\sum_{i\in\mathrm{a}} b_i n_{i+y} + \sum_{i\in\mathrm{c}} b^\dagger_i n_{i+y}\right) \\ & + W^z_{-m}\left(\sum_{i\in\mathrm{a}} b_i n_{i+z} - \sum_{i\in\mathrm{c}} b^\dagger_i n_{i+z}\right) + \mathrm{h.c.}\Bigg\}\,, \end{aligned} \tag{2.60}$$

where we defined the interaction matrix elements

$$W^\alpha_{m\,\sigma} \equiv \boldsymbol{m}\cdot\boldsymbol{W}^\alpha\,\boldsymbol{t}^\sigma\,, \tag{2.61a}$$
$$W^\alpha_{\sigma\,m} \equiv \boldsymbol{t}^\sigma\cdot\boldsymbol{W}^\alpha\,\boldsymbol{m}\,. \tag{2.61b}$$

Note that $W^\alpha_{m\sigma} = W^\alpha_{\sigma m}$ and $W^\alpha_{m+} = (W^\alpha_{m-})^*$ because the matrices $\boldsymbol{W}^\alpha$ given in Eq. (2.17) are symmetric and real.

2.5.3 Fourier transformation

We define the Fourier transformation of the bosonic annihilation operators as

$$b_i = \sqrt{\frac{4}{N}}\sum_{\boldsymbol{k}} e^{i\boldsymbol{k}\cdot\boldsymbol{R}_i} \times \begin{cases} a_{\boldsymbol{k}} & \text{if } \boldsymbol{R}_i \in \mathrm{a} \\ b_{\boldsymbol{k}} & \boldsymbol{R}_i \in \mathrm{b} \\ c_{\boldsymbol{k}} & \boldsymbol{R}_i \in \mathrm{c} \\ d_{\boldsymbol{k}} & \boldsymbol{R}_i \in \mathrm{d} \end{cases} \tag{2.62}$$

where $\boldsymbol{R}_i$ is the position vector of lattice site i and the coordinate origin is chosen such that it coincides with a site of sublattice a. The sum over the crystal momenta $\boldsymbol{k}$ iterates over the first Brillouin zone of the zigzag lattice. Note that the operators $b_{\boldsymbol{k}}, c_{\boldsymbol{k}}, d_{\boldsymbol{k}}$ are not periodic with respect to the first Brillouin zone. This is because in the exponential of the Fourier transformation, we chose the actual position vector of the lattice site $\boldsymbol{R}_i$. The more conventional choice would be the basis vector of the unit cell. Calling these basis vectors $\tilde{\boldsymbol{R}}_i$, the position vectors are related to the basis

vectors as

$$\boldsymbol{R}_i = \begin{cases} \tilde{\boldsymbol{R}}_{\boldsymbol{i}} & \text{if } i \in \text{a} \\ \tilde{\boldsymbol{R}}_{\boldsymbol{i}} + \boldsymbol{d_z} & i \in \text{b} \\ \tilde{\boldsymbol{R}}_{\boldsymbol{i}} + \boldsymbol{a}_1 & i \in \text{c} \\ \tilde{\boldsymbol{R}}_{\boldsymbol{i}} + \boldsymbol{d}_x & i \in \text{d} \end{cases} , \tag{2.63}$$

as can be seen from Fig. 2.8. The Fourier transformation of b_i on sublattice b for instance can be written as

$$b_i = \sqrt{\frac{4}{N}} \sum_{\boldsymbol{k}} e^{i\boldsymbol{k}\cdot\boldsymbol{R}_i} b_{\boldsymbol{k}} = \sqrt{\frac{4}{N}} \sum_{\boldsymbol{k}} e^{i\boldsymbol{k}\cdot\tilde{\boldsymbol{R}}_i} e^{i\boldsymbol{k}\cdot\boldsymbol{d}_z} b_{\boldsymbol{k}} , \tag{2.64}$$

which has the inverse Fourier transform

$$e^{i\boldsymbol{k}\cdot\boldsymbol{d}_z} b_{\boldsymbol{k}} = \sqrt{\frac{4}{N}} \sum_{i\in\text{b}} e^{-i\boldsymbol{k}\cdot\tilde{\boldsymbol{R}}_i} b_i \quad \Leftrightarrow \quad b_{\boldsymbol{k}} = \sqrt{\frac{4}{N}} e^{i\boldsymbol{k}\cdot\boldsymbol{d}_z} \sum_{i\in\text{b}} e^{-i\boldsymbol{k}\cdot\tilde{\boldsymbol{R}}_i} b_i . \tag{2.65}$$

Consider a shift by a reciprocal lattice vector $\boldsymbol{G}$, i.e. $b_{\boldsymbol{k}+\boldsymbol{G}}$. We have $\boldsymbol{G}\cdot\tilde{\boldsymbol{R}}_i = 0$, but the term $\boldsymbol{G}\cdot\boldsymbol{d}_z$ does not vanish. Hence, $b_{\boldsymbol{k}}$ acquires a phase factor upon shifting its momentum by a reciprocal lattice vector. As we will see later, these phase factors become important when considering umklapp scattering. Analogous relations hold for the other sublattices and we get

$$a_{\boldsymbol{k}+\boldsymbol{G}} = a_{\boldsymbol{k}} , \tag{2.66a}$$
$$b_{\boldsymbol{k}+\boldsymbol{G}} = e^{i\boldsymbol{G}\cdot\boldsymbol{d}_z} b_{\boldsymbol{k}} , \tag{2.66b}$$
$$c_{\boldsymbol{k}+\boldsymbol{G}} = e^{i\boldsymbol{G}\cdot\boldsymbol{a}_1} c_{\boldsymbol{k}} , \tag{2.66c}$$
$$d_{\boldsymbol{k}+\boldsymbol{G}} = e^{i\boldsymbol{G}\cdot\boldsymbol{d}_x} d_{\boldsymbol{k}} . \tag{2.66d}$$

At first sight, this non-periodic choice of Fourier transformation seems to make the calculations more complicated. It does however simplify the analytical expressions that appear in the special case $\Gamma = K > 0$ that we will consider later.

We proceed by transforming H_2 given in Eq. (2.58) term by term. We begin with the sum over the number operators,

$$\sum_i n_i = \left(\sum_{i\in\text{a}} + \sum_{i\in\text{b}} + \sum_{i\in\text{c}} + \sum_{i\in\text{d}} \right) b_i^\dagger b_i . \tag{2.67}$$

On sublattice a, this is straightforward to transform,

$$\begin{aligned}\sum_{i\in\mathrm{a}} b_i^\dagger b_i =& \sum_{i\in\mathrm{a}} \frac{4}{N} \sum_{\boldsymbol{k}} e^{-i\boldsymbol{k}\cdot\boldsymbol{R}_i} a_{\boldsymbol{k}}^\dagger \sum_{\boldsymbol{k'}} e^{i\boldsymbol{k'}\cdot\boldsymbol{R}_i} a_{\boldsymbol{k'}} \\ =& \frac{4}{N} \sum_{\boldsymbol{k},\boldsymbol{k'}} a_{\boldsymbol{k}}^\dagger a_{\boldsymbol{k'}} \sum_{i\in\mathrm{a}} e^{i(\boldsymbol{k'}-\boldsymbol{k})\cdot\boldsymbol{R}_i} \\ =& \frac{4}{N} \sum_{\boldsymbol{k},\boldsymbol{k'}} a_{\boldsymbol{k}}^\dagger a_{\boldsymbol{k'}} \frac{N}{4} \delta_{\boldsymbol{k},\boldsymbol{k'}} \\ =& \sum_{\boldsymbol{k}} n_{\mathrm{a},\boldsymbol{k}} \ , \end{aligned} \tag{2.68}$$

where we defined $n_{\mathrm{a},\boldsymbol{k}} = a_{\boldsymbol{k}}^\dagger a_{\boldsymbol{k}}$. Before transforming the sum over sublattice b, we note that the position vectors of sublattice b can be obtained by translating sublattice a by the vector $\boldsymbol{d}_z$, see Fig. 2.8. This leads to

$$\begin{aligned}\sum_{i\in\mathrm{b}} b_i^\dagger b_i =& \sum_{i\in\mathrm{b}} \frac{4}{N} \sum_{\boldsymbol{k}} e^{-i\boldsymbol{k}\cdot\boldsymbol{R}_i} b_{\boldsymbol{k}}^\dagger \sum_{\boldsymbol{k'}} e^{i\boldsymbol{k'}\cdot\boldsymbol{R}_i} b_{\boldsymbol{k'}} \\ =& \sum_{i\in\mathrm{a}} \frac{4}{N} \sum_{\boldsymbol{k}} e^{-i\boldsymbol{k}\cdot(\boldsymbol{R}_i+\boldsymbol{d}_z)} b_{\boldsymbol{k}}^\dagger \sum_{\boldsymbol{k'}} e^{i\boldsymbol{k'}\cdot(\boldsymbol{R}_i+\boldsymbol{d}_z)} b_{\boldsymbol{k'}} \\ =& \frac{4}{N} \sum_{\boldsymbol{k},\boldsymbol{k'}} b_{\boldsymbol{k}}^\dagger b_{\boldsymbol{k'}} \ e^{i(\boldsymbol{k'}-\boldsymbol{k})\cdot\boldsymbol{d}_z} \sum_{i\in\mathrm{a}} e^{i(\boldsymbol{k'}-\boldsymbol{k})\cdot\boldsymbol{R}_i} \\ =& \frac{4}{N} \sum_{\boldsymbol{k},\boldsymbol{k'}} b_{\boldsymbol{k}}^\dagger b_{\boldsymbol{k'}} \ e^{i(\boldsymbol{k'}-\boldsymbol{k})\cdot\boldsymbol{d}_z} \frac{N}{4} \delta_{\boldsymbol{k},\boldsymbol{k'}} \\ =& \sum_{\boldsymbol{k}} n_{\mathrm{b},\boldsymbol{k}} \ . \end{aligned} \tag{2.69}$$

The remaining number operators are transformed similarly, yielding

$$\sum_i n_i = \sum_{\boldsymbol{k}} \left(n_{\mathrm{a},\boldsymbol{k}} + n_{\mathrm{b},\boldsymbol{k}} + n_{\mathrm{c},\boldsymbol{k}} + n_{\mathrm{d},\boldsymbol{k}} \right) \ . \tag{2.70}$$

The remaining terms in H_2 mix bosonic operators from different sublattices. This introduces momentum dependent phase factors, as we show exemplarily for

$$\begin{aligned}\sum_{i\in\mathrm{a}} b_i b_{i+x}^\dagger =& \sum_{i\in\mathrm{a}} \frac{4}{N} \sum_{\boldsymbol{k}} e^{i\boldsymbol{k}\cdot\boldsymbol{R}_i} a_{\boldsymbol{k}} \sum_{\boldsymbol{k'}} e^{-i\boldsymbol{k'}\cdot(\boldsymbol{R}_i+\boldsymbol{d}_x)} d_{\boldsymbol{k'}}^\dagger \\ =& \frac{4}{N} \sum_{\boldsymbol{k},\boldsymbol{k'}} a_{\boldsymbol{k}} d_{\boldsymbol{k'}}^\dagger \ e^{-i\boldsymbol{k'}\cdot\boldsymbol{d}_x} \sum_{i\in\mathrm{a}} e^{i(\boldsymbol{k}-\boldsymbol{k'})\cdot\boldsymbol{R}_i} \\ =& \sum_{\boldsymbol{k}} a_{\boldsymbol{k}} d_{\boldsymbol{k}}^\dagger \ e^{-i\boldsymbol{k}\cdot\boldsymbol{d}_x} \ . \end{aligned} \tag{2.71}$$

In the first line we used the fact that the lattice site $i+x$ belongs to sublattice d if i belongs to sublattice a. The remaining terms of H_2 are transformed similarly, with the result

$$\begin{aligned}
H_2 = &- S\lambda^{\text{zigzag}} \sum_{\boldsymbol{k}} \left(n_{\text{a},\boldsymbol{k}} + n_{\text{b},\boldsymbol{k}} + n_{\text{c},\boldsymbol{k}} + n_{\text{d},\boldsymbol{k}}\right) \\
&+ \frac{S}{2} \sum_{\boldsymbol{k}} \Bigg\{ \left(W^x_{-+} e^{-i\boldsymbol{k}\cdot\boldsymbol{d}_x} + W^y_{-+} e^{-i\boldsymbol{k}\cdot\boldsymbol{d}_y}\right) a_{\boldsymbol{k}} d^\dagger_{\boldsymbol{k}} \\
&\qquad + \left(W^x_{-+} e^{i\boldsymbol{k}\cdot\boldsymbol{d}_x} + W^y_{-+} e^{i\boldsymbol{k}\cdot\boldsymbol{d}_y}\right) c^\dagger_{\boldsymbol{k}} b_{\boldsymbol{k}} \\
&\qquad + W^z_{--} e^{-i\boldsymbol{k}\cdot\boldsymbol{d}_z} a_{\boldsymbol{k}} b^\dagger_{\boldsymbol{k}} \\
&\qquad + W^z_{--} e^{i\boldsymbol{k}\cdot\boldsymbol{d}_z} c^\dagger_{\boldsymbol{k}} d_{\boldsymbol{k}} \\
&\qquad + \left(W^z_{-+} e^{i\boldsymbol{k}\cdot\boldsymbol{d}_z} + 2J_3 \sum_\alpha e^{-2i\boldsymbol{k}\cdot\boldsymbol{d}_\alpha}\right) a_{-\boldsymbol{k}} b_{\boldsymbol{k}} \\
&\qquad + \left(W^z_{-+} e^{-i\boldsymbol{k}\cdot\boldsymbol{d}_z} + 2J_3 \sum_\alpha e^{2i\boldsymbol{k}\cdot\boldsymbol{d}_\alpha}\right) c^\dagger_{-\boldsymbol{k}} d^\dagger_{\boldsymbol{k}} \\
&\qquad + \left(W^x_{--} e^{i\boldsymbol{k}\cdot\boldsymbol{d}_x} + W^y_{--} e^{i\boldsymbol{k}\cdot\boldsymbol{d}_y}\right) a_{-\boldsymbol{k}} d_{\boldsymbol{k}} \\
&\qquad + \left(W^x_{--} e^{-i\boldsymbol{k}\cdot\boldsymbol{d}_x} + W^y_{--} e^{-i\boldsymbol{k}\cdot\boldsymbol{d}_y}\right) c^\dagger_{-\boldsymbol{k}} b^\dagger_{\boldsymbol{k}} + \text{h.c.} \Bigg\} . \qquad (2.72)
\end{aligned}$$

It is convenient to write this expression in matrix form as

$$H_2 = \sum_{\boldsymbol{k}} \sum_{m,n} \left\{ A^{mn}_{\boldsymbol{k}}\ a^\dagger_{\boldsymbol{k}m} a_{\boldsymbol{k}n} + \frac{1}{2} \left[B^{mn}_{\boldsymbol{k}}\ a^\dagger_{\boldsymbol{k}m} a^\dagger_{-\boldsymbol{k}n} + (B^{nm}_{\boldsymbol{k}})^*\ a_{-\boldsymbol{k}m} a_{\boldsymbol{k}n} \right] \right\} , \qquad (2.73)$$

where we now distinguish the sublattices by a subscript index $m, n = 1, 2, 3, 4$ such that the annihilation operators are given by $a_{\boldsymbol{k}1} = a_{\boldsymbol{k}}$, $a_{\boldsymbol{k}2} = b_{\boldsymbol{k}}$, $a_{\boldsymbol{k}3} = c_{\boldsymbol{k}}$, $a_{\boldsymbol{k}4} = d_{\boldsymbol{k}}$, and equivalently for the creation operators. $A^{mn}_{\boldsymbol{k}}$ and $B^{mn}_{\boldsymbol{k}}$ are the sublattice components of the 4×4 matrices

$$\boldsymbol{A}_{\boldsymbol{k}} = \left(\begin{array}{cc|cc} \lambda & \beta_{\boldsymbol{k}} & 0 & \alpha_{\boldsymbol{k}} \\ \beta^*_{\boldsymbol{k}} & \lambda & \alpha^*_{\boldsymbol{k}} & 0 \\ \hline 0 & \alpha_{\boldsymbol{k}} & \lambda & \beta^*_{-\boldsymbol{k}} \\ \alpha^*_{\boldsymbol{k}} & 0 & \beta_{-\boldsymbol{k}} & \lambda \end{array}\right) , \qquad (2.74a)$$

$$\boldsymbol{B}_{\boldsymbol{k}} = \left(\begin{array}{cc|cc} 0 & \mu_{\boldsymbol{k}} & 0 & \nu_{\boldsymbol{k}} \\ \mu_{-\boldsymbol{k}} & 0 & \nu^*_{\boldsymbol{k}} & 0 \\ \hline 0 & \nu^*_{-\boldsymbol{k}} & 0 & \mu_{\boldsymbol{k}} \\ \nu_{-\boldsymbol{k}} & 0 & \mu_{-\boldsymbol{k}} & 0 \end{array}\right) , \qquad (2.74b)$$

with

$$\lambda = -S\lambda^{\text{zigzag}} , \tag{2.75a}$$
$$\alpha_{\boldsymbol{k}} = S\,W^{x}_{+-}e^{i\boldsymbol{k}\cdot\boldsymbol{d}_x} + S\,W^{y}_{+-}e^{i\boldsymbol{k}\cdot\boldsymbol{d}_y} , \tag{2.75b}$$
$$\beta_{\boldsymbol{k}} = S\,W^{z}_{++}e^{i\boldsymbol{k}\cdot\boldsymbol{d}_z} , \tag{2.75c}$$
$$\mu_{\boldsymbol{k}} = S\,W^{z}_{+-}e^{i\boldsymbol{k}\cdot\boldsymbol{d}_z} + 2\,SJ_3\sum_{\alpha} e^{-2i\boldsymbol{k}\cdot\boldsymbol{d}_\alpha} , \tag{2.75d}$$
$$\nu_{\boldsymbol{k}} = S\,W^{x}_{++}e^{i\boldsymbol{k}\cdot\boldsymbol{d}_x} + S\,W^{y}_{++}e^{i\boldsymbol{k}\cdot\boldsymbol{d}_y} , \tag{2.75e}$$

where we used the relations $W^{\alpha}_{+-} = (W^{\alpha}_{-+})^*$ and $W^{\alpha}_{++} = (W^{\alpha}_{--})^*$.

The Fourier transformation of H_3 given in Eq. (2.60) involves terms of the form

$$\begin{aligned}\sum_{i\in\mathrm{a}} n_i b^{\dagger}_{i+x} &= \sum_{i\in\mathrm{a}}\left(\frac{4}{N}\right)^{\frac{3}{2}}\sum_{\boldsymbol{k}} e^{-i\boldsymbol{k}\cdot\boldsymbol{R}_i}\; a^{\dagger}_{\boldsymbol{k}}\sum_{\boldsymbol{k'}} e^{i\boldsymbol{k'}\cdot\boldsymbol{R}_i}\; a_{\boldsymbol{k'}}\sum_{\boldsymbol{k''}} e^{-i\boldsymbol{k''}\cdot(\boldsymbol{R}_i+\boldsymbol{d}_x)}\; d^{\dagger}_{\boldsymbol{k''}} \\ &= \left(\frac{4}{N}\right)^{\frac{3}{2}}\sum_{\boldsymbol{k},\boldsymbol{k'},\boldsymbol{k''}} a^{\dagger}_{\boldsymbol{k}}\; a_{\boldsymbol{k'}}\; d^{\dagger}_{\boldsymbol{k''}}\; e^{-i\boldsymbol{k''}\cdot\boldsymbol{d}_x}\sum_{i\in\mathrm{a}} e^{i(-\boldsymbol{k}+\boldsymbol{k'}-\boldsymbol{k''})\cdot\boldsymbol{R}_i} .\end{aligned} \tag{2.76}$$

The last sum evaluates to one in all cases where $(-\boldsymbol{k}+\boldsymbol{k'}-\boldsymbol{k''})$ equals a reciprocal lattice vector. We write such terms as

$$\sum_{i\in\mathrm{a}} e^{i(\boldsymbol{k}+\boldsymbol{k'}+\boldsymbol{k''})\cdot\boldsymbol{R}_i} = \frac{N}{4}\sum_{\boldsymbol{G}}\delta_{\boldsymbol{k}+\boldsymbol{k'}+\boldsymbol{k''},\boldsymbol{G}} , \tag{2.77}$$

where $\boldsymbol{G}$ iterates over all reciprocal lattice vectors. This distinction from a single Kronecker delta is important because the vector $(\boldsymbol{k}+\boldsymbol{k'}+\boldsymbol{k''})$ does not always fall into the first Brillouin zone (*umklapp*-scattering). Thus, all terms with $\boldsymbol{k}+\boldsymbol{k'}+\boldsymbol{k''} = \boldsymbol{G}$ contribute and a phase factor like $e^{-i\boldsymbol{k''}\cdot\boldsymbol{d}_x}$ cannot be expressed in terms of $\boldsymbol{k},\boldsymbol{k'}$ without knowing the correct umklapp vector $\boldsymbol{G}$. This is because $\boldsymbol{d}_x$ is not a lattice vector and hence $\boldsymbol{G}\cdot\boldsymbol{d}_x \neq 0$. These phase factors arise because of our non-periodic choice of the Fourier transformation, as we explained after Eq. (2.62).

Fourier transforming H_3 given in Eq. (2.60) then gives

$$\begin{aligned}H_3 = \sqrt{\frac{4}{N}}\sum_{\boldsymbol{k}\boldsymbol{k'}\boldsymbol{k''}}\sum_{\boldsymbol{G}}\delta_{\boldsymbol{k}+\boldsymbol{k'}+\boldsymbol{k''},\boldsymbol{G}}\Big\{ &-\left[V_{\boldsymbol{k}}d^{\dagger}_{-\boldsymbol{k}} + U^{*}_{-\boldsymbol{k}}b^{\dagger}_{-\boldsymbol{k}}\right]a^{\dagger}_{-\boldsymbol{k'}}a_{\boldsymbol{k''}} \\ &+e^{i\boldsymbol{G}\cdot\boldsymbol{d}_z}\left[V^{*}_{\boldsymbol{k}}c^{\dagger}_{-\boldsymbol{k}} + U_{-\boldsymbol{k}}a^{\dagger}_{-\boldsymbol{k}}\right]b^{\dagger}_{-\boldsymbol{k'}}b_{\boldsymbol{k''}} \\ &+e^{i\boldsymbol{G}\cdot\boldsymbol{a}_1}\left[V^{*}_{-\boldsymbol{k}}b^{\dagger}_{-\boldsymbol{k}} + U_{\boldsymbol{k}}d^{\dagger}_{-\boldsymbol{k}}\right]c^{\dagger}_{-\boldsymbol{k'}}c_{\boldsymbol{k''}} \\ &-e^{i\boldsymbol{G}\cdot\boldsymbol{d}_x}\left[V_{-\boldsymbol{k}}a^{\dagger}_{-\boldsymbol{k}} + U^{*}_{\boldsymbol{k}}c^{\dagger}_{-\boldsymbol{k}}\right]d^{\dagger}_{-\boldsymbol{k'}}d_{\boldsymbol{k''}} + \text{h.c.}\Big\},\end{aligned} \tag{2.78}$$

where we defined

$$U_{\boldsymbol{k}} = \frac{\sqrt{2S}}{2} W^z_{m+} e^{i\boldsymbol{k}\cdot\boldsymbol{d}_z} \,, \tag{2.79a}$$

$$V_{\boldsymbol{k}} = \frac{\sqrt{2S}}{2} \left(W^x_{m+} e^{i\boldsymbol{k}\cdot\boldsymbol{d}_x} + W^y_{m+} e^{i\boldsymbol{k}\cdot\boldsymbol{d}_y} \right) \,. \tag{2.79b}$$

To reach expression (2.78) we used the relations

$$e^{i\boldsymbol{G}\cdot\boldsymbol{d}_y} = e^{i\boldsymbol{G}\cdot(\boldsymbol{d}_y - \boldsymbol{d}_x)} e^{i\boldsymbol{G}\cdot\boldsymbol{d}_x} = e^{i\boldsymbol{G}\cdot\boldsymbol{d}_x} \,, \tag{2.80a}$$

$$e^{i\boldsymbol{G}\cdot\boldsymbol{a}_2} = e^{i\boldsymbol{G}\cdot(\boldsymbol{a}_2 - \boldsymbol{a}_1)} e^{i\boldsymbol{G}\cdot\boldsymbol{a}_1} = e^{i\boldsymbol{G}\cdot\boldsymbol{a}_1} \,, \tag{2.80b}$$

which hold because $\boldsymbol{d}_y - \boldsymbol{d}_x$ as well as $\boldsymbol{a_2} - \boldsymbol{a_1}$ are lattice vectors.

Next, we express the couplings in momentum space, i.e. λ, $\alpha_{\boldsymbol{k}}$, $\beta_{\boldsymbol{k}}$, $\mu_{\boldsymbol{k}}$, $\nu_{\boldsymbol{k}}$, $U_{\boldsymbol{k}}$, $V_{\boldsymbol{k}}$, in terms of the original model parameters J, K, Γ, J_3. To do so, we first fix the local basis $\{\boldsymbol{t}^x, \boldsymbol{t}^y, \boldsymbol{m}\}$ introduced in Eq. (2.47). We find that every zigzag phase appearing in the phase diagrams in Fig. 2.7) is described by the eigenvalue

$$\lambda^{\text{zigzag}} = \lambda_6 = -J + 3J_3 + \frac{\Gamma}{2}\Gamma + \frac{R}{2} \tag{2.81}$$

given in Eq. 2.33c). Hence the direction of magnetization is given by

$$\boldsymbol{m} = \boldsymbol{v}_6 = \frac{\text{sign}(s)}{\sqrt{2+s^2}} \begin{pmatrix} 1 \\ 1 \\ s \end{pmatrix} \,. \tag{2.82}$$

In order to correctly represent the spin components, the basis $\{\boldsymbol{t}^x, \boldsymbol{t}^y, \boldsymbol{m}\}$ must be orthonormal and right handed which leaves a rotational freedom in the choice of $\boldsymbol{t}^x$ and $\boldsymbol{t}^y$. This gauge freedom results in a momentum independent phase factor for the couplings. We find that it is most convenient to fix the gauge and align the local basis $\{\boldsymbol{t}^x, \boldsymbol{t}^y, \boldsymbol{m}\}$ with the eigensystem given in Eq. (2.33), i.e.

$$\boldsymbol{t}^x = \boldsymbol{v}_4 = \frac{1}{\sqrt{2+r^2}} \begin{pmatrix} 1 \\ 1 \\ r \end{pmatrix} \,, \tag{2.83a}$$

$$\boldsymbol{t}^y = \boldsymbol{v}_5 = \frac{1}{\sqrt{2}} \begin{pmatrix} -1 \\ 1 \\ 0 \end{pmatrix} \,. \tag{2.83b}$$

It is then straightforward to evaluate the matrix elements $W^{\alpha}_{\sigma\sigma'}$ defined in Eq. (2.59) and $W^{\alpha}_{m\sigma'}$ defined in Eq. (2.61b) to express the couplings given

in Eqs. (2.75) and (2.79) as

$$\lambda = S\left[J - 3J_3 - \frac{\Gamma}{2}\Gamma - \frac{R}{2}\right], \tag{2.84a}$$

$$\alpha_{\boldsymbol{k}} = S\left[J + \frac{K}{4}\frac{4+r^2}{2+r^2} + \Gamma\frac{r}{2+r^2}\right]\left(e^{i\boldsymbol{k}\cdot\boldsymbol{d}_x} + e^{i\boldsymbol{k}\cdot\boldsymbol{d}_y}\right), \tag{2.84b}$$

$$\beta_{\boldsymbol{k}} = -S\left[\frac{K}{2}\frac{r^2}{2+r^2} + \frac{\Gamma}{2}\frac{4+r^2}{2+r^2}\right]e^{i\boldsymbol{k}\cdot\boldsymbol{d}_z}, \tag{2.84c}$$

$$\mu_{\boldsymbol{k}} = S\left[J + \frac{K-\Gamma}{2}\frac{r^2}{2+r^2}\right]e^{i\boldsymbol{k}\cdot\boldsymbol{d}_z}, \tag{2.84d}$$

$$\begin{aligned}\nu_{\boldsymbol{k}} = S\Bigg\{&\left[\frac{K}{4}\frac{r^2}{2+r^2} - \Gamma\frac{r}{2+r^2}\right]\left(e^{i\boldsymbol{k}\cdot\boldsymbol{d}_x} + e^{i\boldsymbol{k}\cdot\boldsymbol{d}_y}\right)\\ &+ i\frac{K-\Gamma r}{2}\sqrt{\frac{2}{2+r^2}}\left(e^{i\boldsymbol{k}\cdot\boldsymbol{d}_x} - e^{i\boldsymbol{k}\cdot\boldsymbol{d}_y}\right)\Bigg\},\end{aligned} \tag{2.84e}$$

and

$$\begin{aligned}V_{\boldsymbol{k}} = \frac{\sqrt{2S}}{2}\frac{\mathrm{sign}(s)}{\sqrt{2+s^2}}\Bigg[&\frac{K-\Gamma s}{\sqrt{2}}(e^{i\boldsymbol{k}\cdot\boldsymbol{d}_x} - e^{i\boldsymbol{k}\cdot\boldsymbol{d}_y})\\ &+ i\frac{\Gamma-K}{\sqrt{2+r^2}}(e^{i\boldsymbol{k}\cdot\boldsymbol{d}_x} + e^{i\boldsymbol{k}\cdot\boldsymbol{d}_y})\Bigg],\end{aligned} \tag{2.85a}$$

$$U_{\boldsymbol{k}} = \sqrt{2S}\frac{\mathrm{sign}(s)}{\sqrt{2+s^2}}\frac{\Gamma-K}{\sqrt{2+r^2}}e^{i\boldsymbol{k}\cdot\boldsymbol{d}_z}. \tag{2.85b}$$

Note that $\alpha_{-\boldsymbol{k}} = \alpha^*_{\boldsymbol{k}}$ and $\beta_{-\boldsymbol{k}} = \beta^*_{\boldsymbol{k}}$ with our choice of basis, which implies $\boldsymbol{A}_{-\boldsymbol{k}} = \boldsymbol{A}^*_{\boldsymbol{k}}$ for the matrix $\boldsymbol{A}_{\boldsymbol{k}}$ defined in Eq. (2.74a). Because $\nu_{-\boldsymbol{k}} \neq \nu^*_{\boldsymbol{k}}$, a similar relation for the matrix $\boldsymbol{B}_{\boldsymbol{k}}$ (2.74b) does not hold and $\boldsymbol{B}_{\boldsymbol{k}}$ is not hermitian in general. However, if the imaginary coefficient in the expression (2.84e) vanishes, $\boldsymbol{B}_{\boldsymbol{k}}$ does become hermitian. This is fulfilled if

$$K = \Gamma r\,, \tag{2.86}$$

and will become important later when we identify the special parameter region where the Bogolioubov transformation can be simplified.

2.6 Bogoliubov transformation and special parameter region

The quadratic Hamiltonian (2.73) of our model can be written in symmetrized matrix form as

$$H_2 = \sum_{\boldsymbol{k}} \begin{pmatrix} \boldsymbol{a}_{\boldsymbol{k}} \\ \boldsymbol{a}^*_{-\boldsymbol{k}} \end{pmatrix}^\dagger \begin{pmatrix} \boldsymbol{A}_{\boldsymbol{k}} & \boldsymbol{B}_{\boldsymbol{k}} \\ \boldsymbol{B}^\dagger_{\boldsymbol{k}} & \boldsymbol{A}^T_{-\boldsymbol{k}} \end{pmatrix} \begin{pmatrix} \boldsymbol{a}_{\boldsymbol{k}} \\ \boldsymbol{a}^*_{-\boldsymbol{k}} \end{pmatrix}, \tag{2.87}$$

where we defined the 4 dimensional operator-valued vectors

$$\boldsymbol{a}_{\boldsymbol{k}} = \begin{pmatrix} a_{\boldsymbol{k}} \\ b_{\boldsymbol{k}} \\ c_{\boldsymbol{k}} \\ d_{\boldsymbol{k}} \end{pmatrix} . \tag{2.88}$$

To diagonalize this Hamiltonian, we apply a canonical transformation

$$\begin{pmatrix} \boldsymbol{a}_{\boldsymbol{k}} \\ \boldsymbol{a}^*_{-\boldsymbol{k}} \end{pmatrix} = \mathbb{T}_{\boldsymbol{k}} \begin{pmatrix} \boldsymbol{b}_{\boldsymbol{k}} \\ \boldsymbol{b}^*_{-\boldsymbol{k}} \end{pmatrix} . \tag{2.89}$$

The condition that the transformation must be canonical, i.e. that the bosonic commutation relations must be preserved, translates to the condition that the transformation matrices $\mathbb{T}_{\boldsymbol{k}}$ are pseudo-unitary,

$$\mathbb{T}_{\boldsymbol{k}} \begin{pmatrix} \mathbb{1} & 0 \\ 0 & -\mathbb{1} \end{pmatrix} \mathbb{T}^{\dagger}_{\boldsymbol{k}} = \begin{pmatrix} \mathbb{1} & 0 \\ 0 & -\mathbb{1} \end{pmatrix} . \tag{2.90}$$

Here, $\mathbb{1}$ denotes the 4×4 identity matrix. An algorithm that allows to find these transformations by reducing the problem to a unitary diagonalization can be found in the literature [63, 64] and in known by the name *Colpa algorithm*. We presented this algorithm in Appendix A of our publication [1]. However, in this work we prefer to use a different method, the *hermitian field parametrization*. The hermitian field parametrization has the advantage that it allows us to identify the aforementioned special parameter region and that it halves the dimensionality of the diagonalization problem. It has also turned out to be useful in other magnetically ordered systems [52, 53, 54, 55], and can in principle be applied to any bosonic Hamiltonian.

Our strategy is as follows. First, we introduce the hermitian field parametrization in Sec. 2.6.1. Working in the path integral formulation, we use the hermitian field parametrization to transform the complex fields (which represent the bosonic creation and annihilation operators) into the new hermitian fields. In Sec. 2.6.2 we identify a special parameter region where the quadratic part of the action of the hermitian fields simplifies. In Sec. 2.6.3, we derive analytical expressions for canonical transformation matrices which diagonalize the quadratic part of this action. In Sec. 2.6.4, we invert the hermitian field parametrization, which results in an action for complex fields, i.e. for bosons, which has a diagonal quadratic part. This means that we succeeded in finding the Bogoliubov transformation and obtained the diagonal form of the free magnon propagator. For the readers orientation, we show a summary of this string of transformations in Fig. 2.9. Lastly, in Sec. 2.6.5, we apply the Bogoliubov transformation to the interaction vertices, which we need later for the perturbative calculation of the magnon damping in Sec. 2.7.

$$\begin{pmatrix} \boldsymbol{a}_K \\ \bar{\boldsymbol{a}}_{-K} \end{pmatrix} = \mathbb{T}_{\boldsymbol{k}} \begin{pmatrix} \boldsymbol{b}_K \\ \bar{\boldsymbol{b}}_{-K} \end{pmatrix} = \mathbb{N} \underbrace{\mathbb{M}_{\boldsymbol{k}} \overbrace{\mathbb{N}^{-1} \begin{pmatrix} \boldsymbol{b}_K \\ \bar{\boldsymbol{b}}_{-K} \end{pmatrix}}^{= \begin{pmatrix} \boldsymbol{X}'_K \\ \boldsymbol{P}'_K \end{pmatrix}}}_{= \begin{pmatrix} \boldsymbol{X}_K \\ \boldsymbol{P}_K \end{pmatrix}}$$

Figure 2.9: The Bogoliubov transformation which diagonalizes the original bosonic fields $(\boldsymbol{a}_K, \bar{\boldsymbol{a}}_{-k})^T$ to the magnon modes $(\boldsymbol{b}_K, \bar{\boldsymbol{b}}_{-K})^T$ is expressed by a matrix $\mathbb{T}_{\boldsymbol{k}}$. This transformation is subdivided into three steps: (1) hermitian parametrization $(\boldsymbol{a}_K, \bar{\boldsymbol{a}}_{-K})^T = \mathbb{N} \cdot (\boldsymbol{X}_K, \boldsymbol{P}_K)^T$, (2) canonical diagonalization of the hermitian field $(\boldsymbol{X}_K, \boldsymbol{P}_K)^T = \mathbb{M}_{\boldsymbol{k}} \cdot (\boldsymbol{X}'_K, \boldsymbol{P}'_K)^T$, (3) reparametrization to complex (bosonic) fields $(\boldsymbol{X}'_K, \boldsymbol{P}'_K)^T = \mathbb{N}^{-1} \cdot (\boldsymbol{b}_K, \bar{\boldsymbol{b}}_{-k})^T$.

2.6.1 Hermitian field parameterization

Going to the real space representation for a moment, we express the bosonic operators b_i and $b_i^\dagger$ at any lattice site i in terms of two hermitian operators x_i and p_i as

$$b_i = \frac{1}{\sqrt{2}} \left[x_i + i p_i \right] \ , \tag{2.91a}$$

$$b_i^\dagger = \frac{1}{\sqrt{2}} \left[x_i - i p_i \right] \ . \tag{2.91b}$$

The hermitian operators are chosen in analogy to the harmonic oscillator, they have the same commutation relations as position and momentum operators. Physically, the real fields established by x_i and p_i can be interpreted as fluctuations of the transversal spin components. This can be seen by noting that b_i and $b_i^\dagger$ are approximately proportional to the spin ladder operators by the Holstein-Primakoff transformation (2.55). Then, it becomes clear that the relation (2.91) resembles the relation $S^\pm = S^x \pm i S^y$ between spin ladder operators and transversal spin components.

We use the Fourier transformation defined in Eq. (2.62) to obtain the hermitian parameterization in momentum space,

$$a_{\boldsymbol{k}m} = \frac{1}{\sqrt{2}} \left[x_{\boldsymbol{k}m} + i p_{\boldsymbol{k}m} \right] \ , \tag{2.92a}$$

$$a_{-\boldsymbol{k}m}^\dagger = \frac{1}{\sqrt{2}} \left[x_{\boldsymbol{k}m} - i p_{\boldsymbol{k}_m} \right] \ , \tag{2.92b}$$

where the Fourier transformed hermitian field operators satisfy

$$x_{-\boldsymbol{k}m} = x_{\boldsymbol{k}m}^\dagger \ , \quad p_{-\boldsymbol{k}m} = p_{\boldsymbol{k}m}^\dagger \ . \tag{2.93}$$

Note that these operators fulfill the commutation relation

$$[x_{\boldsymbol{k}m}, p_{\boldsymbol{k}'m'}] = i\delta_{\boldsymbol{k},-\boldsymbol{k}'}\delta_{m,m'} \ . \tag{2.94}$$

We will express the Bogoliubov transformation in the path integral formulation [5, 6, 65], where the annihilation operators $a_{\boldsymbol{k}m}$ are represented by complex fields a_{Km} and the creation operators $a^\dagger_{\boldsymbol{k}m}$ are represented by the complex conjugates $\bar{a}_{Km}$. The label $K = (i\omega, \boldsymbol{k})$ summarizes the crystal momentum and the bosonic Matsubara frequency $i\omega$. The quadratic part of the Euclidean action can be constructed from the quadratic Hamiltonian (2.95) and reads

$$S_2 = \beta \sum_K \sum_{mn} \Big\{ (A^{mn}_{\boldsymbol{k}} - i\omega\delta_{mn})\bar{a}_{Km}a_{Kn} + \frac{1}{2}\left[B^{mn}_{\boldsymbol{k}}\bar{a}_{Km}\bar{a}_{-Kn} + (B^{nm}_{\boldsymbol{k}})^* a_{-Km}a_{Kn}\right] \Big\}, \tag{2.95}$$

where β is the inverse temperature. We define the vectors in flavor space

$$\boldsymbol{a}_K = \begin{pmatrix} a_{K1} \\ a_{K2} \\ a_{K3} \\ a_{K4} \end{pmatrix}, \quad \bar{\boldsymbol{a}}_K = \begin{pmatrix} \bar{a}_{K1} \\ \bar{a}_{K2} \\ \bar{a}_{K3} \\ \bar{a}_{K4} \end{pmatrix} \tag{2.96}$$

and write the action (2.95) in block matrix form as

$$S_2[a,\bar{a}] = \frac{\beta}{2} \sum_K \begin{pmatrix} \boldsymbol{a}_K \\ \bar{\boldsymbol{a}}_{-K} \end{pmatrix}^\dagger \begin{pmatrix} \boldsymbol{A}_{\boldsymbol{k}} - i\omega & \boldsymbol{B}_{\boldsymbol{k}} \\ \boldsymbol{B}^\dagger_{\boldsymbol{k}} & \boldsymbol{A}^T_{-\boldsymbol{k}} + i\omega \end{pmatrix} \begin{pmatrix} \boldsymbol{a}_K \\ \bar{\boldsymbol{a}}_{-K} \end{pmatrix} . \tag{2.97}$$

Since the bosons are now represented by complex numbers instead of operators, we do not need to take the commutation relations into account explicitly, they are encoded implicitly by the frequency dependence of the action. The hermitian operators x_i and p_i become real fields and their Fourier components X_{Km} and P_{Km} are defined by

$$a_{Km} = \frac{1}{\sqrt{2}}\left[X_{Km} + iP_{Km}\right] \ , \tag{2.98a}$$

$$\bar{a}_{-Km} = \frac{1}{\sqrt{2}}\left[X_{Km} - iP_{Km}\right] \ , \tag{2.98b}$$

with the restriction

$$X_{-Km} = X^*_{Km} \ , \quad P_{-Km} = P^*_{Km} \ . \tag{2.99}$$

We write this transformation in block matrix form as

$$\begin{pmatrix} \boldsymbol{a}_K \\ \bar{\boldsymbol{a}}_{-K} \end{pmatrix} = \mathbb{N} \begin{pmatrix} \boldsymbol{X}_K \\ \boldsymbol{P}_K \end{pmatrix} \ , \tag{2.100}$$

where we defined the 8×8 matrix

$$\mathbb{N} = \frac{1}{\sqrt{2}} \begin{pmatrix} \mathbb{1} & i\mathbb{1} \\ \mathbb{1} & -i\mathbb{1} \end{pmatrix} , \tag{2.101}$$

and the vectors

$$\boldsymbol{X}_K = \begin{pmatrix} X_{K1} \\ X_{K2} \\ X_{K3} \\ X_{K4} \end{pmatrix}, \quad \boldsymbol{P}_K = \begin{pmatrix} P_{K1} \\ P_{K2} \\ P_{K3} \\ P_{K4} \end{pmatrix}. \tag{2.102}$$

Applying this transformation to the quadratic action (2.97) leads to

$$S_2[X,P] = \frac{\beta}{2} \sum_K \begin{pmatrix} \boldsymbol{X}_{-K} \\ \boldsymbol{P}_{-K} \end{pmatrix}^T \begin{pmatrix} \boldsymbol{V_k} & \boldsymbol{W_k} + \omega \\ \boldsymbol{W_k^\dagger} - \omega & \boldsymbol{T_k} \end{pmatrix} \begin{pmatrix} \boldsymbol{X}_K \\ \boldsymbol{P}_K \end{pmatrix} , \tag{2.103}$$

with the matrices

$$\boldsymbol{T_k} = \boldsymbol{A_k^R} - \boldsymbol{B_k^R}, \tag{2.104a}$$
$$\boldsymbol{V_k} = \boldsymbol{A_k^R} + \boldsymbol{B_k^R}, \tag{2.104b}$$
$$\boldsymbol{W_k} = \boldsymbol{A_k^I} + \boldsymbol{B_k^I}. \tag{2.104c}$$

Here, the matrices

$$\boldsymbol{A_k^R} = \frac{\boldsymbol{A_k} + \boldsymbol{A_{-k}^T}}{2} , \tag{2.105a}$$
$$\boldsymbol{A_k^I} = \frac{\boldsymbol{A_k} - \boldsymbol{A_{-k}^T}}{2i} , \tag{2.105b}$$
$$\boldsymbol{B_k^R} = \frac{\boldsymbol{B_k} + \boldsymbol{B_k^\dagger}}{2} , \tag{2.105c}$$
$$\boldsymbol{B_k^I} = \frac{\boldsymbol{B_k} - \boldsymbol{B_k^\dagger}}{2i} , \tag{2.105d}$$

are combinations of the matrices appearing in the momentum representation of the quadratic Hamiltonian given in Eqs. (2.74). In the transformation leading to Eq. (2.103), we used that $(\boldsymbol{A_k^I})^\dagger = -\boldsymbol{A_k^I}$ which follows because the Hamiltonian, and as a consequence also the matrix $\boldsymbol{A_k}$, is hermitian.

2.6.2 Special parameter region

We note that the quadratic action (2.103) simplifies if the matrix $\boldsymbol{W_k}$ vanishes. Since in our case $\boldsymbol{A_k^I} = 0$, this happens if $\boldsymbol{B_k}$ is hermitian, as can be seen from Eq. (2.105d). As we noted earlier in Sec. 2.5 before Eq. (2.86), this is the case if the model parameters fulfill

$$K = \Gamma r \, . \tag{2.106}$$

In this region the coupling $\nu_{\boldsymbol{k}}$ (2.84e) satisfies the symmetry $\nu_{-\boldsymbol{k}} = \nu_{\boldsymbol{k}}^*$ so that the matrix $\boldsymbol{B}_{\boldsymbol{k}}$ (2.74b) becomes hermitian. Eq. (2.106) has three solutions,

$$(1) \quad \Gamma = 0 \quad \text{and} \quad K < 0 \,, \tag{2.107a}$$

$$(2) \quad \Gamma = K > 0 \,, \tag{2.107b}$$

$$(3) \quad \Gamma = -\frac{3}{2} K < 0 \,. \tag{2.107c}$$

The first solution constitutes the Heisenberg-Kitaev model which has been studied in the literature [66, 67, 68] but is presently not of interest to us. The third solution does not intersect the zigzag phase for any reasonable choice of the third nearest neighbor coupling J_3. The solution $\Gamma = K > 0$ does intersect the zigzag phase for $J_3 > 0$. This can be seen in the phase diagram depicted Fig. 2.7 b, where the region $\Gamma = K > 0$ is depicted by a dashed line.

At $\Gamma = K > 0$, the variables r and s given in Eq. (2.35) simplify to $r = 1$ and $s = -2$, so that the couplings (2.75) and (2.79) are given by

$$\lambda = S\left(-J + 2K + 3J_3\right) \,, \tag{2.108a}$$

$$\alpha_{\boldsymbol{k}} = S\left(J + \frac{3}{4}K\right)\left(e^{i\boldsymbol{k}\cdot\boldsymbol{d}_x} + e^{i\boldsymbol{k}\cdot\boldsymbol{d}_y}\right) \,, \tag{2.108b}$$

$$\beta_{\boldsymbol{k}} = -SKe^{i\boldsymbol{k}\cdot\boldsymbol{d}_z} \,, \tag{2.108c}$$

$$\mu_{\boldsymbol{k}} = SJe^{i\boldsymbol{k}\cdot\boldsymbol{d}_z} + SJ_3 \sum_{\alpha} e^{-2i\boldsymbol{k}\cdot\boldsymbol{d}_{\boldsymbol{\alpha}}} \,, \tag{2.108d}$$

$$\nu_{\boldsymbol{k}} = -\frac{1}{4}SK\left(e^{i\boldsymbol{k}\cdot\boldsymbol{d}_x} + e^{i\boldsymbol{k}\cdot\boldsymbol{d}_y}\right) \,, \tag{2.108e}$$

and

$$U_{\boldsymbol{k}} = 0 \,, \tag{2.109a}$$

$$V_{\boldsymbol{k}} = -\frac{\sqrt{6S}}{4} K(e^{i\boldsymbol{k}\cdot\boldsymbol{d}_x} - e^{i\boldsymbol{k}\cdot\boldsymbol{d}_y}) \,. \tag{2.109b}$$

The magnetization vector (2.82) is then

$$\boldsymbol{m} = \boldsymbol{e}_2 \,, \tag{2.110}$$

with $\boldsymbol{e}_2$ given in Eq. (2.9a), i.e. the magnetization lies in the lattice plane. In the remainder of this chapter our calculations will be restricted to this region.

2.6.3 Diagonalization of H_2 in hermitian field representation

In the region $\Gamma = K > 0$, where $\boldsymbol{W}_{\boldsymbol{k}} = 0$, the quadratic action (2.103) simplifies to

$$S_2[X, P] = \frac{\beta}{2} \sum_K \begin{pmatrix} \boldsymbol{X}_{-K} \\ \boldsymbol{P}_{-K} \end{pmatrix}^T \begin{pmatrix} \boldsymbol{V}_{\boldsymbol{k}} & \omega \\ -\omega & \boldsymbol{T}_{\boldsymbol{k}} \end{pmatrix} \begin{pmatrix} \boldsymbol{X}_K \\ \boldsymbol{P}_K \end{pmatrix} \,, \tag{2.111}$$

with $\boldsymbol{T_k} = \boldsymbol{A_k} - \boldsymbol{B_k}$ and $\boldsymbol{V_k} = \boldsymbol{A_k} + \boldsymbol{B_k}$. We wish to diagonalize all four blocks in the quadratic action by means of a canonical transformation

$$\begin{pmatrix} \boldsymbol{X}_K \\ \boldsymbol{P}_K \end{pmatrix} = \mathbb{M}_{\boldsymbol{k}} \begin{pmatrix} \boldsymbol{X}'_K \\ \boldsymbol{P}'_K \end{pmatrix} , \tag{2.112}$$

where $\mathbb{M}_{\boldsymbol{k}}$ is an 8×8 matrix. The fact that the two off-diagonal blocks are proportional to a unit matrix due to our restriction $\Gamma = K > 0$ will greatly simplify this task. A canonical transformation must preserve the commutation relations (2.94) of the field operators. One finds that this property is fulfilled if the matrix $\mathbb{M}_{\boldsymbol{k}}$ is of the form

$$\mathbb{M}_{\boldsymbol{k}} = \begin{pmatrix} \boldsymbol{M_k} & 0 \\ 0 & (\boldsymbol{M_k^\dagger})^{-1} \end{pmatrix} . \tag{2.113}$$

In the remainder of this subsection, we will derive an analytical expression for the matrix $\mathbb{M}_{\boldsymbol{k}}$. Since two successive canonical transformations constitute again a cononical transformation, we subdivide this task into two. In a first step, we find a canonical transformation which diagonalizes the lower left 4×4 matrix $\boldsymbol{T_k}$ in the action (2.103) into a unit matrix. In the second step, we will then diagonalize the transformed upper right block.

We find the first transformation by noting that $\boldsymbol{T_k}$ is a hermitian matrix, which means that there is a hermitian matrix $\boldsymbol{T_k}^{1/2}$ which fulfills $(\boldsymbol{T_k}^{1/2})^2 = \boldsymbol{T_k}$. Then, applying the canonical transformation

$$\begin{pmatrix} \boldsymbol{X}_K \\ \boldsymbol{P}_K \end{pmatrix} = \begin{pmatrix} \boldsymbol{T_k}^{1/2} & 0 \\ 0 & \boldsymbol{T_k}^{-1/2} \end{pmatrix} \begin{pmatrix} \tilde{\boldsymbol{X}}_K \\ \tilde{\boldsymbol{P}}_K \end{pmatrix} \tag{2.114}$$

to the action (2.103) diagonalizes the lower left block,

$$S_2[\tilde{X}, \tilde{P}] = \frac{\beta}{2} \sum_K \begin{pmatrix} \tilde{\boldsymbol{X}}_{-K} \\ \tilde{\boldsymbol{P}}_{-K} \end{pmatrix}^T \begin{pmatrix} \tilde{\boldsymbol{V}}_{\boldsymbol{k}} & \omega \\ -\omega & \mathbb{1} \end{pmatrix} \begin{pmatrix} \tilde{\boldsymbol{X}}_K \\ \tilde{\boldsymbol{P}}_K \end{pmatrix} , \tag{2.115}$$

with

$$\tilde{\boldsymbol{V}}_{\boldsymbol{k}} = \boldsymbol{T_k}^{1/2} \, \boldsymbol{V_k} \, \boldsymbol{T_k}^{1/2} . \tag{2.116}$$

Note that the ω blocks are invariant with respect to this transformation since they represent the matrix $\omega \mathbb{1}_{4\times 4}$. Before diagonalizing the matrix $\tilde{\boldsymbol{V}}_{\boldsymbol{k}}$ by a second canonical transformation, we need to find analytical expressions for the first transformation. An analytical expression for the matrix $\boldsymbol{T_k}^{1/2}$ can be constructed by first diagonalizing the matrix $\boldsymbol{T_k}$ by a unitary transformation $\boldsymbol{U_k}$,

$$\boldsymbol{U_k^\dagger} \, \boldsymbol{T_k} \, \boldsymbol{U_k} = \boldsymbol{D_k} \quad \text{diagonal.} \tag{2.117}$$

Given the matrix $\boldsymbol{T_k} = \boldsymbol{A_k} - \boldsymbol{B_k}$ with $\boldsymbol{A_k}$ and $\boldsymbol{B_k}$ given in Eq. (2.74) and the matrix elements at $\Gamma = K > 0$ given in Eq. (2.108), a possible choice

for $\boldsymbol{U}_{\boldsymbol{k}}$ is

$$\boldsymbol{U}_{\boldsymbol{k}} = \frac{1}{2}\begin{pmatrix} -\mathrm{sign}(\eta_{1,\boldsymbol{k}}) & \mathrm{sign}(\eta_{1,\boldsymbol{k}}) & -\mathrm{sign}(\eta_{2,\boldsymbol{k}}) & \mathrm{sign}(\eta_{2,\boldsymbol{k}}) \\ 1 & 1 & -1 & -1 \\ -\mathrm{sign}(\eta_{1,\boldsymbol{k}}) & \mathrm{sign}(\eta_{1,\boldsymbol{k}}) & \mathrm{sign}(\eta_{2,\boldsymbol{k}}) & -\mathrm{sign}(\eta_{2,\boldsymbol{k}}) \\ 1 & 1 & 1 & 1 \end{pmatrix} , \tag{2.118}$$

where we defined the complex sign function

$$\mathrm{sign}(z) \equiv \frac{z}{|z|} , \tag{2.119}$$

and

$$\eta_{1,\boldsymbol{k}} = \alpha_{\boldsymbol{k}} + \beta_{\boldsymbol{k}} - \mu_{\boldsymbol{k}} - \nu_{\boldsymbol{k}} , \tag{2.120a}$$
$$\eta_{2,\boldsymbol{k}} = \alpha_{\boldsymbol{k}} - \beta_{\boldsymbol{k}} + \mu_{\boldsymbol{k}} - \nu_{\boldsymbol{k}} . \tag{2.120b}$$

The matrix $\boldsymbol{D}_{\boldsymbol{k}}$ is then

$$\boldsymbol{D}_{\boldsymbol{k}} = \begin{pmatrix} \lambda - |\eta_{1,\boldsymbol{k}}| & 0 & 0 & 0 \\ 0 & \lambda + |\eta_{1,\boldsymbol{k}}| & 0 & 0 \\ 0 & 0 & \lambda - |\eta_{2,\boldsymbol{k}}| & 0 \\ 0 & 0 & 0 & \lambda + |\eta_{2,\boldsymbol{k}}| \end{pmatrix} . \tag{2.121}$$

Because $\boldsymbol{D}_{\boldsymbol{k}}$ is diagonal, we can simply take the square root of the diagonal elements to construct the matrix $\boldsymbol{D}_{\boldsymbol{k}}^{1/2}$ which fulfills $(\boldsymbol{D}_{\boldsymbol{k}}^{1/2})^2 = \boldsymbol{D}_{\boldsymbol{k}}$. Reversing the unitary transformation $\boldsymbol{U}_{\boldsymbol{k}}$ then yields

$$\boldsymbol{T}_{\boldsymbol{k}}^{1/2} = \boldsymbol{U}_{\boldsymbol{k}}\, \boldsymbol{D}_{\boldsymbol{k}}^{1/2}\, \boldsymbol{U}_{\boldsymbol{k}}^{\dagger} , \tag{2.122}$$

which we can write explicitly as

$$\boldsymbol{T}_{\boldsymbol{k}}^{1/2} = \begin{pmatrix} t_{1,\boldsymbol{k}} & t_{3,\boldsymbol{k}} & t_{2,\boldsymbol{k}} & t_{4,\boldsymbol{k}} \\ t_{3,\boldsymbol{k}}^{*} & t_{1,\boldsymbol{k}} & t_{4,\boldsymbol{k}}^{*} & t_{2,\boldsymbol{k}} \\ t_{2,\boldsymbol{k}}^{*} & t_{4,\boldsymbol{k}} & t_{1,\boldsymbol{k}} & t_{3,\boldsymbol{k}} \\ t_{4,\boldsymbol{k}}^{*} & t_{2,\boldsymbol{k}}^{*} & t_{3,\boldsymbol{k}}^{*} & t_{1,\boldsymbol{k}} \end{pmatrix} , \tag{2.123}$$

with the matrix elements

$$t_{1,\boldsymbol{k}} = \frac{1}{4}\left\{\sqrt{\lambda - |\eta_{1,\boldsymbol{k}}|} + \sqrt{\lambda + |\eta_{1,\boldsymbol{k}}|} + \sqrt{\lambda - |\eta_{2,\boldsymbol{k}}|} + \sqrt{\lambda + |\eta_{2,\boldsymbol{k}}|}\right\}, \tag{2.124a}$$

$$t_{2,\boldsymbol{k}} = \frac{1}{4}\left\{\sqrt{\lambda - |\eta_{1,\boldsymbol{k}}|} + \sqrt{\lambda + |\eta_{1,\boldsymbol{k}}|} - \sqrt{\lambda - |\eta_{2,\boldsymbol{k}}|} - \sqrt{\lambda + |\eta_{2,\boldsymbol{k}}|}\right\}, \tag{2.124b}$$

$$\begin{aligned} t_{3,\boldsymbol{k}} = \frac{1}{4}\Bigg\{ &- \operatorname{sign}(\eta_{1,\boldsymbol{k}}) \left[\sqrt{\lambda - |\eta_{1,\boldsymbol{k}}|} - \sqrt{\lambda + |\eta_{1,\boldsymbol{k}}|}\right] \\ &+ \operatorname{sign}(\eta_{2,\boldsymbol{k}}) \left[\sqrt{\lambda - |\eta_{2,\boldsymbol{k}}|} - \sqrt{\lambda + |\eta_{2,\boldsymbol{k}}|}\right] \Bigg\}, \end{aligned} \tag{2.124c}$$

$$\begin{aligned} t_{4,\boldsymbol{k}} = \frac{1}{4}\Bigg\{ &- \operatorname{sign}(\eta_{1,\boldsymbol{k}}) \left[\sqrt{\lambda - |\eta_{1,\boldsymbol{k}}|} - \sqrt{\lambda + |\eta_{1,\boldsymbol{k}}|}\right] \\ &- \operatorname{sign}(\eta_{2,\boldsymbol{k}}) \left[\sqrt{\lambda - |\eta_{2,\boldsymbol{k}}|} - \sqrt{\lambda + |\eta_{2,\boldsymbol{k}}|}\right] \Bigg\}. \end{aligned} \tag{2.124d}$$

We use this result to write down an explicit expression for the matrix $\tilde{\boldsymbol{V}}_{\boldsymbol{k}}$ given in Eq. (2.116),

$$\tilde{\boldsymbol{V}}_{\boldsymbol{k}} = \begin{pmatrix} v_{1,\boldsymbol{k}} & v_{2,\boldsymbol{k}} & v_{3,\boldsymbol{k}} & v_{4,\boldsymbol{k}} \\ v_{2,\boldsymbol{k}}^* & v_{1,\boldsymbol{k}} & v_{4,\boldsymbol{k}}^* & v_{3,\boldsymbol{k}} \\ v_{3,\boldsymbol{k}}^* & v_{4,\boldsymbol{k}} & v_{1,\boldsymbol{k}} & v_{2,\boldsymbol{k}} \\ v_{4,\boldsymbol{k}}^* & v_{3,\boldsymbol{k}}^* & v_{2,\boldsymbol{k}}^* & v_{1,\boldsymbol{k}} \end{pmatrix}, \tag{2.125}$$

where we defined

$$\begin{aligned} v_{1,\boldsymbol{k}} = \lambda &\left(t_{1,\boldsymbol{k}}^2 + t_{2,\boldsymbol{k}}^2 + |t_{3,\boldsymbol{k}}|^2 + |t_{4,\boldsymbol{k}}|^2\right) \\ &+ 2\mathrm{Re}\left\{(\beta_{\boldsymbol{k}} + \mu_{\boldsymbol{k}})\left(t_{1,\boldsymbol{k}} t_{3,\boldsymbol{k}}^* + t_{2,\boldsymbol{k}} t_{4,\boldsymbol{k}}^*\right)\right\} \\ &+ 2\mathrm{Re}\left\{(\alpha_{\boldsymbol{k}} + \nu_{\boldsymbol{k}})\left(t_{2,\boldsymbol{k}} t_{3,\boldsymbol{k}}^* + t_{1,\boldsymbol{k}} t_{4,\boldsymbol{k}}^*\right)\right\}, \end{aligned} \tag{2.126a}$$

$$\begin{aligned} v_{2,\boldsymbol{k}} = 2\lambda &\left(t_{1,\boldsymbol{k}} t_{3,\boldsymbol{k}} + t_{2,\boldsymbol{k}} t_{4,\boldsymbol{k}}\right) \\ &+ (\beta_{\boldsymbol{k}} + \mu_{\boldsymbol{k}})\left(t_{1,\boldsymbol{k}}^2 + t_{2,\boldsymbol{k}}^2\right) + (\beta_{\boldsymbol{k}} + \mu_{\boldsymbol{k}})^*\left(t_{3,\boldsymbol{k}}^2 + t_{4,\boldsymbol{k}}^2\right) \\ &+ 2(\alpha_{\boldsymbol{k}} + \nu_{\boldsymbol{k}}) t_{1,\boldsymbol{k}} t_{2,\boldsymbol{k}} + 2(\alpha_{\boldsymbol{k}} + \nu_{\boldsymbol{k}})^* t_{3,\boldsymbol{k}} t_{4,\boldsymbol{k}}, \end{aligned} \tag{2.126b}$$

$$\begin{aligned} v_{3,\boldsymbol{k}} = 2\lambda t_{1,\boldsymbol{k}} t_{2,\boldsymbol{k}} &+ 2\mathrm{Re}\left\{t_{3,\boldsymbol{k}} t_{4,\boldsymbol{k}}^*\right\} \\ &+ 2\mathrm{Re}\left\{(\beta_{\boldsymbol{k}} + \mu_{\boldsymbol{k}})\left(t_{2,\boldsymbol{k}} t_{3,\boldsymbol{k}}^* + t_{1,\boldsymbol{k}} t_{4,\boldsymbol{k}}^*\right)\right\} \\ &+ 2\mathrm{Re}\left\{(\alpha_{\boldsymbol{k}} + \nu_{\boldsymbol{k}})\left(t_{1,\boldsymbol{k}} t_{3,\boldsymbol{k}}^* + t_{2,\boldsymbol{k}} t_{4,\boldsymbol{k}}^*\right)\right\}, \end{aligned} \tag{2.126c}$$

$$\begin{aligned} v_{4,\boldsymbol{k}} = 2\lambda\,&(t_{1,\boldsymbol{k}}t_{4,\boldsymbol{k}} + t_{2,\boldsymbol{k}}t_{3,\boldsymbol{k}}) \\ &+ 2\,(\beta_{\boldsymbol{k}} + \mu_{\boldsymbol{k}})\,t_{1,\boldsymbol{k}}t_{2,\boldsymbol{k}} + 2\,(\beta_{\boldsymbol{k}} + \mu_{\boldsymbol{k}})^*\,t_{3,\boldsymbol{k}}t_{4,\boldsymbol{k}} \\ &+ (\alpha_{\boldsymbol{k}} + \nu_{\boldsymbol{k}})\left(t_{1,\boldsymbol{k}}^2 + t_{2,\boldsymbol{k}}^2\right) + (\alpha_{\boldsymbol{k}} + \nu_{\boldsymbol{k}})^*\left(t_{3,\boldsymbol{k}}^2 + t_{4,\boldsymbol{k}}^2\right) . \end{aligned} \tag{2.126d}$$

Thus, we have successfully diagonalized the lower right block of the quadratic action. Next, we diagonalize the matrix $\tilde{\boldsymbol{V}}_{\boldsymbol{k}}$ in the top left block of the quadratic action (2.115) by a second canonical transformation. We do this by means of a unitary transformation $\boldsymbol{S}_{\boldsymbol{k}}$ which fulfills

$$\boldsymbol{S}_{\boldsymbol{k}}\,\tilde{\boldsymbol{V}}_{\boldsymbol{k}}\,\boldsymbol{S}_{\boldsymbol{k}}^{\dagger} = \boldsymbol{\Omega}_{\boldsymbol{k}}^2 \quad \text{diagonal.} \tag{2.127}$$

A suitable transformation matrix is

$$\boldsymbol{S}_{\boldsymbol{k}} = \frac{1}{2}\begin{pmatrix} s_{1,\boldsymbol{k}} & -s_{1,\boldsymbol{k}} & -s_{2,\boldsymbol{k}} & s_{2,\boldsymbol{k}} \\ -1 & -1 & 1 & 1 \\ -s_{1,\boldsymbol{k}} & s_{1,\boldsymbol{k}} & -s_{2,\boldsymbol{k}} & s_{2,\boldsymbol{k}} \\ 1 & 1 & 1 & 1 \end{pmatrix}, \tag{2.128}$$

with

$$\begin{aligned} s_{1,\boldsymbol{k}} = \operatorname{sign}(\eta_{2,\boldsymbol{k}})\,\operatorname{sgn}\Big(&2\lambda\,\operatorname{Re}\left\{(-\alpha_{\boldsymbol{k}} + \beta_{\boldsymbol{k}})\operatorname{sgn}(\eta_{2,\boldsymbol{k}}^*)\right\} \\ &+ 2i\sqrt{\lambda^2 - |\eta_{2,\boldsymbol{k}}|^2}\,\operatorname{Im}\left\{(-\alpha_{\boldsymbol{k}} + \beta_{\boldsymbol{k}})\operatorname{sgn}(\eta_{2,\boldsymbol{k}}^*)\right\}\Big) , \end{aligned} \tag{2.129a}$$

$$\begin{aligned} s_{2,\boldsymbol{k}} = \operatorname{sign}(\eta_{1,\boldsymbol{k}})\,\operatorname{sgn}\Big(&2\lambda\,\operatorname{Re}\left\{(\alpha_{\boldsymbol{k}} + \beta_{\boldsymbol{k}})\operatorname{sgn}(\eta_{1,\boldsymbol{k}}^*)\right\} \\ &+ 2i\sqrt{\lambda^2 - |\eta_{1,\boldsymbol{k}}|^2}\,\operatorname{Im}\left\{(\alpha_{\boldsymbol{k}} + \beta_{\boldsymbol{k}})\operatorname{sgn}(\eta_{1,\boldsymbol{k}}^*)\right\}\Big) . \end{aligned} \tag{2.129b}$$

The resulting diagonal matrix is

$$\boldsymbol{\Omega}_{\boldsymbol{k}}^2 = \begin{pmatrix} (\omega_{\boldsymbol{k},1})^2 & 0 & 0 & 0 \\ 0 & (\omega_{\boldsymbol{k},2})^2 & 0 & 0 \\ 0 & 0 & (\omega_{\boldsymbol{k},3})^2 & 0 \\ 0 & 0 & 0 & (\omega_{\boldsymbol{k},4})^2 \end{pmatrix}, \tag{2.130}$$

which has the squares of the magnon energies as its elements as will become clear later. Using the transformation (2.127) and our explicit expressions for $\tilde{\boldsymbol{V}}_{\boldsymbol{k}}$ and $\boldsymbol{S}_{\boldsymbol{k}}$ we obtain the analytic expressions for the squared magnon spectrum,

$$(\omega_{\boldsymbol{k},1})^2 = (\omega_{\boldsymbol{k},-}^-)^2 , \tag{2.131a}$$

$$(\omega_{\boldsymbol{k},2})^2 = (\omega_{\boldsymbol{k},+}^-)^2 , \tag{2.131b}$$

$$(\omega_{\boldsymbol{k},3})^2 = (\omega_{\boldsymbol{k},-}^+)^2 , \tag{2.131c}$$

$$(\omega_{\boldsymbol{k},4})^2 = (\omega_{\boldsymbol{k},+}^+)^2 , \tag{2.131d}$$

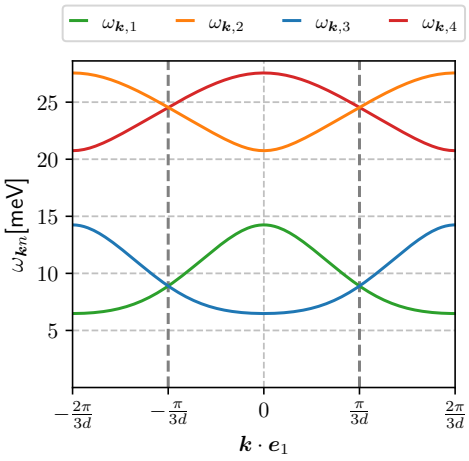

Figure 2.10: Dispersions of the four magnon branches given by Eqs. (2.131) and (2.132) for the arbitrary parameters $J = -12\text{meV}$, $K = \Gamma = 7\text{meV}$, $J_3 = 3\text{meV}$. Shown is the spectrum on the $\boldsymbol{e}_1$-axis perpendicular to the zigzag stripes. The border of the first magnetic Brillouin zone is marked by the thick dashed vertical lines. The individual functions $\omega_{\boldsymbol{k}n}$ are not periodic within the first Brillouin zone, but the full spectrum is.

where we defined

$$(\omega^{+}_{\boldsymbol{k},\pm})^2 = \lambda^2 + |\alpha_{\boldsymbol{k}} + \beta_{\boldsymbol{k}}|^2 - |\mu_{\boldsymbol{k}} + \nu_{\boldsymbol{k}}|^2 \pm \sqrt{2|\alpha_{\boldsymbol{k}} + \beta_{\boldsymbol{k}}|^2(2\lambda^2 - |\mu_{\boldsymbol{k}} + \nu_{\boldsymbol{k}}|^2) + 2\mathrm{Re}[(\alpha_{\boldsymbol{k}} + \beta_{\boldsymbol{k}})^2(\mu^*_{\boldsymbol{k}} + \nu^*_{\boldsymbol{k}})^2]}\,, \tag{2.132a}$$

$$(\omega^{-}_{\boldsymbol{k},\pm})^2 = \lambda^2 + |\alpha_{\boldsymbol{k}} - \beta_{\boldsymbol{k}}|^2 - |\mu_{\boldsymbol{k}} - \nu_{\boldsymbol{k}}|^2 \pm \sqrt{2|\alpha_{\boldsymbol{k}} - \beta_{\boldsymbol{k}}|^2(2\lambda^2 - |\mu_{\boldsymbol{k}} - \nu_{\boldsymbol{k}}|^2) + 2\mathrm{Re}[(\alpha_{\boldsymbol{k}} - \beta_{\boldsymbol{k}})^2(\mu^*_{\boldsymbol{k}} - \nu^*_{\boldsymbol{k}})^2]}\,. \tag{2.132b}$$

For an exemplary set of model parameters J, K, Γ, J_3, we show a plot of the dispersion in Fig. 2.10. Note that the individual functions $\omega_{\boldsymbol{k}n}$ are not periodic with respect to the magnetic Brillouin zone, but the set of all branches is. This is again due to our choice of Fourier transformation (2.62) which produces the phase factors discussed in Sec. 2.5.3. As a result, crossing of the boundary of the Brillouin zone results in a permutation of the pairs $\omega_{\boldsymbol{k},1} \leftrightarrow \omega_{\boldsymbol{k},3}$ and $\omega_{\boldsymbol{k},2} \leftrightarrow \omega_{\boldsymbol{k},4}$.

As long as we stay within the zigzag phase, it is safe to assume that none of the energies are negative because a negative magnon energy would imply an instability of the ordered ground state. We can therefore define the dispersion matrix

$$\boldsymbol{\Omega}_{\boldsymbol{k}} = \begin{pmatrix} \omega_{\boldsymbol{k},1} & 0 & 0 & 0 \\ 0 & \omega_{\boldsymbol{k},2} & 0 & 0 \\ 0 & 0 & \omega_{\boldsymbol{k},3} & 0 \\ 0 & 0 & 0 & \omega_{\boldsymbol{k},4} \end{pmatrix}, \tag{2.133}$$

as well as its square root

$$\boldsymbol{\Omega}_{\boldsymbol{k}}^{1/2} = \begin{pmatrix} (\omega_{\boldsymbol{k},1})^{1/2} & 0 & 0 & 0 \\ 0 & (\omega_{\boldsymbol{k},2})^{1/2} & 0 & 0 \\ 0 & 0 & (\omega_{\boldsymbol{k},3})^{1/2} & 0 \\ 0 & 0 & 0 & (\omega_{\boldsymbol{k},4})^{1/2} \end{pmatrix} , \tag{2.134}$$

and inverse square root

$$\boldsymbol{\Omega}_{\boldsymbol{k}}^{-1/2} = \begin{pmatrix} (\omega_{\boldsymbol{k},1})^{-1/2} & 0 & 0 & 0 \\ 0 & (\omega_{\boldsymbol{k},2})^{-1/2} & 0 & 0 \\ 0 & 0 & (\omega_{\boldsymbol{k},3})^{-1/2} & 0 \\ 0 & 0 & 0 & (\omega_{\boldsymbol{k},4})^{-1/2} \end{pmatrix} . \tag{2.135}$$

We can then write the second canonical transformation as

$$\begin{pmatrix} \tilde{\boldsymbol{X}}_K \\ \tilde{\boldsymbol{P}}_K \end{pmatrix} = \begin{pmatrix} \boldsymbol{S}_{\boldsymbol{k}} \boldsymbol{\Omega}_{\boldsymbol{k}}^{-1/2} & 0 \\ 0 & \boldsymbol{S}_{\boldsymbol{k}} \boldsymbol{\Omega}_{\boldsymbol{k}}^{1/2} \end{pmatrix} \begin{pmatrix} \boldsymbol{X}'_K \\ \boldsymbol{P}'_K \end{pmatrix} . \tag{2.136}$$

The transformed action (2.115) then assumes the block diagonal form

$$S_2[X', P'] = \frac{\beta}{2} \sum_K \begin{pmatrix} \boldsymbol{X}'_{-K} \\ \boldsymbol{P}'_{-K} \end{pmatrix}^T \begin{pmatrix} \boldsymbol{\Omega}_{\boldsymbol{k}} & \omega \\ -\omega & \boldsymbol{\Omega}_{\boldsymbol{k}} \end{pmatrix} \begin{pmatrix} \boldsymbol{X}'_K \\ \boldsymbol{P}'_K \end{pmatrix} . \tag{2.137}$$

We summarize the overall canonical transformation given by Eqs. (2.114) and (2.136) of the hermitian fields by

$$\begin{pmatrix} \boldsymbol{X}_K \\ \boldsymbol{P}_K \end{pmatrix} = \begin{pmatrix} \boldsymbol{T}_{\boldsymbol{k}}^{1/2} \, \boldsymbol{S}_{\boldsymbol{k}} \, \boldsymbol{\Omega}_{\boldsymbol{k}}^{-1/2} & 0 \\ 0 & \boldsymbol{T}_{\boldsymbol{k}}^{-1/2} \, \boldsymbol{S}_{\boldsymbol{k}} \, \boldsymbol{\Omega}_{\boldsymbol{k}}^{1/2} \end{pmatrix} \begin{pmatrix} \boldsymbol{X}'_K \\ \boldsymbol{P}'_K \end{pmatrix} . \tag{2.138}$$

The transformation matrix is of the form given in Eq. (2.113) with the submatrices

$$\boldsymbol{M}_{\boldsymbol{k}} = \boldsymbol{T}_{\boldsymbol{k}}^{1/2} \, \boldsymbol{S}_{\boldsymbol{k}} \, \boldsymbol{\Omega}_{\boldsymbol{k}}^{-1/2} , \tag{2.139a}$$

$$(\boldsymbol{M}_{\boldsymbol{k}}^{\dagger})^{-1} = \boldsymbol{T}_{\boldsymbol{k}}^{-1/2} \, \boldsymbol{S}_{\boldsymbol{k}} \, \boldsymbol{\Omega}_{\boldsymbol{k}}^{1/2} . \tag{2.139b}$$

2.6.4 Reparametrization to complex fields

Having diagonalized the quadratic action in the hermitian field parametrization, we now want to invert the hermitian field parametrization and express the action again in terms of complex fields $b_{Km}^{\dagger}$ and b_{Km} associated with bosonic creation and annihilation operators. We do this by applying the inverse of the transformation (2.100), which reads

$$\begin{pmatrix} \boldsymbol{X}'_K \\ \boldsymbol{P}'_K \end{pmatrix} = \mathbb{N}^{-1} \begin{pmatrix} \boldsymbol{b}_K \\ \bar{\boldsymbol{b}}_{-K} \end{pmatrix} , \tag{2.140}$$

with the 8×8 matrix

$$\mathbb{N}^{-1} = \frac{1}{\sqrt{2}} \begin{pmatrix} \mathbb{1} & \mathbb{1} \\ -i\mathbb{1} & i\mathbb{1} \end{pmatrix} . \tag{2.141}$$

Using this transformation, the quadratic action (2.137) becomes

$$\begin{aligned} S_2[b, \bar{b}] =& \frac{\beta}{2} \sum_K \begin{pmatrix} \bar{\boldsymbol{b}}_K \\ \boldsymbol{b}_{-K} \end{pmatrix}^T \begin{pmatrix} \boldsymbol{\Omega}_{\boldsymbol{k}} - i\omega & 0 \\ 0 & \boldsymbol{\Omega}_{\boldsymbol{k}} + i\omega \end{pmatrix} \begin{pmatrix} \boldsymbol{b}_K \\ \bar{\boldsymbol{b}}_{-K} \end{pmatrix} \\ =& \beta \sum_K \bar{\boldsymbol{b}}_K^T \left(\boldsymbol{\Omega}_{\boldsymbol{k}} - i\omega \right) \boldsymbol{b}_K , \end{aligned} \tag{2.142}$$

which is fully diagonal. In this expressions we see explicitly that the diagonal matrix $\boldsymbol{\Omega}_{\boldsymbol{k}}$ does indeed contain the magnon energies as we claimed earlier. In the last step we relabeled the summation index $K \to -K$ for the lower right matrix block and used $\boldsymbol{\Omega}_{\boldsymbol{k}} = \boldsymbol{\Omega}_{-\boldsymbol{k}}$. The complete Bogoliubov transformation from the Holstein-Primakoff bosons $\bar{\boldsymbol{a}}_K$ and $\boldsymbol{a}_K$ to the spin wave modes $\bar{\boldsymbol{b}}_K$ and $\boldsymbol{b}_K$ can now be expressed in matrix form as

$$\begin{pmatrix} \boldsymbol{a}_K \\ \bar{\boldsymbol{a}}_{-K} \end{pmatrix} = \mathbb{T}_{\boldsymbol{k}} \begin{pmatrix} \boldsymbol{b}_K \\ \bar{\boldsymbol{b}}_{-K} \end{pmatrix} , \tag{2.143}$$

where the 8×8 matrix $\mathbb{T}_{\boldsymbol{k}}$ is given by

$$\begin{aligned} \mathbb{T}_{\boldsymbol{k}} =& \mathbb{N} \begin{pmatrix} \boldsymbol{M}_{\boldsymbol{k}} & 0 \\ 0 & (\boldsymbol{M}_{\boldsymbol{k}}^\dagger)^{-1} \end{pmatrix} \mathbb{N}^{-1} \\ =& \frac{1}{2} \begin{pmatrix} \boldsymbol{M}_{\boldsymbol{k}} + (\boldsymbol{M}_{\boldsymbol{k}}^\dagger)^{-1} & \boldsymbol{M}_{\boldsymbol{k}} - (\boldsymbol{M}_{\boldsymbol{k}}^\dagger)^{-1} \\ \boldsymbol{M}_{\boldsymbol{k}} - (\boldsymbol{M}_{\boldsymbol{k}}^\dagger)^{-1} & \boldsymbol{M}_{\boldsymbol{k}} + (\boldsymbol{M}_{\boldsymbol{k}}^\dagger)^{-1} \end{pmatrix} , \end{aligned} \tag{2.144}$$

and the matrices $\boldsymbol{M}_{\boldsymbol{k}}$ and $(\boldsymbol{M}_{\boldsymbol{k}}^\dagger)^{-1}$ are given in Eqs. (2.139). Analytical expressions for these matrices can be written as

$$\boldsymbol{M}_{\boldsymbol{k}} = \left(\begin{array}{cc|cc} s_{1,\boldsymbol{k}}\vartheta_{\boldsymbol{k}}^+ - \vartheta_{\boldsymbol{k}}^- & -\vartheta_{\boldsymbol{k}}^- - s_{1,\boldsymbol{k}}\vartheta_{\boldsymbol{k}}^+ & -\varphi_{\boldsymbol{k}}^- - s_{2,\boldsymbol{k}}\varphi_{\boldsymbol{k}}^+ & s_{2,\boldsymbol{k}}\varphi_{\boldsymbol{k}}^+ - \varphi_{\boldsymbol{k}}^- \\ s_{1,\boldsymbol{k}}\vartheta_{\boldsymbol{k}}^{-*} - \vartheta_{\boldsymbol{k}}^+ & -\vartheta_{\boldsymbol{k}}^+ - s_{1,\boldsymbol{k}}\vartheta_{\boldsymbol{k}}^{-*} & \varphi_{\boldsymbol{k}}^+ + s_{2,\boldsymbol{k}}\varphi_{\boldsymbol{k}}^{-*} & \varphi_{\boldsymbol{k}}^+ - s_{2,\boldsymbol{k}}\varphi_{\boldsymbol{k}}^{-*} \\ \hline \vartheta_{\boldsymbol{k}}^- - s_{1,\boldsymbol{k}}\vartheta_{\boldsymbol{k}}^+ & \vartheta_{\boldsymbol{k}}^- + s_{1,\boldsymbol{k}}\vartheta_{\boldsymbol{k}}^+ & -\varphi_{\boldsymbol{k}}^- - s_{2,\boldsymbol{k}}\varphi_{\boldsymbol{k}}^+ & s_{2,\boldsymbol{k}}\varphi_{\boldsymbol{k}}^+ - \varphi_{\boldsymbol{k}}^- \\ \vartheta_{\boldsymbol{k}}^+ - s_{1,\boldsymbol{k}}\vartheta_{\boldsymbol{k}}^{-*} & \vartheta_{\boldsymbol{k}}^+ + s_{1,\boldsymbol{k}}\vartheta_{\boldsymbol{k}}^{-*} & \varphi_{\boldsymbol{k}}^+ + s_{2,\boldsymbol{k}}\varphi_{\boldsymbol{k}}^{-*} & \varphi_{\boldsymbol{k}}^+ - s_{2,\boldsymbol{k}}\varphi_{\boldsymbol{k}}^{-*} \end{array} \right) \boldsymbol{\Omega}_{\boldsymbol{k}}^{-1/2} \tag{2.145a}$$

and

$$(\boldsymbol{M}_{\boldsymbol{k}}^\dagger)^{-1} = \left(\begin{array}{cc|cc} q_{2,\boldsymbol{k}}\left(\vartheta_{\boldsymbol{k}}^- + s_{1,\boldsymbol{k}}\vartheta_{\boldsymbol{k}}^+\right) & q_{2,\boldsymbol{k}}\left(\vartheta_{\boldsymbol{k}}^- - s_{1,\boldsymbol{k}}\vartheta_{\boldsymbol{k}}^+\right) & q_{1,\boldsymbol{k}}\left(\varphi_{\boldsymbol{k}}^- - s_{2,\boldsymbol{k}}\varphi_{\boldsymbol{k}}^+\right) & q_{1,\boldsymbol{k}}\left(\varphi_{\boldsymbol{k}}^- + s_{2,\boldsymbol{k}}\varphi_{\boldsymbol{k}}^+\right) \\ -q_{2,\boldsymbol{k}}\left(\vartheta_{\boldsymbol{k}}^+ + s_{1,\boldsymbol{k}}\vartheta_{\boldsymbol{k}}^{-*}\right) & -q_{2,\boldsymbol{k}}\left(\vartheta_{\boldsymbol{k}}^+ - s_{1,\boldsymbol{k}}\vartheta_{\boldsymbol{k}}^{-*}\right) & q_{1,\boldsymbol{k}}\left(\varphi_{\boldsymbol{k}}^+ - s_{2,\boldsymbol{k}}\varphi_{\boldsymbol{k}}^{-*}\right) & q_{1,\boldsymbol{k}}\left(\varphi_{\boldsymbol{k}}^+ + s_{2,\boldsymbol{k}}\varphi_{\boldsymbol{k}}^{-*}\right) \\ \hline -q_{2,\boldsymbol{k}}\left(\vartheta_{\boldsymbol{k}}^- + s_{1,\boldsymbol{k}}\vartheta_{\boldsymbol{k}}^+\right) & -q_{2,\boldsymbol{k}}\left(\vartheta_{\boldsymbol{k}}^- - s_{1,\boldsymbol{k}}\vartheta_{\boldsymbol{k}}^+\right) & q_{1,\boldsymbol{k}}\left(\varphi_{\boldsymbol{k}}^- - s_{2,\boldsymbol{k}}\varphi_{\boldsymbol{k}}^+\right) & q_{1,\boldsymbol{k}}\left(\varphi_{\boldsymbol{k}}^- + s_{2,\boldsymbol{k}}\varphi_{\boldsymbol{k}}^+\right) \\ q_{2,\boldsymbol{k}}\left(\vartheta_{\boldsymbol{k}}^+ + s_{1,\boldsymbol{k}}\vartheta_{\boldsymbol{k}}^{-*}\right) & q_{2,\boldsymbol{k}}\left(\vartheta_{\boldsymbol{k}}^+ - s_{1,\boldsymbol{k}}\vartheta_{\boldsymbol{k}}^{-*}\right) & q_{1,\boldsymbol{k}}\left(\varphi_{\boldsymbol{k}}^+ - s_{2,\boldsymbol{k}}\varphi_{\boldsymbol{k}}^{-*}\right) & q_{1,\boldsymbol{k}}\left(\varphi_{\boldsymbol{k}}^+ + s_{2,\boldsymbol{k}}\varphi_{\boldsymbol{k}}^{-*}\right) \end{array} \right) \boldsymbol{\Omega}_{\boldsymbol{k}}^{1/2} , \tag{2.145b}$$

where we leave the last multiplications with the diagonal matrices $\boldsymbol{\Omega}_{\boldsymbol{k}}^{\pm 1/2}$ to the reader's imagination and defined

$$q_{i,\boldsymbol{k}} = \frac{1}{\sqrt{\lambda^2 - |\eta_{i,\boldsymbol{k}}|^2}}, \quad i = 1, 2, \tag{2.146}$$

as well as

$$\varphi_{\boldsymbol{k}}^{+} = \frac{1}{4}\left(\sqrt{\lambda - |\eta_{1,\boldsymbol{k}}|} + \sqrt{\lambda + |\eta_{1,\boldsymbol{k}}|}\right) , \tag{2.147a}$$

$$\varphi_{\boldsymbol{k}}^{-} = \frac{1}{4}\left(\sqrt{\lambda - |\eta_{1,\boldsymbol{k}}|} - \sqrt{\lambda + |\eta_{1,\boldsymbol{k}}|}\right) \mathrm{sgn}(\eta_{1,\boldsymbol{k}}) , \tag{2.147b}$$

$$\vartheta_{\boldsymbol{k}}^{+} = \frac{1}{4}\left(\sqrt{\lambda - |\eta_{2,\boldsymbol{k}}|} + \sqrt{\lambda + |\eta_{2,\boldsymbol{k}}|}\right) , \tag{2.147c}$$

$$\vartheta_{\boldsymbol{k}}^{-} = \frac{1}{4}\left(\sqrt{\lambda - |\eta_{2,\boldsymbol{k}}|} - \sqrt{\lambda + |\eta_{2,\boldsymbol{k}}|}\right) \mathrm{sgn}(\eta_{2,\boldsymbol{k}}) . \tag{2.147d}$$

2.6.5 Transformation of H_3

To calculate the magnon damping, we need to apply the Bogoliubov transformation to the leading interaction. The leading interaction is given by the three legged vertices represented by the cubic part of the Hamiltonian H_3 given in Eq. (2.78). Written as a Euclidian action, this reads

$$\begin{aligned}\mathcal{S}_3 = \beta\sqrt{\frac{4}{N}} \sum_{KK'K''} \sum_{\boldsymbol{G}} \delta_{\boldsymbol{k}+\boldsymbol{k}'+\boldsymbol{k}'',\boldsymbol{G}}\delta_{\omega+\omega'+\omega'',0} \Big\{ & \\ - V_{\boldsymbol{k}} \left[\bar{d}_{-K}\bar{a}_{-K'}a_{K''} + d_K a_{K'}\bar{a}_{-K''}\right] & \\ + e^{i\boldsymbol{G}\cdot\boldsymbol{d}_z} V_{\boldsymbol{k}}^{*} \left[\bar{c}_{-K}\bar{b}_{-K'}b_{K''} + c_K b_{K'}\bar{b}_{-K''}\right] & \\ + e^{i\boldsymbol{G}\cdot\boldsymbol{a}_1} V_{\boldsymbol{k}} \left[\bar{b}_{-K}\bar{c}_{-K'}c_{K''} + b_K c_{K'}\bar{c}_{-K''}\right] & \\ - e^{i\boldsymbol{G}\cdot\boldsymbol{d}_x} V_{\boldsymbol{k}}^{*} \left[\bar{a}_{-K}\bar{d}_{-K'}d_{K''} + a_K d_{K'}\bar{d}_{-K''}\right] \Big\} , &\end{aligned} \tag{2.148}$$

where we used that $\boldsymbol{U}_{\boldsymbol{k}} = 0$ at $\Gamma = K > 0$ and $\boldsymbol{V}_{\boldsymbol{k}}$ is given by Eq. (2.109b). We will write the transformation of the Holstein-Primakoff bosons $\bar{\boldsymbol{a}}_K$ and $\boldsymbol{a}_K$ to the original spin wave modes $\bar{\boldsymbol{b}}_K$ and $\boldsymbol{b}_K$ in tensor component form and therefore define the 8-dimensional complex vectors

$$\boldsymbol{\phi}_K = \begin{pmatrix} \boldsymbol{a}_K \\ \bar{\boldsymbol{a}}_{-K} \end{pmatrix} , \quad \boldsymbol{\psi}_K = \begin{pmatrix} \boldsymbol{b}_K \\ \bar{\boldsymbol{b}}_{-K} \end{pmatrix} . \tag{2.149}$$

The Bogoliubov transformation (2.143) can then be written as

$$\phi_K^{\mu} = \sum_{\mu'} \mathbb{T}_{\boldsymbol{k}}^{\mu\mu'} \psi_K^{\mu'}, \tag{2.150}$$

where the matrix $\mathbb{T}^{\mu\mu'}_{\boldsymbol{k}}$ is defined in Eq. (2.144) and the Greek indices range from 1 to 8 and enumerate the vector- and matrix components. Following this logic, we rewrite the cubic action (2.148) in tensor form as

$$\begin{aligned} S_3[\phi] =& \beta\sqrt{\frac{4}{N}} \sum_{KK'K''} \sum_{\boldsymbol{G}} \delta_{\boldsymbol{k}+\boldsymbol{k}'+\boldsymbol{k}'',\boldsymbol{G}} \delta_{\omega+\omega'+\omega'',0} \\ & \times \sum_{\mu\nu\lambda} \frac{1}{3!} \Gamma^{\mu\nu\lambda}(\boldsymbol{k},\boldsymbol{k}',\boldsymbol{k}'') \phi^{\mu}_{K} \phi^{\nu}_{K'} \phi^{\lambda}_{K''} \,. \end{aligned} \tag{2.151}$$

Here, the vertex $\Gamma^{\mu\nu\lambda}(\boldsymbol{k},\boldsymbol{k}',\boldsymbol{k}')$ is symmetrized with respect to permutation of the complex variables $\phi^{\mu}_{K}, \phi^{\nu}_{K'}, \phi^{\lambda}_{K''}$. Most of its $8^3 = 512$ components vanish, and there are only 48 non-zero components, namely

$$\begin{aligned} &\Gamma^{851}(\boldsymbol{k},\boldsymbol{k}',\boldsymbol{k}'') = \Gamma^{815}(\boldsymbol{k},\boldsymbol{k}',\boldsymbol{k}'') \\ &= \Gamma^{415}(\boldsymbol{k},\boldsymbol{k}',\boldsymbol{k}'') = \Gamma^{451}(\boldsymbol{k},\boldsymbol{k}',\boldsymbol{k}'') = -V_{\boldsymbol{k}}, \end{aligned} \tag{2.152a}$$

$$\begin{aligned} &\Gamma^{581}(\boldsymbol{k},\boldsymbol{k}',\boldsymbol{k}'') = \Gamma^{185}(\boldsymbol{k},\boldsymbol{k}',\boldsymbol{k}'') \\ &= \Gamma^{145}(\boldsymbol{k},\boldsymbol{k}',\boldsymbol{k}'') = \Gamma^{541}(\boldsymbol{k},\boldsymbol{k}',\boldsymbol{k}'') = -V_{\boldsymbol{k}'}, \end{aligned} \tag{2.152b}$$

$$\begin{aligned} &\Gamma^{518}(\boldsymbol{k},\boldsymbol{k}',\boldsymbol{k}'') = \Gamma^{158}(\boldsymbol{k},\boldsymbol{k}',\boldsymbol{k}'') \\ &= \Gamma^{154}(\boldsymbol{k},\boldsymbol{k}',\boldsymbol{k}'') = \Gamma^{514}(\boldsymbol{k},\boldsymbol{k}',\boldsymbol{k}'') = -V_{\boldsymbol{k}''}, \end{aligned} \tag{2.152c}$$

$$\begin{aligned} &\Gamma^{762}(\boldsymbol{k},\boldsymbol{k}',\boldsymbol{k}'') = \Gamma^{726}(\boldsymbol{k},\boldsymbol{k}',\boldsymbol{k}'') \\ &= \Gamma^{326}(\boldsymbol{k},\boldsymbol{k}',\boldsymbol{k}'') = \Gamma^{362}(\boldsymbol{k},\boldsymbol{k}',\boldsymbol{k}'') = e^{i(\boldsymbol{k}+\boldsymbol{k}'+\boldsymbol{k}'')\cdot\boldsymbol{d}_z} V^*_{\boldsymbol{k}}, \end{aligned} \tag{2.152d}$$

$$\begin{aligned} &\Gamma^{672}(\boldsymbol{k},\boldsymbol{k}',\boldsymbol{k}'') = \Gamma^{276}(\boldsymbol{k},\boldsymbol{k}',\boldsymbol{k}'') \\ &= \Gamma^{236}(\boldsymbol{k},\boldsymbol{k}',\boldsymbol{k}'') = \Gamma^{632}(\boldsymbol{k},\boldsymbol{k}',\boldsymbol{k}'') = e^{i(\boldsymbol{k}+\boldsymbol{k}'+\boldsymbol{k}'')\cdot\boldsymbol{d}_z} V^*_{\boldsymbol{k}'}, \end{aligned} \tag{2.152e}$$

$$\begin{aligned} &\Gamma^{627}(\boldsymbol{k},\boldsymbol{k}',\boldsymbol{k}'') = \Gamma^{267}(\boldsymbol{k},\boldsymbol{k}',\boldsymbol{k}'') \\ &= \Gamma^{263}(\boldsymbol{k},\boldsymbol{k}',\boldsymbol{k}'') = \Gamma^{623}(\boldsymbol{k},\boldsymbol{k}',\boldsymbol{k}'') = e^{i(\boldsymbol{k}+\boldsymbol{k}'+\boldsymbol{k}'')\cdot\boldsymbol{d}_z} V^*_{\boldsymbol{k}''}, \end{aligned} \tag{2.152f}$$

$$\begin{aligned} &\Gamma^{673}(\boldsymbol{k},\boldsymbol{k}',\boldsymbol{k}'') = \Gamma^{637}(\boldsymbol{k},\boldsymbol{k}',\boldsymbol{k}'') \\ &= \Gamma^{237}(\boldsymbol{k},\boldsymbol{k}',\boldsymbol{k}'') = \Gamma^{273}(\boldsymbol{k},\boldsymbol{k}',\boldsymbol{k}'') = e^{i(\boldsymbol{k}+\boldsymbol{k}'+\boldsymbol{k}'')\cdot\boldsymbol{a}_1} V_{\boldsymbol{k}}, \end{aligned} \tag{2.152g}$$

$$\begin{aligned} &\Gamma^{763}(\boldsymbol{k},\boldsymbol{k}',\boldsymbol{k}'') = \Gamma^{367}(\boldsymbol{k},\boldsymbol{k}',\boldsymbol{k}'') \\ &= \Gamma^{327}(\boldsymbol{k},\boldsymbol{k}',\boldsymbol{k}'') = \Gamma^{723}(\boldsymbol{k},\boldsymbol{k}',\boldsymbol{k}'') = e^{i(\boldsymbol{k}+\boldsymbol{k}'+\boldsymbol{k}'')\cdot\boldsymbol{a}_1} V_{\boldsymbol{k}'}, \end{aligned} \tag{2.152h}$$

$$\begin{aligned} &\Gamma^{736}(\boldsymbol{k},\boldsymbol{k}',\boldsymbol{k}'') = \Gamma^{376}(\boldsymbol{k},\boldsymbol{k}',\boldsymbol{k}'') \\ &= \Gamma^{372}(\boldsymbol{k},\boldsymbol{k}',\boldsymbol{k}'') = \Gamma^{732}(\boldsymbol{k},\boldsymbol{k}',\boldsymbol{k}'') = e^{i(\boldsymbol{k}+\boldsymbol{k}'+\boldsymbol{k}'')\cdot\boldsymbol{a}_1} V_{\boldsymbol{k}''}, \end{aligned} \tag{2.152i}$$

$$\Gamma^{584}(\boldsymbol{k},\boldsymbol{k'},\boldsymbol{k''}) = \Gamma^{548}(\boldsymbol{k},\boldsymbol{k'},\boldsymbol{k''})$$
$$= \Gamma^{148}(\boldsymbol{k},\boldsymbol{k'},\boldsymbol{k''}) = \Gamma^{362}(\boldsymbol{k},\boldsymbol{k'},\boldsymbol{k''}) = -e^{i(\boldsymbol{k}+\boldsymbol{k'}+\boldsymbol{k''})\cdot\boldsymbol{d}_x} V^*_{\boldsymbol{k}}, \tag{2.152j}$$

$$\Gamma^{854}(\boldsymbol{k},\boldsymbol{k'},\boldsymbol{k''}) = \Gamma^{458}(\boldsymbol{k},\boldsymbol{k'},\boldsymbol{k''})$$
$$= \Gamma^{418}(\boldsymbol{k},\boldsymbol{k'},\boldsymbol{k''}) = \Gamma^{814}(\boldsymbol{k},\boldsymbol{k'},\boldsymbol{k''}) = -e^{i(\boldsymbol{k}+\boldsymbol{k'}+\boldsymbol{k''})\cdot\boldsymbol{d}_x} V^*_{\boldsymbol{k'}}, \tag{2.152k}$$

$$\Gamma^{845}(\boldsymbol{k},\boldsymbol{k'},\boldsymbol{k''}) = \Gamma^{485}(\boldsymbol{k},\boldsymbol{k'},\boldsymbol{k''})$$
$$= \Gamma^{481}(\boldsymbol{k},\boldsymbol{k'},\boldsymbol{k''}) = \Gamma^{841}(\boldsymbol{k},\boldsymbol{k'},\boldsymbol{k''}) = -e^{i(\boldsymbol{k}+\boldsymbol{k'}+\boldsymbol{k''})\cdot\boldsymbol{d}_x} V^*_{\boldsymbol{k''}}. \tag{2.152l}$$

Using the Bogoliubov transformation in the tensor form given in Eq. (2.150), we can write the action (2.151) as

$$S_3[\psi] = \beta\sqrt{\frac{4}{N}} \sum_{KK'K''} \sum_{\boldsymbol{G}} \delta_{\boldsymbol{k}+\boldsymbol{k'}+\boldsymbol{k''},\boldsymbol{G}} \delta_{\omega+\omega'+\omega'',0} \times \sum_{\mu\nu\lambda} \frac{1}{3!} \tilde{\Gamma}^{\mu\nu\lambda}(\boldsymbol{k},\boldsymbol{k'},\boldsymbol{k'}) \psi^{\mu}_{K} \psi^{\nu}_{K'} \psi^{\lambda}_{K''} \,, \tag{2.153}$$

with the transformed vertices

$$\tilde{\Gamma}^{\mu\nu\lambda}(\boldsymbol{k},\boldsymbol{k'},\boldsymbol{k''}) = \sum_{\mu'\nu'\lambda'} \Gamma^{\mu'\nu'\lambda'}(\boldsymbol{k},\boldsymbol{k'},\boldsymbol{k''}) \mathbb{T}^{\mu'\mu}_{\boldsymbol{k}} \mathbb{T}^{\nu'\nu}_{\boldsymbol{k'}} \mathbb{T}^{\lambda'\lambda}_{\boldsymbol{k''}} \,. \tag{2.154}$$

The analytical expressions for $\tilde{\Gamma}^{\mu\nu\lambda}(\boldsymbol{k},\boldsymbol{k'},\boldsymbol{k''})$ are long enough to discourage us from proceeding analytically. When we calculate the magnon damping in the next section, we will therefore translate our analytical expressions for the transformation matrices $\mathbb{T}^{\mu\mu'}_{\boldsymbol{k}}$ to numerical matrices at the desired values of $\boldsymbol{k}$. Still, this leaves us with an advantage compared to a fully numerical treatment, since we do not have to perform the diagonalization for each $\boldsymbol{k}$-point separately but can merely substitute numerical values in our analytical expressions.

2.7 Magnon damping at zero temperature

Let us recall how quasiparticle damping is related to the imaginary part of the self energy. The retarded Green's function for the magnons can be written as

$$G^{\mathrm{ret}}_{\boldsymbol{k}n}(\omega) = \frac{1}{\omega - \omega_{\boldsymbol{k}n} - \Sigma^{\mathrm{ret}}_{\boldsymbol{k}n}(\omega)} \,, \tag{2.155}$$

where $\omega_{\boldsymbol{k}n}$ are the magnon energies and $\Sigma^{\mathrm{ret}}_{\boldsymbol{k}n}(\omega)$ is the retarded self energy of the magnons. The real time representation of the retarded Green's function

is given by the Fourier transform, and may be written as

$$\begin{aligned} G^{\mathrm{ret}}_{\boldsymbol{k}n}(t) &= \int_{-\infty}^{\infty} \frac{d\omega}{2\pi}\, G^{\mathrm{ret}}_{\boldsymbol{k}n}(\omega) e^{-i\omega t} \\ &= e^{-i\omega_{\boldsymbol{k}n} t} \int_{-\infty}^{\infty} \frac{d\omega}{2\pi}\, G^{\mathrm{ret}}_{\boldsymbol{k}n}(\omega_{\boldsymbol{k}n} - \omega) e^{-i\omega t} \\ &= e^{-i\omega_{\boldsymbol{k}n} t} \int_{-\infty}^{\infty} \frac{d\omega}{2\pi}\, \frac{-e^{-i\omega t}}{\omega + \Sigma^{\mathrm{ret}}_{\boldsymbol{k}n}(\omega_{\boldsymbol{k}n} - \omega)} \,. \end{aligned} \tag{2.156}$$

From the first to the second line, we shifted the integration variable $\omega \to \omega_{\boldsymbol{k}n} - \omega$. In the simplest approximation, we neglect the momentum dependence of the self energy in the integral, i.e. $\Sigma^{\mathrm{ret}}_{\boldsymbol{k}n}(\omega_{\boldsymbol{k}n} - \omega) \approx \Sigma^{\mathrm{ret}}_{\boldsymbol{k}n}(\omega_{\boldsymbol{k}n})$. Anticipating that $\mathrm{Im}\, \Sigma^{\mathrm{ret}}_{\boldsymbol{k}n}(\omega_{\boldsymbol{k}n}) < 0$, we can evaluate the Fourier transform and write

$$\begin{aligned} G^{\mathrm{ret}}_{\boldsymbol{k}n}(t) &= -e^{-i\omega_{\boldsymbol{k}n} t} i\theta(t)\; e^{-i\Sigma^{\mathrm{ret}}_{\boldsymbol{k}n}(\omega_{\boldsymbol{k}n}) t} \\ &= -i\theta(t)\; e^{-i(\omega_{\boldsymbol{k}n} + R_{\boldsymbol{k}n}) t}\; e^{-\gamma_{\boldsymbol{k}n} t} \,, \end{aligned} \tag{2.157}$$

where we separated the real and imaginary part of $\Sigma^{\mathrm{ret}}_{\boldsymbol{k}n}(\omega_{\boldsymbol{k}n})$ as

$$R_{\boldsymbol{k}n} \equiv \mathrm{Re}\, \Sigma^{\mathrm{ret}}_{\boldsymbol{k}n}(\omega_{\boldsymbol{k}n}) \,, \tag{2.158a}$$

$$\gamma_{\boldsymbol{k}n} \equiv -\mathrm{Im}\, \Sigma^{\mathrm{ret}}_{\boldsymbol{k}n}(\omega_{\boldsymbol{k}n}) \,. \tag{2.158b}$$

We see that $\gamma_{\boldsymbol{k}n}$ is the decay rate of the retarded Green's function. As long as the decay rate is small compared to the frequency $\omega_{\boldsymbol{k}n} + R_{\boldsymbol{k}n}$, we may call $\gamma_{\boldsymbol{k}n}$ the damping of the corresponding mode. The real part $R_{\boldsymbol{k}n}$ of the self energy shifts the magnon energies and thus contributes to the damping only at higher orders. We will neglect this part in our calculations and comment on the implications of this approximation in the discussion in Sec. 2.9.1.

2.7.1 Born approximation

To proceed, we derive expressions for the magnon damping to leading order in perturbation theory, which we refer to as the Born approximation. The self energy is then given by the Feynman diagrams with two interaction vertices and two external legs. Of these, only those diagrams where the outer indices connect to different vertices produce an imaginary part. These diagrams are given by

$$\Sigma^{(a)}_n(K) = -\frac{2}{2\beta}(3!)^2$$  , (2.159a)

$$\Sigma^{(b)}_n(K) = -\frac{1}{2\beta}(3!)^2$$  , (2.159b)

$$\Sigma^{(c)}_n(K) = -\frac{1}{2\beta}(3!)^2$$  . (2.159c)

Here, a directed line between two vertices represents the free magnon propagator,

$$G_n^0(K) = \frac{1}{i\omega - \omega_{\boldsymbol{k}n}} \,. \tag{2.160}$$

The vertices are given by the cubic action (2.153). The factor of $(3!)^2$ arises because we symmetrized the three-point vertex in Eq. (2.151). This symmetry carries over to the transformed three-point vertex (2.154), giving (3!) equivalent possibilities to connect the propagator indices to each vertex. We write out the first contribution as

$$\begin{aligned}\Sigma_n^{(a)}(K) = &- \frac{4\beta}{N(3!)^2} \sum_{K'} \sum_{n'm} (3!)^2 \frac{1}{\beta} G^0_{n'}(K') \frac{1}{\beta} G^0_m(G_1 - K - K') \\ &\qquad \times \left| \tilde{\Gamma}^{nn'm+4}(\boldsymbol{k}, \boldsymbol{k'}, \boldsymbol{G}_1 - \boldsymbol{k} - \boldsymbol{k'}) \right|^2 \\ = &- \frac{4}{N} \sum_{\boldsymbol{k'}} \sum_{n'm} \left| \tilde{\Gamma}^{nn'm+4}(\boldsymbol{k}, \boldsymbol{k'}, \boldsymbol{G}_1 - \boldsymbol{k} - \boldsymbol{k'}) \right|^2 \\ &\qquad \times \frac{1}{\beta} \sum_{\omega'} \frac{1}{\omega_{\boldsymbol{k'}n'} - i\omega'} \frac{1}{\omega_{\boldsymbol{G}_1 - \boldsymbol{k} - \boldsymbol{k'}, m} - i\omega - i\omega'} .\end{aligned} \tag{2.161}$$

Here we have defined the reciprocal lattice vector $\boldsymbol{G}_1$ via the requirement that $\boldsymbol{G}_1 - \boldsymbol{k} - \boldsymbol{k'}$ lies within the first Brillouin zone. This is because in the cubic action (2.153), momentum is conserved modulo reciprocal lattice vectors and the momentum sums go over the first Brillouin zone. The indices n' and m sum over the four values 1, 2, 3, 4, and the index $m+4$ consequently takes the values 5, 6, 7, 8. The reason for a separate treatment of these two sectors is that incoming propagator lines connect via Wick's theorem to a creation operator of the interaction vertex. In the collective variable ψ_K (2.149), the creation operators are listed in the positions 1...4. Similarly, the annihilation operators listed in the positions 5...8 correspond to outgoing lines.

The sum over the bosonic Matsubara frequencies in above Eq. (2.161) can be done analytically by using the residue theorem, giving

$$\begin{aligned}\Sigma_n^{(a)}(K) = &- \frac{4}{N} \sum_{\boldsymbol{k'}} \sum_{n'm} \left| \tilde{\Gamma}^{nn'm+4}(\boldsymbol{k}, \boldsymbol{k'}, \boldsymbol{G}_1 - \boldsymbol{k} - \boldsymbol{k'}) \right|^2 \\ &\qquad \times \frac{n(\omega_{\boldsymbol{k'}n'}) - n(\omega_{\boldsymbol{G}_1 - \boldsymbol{k} - \boldsymbol{k'}, m})}{\omega_{\boldsymbol{k'}n'} - \omega_{\boldsymbol{G}_1 - \boldsymbol{k} - \boldsymbol{k'}, m} + i\omega} \,,\end{aligned} \tag{2.162}$$

with the Bose function

$$n(E) = \frac{1}{e^{\beta E} - 1} \,. \tag{2.163}$$

The retarded self energy is obtained by the Wick rotation $i\omega \to \omega + i0^+$, where 0^+ denotes an infinitesimal positive real number. Identifying the

representation of the Dirac-delta by the Sokhotski–Plemelj formula,

$$\frac{1}{x \pm i0^+} = \mathcal{P}\left(\frac{1}{x}\right) \mp i\pi\delta(x)\,, \tag{2.164}$$

where $\mathcal{P}$ denotes the principal value, we find

$$\begin{aligned}\operatorname{Im}\Sigma_n^{(a),ret}(\boldsymbol{k},\omega) =& \operatorname{Im}\Sigma_n^{(a)}(\boldsymbol{k},\omega+i0^+)\\ =& \pi\frac{4}{N}\sum_{\boldsymbol{k'}}\sum_{n'm}\left|\tilde{\Gamma}^{nn'm+4}(\boldsymbol{k},\boldsymbol{k'},\boldsymbol{G}_1-\boldsymbol{k}-\boldsymbol{k'})\right|^2\\ &\times\left[n(\omega_{\boldsymbol{k'}n'})-n(\omega_{\boldsymbol{G}_1-\boldsymbol{k}-\boldsymbol{k'}m})\right]\\ &\times\delta\left(\omega+\omega_{\boldsymbol{k'}n'}-\omega_{\boldsymbol{G}_1-\boldsymbol{k}-\boldsymbol{k'}m}\right).\end{aligned} \tag{2.165a}$$

The other two contributions to the imaginary part of the self energy given in Eqs. (2.159) can be evaluated analogously, with the results

$$\begin{aligned}\operatorname{Im}\Sigma_n^{(b),ret}(\boldsymbol{k},\omega) =& \operatorname{Im}\Sigma_n^{(b)}(\boldsymbol{k},\omega+i0^+)\\ =& -\frac{\pi}{2}\frac{4}{N}\sum_{\boldsymbol{k'}}\sum_{n'm}\left|\tilde{\Gamma}^{n+4\,n'm}(-\boldsymbol{k},\boldsymbol{k'},\boldsymbol{G}_2+\boldsymbol{k}-\boldsymbol{k'})\right|^2\\ &\times\left[1+n(\omega_{\boldsymbol{k'}n'})+n(\omega_{\boldsymbol{G}_2+\boldsymbol{k}-\boldsymbol{k'}m})\right]\\ &\times\delta\left(\omega-\omega_{\boldsymbol{k'}n'}-\omega_{\boldsymbol{G}_2+\boldsymbol{k}-\boldsymbol{k'}m}\right),\end{aligned} \tag{2.165b}$$

$$\begin{aligned}\operatorname{Im}\Sigma_n^{(c),ret}(\boldsymbol{k},\omega) =& \operatorname{Im}\Sigma_n^{(c)}(\boldsymbol{k},\omega+i0^+)\\ =& \frac{\pi}{2}\frac{4}{N}\sum_{\boldsymbol{k'}}\sum_{n'm}\left|\tilde{\Gamma}^{nn'm}(\boldsymbol{k},\boldsymbol{k'},\boldsymbol{G}_1-\boldsymbol{k}-\boldsymbol{k'})\right|^2\\ &\times\left[1+n(\omega_{\boldsymbol{k'}n'})+n(\omega_{\boldsymbol{G}_1-\boldsymbol{k}-\boldsymbol{k'}m})\right]\\ &\times\delta\left(\omega+\omega_{\boldsymbol{k'}n'}+\omega_{\boldsymbol{G}_1-\boldsymbol{k}-\boldsymbol{k'}m}\right).\end{aligned} \tag{2.165c}$$

Here, the reciprocal lattice vector $\boldsymbol{G}_2$ must be chosen such that $\boldsymbol{G}_2+\boldsymbol{k}-\boldsymbol{k'}$ lies within the first Brillouin zone.

In the lowest order approximation for the damping $\gamma_{\boldsymbol{k}n}$ given in Eq. (2.158b), we need to evaluate the imaginary part of the self energy at $\omega=\omega_{\boldsymbol{k}n}$. Then, the Dirac-delta in $\operatorname{Im}\Sigma_n^{(c),ret}(\boldsymbol{k},\omega_{\boldsymbol{k}n})$ vanishes because all magnon energies are positive. Moreover, at zero temperature, the Bose functions in the above expression vanish. We are thus left with only one term stemming from $\operatorname{Im}\Sigma_n^{(b),ret}(\boldsymbol{k},\omega_{\boldsymbol{k}n})$, and get

$$\begin{aligned}\gamma_{\boldsymbol{k}n} =& \frac{\pi}{2}\frac{4}{N}\sum_{\boldsymbol{k'}}\sum_{n'm}\left|\tilde{\Gamma}^{n+4\,n'm}(-\boldsymbol{k},\boldsymbol{k'},\boldsymbol{G}_2+\boldsymbol{k}-\boldsymbol{k'})\right|^2\\ &\times\delta\left(\omega_{\boldsymbol{k}n}-\omega_{\boldsymbol{k'}n'}-\omega_{\boldsymbol{G}_2+\boldsymbol{k}-\boldsymbol{k'}m}\right).\end{aligned} \tag{2.166}$$

A remark about the reciprocal lattice vector $\boldsymbol{G}_2$ appearing in the above integral is appropriate here. Recall that that $\boldsymbol{G}_2$ ensures that all crystal

momenta lie within the first Brillouin zone. This is so because all momentum sums in the action go over momenta in the first Brillouin zone. In principle however, the analytical expressions for the couplings (2.108, 2.109) can be analytically continued beyond the first Brillouin zone. As discussed in Sec. 2.6.3, crossing of the border of a Brillouin zone then corresponds to switching the analytical expressions for the magnon branches pairwise with one another. It seems plausible that a similar principle might hold for the interaction vertices as well. Although we did not investigate this rigorously, we found that omitting the vector $\boldsymbol{G}_2$ in the numerical calculation does not alter the results up to switching of the magnon branches. In our publication [1] we used the results with $\boldsymbol{G}_2$ omitted in order to conform with our collaborators. For the sake of consistency, we will keep $\boldsymbol{G}_2$ in this thesis.

In the thermodynamic limit of a large system, $N \to \infty$, the crystal momentum becomes a continuous variable and momentum sums become integrals. The magnon damping (2.166) then reads

$$\gamma_{\boldsymbol{k}n} = \frac{\pi}{2} \sum_{n'm} \int_{\mathrm{BZ}} \frac{d^2k'}{V_{\mathrm{BZ}}} \left| \tilde{\Gamma}^{n+4\, n'm}(-\boldsymbol{k}, \boldsymbol{k'}, \boldsymbol{G}_2 + \boldsymbol{k} - \boldsymbol{k'}) \right|^2 \times \delta\left(\omega_{\boldsymbol{k}n} - \omega_{\boldsymbol{k'}n'} - \omega_{\boldsymbol{k}-\boldsymbol{k'}m}\right), \tag{2.167}$$

where the integral extends over the first Brillouin zone and

$$V_{\mathrm{BZ}} = \sqrt{3} \left(\frac{2\pi}{3d}\right)^2 \tag{2.168}$$

is the volume of the first Brillouin zone.

For a given set of model parameters in the overlap of the special region $\Gamma = K > 0$ with the zigzag phase, we can use our analytical expressions to construct an efficient numerical algorithm to compute the magnon damping given in Eq. (2.167). Substituting the model parameters and the relevant crystal momenta into the expression for the the transformed three-point vertices given in Eq. (2.154) and performing the tensor contraction numerically, we obtain a numerical tensor for $\tilde{\Gamma}^{n+4\, n'm}(-\boldsymbol{k}, \boldsymbol{k'}, \boldsymbol{G}_2 + \boldsymbol{k} - \boldsymbol{k'})$ at arbitrary $\boldsymbol{k}, \boldsymbol{k'}$. This procedure is much faster than a numerical diagonalization of the 8×8 propagator matrix at each point in $\boldsymbol{k}$-space. The remaining problem is then to solve the two-dimensional integral over the Brillouin zone appearing in the expression (2.167) for the magnon damping.

2.7.2 Numerical integration by triangulation

The Brillouin zone integrals in Eq. (2.167) are of the form

$$I = \int_A f(\boldsymbol{k})\, \delta(g(\boldsymbol{k}))\, dk_1\, dk_2\,. \tag{2.169}$$

In his doctoral thesis [69], Johannes Hick described a 'triangular method' to solve such integrals. He divides the area A into small triangles and approximates the functions $f(\boldsymbol{k})$ and $g(\boldsymbol{k})$ as linear on each triangle. These linear functions are uniquely determined on each triangle by the function values on the corners. If the triangles are small enough, this patchwork of linear functions provides a good approximation for the function on the whole area A. Consequently, the integral over the whole area A can be approximated by the sum of the integrals over the single triangles. The integral over a single triangle is simple because of the linearity of the involved functions. We note that although it seems likely that such a procedure has been used prior to Hick's thesis, we are not aware of any additional references. Hick formulated this procedure for a specific alignment of the triangles, and we wish to generalize this approach now. For this, we consider a general triangle with the coordinates of the corners given by

$$\boldsymbol{k}_a = \begin{pmatrix} k_{a,1} \\ k_{a,2} \end{pmatrix} \ , \ \boldsymbol{k}_b = \begin{pmatrix} k_{b,1} \\ k_{b,2} \end{pmatrix} \ , \ \boldsymbol{k}_c = \begin{pmatrix} k_{c,1} \\ k_{c,2} \end{pmatrix} \ . \tag{2.170}$$

We suppose that that the numerical values of the functions $f(\boldsymbol{k})$ and $g(\boldsymbol{k})$ at the corners of the triangle are known and denote them by f_a, f_b, f_c and g_a, g_b, g_c. Then the linearized version of $f(\boldsymbol{k})$ can be defined as

$$f^L(\boldsymbol{k}) = f(\boldsymbol{k}_a) + \boldsymbol{\nabla} f^L \cdot (\boldsymbol{k} - \boldsymbol{k}_a) \ , \tag{2.171}$$

where the constant gradient $\boldsymbol{\nabla} f^L$ is uniquely determined by f_a, f_b, f_c and the corner coordinates of the triangle. To find the relation between the gradient and the function values f_a, f_b, f_c, we write the linearized function alternatively as

$$f^L(\beta, \gamma) = f_a + \beta(f_b - f_a) + \gamma(f_c - f_a) \ , \tag{2.172}$$

where β and γ parameterize $\boldsymbol{k}$ such that

$$\boldsymbol{k} = \boldsymbol{k}_a + \beta(\boldsymbol{k}_b - \boldsymbol{k}_a) + \gamma(\boldsymbol{k}_c - \boldsymbol{k}_a) \ . \tag{2.173}$$

Note that β and γ are just different coordinates for the $\boldsymbol{k}$-space, chosen such that the corners of the triangle lie at $(0,0)$, $(0,1)$, and $(1,0)$. We define the relative vectors

$$\boldsymbol{r}(\boldsymbol{k}) = \boldsymbol{k} - \boldsymbol{k}_a \ , \tag{2.174a}$$
$$\boldsymbol{r}_b = \boldsymbol{k}_b - \boldsymbol{k}_a \ , \tag{2.174b}$$
$$\boldsymbol{r}_c = \boldsymbol{k}_c - \boldsymbol{k}_a \ , \tag{2.174c}$$

and write the transformation (2.173) in matrix form as

$$\boldsymbol{r} = (\boldsymbol{r}_b, \boldsymbol{r}_c) \begin{pmatrix} \beta \\ \gamma \end{pmatrix} = \boldsymbol{A} \begin{pmatrix} \beta \\ \gamma \end{pmatrix} \ , \tag{2.175}$$

with the matrix

$$\boldsymbol{A} = \begin{pmatrix} r_{b,1} & r_{c,1} \\ r_{b,2} & r_{c,2} \end{pmatrix} . \tag{2.176}$$

We invert the transformation (2.175) to find

$$\begin{pmatrix} \beta \\ \gamma \end{pmatrix} = \frac{1}{\det \boldsymbol{A}} \begin{pmatrix} r_{c,2} & -r_{c,1} \\ -r_{b,2} & r_{b,1} \end{pmatrix} \boldsymbol{r} , \tag{2.177}$$

where

$$\det \boldsymbol{A} = r_{b,1} r_{c,2} - r_{b,2} r_{c,1} . \tag{2.178}$$

We now substitute the expressions for β and γ given in the above transformation (2.177) in the expression (2.172) for the linearized function and find

$$\begin{aligned} f^L(\boldsymbol{k}) =& f_a + \frac{r_{c,2} r_1 - r_{c,1} r_2}{\det \boldsymbol{A}} (f_b - f_a) + \frac{-r_{b,2} r_1 + r_{b,1} r_2}{\det \boldsymbol{A}} (f_c - f_a) \\ =& f_a + \frac{r_{c,2}(f_b - f_a) - r_{b,2}(f_c - f_a)}{\det \boldsymbol{A}} r_1 \\ & + \frac{-r_{c,1}(f_b - f_a) + r_{b,1}(f_c - f_a)}{\det \boldsymbol{A}} r_2 \\ =& f_a + \frac{1}{\det \boldsymbol{A}} \left[(f_b - f_a) \begin{pmatrix} r_{c,2} \\ -r_{c,1} \end{pmatrix} + (f_c - f_a) \begin{pmatrix} -r_{b,2} \\ r_{b,1} \end{pmatrix} \right] \cdot \boldsymbol{r} . \end{aligned} \tag{2.179}$$

Comparing this with the expression (2.171), we thus find

$$\boldsymbol{\nabla} f^L = \frac{1}{\det \boldsymbol{A}} \left[(f_b - f_a) \begin{pmatrix} r_{c,2} \\ -r_{c,1} \end{pmatrix} + (f_c - f_a) \begin{pmatrix} -r_{b,2} \\ r_{b,1} \end{pmatrix} \right] . \tag{2.180}$$

In above derivation, one can of course replace f with g to find the linear approximation and the gradient of the function $g(\boldsymbol{k})$ on the triangle. To evaluate the integral (2.169), we first rewrite it to

$$I = \int_{\mathcal{C}} \frac{f(\boldsymbol{k}(l))}{|\boldsymbol{\nabla} g(\boldsymbol{k}(l))|} dl , \tag{2.181}$$

where the integral goes over those curves $\mathcal{C}$ which are defined by $g(\boldsymbol{k}) = 0$ and lie within the area A. dl is the corresponding line measure. We evaluate this integral for one triangle by using the linearized functions $f^L(\boldsymbol{k})$ and $g^L(\boldsymbol{k})$ as approximation, where $f^L(\boldsymbol{k})$ is given in Eq. (2.171) and $g^L(\boldsymbol{k})$ is defined analogously. Then, the gradient is constant, and the curve $\mathcal{C}$ is just a straight line. If this line does not cross the triangle, the integral vanishes. If $\mathcal{C}$ does cross the triangle, we need to find the two points where the line intersects the triangle. We call these points $\boldsymbol{p}_a$ and $\boldsymbol{p}_b$ as depicted in Fig. 2.11a. We

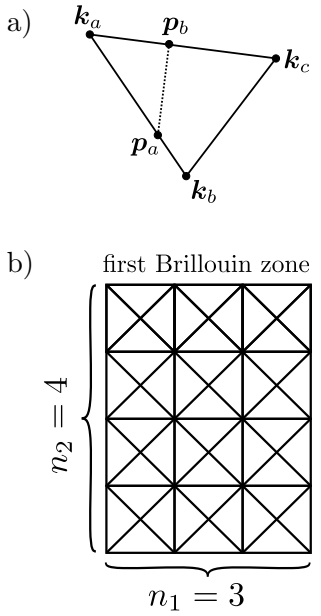

Figure 2.11: a) Three arbitrary points $\boldsymbol{k}_a, \boldsymbol{k}_b, \boldsymbol{k}_c$ define the corners of a triangle. The two points $\boldsymbol{p}_a, \boldsymbol{p}_b$ mark the intersection of the triangle with the line where $g^L(\boldsymbol{k})$ (the linearized version of $g(\boldsymbol{k})$ appearing in the Dirac-delta in the integral (2.169)) vanishes.
b) Subdivision of the first Brillouin zone into $4 \times n_1 \times n_2$ triangles, here shown for the case $n_1 = 3$, $n_2 = 4$.

thus get

$$\begin{aligned} I =& \frac{1}{|\boldsymbol{\nabla} g^L|} \int_{\boldsymbol{p}_a}^{\boldsymbol{p}_b} f^L(\boldsymbol{k}(l)) dl \\ =& \frac{1}{|\boldsymbol{\nabla} g^L|} \left[f_a |\boldsymbol{p}_b - \boldsymbol{p}_a| + \boldsymbol{\nabla} f^L \cdot \int_{\boldsymbol{p}_a}^{\boldsymbol{p}_b} (\boldsymbol{k}(l) - \boldsymbol{k}_a) dl \right] \\ =& \frac{|\boldsymbol{p}_b - \boldsymbol{p}_a|}{|\boldsymbol{\nabla} g^L|} \left[f_a + \boldsymbol{\nabla} f^L \cdot \left(\frac{\boldsymbol{p}_a + \boldsymbol{p}_b}{2} - \boldsymbol{k}_a \right) \right] , \end{aligned} \tag{2.182}$$

where the integral goes along the straight line connecting $\boldsymbol{p}_a$ and $\boldsymbol{p}_b$ and we substituted expression (2.171) for $f^L(\boldsymbol{k})$.

2.7.3 Numerical calculation of the magnon damping

Having established an approximate expression for the integral over a single triangle, we subdivide the first Brillouin zone into triangles as depicted exemplarily in Fig. 2.11b. In the expression (2.167) for the magnon damping at momentum $\boldsymbol{k}$, we integrate over $\boldsymbol{k'}$ and the function $g(\boldsymbol{k'})$ appears as $\omega_{\boldsymbol{k}n} - \omega_{\boldsymbol{k'}n'} - \omega_{\boldsymbol{k}-\boldsymbol{k'}m}$ and the function $f(\boldsymbol{k'})$ as $\left|\tilde{\Gamma}^{n+4\,n'm}(-\boldsymbol{k}, \boldsymbol{k'}, \boldsymbol{G}_2 + \boldsymbol{k} - \boldsymbol{k'})\right|^2$. We extract their numerical values for given $\boldsymbol{k}$ and for $\boldsymbol{k'}$ on all triangle corners from our analytical expressions given in Eq. (2.154) and Eqs. (2.132). To do so, we need to choose the model parameters first. With the restriction that the model parameters lie on the line $\Gamma = K > 0$ and within the

zigzag-phase, we arbitrarily choose

$$J = -12\text{meV}, \tag{2.183a}$$
$$K = \Gamma = 7\text{meV}, \tag{2.183b}$$
$$J_3 = 3\text{meV}. \tag{2.183c}$$

The position of this point within the phase diagram is visualized in Fig. 2.12. We want to plot the magnon damping for values of $\boldsymbol{k}$ along the path through

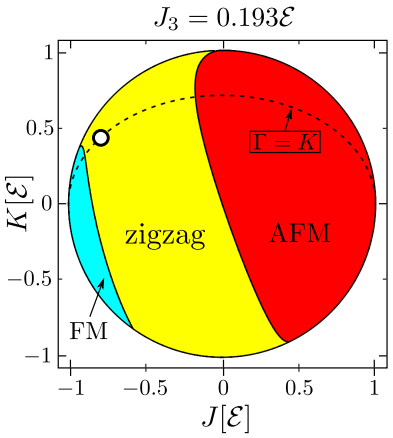

Figure 2.12: Phase diagram for $J_3 = 0.193\mathcal{E}$, which includes the point in parameter space given by Eqs. (2.183) used for numerical calculations. This point is marked by the white dot. The dashed line marks the region where $\Gamma = K$.

$\boldsymbol{k}$-space depicted in Fig. 2.13. This is the same path as was used in the prior literature [2]. Note that for the magnon damping, there is some redundancy in this choice of momentum path, because our Hamiltonian is periodic with respect to the first magnetic Brillouin zone. The momentum path is however adjusted for the Brillouin zone of the honeycomb lattice, which is twice as large as the magnetic Brillouin zone. We thus expect that the periodicity of the magnon damping leads to repeating patterns on path sections that are equivalent modulo the magnetic Brillouin zone, i.e. the section between X and Γ is equivalent to the section between Y and Γ'. We nevertheless keep the redundant parts of the momentum path because later, we evaluate

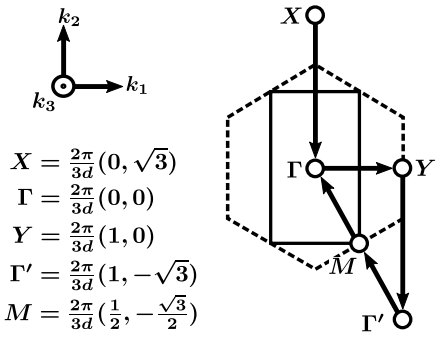

Figure 2.13: The momentum-space path used in our numerical evaluation of the magnon damping. The rectangle indicates the first magnetic Brillouin zone of the zigzag ground state. Note that the component k_1 is perpendicular to the zigzag stripes. The dashed hexagon indicates the Brillouin zone of the honeycomb lattice

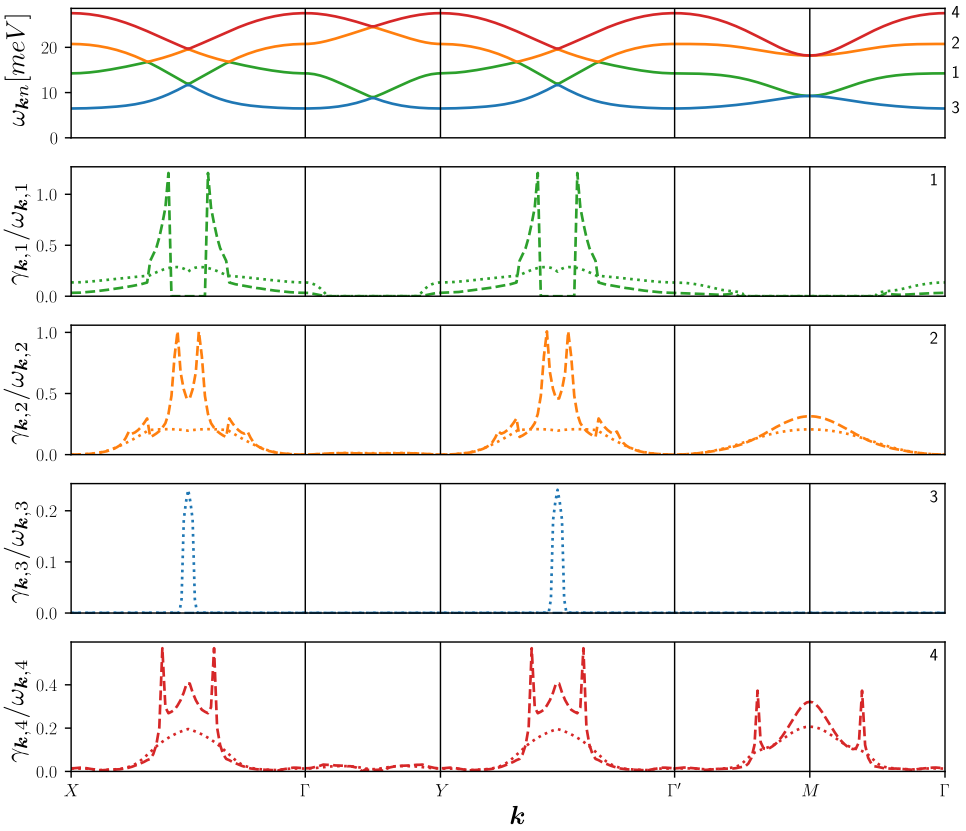

Figure 2.14: *Top panel:* Magnon energies along the momentum-contour depicted in Fig. 2.13. The numbers to the right of the graph label the branch index n as used in the analytical expressions. *Lower panels:* Magnon damping in Born approximation (dashed) and in iDE approximation (dotted). Here, the damping for each of the four magnon branches is shown in a separate graph.

the dynamical structure factor which is not periodic with respect to the magnetic Brillouin zone. The resulting magnon damping for each of the four branches is shown in Fig. 2.14.

2.7.4 Imaginary Dyson equation approach

The magnon damping in Born approximation shown in Fig. 2.14 shows van-Hove singularities [4, 70] in the form of pronounced peaks where the gradient of the argument in the Dirac-deltas in the expession for the magnon damping (2.167) vanishes. As these are unphysical artifacts of the Born approximation, we will self consistently consider a higher order approximation. Recall the approximate expression (2.157) for the retarded Greens function written in terms of the magnon energies and damping. In the derivation of this expression, we used an on-shell approximation $\Sigma^{\mathrm{ret}}_{\boldsymbol{k}n}(\omega_{\boldsymbol{k}n} - \omega) \approx \Sigma^{\mathrm{ret}}_{\boldsymbol{k}n}(\omega_{\boldsymbol{k}n})$. A better approximation would self-consistently take into account

the renormalization of the magnon energies, i.e. $\Sigma^{\mathrm{ret}}_{\boldsymbol{k}n}(\omega_{\boldsymbol{k}n} - \omega) \approx \Sigma^{\mathrm{ret}}_{\boldsymbol{k}n}(\tilde{\omega}_{\boldsymbol{k}n})$ with $\tilde{\omega}_{\boldsymbol{k}n} = \omega_{\boldsymbol{k}n} + \Sigma^{\mathrm{ret}}_{\boldsymbol{k}n}(\tilde{\omega}_{\boldsymbol{k}n})$. Neglecting the real part of the self energy leads to $\tilde{\omega}_{\boldsymbol{k}n} = \omega_{\boldsymbol{k}n} - i\gamma_{\boldsymbol{k}n}$. By the expression for the magnon damping in terms of the imaginary part of the self energy given in Eq. (2.157), we then get a self consistent equation for the magnon damping,

$$\gamma_{\boldsymbol{k}n} = -\mathrm{Im}\, \Sigma^{\mathrm{ret}}_{\boldsymbol{k}n}(\omega_{\boldsymbol{k}n} - i\gamma_{\boldsymbol{k}n}) \,. \tag{2.184}$$

This approximation was originally proposed as the imaginary Dyson equation (iDE) approach [71, 72], where the name refers to the fact that above formula is the imaginary part of the Dyson equation. We already derived perturbative expressions for the imaginary part of the self energy in Sec. 2.7.1. The substitution $\omega_{\boldsymbol{k}n} \to \omega_{\boldsymbol{k}n} - i\gamma_{\boldsymbol{k}n}$ does not alter the derivation in a major way. The only difference is that due to the imaginary part $i\gamma_{\boldsymbol{k}n}$ introduced to the inverse propagator, the Wick rotation produces Lorentzians instead of Dirac-Deltas in Eqs. (2.165). This can be taken into account by simply interpreting the Dirac-Deltas with complex argument as Lorentzians, i.e.

$$\delta(x - iy) \equiv \frac{1}{\pi} \frac{y}{x^2 + y^2} \,. \tag{2.185}$$

We thus find in analogy to Eq. (2.167) that

$$\gamma_{\boldsymbol{k}n} = \frac{\pi}{2} \sum_{n'm} \int_{\mathrm{BZ}} \frac{d^2k'}{V_{\mathrm{BZ}}} \left| \tilde{\Gamma}^{n+4\, n'm}(-\boldsymbol{k}, \boldsymbol{k'}, \boldsymbol{G}_2 + \boldsymbol{k} - \boldsymbol{k'}) \right|^2 \times \delta\left(\omega_{\boldsymbol{k}n} - i\gamma_{\boldsymbol{k}n} - \omega_{\boldsymbol{k'}n'} - \omega_{\boldsymbol{k}-\boldsymbol{k'}m}\right) \,. \tag{2.186}$$

This equation can be solved by successive iteration. We start with our Born result for $\gamma_{\boldsymbol{k}n}$. If $\gamma_{\boldsymbol{k}n} = 0$, the iteration can already be terminated. If $\gamma_{\boldsymbol{k}n} > 0$, the Dirac-delta becomes a Lorenzian and the integral can be solved numerically by the method of Gaussian quadratures. The new result for $\gamma_{\boldsymbol{k}n}$ is then used in the next iteration. In our case, the iteration converged everywhere after less than 30 iterations. We show the results as dotted lines in Fig. 2.14.

2.8 Dynamical structure factor

The dynamical structure factor $S^{\alpha\beta}(\boldsymbol{k}, \omega)$ plays a central role in connecting the quasiparticle properties to experimental results. Most notably for our purposes, it is straightforwardly connected to the neutron scattering intensity $\mathcal{I}(\boldsymbol{k}, \omega)$ by

$$\mathcal{I}(\boldsymbol{k}, \omega) = F^2(\boldsymbol{k}) \sum_{\alpha\beta} \left(\delta_{\alpha\beta} - k_\alpha k_\beta / k^2\right) S^{\alpha\beta}(\boldsymbol{k}, \omega) \,, \tag{2.187}$$

where $F(\boldsymbol{k})$ is a molecular or atomic structure factor. A detailed derivation can be found in Ref. [73]. The dynamical structure factor is the Fourier transform of the two-spin correlation function $\langle S_i^\alpha(t) S_j^\beta(0)\rangle$ and defined by

$$\begin{aligned} S^{\alpha\beta}(\boldsymbol{k},\omega) &= \int_{-\infty}^{\infty} \frac{dt}{2\pi} \frac{1}{N} \sum_{ij} \langle S_i^\alpha(t) S_j^\beta(0)\rangle e^{-i\boldsymbol{k}\cdot(\boldsymbol{R}_i-\boldsymbol{R}_j)+i\omega t} \\ &= \int \frac{dt}{2\pi} \langle S_{-\boldsymbol{k}}^\alpha(t) S_{\boldsymbol{k}}^\beta(0)\rangle e^{i\omega t} \ . \end{aligned} \tag{2.188}$$

In the second line we have introduced the Fourier components of the spin operators,

$$\boldsymbol{S}_{\boldsymbol{k}}(t) = \frac{1}{\sqrt{N}} \sum_i \boldsymbol{S}_i(t) e^{-i\boldsymbol{k}\cdot\boldsymbol{R}_i}. \tag{2.189}$$

In the planar basis $\{\boldsymbol{e}_1, \boldsymbol{e}_2, \boldsymbol{e}_3\}$ given in Eq. (2.9), the components of the Fourier transformed spin vector operators $\boldsymbol{S}_{\boldsymbol{k}}(t)$ are

$$S_{\boldsymbol{k}}^\alpha = \boldsymbol{e}_\alpha \cdot \boldsymbol{S}_{\boldsymbol{k}} = \frac{1}{\sqrt{N}} \sum_i e^{-i\boldsymbol{k}\cdot\boldsymbol{R}_i} \boldsymbol{e}_\alpha \cdot \boldsymbol{S}_i \ . \tag{2.190}$$

We wish to express those in terms of the bosons defined by the $1/S$ expansion (2.55). Because the $1/S$ expansion in the zigzag phase is given in terms of the local spin basis $\{\boldsymbol{t}_i^x, \boldsymbol{t}_i^y, \boldsymbol{m}_i\}$ defined in Eq. (2.46), we need to reexpress the basis vectors $\boldsymbol{e}_\alpha$. Noting that in our special parameter region $\Gamma = K > 0$ we have $s = -2$ and $r = 1$, we find from the explicit expressions of the local basis vectors given in Eqs. (2.82), (2.83) and from their relations to the global spin basis (2.47) that

$$\boldsymbol{e}_1 = -\boldsymbol{t}^x = -\boldsymbol{t}_i^x \ , \tag{2.191a}$$

$$\boldsymbol{e}_2 = \boldsymbol{m} = \begin{cases} \boldsymbol{m}_i & \text{for i on sublattices a, d ,} \\ -\boldsymbol{m}_i & \text{for i on sublattices b, c ,} \end{cases} \tag{2.191b}$$

$$\boldsymbol{e}_3 = \boldsymbol{t}^y = \begin{cases} \boldsymbol{t}_i^y & \text{for i on sublattices a, d ,} \\ -\boldsymbol{t}_i^y & \text{for i on sublattices b, c .} \end{cases} \tag{2.191c}$$

With these relations, we can write the Fourier transformed spin operators in the planar basis as

$$S_{\boldsymbol{k}}^1 = -\frac{1}{\sqrt{N}} \sum_i e^{-i\boldsymbol{k}\cdot\boldsymbol{R}_i} \ \boldsymbol{t}_i^x \cdot \boldsymbol{S}_i \ , \tag{2.192a}$$

$$S_{\boldsymbol{k}}^2 = \frac{1}{\sqrt{N}} \left[\sum_{i\in a,d} e^{-i\boldsymbol{k}\cdot\boldsymbol{R}_i} \ \boldsymbol{m}_i \cdot \boldsymbol{S}_i - \sum_{i\in c,b} e^{-i\boldsymbol{k}\cdot\boldsymbol{R}_i} \ \boldsymbol{m}_i \cdot \boldsymbol{S}_i \right] \ , \tag{2.192b}$$

$$S_{\boldsymbol{k}}^3 = \frac{1}{\sqrt{N}} \left[\sum_{i\in a,d} e^{-i\boldsymbol{k}\cdot\boldsymbol{R}_i} \ \boldsymbol{t}_i^y \cdot \boldsymbol{S}_i - \sum_{i\in c,b} e^{-i\boldsymbol{k}\cdot\boldsymbol{R}_i} \ \boldsymbol{t}_i^y \cdot \boldsymbol{S}_i \right] \ . \tag{2.192c}$$

In these expressions, we identify the spin components with the Holstein-Primakoff bosons in the $1/S$ expansion (2.55) as

$$\boldsymbol{t}_i^x \cdot \boldsymbol{S}_i = S_i^x = \frac{1}{2}\left(S_i^+ + S_i^-\right) = \frac{\sqrt{2S}}{2}\left(b_i + b_i^\dagger\right) + \mathcal{O}\left(S^0\right) \ , \tag{2.193a}$$

$$\boldsymbol{t}_i^y \cdot \boldsymbol{S}_i = S_i^y = \frac{1}{2i}\left(S_i^+ - S_i^-\right) = \frac{\sqrt{2S}}{2i}\left(b_i - b_i^\dagger\right) + \mathcal{O}\left(S^0\right) \ , \tag{2.193b}$$

$$\boldsymbol{m}_i \cdot \boldsymbol{S}_i = S_i^{\parallel} = S - n_i \ . \tag{2.193c}$$

From these relations it is transparent that, as expected, the longitudinal parts of the structure factor are of higher order in $1/S$ than the purely transversal components, as to lowest order we get $S^{\alpha\beta} \propto S$ and the expectation value of the number operator vanishes as $T \to 0$. We will therefore omit the longitudinal spin components. Substituting the above relations (2.193) into Eqs. (2.192) then yields for the transversal spin components

$$S_{\boldsymbol{k}}^1 = -\frac{\sqrt{2S}}{4}\sum_i e^{-i\boldsymbol{k}\cdot\boldsymbol{R}_i}\left(b_i + b_i^\dagger\right) \ , \tag{2.194a}$$

$$S_{\boldsymbol{k}}^3 = \frac{\sqrt{2S}}{4i}\left[\sum_{i\in a,d} e^{-i\boldsymbol{k}\cdot\boldsymbol{R}_i}\left(b_i - b_i^\dagger\right) - \sum_{i\in c,b} e^{-i\boldsymbol{k}\cdot\boldsymbol{R}_i}\left(b_i - b_i^\dagger\right)\right] \ . \tag{2.194b}$$

We can now identify the Fourier transformed bosons from Eq. (2.62). However, the structure factor is periodic with respect to the first Brillouin zone of the lattice, which is twice as large as the magnetic Brillouin zone of the zigzag ground state. We thus have to take into account the phase factors (2.66) associated with the non-periodicity of the boson operators. We do this by writing

$$\boldsymbol{k} = \tilde{\boldsymbol{k}} + \boldsymbol{G} \ , \tag{2.195}$$

such that $\boldsymbol{G}$ is a reciprocal lattice vector of the magnetic Bravais lattice and $\tilde{\boldsymbol{k}}$ lies in the first magnetic Brillouin zone. Then, the spin components (2.194)

can be written as

$$\begin{aligned} S^1_{\boldsymbol{k}} =& -\frac{\sqrt{2S}}{4}\Big[\left(a_{\tilde{\boldsymbol{k}}}+a^\dagger_{-\tilde{\boldsymbol{k}}}\right)+e^{i\boldsymbol{G}\cdot\boldsymbol{d_x}}\left(b_{\tilde{\boldsymbol{k}}}+b^\dagger_{-\tilde{\boldsymbol{k}}}\right) \\ &+e^{i\boldsymbol{G}\cdot\boldsymbol{a_1}}\left(c_{\tilde{\boldsymbol{k}}}+c^\dagger_{-\tilde{\boldsymbol{k}}}\right)+e^{i\boldsymbol{G}\cdot\boldsymbol{d_z}}\left(d_{\tilde{\boldsymbol{k}}}+d^\dagger_{-\tilde{\boldsymbol{k}}}\right)\Big] \\ \equiv& -\frac{\sqrt{2S}}{4}\sum_\mu \nu^\mu_{\boldsymbol{G}}\,\phi^\mu_{\tilde{\boldsymbol{k}}}\,, \end{aligned} \tag{2.196a}$$

$$\begin{aligned} S^3_{\boldsymbol{k}} =& \frac{\sqrt{2S}}{4i}\Big[\left(a_{\tilde{\boldsymbol{k}}}-a^\dagger_{-\tilde{\boldsymbol{k}}}\right)-e^{i\boldsymbol{G}\cdot\boldsymbol{d_x}}\left(b_{\tilde{\boldsymbol{k}}}-b^\dagger_{-\tilde{\boldsymbol{k}}}\right) \\ &-e^{i\boldsymbol{G}\cdot\boldsymbol{a_1}}\left(c_{\tilde{\boldsymbol{k}}}-c^\dagger_{-\tilde{\boldsymbol{k}}}\right)+e^{i\boldsymbol{G}\cdot\boldsymbol{d_z}}\left(d_{\tilde{\boldsymbol{k}}}-d^\dagger_{-\tilde{\boldsymbol{k}}}\right)\Big] \\ \equiv& \frac{\sqrt{2S}}{4i}\sum_\mu \sigma_\mu\,\nu^\mu_{\boldsymbol{G}}\,\phi^\mu_{\tilde{\boldsymbol{k}}}\,. \end{aligned} \tag{2.196b}$$

Here, we used the collective 8-component operator-valued vector

$$\phi^\mu_{\boldsymbol{k}} = (a_{\boldsymbol{k}}, b_{\boldsymbol{k}}, c_{\boldsymbol{k}}, d_{\boldsymbol{k}}, a^\dagger_{-\boldsymbol{k}}, b^\dagger_{-\boldsymbol{k}}, c^\dagger_{-\boldsymbol{k}}, d^\dagger_{-\boldsymbol{k}}) \tag{2.197}$$

in analogy to the definition (2.149) from the path integral approach, and defined the vectors $\nu^\mu_{\boldsymbol{G}}$ and σ_μ with components

$$\nu^\mu_{\boldsymbol{G}} = (1, e^{i\boldsymbol{G}\cdot\boldsymbol{d_x}}, e^{i\boldsymbol{G}\cdot\boldsymbol{a_1}}, e^{i\boldsymbol{G}\cdot\boldsymbol{d_z}}, 1, e^{i\boldsymbol{G}\cdot\boldsymbol{d_x}}, e^{i\boldsymbol{G}\cdot\boldsymbol{a_1}}, e^{i\boldsymbol{G}\cdot\boldsymbol{d_z}})\,, \tag{2.198}$$

$$\sigma_\mu = (+1,-1,-1,+1,-1,+1,+1,-1)\,. \tag{2.199}$$

In a next step, we use the Bogoliubov transformation (2.150) to express the Holstein-Primakoff bosons $\phi^\mu_{\tilde{\boldsymbol{k}}}$ in terms of the Bogoliubov bosons as

$$\phi^\mu_{\tilde{\boldsymbol{k}}} = \sum_{\mu'} \mathbb{T}^{\mu\mu'}_{\tilde{\boldsymbol{k}}}\,\psi^{\mu'}_{\tilde{\boldsymbol{k}}}\,, \tag{2.200}$$

where

$$\psi^\mu_{\boldsymbol{k}} = (b_{\boldsymbol{k}1}, b_{\boldsymbol{k}2}, b_{\boldsymbol{k}3}, b_{\boldsymbol{k}4}, b^\dagger_{-\boldsymbol{k}1}, b^\dagger_{-\boldsymbol{k}2}, b^\dagger_{-\boldsymbol{k}3}, b^\dagger_{-\boldsymbol{k}4})\,, \tag{2.201}$$

and $b_{\boldsymbol{k}n}$ and $b^\dagger_{\boldsymbol{k}n}$ are the annihilation and creation operators of the four different magnon branches. We thus get

$$S^1_{\boldsymbol{k}} = -\frac{\sqrt{2S}}{4}\sum_{\mu\mu'} \nu^\mu_{\boldsymbol{G}}\,\mathbb{T}^{\mu\mu'}_{\tilde{\boldsymbol{k}}}\,\psi^{\mu'}_{\tilde{\boldsymbol{k}}}\,, \tag{2.202a}$$

$$S^3_{\boldsymbol{k}} = \frac{\sqrt{2S}}{4i}\sum_{\mu\mu'} \sigma_\mu\,\nu^\mu_{\boldsymbol{G}}\,\mathbb{T}^{\mu\mu'}_{\tilde{\boldsymbol{k}}}\,\psi^{\mu'}_{\tilde{\boldsymbol{k}}}\,. \tag{2.202b}$$

Substitution into the definition (2.188) of the dynamical structure factor then yields for the transversal components

$$S^{11}(\boldsymbol{k},\omega) = \frac{2S}{16}\sum_{\mu\mu'}\nu^{\mu}_{-\boldsymbol{G}}\,\mathbb{T}^{\mu\mu'}_{-\tilde{\boldsymbol{k}}}\sum_{\nu\nu'}\nu^{\nu}_{\boldsymbol{G}}\,\mathbb{T}^{\nu\nu'}_{\tilde{\boldsymbol{k}}}\int\frac{dt}{2\pi}\langle\psi^{\mu'}_{-\tilde{\boldsymbol{k}}}(t)\psi^{\nu'}_{\tilde{\boldsymbol{k}}}(0)\rangle e^{i\omega t}\ , \tag{2.203a}$$

$$S^{13}(\boldsymbol{k},\omega) = -\frac{2S}{16i}\sum_{\mu\mu'}\nu^{\mu}_{-\boldsymbol{G}}\,\mathbb{T}^{\mu\mu'}_{-\tilde{\boldsymbol{k}}}\sum_{\nu\nu'}\sigma_\nu\nu^{\nu}_{\boldsymbol{G}}\,\mathbb{T}^{\nu\nu'}_{\tilde{\boldsymbol{k}}}\int\frac{dt}{2\pi}\langle\psi^{\mu'}_{-\tilde{\boldsymbol{k}}}(t)\psi^{\nu'}_{\tilde{\boldsymbol{k}}}(0)\rangle e^{i\omega t}\ , \tag{2.203b}$$

$$S^{33}(\boldsymbol{k},\omega) = -\frac{2S}{16}\sum_{\mu\mu'}\sigma_\mu\nu^{\mu}_{-\boldsymbol{G}}\,\mathbb{T}^{\mu\mu'}_{-\tilde{\boldsymbol{k}}}\sum_{\nu\nu'}\sigma_\nu\nu^{\nu}_{\boldsymbol{G}}\,\mathbb{T}^{\nu\nu'}_{\tilde{\boldsymbol{k}}}\int\frac{dt}{2\pi}\langle\psi^{\mu'}_{-\tilde{\boldsymbol{k}}}(t)\psi^{\nu'}_{\tilde{\boldsymbol{k}}}(0)\rangle e^{i\omega t}\ . \tag{2.203c}$$

The integrals appearing in these expressions are related to the imaginary part of the retarded Green's functions by the Kramers-Kronig-relations [8]. Some care has to be taken because $\psi^{\mu}_{\boldsymbol{k}}$ lists both creation and annihilation operators, see Eq. (2.201). In our approximation, the off diagonal elements of the full propagator are of higher order in $1/S$ than the diagonal elements, so we only take into account the diagonal elements, giving

$$\begin{aligned}\int\frac{dt}{2\pi}\langle\psi^{n+4}_{-\boldsymbol{k}}(t)\psi^{n}_{\boldsymbol{k}}(0)\rangle e^{i\omega t} &= \int\frac{dt}{2\pi}\langle b^{\dagger}_{\boldsymbol{k}n}(t)b_{\boldsymbol{k}n}(0)\rangle e^{i\omega t}\\ &= \frac{1}{e^{-\beta\omega}-1}\frac{1}{\pi}\mathrm{Im}\,G^{\mathrm{ret}}_{n}(\boldsymbol{k},\omega)\ ,\end{aligned} \tag{2.204a}$$

$$\begin{aligned}\int\frac{dt}{2\pi}\langle\psi^{n}_{-\boldsymbol{k}}(t)\psi^{n+4}_{\boldsymbol{k}}(0)\rangle e^{i\omega t} &= \int\frac{dt}{2\pi}\langle b_{-\boldsymbol{k}n}(t)b^{\dagger}_{-\boldsymbol{k}n}(0)\rangle e^{i\omega t}\\ &= \frac{1}{e^{-\beta\omega}-1}\frac{1}{\pi}\mathrm{Im}\,G^{\mathrm{ret}}_{n}(\boldsymbol{k},-\omega)\ ,\end{aligned} \tag{2.204b}$$

for $n = 1, 2, 3, 4$. At zero temperature, the Bose functions simplify and the structure factor can be written compactly as

$$S^{\alpha\beta}(\boldsymbol{k},\omega) = -\frac{1}{\pi}\sum_{n}W^{\alpha\beta}_{\boldsymbol{k}n}\,\mathrm{Im}\ G^{\mathrm{ret}}_{n}(\tilde{\boldsymbol{k}},\omega)\ , \tag{2.205}$$

where we defined the functions

$$W^{11}_{\boldsymbol{k}n} = \frac{S}{8}\left(\sum_{\mu}\nu^{\mu}_{-\boldsymbol{G}}\,\mathbb{T}^{\mu n}_{-\tilde{\boldsymbol{k}}}\right)\left(\sum_{\nu}\nu^{\nu}_{\boldsymbol{G}}\,\mathbb{T}^{\nu\,n+4}_{\tilde{\boldsymbol{k}}}\right)\ , \tag{2.206a}$$

$$W^{13}_{\boldsymbol{k}n} = \frac{S}{8i}\left(\sum_{\mu}\nu^{\mu}_{-\boldsymbol{G}}\,\mathbb{T}^{\mu n}_{-\tilde{\boldsymbol{k}}}\right)\left(\sum_{\nu}\sigma_\nu\,\nu^{\nu}_{\boldsymbol{G}}\,\mathbb{T}^{\nu\,n+4}_{\tilde{\boldsymbol{k}}}\right)\ , \tag{2.206b}$$

$$W^{33}_{\boldsymbol{k}n} = -\frac{S}{8}\left(\sum_{\mu}\sigma_\mu\,\nu^{\mu}_{-\boldsymbol{G}}\,\mathbb{T}^{\mu n}_{-\tilde{\boldsymbol{k}}}\right)\left(\sum_{\nu}\sigma_\nu\,\nu^{\nu}_{\boldsymbol{G}}\,\mathbb{T}^{\nu\,n+4}_{\tilde{\boldsymbol{k}}}\right)\ . \tag{2.206c}$$

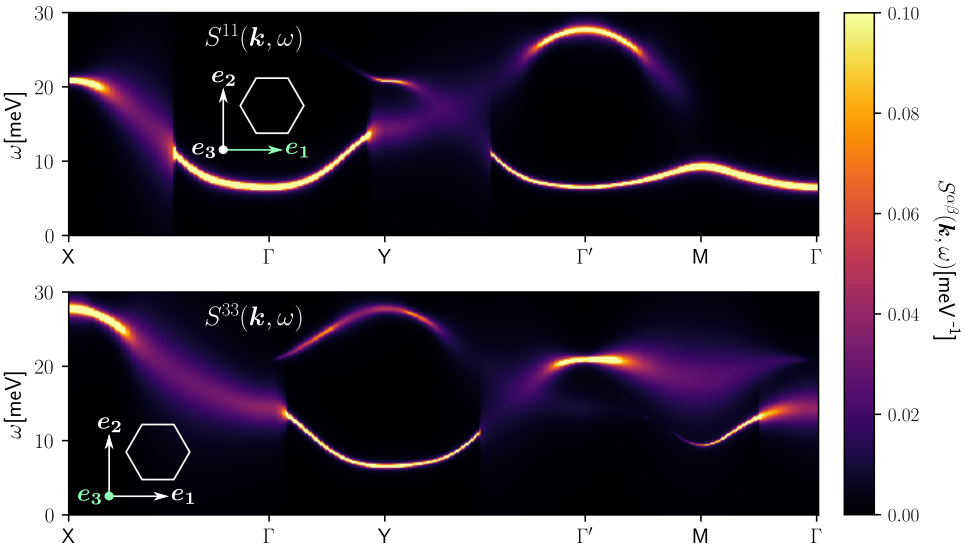

Figure 2.15: Dynamical Structure factor computed from the result of the iDE approximation for the magnon damping. This figure is republished from Ref. [1] with permission of the American Physical Society.

From the Dyson equation (2.155) and the relation (2.158b) between self energy and magnon damping $\gamma_{\boldsymbol{k}n}$, we see that the imaginary part of the retarded Green function within our Born approximation can be written as

$$\operatorname{Im} G_n^{\mathrm{ret}}(\boldsymbol{k},\omega) \approx \frac{-\gamma_{\boldsymbol{k}n}}{(\omega-\omega_{\boldsymbol{k}n})^2+\gamma_{\boldsymbol{k}n}^2}\,. \tag{2.207}$$

Having numerical values for $\gamma_{\boldsymbol{k}n}$ from Sec. 2.7, the structure factor at zero temperature can now be calculated from Eq. (2.205). In Fig. 2.15, we used our results for the damping in the iDE approximation to visualize the dynamical structure factor along the momentum path given in Fig. 2.13.

2.9 Discussion

Our results for the magnon damping shown in Fig. 2.14 confirm the claim made in Ref. [2] that magnon decays in the KHΓ model can become significant due to the decay of single magnons into two-magnon states. This mechanism leads to broad features in the structure factor shown in Fig. 2.15 and can potentially explain scattering continua in inelastic neutron scattering experiments. While our results support the approximation done in Ref. [2], our method is restricted to a region in parameter space which is not compatible with the model parameters found Ref. [2]. In the following, we want to elaborate on this issue as well as on the real part of the self energy, which we neglected throughout our calculations.

2.9.1 Purely imaginary self energy

Let us comment on the fact that in both of our approximations (Born and iDE), we neglected the real part of the self energy. In case of the Born approximation the real and imaginary part of the self energy can be calculated independently because they are calculated purely in terms of the bare propagator and bare vertices. Hence, it is clear that while the real part of the self energy will shift the magnon energies, it will not change our results for the damping. The situation is more complicated with the iDE approximation. The Dyson equation can be interpreted as a self consistent equation for the self energy and a solution must in general include the real and imaginary part. Neglecting the real part must be justified by suitable arguments. In Refs. [71, 72], where the iDE approximation was introduced, it was shown for a different model that the real part is much smaller than the imaginary part, while in Ref. [2] the approximation was justified by agreement with experiments and exact diagonalization results. Another argument was suggested in the supplementary material of Ref. [2], namely that one can regard the model parameters as renormalized couplings, which already take into account the renormalization of the magnon energies. It is clear that such an argument cannot be rigorous, since the magnon spectrum has many more degrees of freedom than the (constant) coupling parameters. For instance, one would expect the formation of energy gaps at some of the naked band crossings, while in other places the spectrum might merely be shifted more or less uniformly. An independent confirmation of the validity of the iDE approximation in the KHΓ model would be desirable. Nevertheless, the agreement with the measurements obtained in Ref. [2] can be seen as evidence that the iDE approximation is indeed applicable.

2.9.2 Special parameter region

A weak point of our calculations is their restriction to couplings which fulfill $\Gamma = K > 0$. While it is unlikely that this particular region in parameter space will be relevant for a real material, our method can be used to validate other approximations. One example is the approximation used in Ref. [2], where the authors neglect the momentum dependence of the interaction vertex. As mentioned in the introduction to this chapter, it was our main motivation to validate this approximation. As we discuss in our publication [1], our results verify the cruder approximation of Ref. [2] in a qualitative way. More concretely, we verified that the magnon decay rates from one-magnon to two-magnon states can be significant in large parts of the Brillouin zone of the Kitaev-Heisenberg-Γ model, which can be seen from the high damping rates in Fig. 2.14. Such magnon decay processes can in principle explain broad incoherent features in inelastic neutron scattering experiments, as was the claim in Ref. [2] and as can be inferred from the

broad features in the dynamical structure factor shown in Fig. 2.15. There is to our knowledge no feasible procedure that manages to produce reliable perturbative results for the magnon damping in KHΓ models or other similarly complicated extended Kitaev models in the whole coupling space. While magnon spectra can reliably be calculated by exact diagonalization, it is only applicable for small systems made up of a few unit cells because the computational cost scales exponentially with the system size due to the exponential growth of the Hilbert space. Numerical perturbation theory, i.e. diagonalization of the propagator matrix by the Colpa algorithm [63], is computationally costly because in order to evaluate the damping to lowest order perturbation, one must integrate over all momenta. This means that the 8×8 propagator matrix needs to be diagonalized for a large number of momenta in order to approximate this integral. With our approach, we are able to systematically identify a region in the coupling space where the problem is reduced to the diagonalization of 4×4 matrices. This allows to perform perturbation theory in more detail than before. We stress that this systematic approach can in principle be applied to any bosonic model, and might be useful to examine other complicated magnetic materials as well.

Chapter 3

Discontinuous phase transition in the SYK model

In this chapter, we examine a toy model with random all-to-all interaction, the SYK model. We have already introduced this model in the introduction in Sec. 1.2.2. Using the functional renormalization group (FRG), which we have introduced in Sec. 1.2.1, we find an unexpected result: strongly correlated critical fluctuations at a discontinuous quantum phase transition.

The structure of this chapter closely follows our publication [3]. In Sec. 3.1, we define the Hamiltonian of the fermionic SYK model and discuss some of the properties of its exact solution. Then, in Sec. 3.2, we perform a disorder average over the random couplings of the SYK model to obtain an average action, and argue that the RG flow of the average action is equivalent to the average RG flow of the SYK model in the thermodynamic limit. We then continue to derive RG flow equations for the average action in Sec. 3.3. In Sec. 3.4, we introduce a sharp frequency cutoff and derive explicit flow equations for the effective chemical potential and effective interaction. In Sec. 3.5, we identify a fixed point which describes a discontinuous phase transition of the SYK. In Sec. 3.6, we construct a method that allows us to integrate the flow equations and plot the RG trajectories. Finally, in Sec. 3.7, we discuss possible physical implications of our results.

3.1 The SYK model

The fermionic SYK model is defined by the Hamiltonian

$$H = -\mu \sum_i c_i^\dagger c_i + \sum_{i<j,k<l} J_{ij,kl} c_i^\dagger c_j^\dagger c_k c_l. \tag{3.1}$$

Here, μ is the chemical potential and $c_i^\dagger$ and c_i are fermionic creation and annihilation operators for a total of N fermionic modes. The indices i, j, k, l iterate over the N fermionic modes in an arbitrary order. Note that there

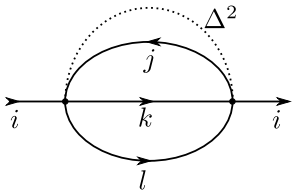

Figure 3.1: Melon diagram contributing to leading order to the average self energy. The dashed line represents the average over the random couplings, $\overline{|J_{ij,kl}|^2} = \Delta^2$.

are no spatial degrees of freedom. $J_{ij,kl}$ is a complex quenched random interaction with Gaussian probability distribution

$$\rho(J_{ij,kl}) = \frac{1}{\pi\Delta^2} \exp\left\{-\frac{|J_{ij,kl}|^2}{\Delta^2}\right\} , \tag{3.2}$$

where the mean of the interaction is zero and the variance is given in terms of a fixed coupling energy J as

$$\Delta^2 \equiv \overline{|J_{ij,kl}|^2} = 2J^2/N^3 . \tag{3.3}$$

Besides the fermionic symmetries

$$J_{ij,kl} = -J_{ji,kl} = -J_{ij,lk} , \tag{3.4}$$

and hermiticity condition

$$J_{ij,kl} = J^*_{kl,ij} , \tag{3.5}$$

all components are statistically independent.

In the thermodynamic limit $N \to \infty$, an exact solution for the single mode dynamics can be constructed [14, 45, 46]. This is possible due to the self averaging property of the SYK model: because all modes interact randomly with each other, the sum in the interaction term of the Hamiltonian (3.1) is effectively an average over all modes. As a result, the dynamics of any given mode is given by the average dynamics of all modes [14]. In the following, we have to distinguish to different averages, the disorder average over the random couplings and the mode average over all fermionic modes. However, these two averages are deeply intertwined by the self averaging property of the SYK-model: since in the thermodynamic limit, all fermionic modes obey the same average dynamics, no physical quantities can depend on the specific configuration of the couplings $J_{ij,kl}$.

Among the Feynman diagrams for the disorder-averaged self energy, only the so-called *melon diagrams* [14, 46] are of leading order in $1/N$. We depicted this diagram in Fig. 3.1. Because the random couplings are statistically independent, the two vertices in the melon diagram connected by the dashed line must have the same indices. But this means that the outer indices on the left and on the right coincide. As a result, the self energy,

and hence also the full propagator, are diagonal to leading order in $1/N$. Considering the self averaging property of the SYK model, this is an expected result [74]. Due to the simplicity of the melon diagrams, a self consistent equation for the mode-averaged self energy in imaginary time can be found [14, 45, 46],

$$\Sigma(\tau) = -J^2 G^2(\tau) G(-\tau) \,, \tag{3.6}$$

where $G(\tau)$ is the mode-averaged full propagator. The solution can then be found by using the Dyson equation in imaginary frequency space,

$$G(\omega) = \frac{1}{i\omega + \mu - \Sigma(\omega)} \,. \tag{3.7}$$

As we have discussed in Sec. 1.2.2, the explicit form of the solution at low temperatures depends on the chemical potential and leads to either the non-Fermi liquid (nFL) or the integer valence (IV) phase, see Fig. 1.1. These phases are separated by a discontinuous phase transition, which we wish to study at zero temperature.

3.2 Disorder average

We are interested in the phase diagram of the SYK model in the thermodynamic limit $N \to \infty$. In this limit, the specific random values of the random couplings do not matter because of the self-averaging property of the SYK model. This allows us to simplify the problem by integrating out the random couplings $J_{ij,kl}$ with the path integral formalism. However, there is a complication. In our FRG analysis, we use the tree expansion to describe the flow of the n-point irreducible vertices $\Gamma^{(n)}_{i_1,\dots,i_n}(\omega_1, \dots \omega_n; \boldsymbol{J})$, where $\boldsymbol{J}$ summarizes the random couplings $J_{ij,kl}$. The vertices depend on the random couplings $J_{ij,kl}$ as well as on the fermionic modes $i_1 \dots i_n$ and the Matsubara frequencies $\omega_1 \dots \omega_n$. The generating functional of the irreducible vertices is the Legendre transform of the generating functional of the connected Green's functions, and the latter is given by the logarithm of the generating functional of the disconnected Green's functions [75, 76]. While the disorder average of the disconnected Green's functions is relatively straightforward, the logarithm poses a challenge for the evaluation of the average irreducible vertices. This is because the logarithm and the average do not commute. This problem can be tackled by the replica trick [5, 77, 78, 79, 80]. In the next subsection 3.2.1, we will use the replica trick to justify that the average RG flow of the SYK model is given by the RG flow of an average action. Then, in Sec. 3.2.2, we will determine the appropriate average action by integrating over the probability distribution of the random couplings $J_{ij,kl}$. Throughout this section, we refer to the disorder average simply as the average.

3.2.1 Replica trick

The replica trick can be expressed as

$$\overline{\ln Z} = \lim_{n\to 0} \frac{\overline{Z^n} - 1}{n} \,, \tag{3.8}$$

where Z is the partition function and the overline indicates an average. Usually, the right hand side of above equation is evaluated for generic integers $n > 0$, and then analytically continued to the case $n = 0$. We can apply this formula to our case by noting that the generating functional for the disconnected Green's functions [5, 75, 76],

$$Z[\boldsymbol{J}, \bar{\boldsymbol{\eta}}, \boldsymbol{\eta}] = \int \mathcal{D}c \, \exp\left\{-S[\boldsymbol{J}, \bar{\boldsymbol{c}}, \boldsymbol{c}] + \bar{\boldsymbol{\eta}}\boldsymbol{c} + \boldsymbol{\eta}\bar{\boldsymbol{c}}\right\} \,, \tag{3.9}$$

is a partition function with a functional dependence on the Grassmann sources $\bar{\boldsymbol{\eta}}, \boldsymbol{\eta}$ and the average is over the random couplings $\boldsymbol{J}$. In the above expression, $\mathcal{D}c$ denotes the Grassmann path integral over the fermionic degrees of freedom and $S[\boldsymbol{J}, \bar{\boldsymbol{c}}, \boldsymbol{c}]$ is the bare action of the SYK model, which we will define later. Note that the formula (3.8) for the replica trick contains an n-th power of the partition function. Effectively, Z^n is the partition function describing n non-interacting copies - or replicas - of the model. However, the average introduces an interaction between the replicas. To see this, we write

$$\begin{aligned}(Z[\boldsymbol{J}, \bar{\boldsymbol{\eta}}, \boldsymbol{\eta}])^n = \int \mathcal{D}c_1 \cdots \int \mathcal{D}c_n \exp\big\{ &- S[\boldsymbol{J}, \bar{\boldsymbol{c}}_1, \boldsymbol{c}_1] + \bar{\boldsymbol{\eta}}\boldsymbol{c}_1 + \boldsymbol{\eta}\bar{\boldsymbol{c}}_1 - \dots \\ &- S[\boldsymbol{J}, \bar{\boldsymbol{c}}_n, \boldsymbol{c}_n] + \bar{\boldsymbol{\eta}}\boldsymbol{c}_n + \boldsymbol{\eta}\bar{\boldsymbol{c}}_n\big\} \,.\end{aligned} \tag{3.10}$$

To perform the average over the random couplings $J_{ij,kl}$, we integrate over the probability measure $\mathcal{D}J\, P(\boldsymbol{J})$ (which we specify later) and write

$$\begin{aligned}\overline{(Z[\boldsymbol{J}, \bar{\boldsymbol{\eta}}, \boldsymbol{\eta}])^n} = \int \mathcal{D}c_1 \cdots \int \mathcal{D}c_n \int \mathcal{D}J\, P(\boldsymbol{J}) \\ \times \exp\big\{ - S[\boldsymbol{J}, \bar{\boldsymbol{c}}_1, \boldsymbol{c}_1] + \bar{\boldsymbol{\eta}}\boldsymbol{c}_1 + \boldsymbol{\eta}\bar{\boldsymbol{c}}_1 - \dots \\ - S[\boldsymbol{J}, \bar{\boldsymbol{c}}_n, \boldsymbol{c}_n] + \bar{\boldsymbol{\eta}}\boldsymbol{c}_n + \boldsymbol{\eta}\bar{\boldsymbol{c}}_n\big\} \,,\end{aligned} \tag{3.11}$$

where we interchanged the order of integration over the fields with the integration over the random couplings. In general, the average of the exponential function does not factorize,

$$\begin{aligned}\int \mathcal{D}J\, P(\boldsymbol{J}) \exp\big\{ - S[\boldsymbol{J}, \bar{\boldsymbol{c}}_1, \boldsymbol{c}_1] - \cdots - S[\boldsymbol{J}, \bar{\boldsymbol{c}}_n, \boldsymbol{c}_n]\big\} \\ \neq \left(\int \mathcal{D}J\, P(\boldsymbol{J}) \exp\big\{ - S[\boldsymbol{J}, \bar{\boldsymbol{c}}, \boldsymbol{c}]\big\}\right)^n \,,\end{aligned} \tag{3.12}$$

which means that the averaging introduces an interaction between the n replicas. However, the SYK model is *replica diagonal* in the thermodynamic limit [14, 81, 82], which means that the average does factorize, giving

$$\overline{(Z[\boldsymbol{J},\bar{\boldsymbol{\eta}},\boldsymbol{\eta}])^n} = \left(\overline{Z[\boldsymbol{J},\bar{\boldsymbol{\eta}},\boldsymbol{\eta}]}\right)^n . \tag{3.13}$$

Inserting this into the formula for the replica trick (3.8) and applying L'Hospital's rule then yields the simple relation

$$\overline{\ln Z} = \ln \overline{Z} \, . \tag{3.14}$$

Because the functional derivative with respect to the sources commutes with the average, the average generating functional for the disconnected Green's functions generates the average disconnected Green's functions. But if Z is the generating functional of the disconnected Green's functions, then $\ln Z$ is, up to normalization, the generating functional of the connected Green's functions [75, 76]. By virtue of Eq. (3.14), this means that the average connected Green's functions coincide with the connected Green's functions obtained from an average action $S[\overline{\boldsymbol{c}},\boldsymbol{c}]$ defined by

$$\exp\big\{ -S[\overline{\boldsymbol{c}},\boldsymbol{c}]\big\} = \int \mathcal{D}J \, P(\boldsymbol{J}) \exp\big\{ -S[\boldsymbol{J},\overline{\boldsymbol{c}},\boldsymbol{c}]\big\} \, . \tag{3.15}$$

The generating functionals of the irreducible vertices and the connected Green's functions are related by a Legendre transform with respect to the sources $\boldsymbol{\eta},\bar{\boldsymbol{\eta}}$ [75, 76]. But because the sources are external variables, and hence the Legendre transform commutes with the averaging. Consequently, the average irreducible vertices coincide with the irreducible vertices obtained from the average action. This simplifies our task tremendously, because we only need to apply the FRG to the average action of the SYK model to find the flow of the average irreducible vertices.

3.2.2 Average action

To find the average action, we write the random action corresponding to the SYK-Hamiltonian (3.1) in imaginary time as

$$S[\boldsymbol{J},\overline{\boldsymbol{c}},\boldsymbol{c}] \;\; = \;\; S_2[\overline{\boldsymbol{c}},\boldsymbol{c}] + S_4[\boldsymbol{J},\overline{\boldsymbol{c}},\boldsymbol{c}] \, , \tag{3.16}$$

with

$$S_2[\overline{\boldsymbol{c}},\boldsymbol{c}] = \sum_i \int_0^\beta d\tau \, \overline{c}_i(\tau) \, (\partial_\tau - \mu) \, c_i(\tau) \, , \tag{3.17}$$

and

$$S_4[\boldsymbol{J},\overline{\boldsymbol{c}},\boldsymbol{c}] = \sum_{i<j} \sum_{k<l} J_{ij,kl} \int_0^\beta d\tau \overline{c}_i(\tau) \overline{c}_j(\tau) c_k(\tau) c_l(\tau) \, , \tag{3.18}$$

where β is the inverse temperature. We define the Fourier transform of the fermionic modes as

$$c_i(\tau) = \frac{1}{\beta} \sum_{\omega} e^{-i\omega\tau} c_i(\omega) \,, \tag{3.19}$$

where the sum iterates over the fermionic Matsubara frequencies ω. Written in terms of Matsubara frequencies, the quadratic action reads

$$S_2[\overline{\boldsymbol{c}}, \boldsymbol{c}] = \frac{1}{\beta} \sum_{i} \sum_{\omega} (-i\omega - \mu)\, \overline{c}_i(\omega) c_i(\omega) \,, \tag{3.20}$$

and the quartic action reads

$$S_4[\boldsymbol{J}, \overline{\boldsymbol{c}}, \boldsymbol{c}] = \sum_{i<j} \sum_{k<l} J_{ij,kl} \frac{1}{\beta^4} \sum_{\omega_1 \ldots \omega_4} \beta\, \delta_{12,34}\, \overline{c}_i(\omega_1) \overline{c}_j(\omega_2) c_k(\omega_3) \,. \tag{3.21}$$

Here, we used the abbreviations

$$\sum_{\omega_{1234}} = \sum_{\omega_1} \sum_{\omega_2} \sum_{\omega_3} \sum_{\omega_4} \qquad \text{and} \qquad \delta_{12,34} = \delta_{\omega_1+\omega_2, \omega_3+\omega_4} \,. \tag{3.22}$$

We wish to calculate the average action $S[\overline{\boldsymbol{c}}, \boldsymbol{c}]$ defined in Eq. (3.15) by integrating over the random couplings $J_{ij,kl}$. We therefore define the integration measure

$$\mathcal{D}J = \prod_{i<j,\,(i)\leq k<l} \frac{dJ^*_{ij,kl}\, dJ_{ij,kl}}{2\pi\, i} = \prod_{i<j,\,(i)\leq k<l} \left(dJ^{\mathrm{Re}}_{ij,kl}\, dJ^{\mathrm{Im}}_{ij,kl} \right) , \tag{3.23}$$

and the probability density

$$P(\boldsymbol{J}) = \prod_{i<j,\,(i)\leq k<l} \rho(J_{ij,kl}) \,, \tag{3.24}$$

where $\rho(J_{ij,kl})$ is the Gaussian probability distribution given in Eq. (3.2). In the above expressions, the product goes over all quadruples i, j, k, l which fulfill $i < j$ and $i \leq k < l$. These relations ensure that the symmetries $J_{ij,kl} = -J_{ji,kl} = -J_{ij,lk}$ and $J_{ij,kl} = J^*_{kl,ij}$ given in Eqs. (3.4) and (3.5) are respected without double counting of degrees of freedom. The superscripts Re and Im denote the real and imaginary parts of the respective variable. The integral over the random couplings can be evaluated explicitly. To show this, we note that the quadratic part of the action is independent of

the random couplings. For the quartic part, we write

$$\begin{aligned}
&\int \mathcal{D}J\, P(\boldsymbol{J})\, e^{-S_4[\boldsymbol{J},\overline{\boldsymbol{c}},\boldsymbol{c}]} \\
&= \prod_{i<j,\,(i)\le k<l} \Bigg(\int \frac{dJ^*_{ij,kl}\, dJ_{ij,kl}}{2\pi\, i} \frac{1}{\pi\, \Delta^2}\, \exp\Bigg\{ -\frac{1}{\Delta^2} J^*_{ij,kl}\, J_{ij,kl} \\
&\qquad - \frac{1}{\beta^4} \sum_{\omega_{1234}} \beta\delta_{12,34} \big[J_{ij,kl}\, \overline{c}_i(\omega_1)\overline{c}_j(\omega_2) c_k(\omega_3) c_l(\omega_4) \\
&\qquad\qquad + J^*_{ij,kl}\, \overline{c}_k(\omega_3)\overline{c}_l(\omega_4) c_i(\omega_1) c_j(\omega_2) \big] \Bigg\} \Bigg) \,. \qquad (3.25)
\end{aligned}$$

The integration over real and imaginary parts of $J_{ij,kl}$ can be separated, giving

$$\int \mathcal{D}J\, P(\boldsymbol{J})\, e^{-S_4[\boldsymbol{J},\overline{\boldsymbol{c}},\boldsymbol{c}]} = \prod_{i<j,\,(i)\le k<l} I^{\mathrm{Re}}_{ij,kl}[\overline{\boldsymbol{c}},\boldsymbol{c}]\, I^{\mathrm{Im}}_{ij,kl}[\overline{\boldsymbol{c}},\boldsymbol{c}] \qquad (3.26)$$

with

$$\begin{aligned}
I^{\mathrm{Re}}_{ij,kl}[\overline{\boldsymbol{c}},\boldsymbol{c}] = \int \frac{dJ^{\mathrm{Re}}_{ij,kl}}{\sqrt{\pi}\,\Delta}\, \exp\Bigg\{ &- \frac{\left(J^{\mathrm{Re}}_{ij,kl}\right)^2}{\Delta^2} - \frac{J^{\mathrm{Re}}_{ij,kl}}{\beta^4} \sum_{\omega_{1234}} \beta\delta_{12,34} \\
&\times \big[\overline{c}_i(\omega_1)\overline{c}_j(\omega_2) c_k(\omega_3) c_l(\omega_4) + \overline{c}_k(\omega_3)\overline{c}_l(\omega_4) c_i(\omega_1) c_j(\omega_2) \big] \Bigg\} \,, \qquad (3.27a)
\end{aligned}$$

$$\begin{aligned}
I^{\mathrm{Im}}_{ij,kl}[\overline{\boldsymbol{c}},\boldsymbol{c}] = \int \frac{dJ^{\mathrm{Im}}_{ij,kl}}{\sqrt{\pi}\,\Delta}\, \exp\Bigg\{ &- \frac{\left(J^{\mathrm{Im}}_{ij,kl}\right)^2}{\Delta^2} - \frac{i J^{\mathrm{Im}}_{ij,kl}}{\beta^4} \sum_{\omega_{1234}} \beta\delta_{12,34} \\
&\times \big[\overline{c}_i(\omega_1)\overline{c}_j(\omega_2) c_k(\omega_3) c_l(\omega_4) - \overline{c}_k(\omega_3)\overline{c}_l(\omega_4) c_i(\omega_1) c_j(\omega_2) \big] \Bigg\} \,. \qquad (3.27b)
\end{aligned}$$

To solve those, we expand the exponentials into a power series,

$$\begin{aligned}
I^{\mathrm{Re}}_{ij,kl}[\overline{\boldsymbol{c}},\boldsymbol{c}] = \int \frac{dJ^{\mathrm{Re}}_{ij,kl}}{\sqrt{\pi}\,\Delta}\, \exp\left\{ -\frac{\left(J^{\mathrm{Re}}_{ij,kl}\right)^2}{\Delta^2} \right\} \Bigg\{ \sum_{n=0}^{\infty} \frac{1}{n!} \left(\frac{-J^{\mathrm{Re}}_{ij,kl}}{\beta^4} \right)^n \\
\times \Bigg(\sum_{\omega_{1234}} \beta\delta_{12,34} \big[\overline{c}_i(\omega_1)\overline{c}_j(\omega_2) c_k(\omega_3) c_l(\omega_4) + \overline{c}_k(\omega_3)\overline{c}_l(\omega_4) c_i(\omega_1) c_j(\omega_2) \big] \Bigg)^n \Bigg\} \,, \qquad (3.28a)
\end{aligned}$$

$$I^{\mathrm{Im}}_{ij,kl}[\overline{\boldsymbol{c}},\boldsymbol{c}] = \int \frac{dJ^{\mathrm{Im}}_{ij,kl}}{\sqrt{\pi}\,\Delta}\,\exp\left\{-\frac{\left(J^{\mathrm{Im}}_{ij,kl}\right)^2}{\Delta^2}\right\}\left\{\sum_{n=0}^{\infty}\frac{1}{n!}\left(\frac{-i\,J^{\mathrm{Im}}_{ij,kl}}{\beta^4}\right)^n \right.$$
$$\left.\times\left(\sum_{\omega_{1234}}\beta\delta_{12,34}\left[\overline{c}_i(\omega_1)\overline{c}_j(\omega_2)c_k(\omega_3)c_l(\omega_4)-\overline{c}_k(\omega_3)\overline{c}_l(\omega_4)c_i(\omega_1)c_j(\omega_2)\right]\right)^n\right\}. \tag{3.28b}$$

The remaining integrals in these expressions evaluate to

$$\int\frac{dJ}{\sqrt{\pi}\Delta}\,e^{-\frac{J^2}{\Delta^2}}\,J^n \;=\; \begin{cases}\left(\frac{\Delta^2}{2}\right)^{\frac{n}{2}}\,(n-1)!! & n\text{ even}\\ 0 & n\text{ odd}\end{cases}. \tag{3.29}$$

We insert this into Eqs. (3.28) and rename the summation index $n \to 2n$ (since all odd powers vanish), to obtain

$$I^{\mathrm{Re}}_{ij,kl}[\overline{\boldsymbol{c}},\boldsymbol{c}] = \left\{\sum_{n=0}^{\infty}\frac{(2n-1)!!}{(2n)!}\left(\frac{-\Delta}{\sqrt{2}\,\beta^4}\right)^{2n}\right.$$
$$\left.\times\left(\sum_{\omega_{1234}}\beta\delta_{12,34}\left[\overline{c}_i(\omega_1)\overline{c}_j(\omega_2)c_k(\omega_3)c_l(\omega_4)+\overline{c}_k(\omega_3)\overline{c}_l(\omega_4)c_i(\omega_1)c_j(\omega_2)\right]\right)^{2n}\right\}, \tag{3.30a}$$

$$I^{\mathrm{Im}}_{ij,kl}[\overline{\boldsymbol{c}},\boldsymbol{c}] = \left\{\sum_{n=0}^{\infty}\frac{(2n-1)!!}{(2n)!}\left(\frac{-i\,\Delta}{\sqrt{2}\,\beta^4}\right)^{2n}\right.$$
$$\left.\times\left(\sum_{\omega_{1234}}\beta\delta_{12,34}\left[\overline{c}_i(\omega_1)\overline{c}_j(\omega_2)c_k(\omega_3)c_l(\omega_4)-\overline{c}_k(\omega_3)\overline{c}_l(\omega_4)c_i(\omega_1)c_j(\omega_2)\right]\right)^{2n}\right\}. \tag{3.30b}$$

Using

$$\frac{(2n-1)!!}{(2n)!} \;=\; \frac{1}{n!}\frac{1}{2^n}, \tag{3.31}$$

we can rewrite the sums in Eqs. (3.28) as exponentials,

$$I^{\mathrm{Re}}_{ij,kl}[\overline{\boldsymbol{c}},\boldsymbol{c}] = \exp\left\{\frac{\Delta^2}{4\beta^8}\left(\sum_{\omega_{1234}}\beta\delta_{12,34}\left[\overline{c}_i(\omega_1)\overline{c}_j(\omega_2)c_k(\omega_3)c_l(\omega_4)\right.\right.\right.$$
$$\left.\left.\left.+\,\overline{c}_k(\omega_3)\overline{c}_l(\omega_4)c_i(\omega_1)c_j(\omega_2)\right]\right)^2\right\}, \tag{3.32a}$$

$$I^{\mathrm{Im}}_{ij,kl}[\overline{\boldsymbol{c}},\boldsymbol{c}] = \exp\Bigg\{ -\frac{\Delta^2}{4\beta^8}\Bigg(\sum_{\omega_{1234}} \beta\delta_{12,34}\big[\overline{c}_i(\omega_1)\overline{c}_j(\omega_2)c_k(\omega_3)c_l(\omega_4) - \overline{c}_k(\omega_3)\overline{c}_l(\omega_4)c_i(\omega_1)c_j(\omega_2)\big]\Bigg)^2\Bigg\} . \quad (3.32b)$$

Evaluating the squares and using Eq. (3.26), we can write

$$\int \mathcal{D}J\, P(\boldsymbol{J})\, e^{-S_4[\boldsymbol{J},\overline{\boldsymbol{c}},\boldsymbol{c}]} = e^{-S_8[\overline{\boldsymbol{c}},\boldsymbol{c}]} , \quad (3.33)$$

where we defined

$$S_8[\overline{\boldsymbol{c}},\boldsymbol{c}] = -\frac{\Delta^2}{\beta^8} \sum_{i<j,\,(i)\leq k<l} \sum_{\omega_{1234}} \beta\,\delta_{12,34} \sum_{\omega'_{1234}} \beta\,\delta_{1'2',3'4'} \times \overline{c}_i(\omega_1)\overline{c}_j(\omega_2)c_k(\omega_3)c_l(\omega_4)\overline{c}_k(\omega'_3)\overline{c}_l(\omega'_4)c_i(\omega'_1)c_j(\omega'_2) . \quad (3.34)$$

For the average action defined in Eq. (3.15) we can thus write

$$S[\overline{\boldsymbol{c}},\boldsymbol{c}] = S_2[\overline{\boldsymbol{c}},\boldsymbol{c}] + S_8[\overline{\boldsymbol{c}},\boldsymbol{c}] . \quad (3.35)$$

We conclude that the disorder average transforms the original four-point interaction to an effective eight-point interaction given by S_8. This is the starting point of our FRG analysis: at the initial scale $\Lambda = \Lambda_0$, all irreducible vertices except the eight-point vertex vanish. As the scale Λ decreases, additional vertices will be generated by the flow equations.

3.3 Flow equations at zero temperature

A detailed derivation of the flow equations for the irreducible vertices from a general fermionic action is given in chapter 10 of Ref. [39]. In this section, we use this procedure to find the flow equations for the disorder-averaged action given in Eq. (3.35). From now on, we refer to the mode average simply as the average, because the disorder average has already been performed in the previous section. We simplify the flow equations by several approximations, of which some become exact in the thermodynamic limit. First, in Sec. 3.3.1, we determine the contributions to the flow equations which are leading in orders of the inverse number of modes $1/N$. Then, in Sec. 3.3.2, we discuss the implications of the self averaging property of the SYK-model and derive the flow equations for the average mode. Next, in Sec. 3.3.3, we restrict the flow equations to zero temperature. In Sec. 3.3.4, we apply the Katanin substitution, which is an approximation that simplifies our flow equations. Finally, in Sec. 3.3.6, we expand the vertices for small frequencies, which describe the macroscopic dynamics.

3.3.1 1/N expansion

We start by writing the interacting part of the action S_8 given in Eq. (3.34) in a symmetrized form as

$$\begin{aligned} S_8[\bar{\boldsymbol{c}}, \boldsymbol{c}] = \frac{-1}{(4!)^2\,\beta^8}\frac{1}{N^3}\sum_{ijkl}\sum_{i'j'k'l'}\sum_{\omega_{1234}}\sum_{\omega'_{1234}} \beta\,\delta_{1234,1'2'3'4'} \\ \times\,\Gamma^{(8)}_{0,i'j'k'l',lkji}(\omega'_1,\omega'_2,\omega'_3,\omega'_4;\,\omega_4,\omega_3,\omega_2,\omega_1) \\ \times\,\bar{c}_i(\omega_1)\bar{c}_j(\omega_2)\bar{c}_k(\omega_3)\bar{c}_l(\omega_4)c_l(\omega'_4)c_k(\omega'_3)c_j(\omega'_2)c_i(\omega'_1)\;, \end{aligned} \tag{3.36}$$

with the partially antisymmetric vertex

$$\begin{aligned} &\Gamma^{(8)}_{0,i'j'k'l',lkji}(\omega'_1,\omega'_2,\omega'_3,\omega'_4;\,\omega_4,\omega_3,\omega_2,\omega_1) = \\ &\mathcal{S}_{i'\omega'_1,j'\omega'_2,k'\omega'_3,l'\omega'_4;\,l\omega_4,k\omega_3,j\omega_2,i\omega_1}\left(\frac{-(4!)^2}{8}\,2J^2\,\delta_{i'i}\,\delta_{j'j}\,\delta_{k'k}\,\delta_{l'l}\,\beta\delta_{12,3'4'}\delta_{1'2',34}\right)\;. \end{aligned} \tag{3.37}$$

Here, the operator $\mathcal{S}_{i'\omega'_1,j'\omega'_2,k'\omega'_3,l'\omega'_4;\,l\omega_4,k\omega_3,j\omega_2,i\omega_1}$ antisymmetrizes the two fermionic sectors separated by the semicolon. Following the procedure presented in chapter 10 of Ref. [39], we can now write down the flow equations for the irreducible vertices. We note that the irreducible two point vertex coincides with the self energy and hence, as we argued in Sec. 3.1, is diagonal in the mode-indices to leading order in $1/N$,

$$\Gamma^{(2)}_{\Lambda,i'i}(\omega',\omega) = \delta_{i',i}\delta_{\omega',\omega}\Sigma_{\Lambda,i}(\omega) + \mathcal{O}\left(1/N\right)\;. \tag{3.38}$$

We recall that this also means that the full propagator is diagonal, and obtain the flow equation for the self energy,

$$\partial_\Lambda\Sigma_{\Lambda,i}(\omega_1) = \frac{1}{\beta\,N}\sum_j\sum_\omega \dot{G}_{\Lambda,j}(\omega)\,\Gamma^{(4)}_{\Lambda,ij,ji}(\omega_1,\omega;\,\omega,\omega_1)\;, \tag{3.39}$$

which is exact in the thermodynamic limit $N\to\infty$. Here, we introduced the diagonal *single scale propagator* [39] defined by

$$\dot{G}_{\Lambda,j}(\omega) \equiv -G_{\Lambda,j}(\omega)\,\left[\partial_\Lambda G^{-1}_{0,\Lambda,j}(\omega)\right]G_{\Lambda,j}(\omega)\;, \tag{3.40}$$

where $G^{-1}_{0,\Lambda,j}$ is the inverse of the flowing free propagator. A graphical representation of the flow equation for the two-point vertex is shown in Fig. 3.2. The flow equation for the four-point vertex is given by

$$\partial_\Lambda\Gamma^{(4)}_{\Lambda,i'j',ji}(\omega'_1,\omega'_2;\,\omega_2,\omega_1) = f^{(1)} + f^{(2a)} + f^{(2b)}\;, \tag{3.41}$$

where we abbreviated

$$f^{(1)} = \frac{1}{\beta\,N}\sum_k\sum_\omega \dot{G}_{\Lambda,k}(\omega)\,\Gamma^{(6)}_{\Lambda,i'j'k,kji}(\omega'_1,\omega'_2,\omega;\,\omega,\omega_2,\omega_1)\;, \tag{3.42}$$

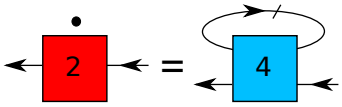

Figure 3.2: Diagrammatic representation of the flow equation (3.39) for the irreducible two-point vertex. The dot represents the derivative with respect to the scale Λ, the directed lines represent the full flowing propagators, and the slashed line represents the single-scale propagator defined in Eq. (3.40).

$$f^{(2a)} = -\frac{1}{\beta^2 N^2} \sum_{k,k'} \sum_{\omega,\omega'} \dot{G}_{\Lambda,k}(\omega)\, G_{\Lambda,k'}(\omega') \times \Gamma^{(4)}_{\Lambda,i'j',k'k}(\omega_1', \omega_2'; \omega', \omega)\, \Gamma^{(4)}_{\Lambda,kk',ij}(\omega, \omega'; \omega_2, \omega_1) \,, \quad (3.43)$$

$$f^{(2b)} = \frac{1}{\beta^2 N^2} \sum_{k,k'} \sum_{\omega,\omega'} \Big[\dot{G}_{\Lambda,k}(\omega)\, G_{\Lambda,k'}(-\omega') + G_{\Lambda,k}(\omega)\, \dot{G}_{\Lambda,k'}(-\omega')\Big] \times \Big[\Gamma^{(4)}_{\Lambda,i'k',ki}(\omega_1', \omega'; \omega, \omega_1)\, \Gamma^{(4)}_{\Lambda,j'k,k'j}(\omega_2', \omega; \omega', \omega_2) - \Gamma^{(4)}_{\Lambda,i'k,k'j}(\omega_1', \omega; \omega', \omega_2)\, \Gamma^{(4)}_{\Lambda,j'k',k'i}(\omega_2', \omega'; \omega, \omega_1')\Big] \,. \quad (3.44)$$

A diagrammatic representation of the flow equation for the four-point vertex is shown in Fig. 3.3. In the thermodynamic limit $N \to \infty$, only $f^{(1)}$ contributes to the flow equation of the four-point vertex. To show this, we anticipate that to leading order in $1/N$, the incoming mode-indices of any vertex coincide with the outgoing indices (up to permutation). Then, the sum over the mode indices in $f^{(2a)}$ given in Eq. (3.43) collapses to $2 = \mathcal{O}(1)$ terms, so that the whole expression is subleading, $f^{(2a)} = \mathcal{O}(1/N^2)$. In $f^{(2b)}$ given in Eq. (3.43), only one of the two sums collapses, and the whole expression is still subleading, $f^{(2b)} = \mathcal{O}(1/N)$. By the same argument, one finds that the only leading contribution to the flow equation of any n-point vertex is given by the $(n+2)$-point vertex with two legs joined by the single scale propagator. Hence, the flow equations in the limit $N \to \infty$ for the four-point and the six-point vertex are given by

$$\partial_\Lambda \Gamma^{(4)}_{\Lambda,i'j',ji}(\omega_1', \omega_2'; \omega_2, \omega_1) = \frac{1}{\beta N} \sum_k \sum_\omega \dot{G}_{\Lambda,k}(\omega)\, \Gamma^{(6)}_{\Lambda,i'j'k,kji}(\omega_1', \omega_2', \omega; \omega, \omega_2, \omega_1) \,, \quad (3.45)$$

$$\partial_\Lambda \Gamma^{(6)}_{\Lambda,i'k'j',kji}(\omega_1', \omega_2', \omega_3'; \omega_3, \omega_2, \omega_1) = \frac{1}{\beta N} \sum_l \sum_\omega \dot{G}_{\Lambda,l}(\omega)\, \Gamma^{(8)}_{\Lambda,i'j'k'l,lkji}(\omega_1', \omega_2', \omega_3', \omega; \omega, \omega_3, \omega_2, \omega_1) \,. \quad (3.46)$$

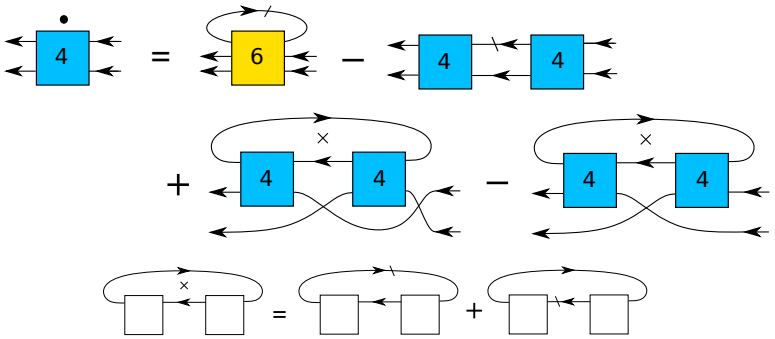

Figure 3.3: Diagrammatic representation of the flow equation (3.41) for the irreducible two-point vertex. the first diagram on the right hand side of flow equation represents $f^{(1)}$ given in Eq. (3.42), the second diagram represents $f^{(2a)}$ given in Eq. (3.43), and the last two diagrams represent $f^{(2b)}$ given in Eq. (3.44). The '$\times$' symbol sums up the two diagrams where one of the enclosing propagators is replaced by a single scale propagator, as indicated in the last row.

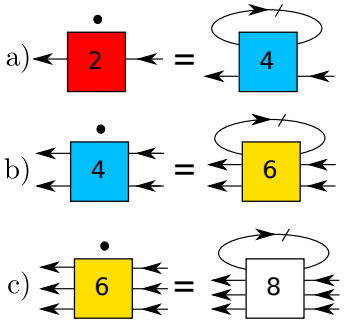

Figure 3.4: Diagrammatic representations of the FRG flow equations to leading order in $1/N$ for the two-point, four-point, and six-point vertices as given in Eqs. (3.39), (3.45), and (3.46) respectively.

We show the diagrammatic representation of the flow equations for the two-point, four-point, and six-point vertices in Fig 3.4.

Next, we want to justify our anticipation that only such vertices are generated where the outgoing indices match the incoming indices. We first note that this is trivially satisfied at the beginning of the flow, since in the microscopic action the only non-vanishing vertex is the eight-point vertex given by Eq. (3.37). Then, to leading order in $1/N$, only the six-point vertex is generated initially. From Fig. 3.4c, it is clear that the outgoing indices of the generated six-point vertex match the incoming indices. The same argument can now successively be repeated for the flow equations of the four- and two-point vertices, leading to the conclusion that our anticipation was correct. One consequence is that the eight-point vertex does not flow

at all,

$$\partial_\Lambda \Gamma_\Lambda^{(8)} = 0 \,, \tag{3.47}$$

where we omitted the mode-indices and frequencies for the sake of brevity.

3.3.2 Mode average

Because to leading order in $1/N$, the incoming and the outgoing mode-indices of all vertices match, we do not need to consider the flow equations in their full generality. We only consider those parts of the flow equations where all incoming and outgoing mode-indices of the vertices match. Furthermore, we consider only those flow equations which contribute to the flowing self energy. This means that we can set all primed frequencies in the flow equations (3.39), (3.45) and (3.46) equal to the unprimed frequencies. Moreover, as a consequence of the self-averaging property of the SYK-model, all propagators, including the single scale propagator, are independent of the mode-index,

$$G_{0,\Lambda,i}(\omega) = G_{0,\Lambda}(\omega) \,, \tag{3.48a}$$

$$G_{\Lambda,i}(\omega) = G_\Lambda(\omega) \,, \tag{3.48b}$$

$$\dot{G}_{\Lambda,i}(\omega) = \dot{G}_\Lambda(\omega) \equiv -G_\Lambda^2(\omega)\, \partial_\Lambda G_{0,\Lambda}^{-1}(\omega) \,. \tag{3.48c}$$

The sum over the mode-indices in the flow equations (3.39), (3.45) and (3.46) then only acts on the vertices. This sum can be identified as the average vertices

$$\Gamma_\Lambda^{(2k)}(\omega_1, \ldots, \omega_k) \equiv \frac{1}{N^k} \sum_{i_1 \ldots i_k} \Gamma^{(2k)}_{\Lambda, i_1 \ldots i_k, i_k \ldots i_1}(\omega_1, \ldots, \omega_k; \omega_k, \ldots, \omega_1) \,. \tag{3.49}$$

With these considerations, the flow equations can written as

$$\partial_\Lambda \Sigma_\Lambda(\omega_1) = \frac{1}{\beta} \sum_\omega \dot{G}_\Lambda(\omega)\, \Gamma_\Lambda^{(4)}(\omega_1, \omega) \,, \tag{3.50a}$$

$$\partial_\Lambda \Gamma_\Lambda^{(4)}(\omega_1, \omega_2) = \frac{1}{\beta} \sum_\omega \dot{G}_\Lambda(\omega)\, \Gamma_\Lambda^{(6)}(\omega_1, \omega_2, \omega) \,, \tag{3.50b}$$

$$\partial_\Lambda \Gamma_\Lambda^{(6)}(\omega_1, \omega_2, \omega_3) = \frac{1}{\beta} \sum_\omega \dot{G}_\Lambda(\omega)\, \Gamma_0^{(8)}(\omega_1, \omega_2, \omega_3, \omega) \,. \tag{3.50c}$$

To solve this system of coupled differential equations, we need an explicit expression for the average eight-point vertex $\Gamma_0^{(8)}(\omega_1, \omega_2, \omega_3, \omega_4)$. This can be found by applying the vertex average (3.49) to the full eight-point vertex given in Eq (3.37), which results in

$$\begin{aligned} \Gamma_0^{(8)}(\omega_1, \omega_2, \omega_3, \omega_4) &= -\frac{1}{4!} \mathcal{S}_{\omega_1, \omega_2, \omega_3, \omega_4} \left(\frac{(4!)^2}{8}\, 2J^2 \beta \delta_{12,34} \right) \\ &= -2J^2 \beta \left(\delta_{12,34} + \delta_{13,24} + \delta_{14,23} \right) \,. \end{aligned} \tag{3.51}$$

3.3.3 Zero temperature limit

At zero temperature, the Matsubara sums become integrals,

$$\frac{1}{\beta}\sum_{\omega} = \int_{-\infty}^{\infty} \frac{d\omega}{2\pi} \,, \tag{3.52}$$

and the averaged flow equations read

$$\partial_\Lambda \Sigma_\Lambda(\omega_1) = \int \frac{d\omega_2}{2\pi}\, \dot{G}_\Lambda(\omega_2)\, \Gamma^{(4)}_\Lambda(\omega_1,\omega_2) \,, \tag{3.53a}$$

$$\partial_\Lambda \Gamma^{(4)}_\Lambda(\omega_1,\omega_2) = \int \frac{d\omega_3}{2\pi}\, \dot{G}_\Lambda(\omega_3)\, \Gamma^{(6)}_\Lambda(\omega_1,\omega_2,\omega_3) \,, \tag{3.53b}$$

$$\partial_\Lambda \Gamma^{(6)}_\Lambda(\omega_1,\omega_2,\omega_3) = \int \frac{d\omega_4}{2\pi}\, \dot{G}_\Lambda(\omega_4)\, \Gamma^{(8)}_0(\omega_1,\omega_2,\omega_3,\omega_4) \,. \tag{3.53c}$$

Noting that in the zero temperature limit $\beta\delta_{12,34} \to 2\pi\,\delta(\omega_1+\omega_2-\omega_3-\omega_3)$, the integral in the flow equation for the six-point vertex can easily be evaluated by using the explicit expression (3.51) for the eight-point vertex, giving

$$\begin{aligned}\partial_\Lambda \Gamma^{(6)}_\Lambda(\omega_1,\omega_2,\omega_3) = -2J^2\Big[&\dot{G}_\Lambda(\omega_1+\omega_2-\omega_3) + \dot{G}_\Lambda(\omega_1-\omega_2+\omega_3) \\ &+ \dot{G}_\Lambda(-\omega_1+\omega_2+\omega_3)\Big] \,.\end{aligned} \tag{3.54}$$

The system of flow equations for the average two-, four- and six-point vertices can be closed by noting that the single scale propagator is determined by the self energy through Eq. (3.48c) and the Dyson equation,

$$G^{-1}_\Lambda(\omega) = G^{-1}_{0,\Lambda}(\omega) - \Sigma_\Lambda(\omega) \,. \tag{3.55}$$

However, due to the many degrees of freedom represented by the Matsubara frequencies, a straightforward analytical solution is impossible. Therefore, we will resort to the Katanin substitution and a series of low frequency expansions to simplify the flow equations.

3.3.4 Katanin substitution

We apply the Katanin substitution [83] on the flow equation (3.54) for the six-point vertex. This amounts to the replacement of the single scale propagator by a simple derivative of the full propagator,

$$\dot{G}_\Lambda(\omega) \to \partial_\Lambda G_\Lambda(\omega) \,. \tag{3.56}$$

With the Katanin substitution, the flow equation (3.54) for the six-point vertex can directly be integrated to

$$\begin{aligned}\Gamma^{(6)}_\Lambda(\omega_1,\omega_2,\omega_3) = -2J^2\big[&G_\Lambda(\omega_1+\omega_2-\omega_3) + G_\Lambda(\omega_1-\omega_2+\omega_3) \\ &+ G_\Lambda(-\omega_1+\omega_2+\omega_3)\big] \,.\end{aligned} \tag{3.57}$$

With this result, the flow equation (3.53b) for the 4-vertex reads

$$\partial_\Lambda \Gamma^{(4)}_\Lambda(\omega_1,\omega_2) = -2J^2 \int \frac{d\omega_3}{2\pi}\, \dot{G}_\Lambda(\omega_3)\big[G_\Lambda(\omega_1+\omega_2-\omega_3) + G_\Lambda(\omega_1-\omega_2+\omega_3) + G_\Lambda(-\omega_1+\omega_2+\omega_3)\big] \,. \tag{3.58}$$

To simplify our notation, we define the generalized susceptibilities

$$\chi_\Lambda(\omega) = \int \frac{d\omega_3}{2\pi}\, G_\Lambda(\omega_3)\, G_\Lambda(\omega-\omega_3) \,, \tag{3.59a}$$

$$\Pi_\Lambda(\omega) = \int \frac{d\omega_3}{2\pi}\, G_\Lambda(\omega_3)\, G_\Lambda(\omega_3-\omega) \,, \tag{3.59b}$$

and their single scale derivatives

$$\begin{aligned}\dot{\chi}_\Lambda(\omega) &\equiv \int \frac{d\omega_3}{2\pi}\left[\dot{G}_\Lambda(\omega_3)\, G_\Lambda(\omega-\omega_3) + G_\Lambda(\omega_3)\, \dot{G}_\Lambda(\omega-\omega_3)\right] \\ &= 2\int \frac{d\omega_3}{2\pi} \dot{G}_\Lambda(\omega_3)\, G_\Lambda(\omega-\omega_3) \,, \end{aligned} \tag{3.60a}$$

$$\begin{aligned}\dot{\Pi}_\Lambda(\omega) &\equiv \int \frac{d\omega_3}{2\pi}\left[\dot{G}_\Lambda(\omega_3)\, G_\Lambda(\omega_3-\omega) + G_\Lambda(\omega_3)\, \dot{G}_\Lambda(\omega_3-\omega)\right] \\ &= \int \frac{d\omega_3}{2\pi} \dot{G}_\Lambda(\omega_3)\, \left[G_\Lambda(\omega_3-\omega) + G_\Lambda(\omega_3+\omega)\right] \,. \end{aligned} \tag{3.60b}$$

With these expressions, we rewrite the flow equation (3.58) in the compact form

$$\partial_\Lambda \Gamma^{(4)}_\Lambda(\omega_1,\omega_2) = -J^2\left[\dot{\chi}_\Lambda(\omega_1+\omega_2) + 2\dot{\Pi}_\Lambda(\omega_1-\omega_2)\right] \,. \tag{3.61}$$

3.3.5 Validity of the Katanin substitution

The validity of the Katanin substitution may be questioned, as it is indeed difficult to justify a priori. We note however, that the known exact solution (3.6) for the self energy can be recovered by repeated applications of the Katanin substitution. To see this, we apply the Katanin substitution to the flow equation (3.58) of the four-point vertex to find

$$\partial_\Lambda \Gamma^{(4)}_\Lambda(\omega_1,\omega_2) = -2J^2 \int \frac{d\omega_3}{2\pi}\, \partial_\Lambda G_\Lambda(\omega_3)\big[G_\Lambda(\omega_1+\omega_2-\omega_3) + G_\Lambda(\omega_1-\omega_2+\omega_3) + G_\Lambda(-\omega_1+\omega_2+\omega_3)\big] \,. \tag{3.62}$$

We symmetrize the frequency arguments by shifts of the integration variable ω_3 and obtain

$$\begin{aligned}\partial_\Lambda \Gamma^{(4)}_\Lambda(\omega_1,\omega_2) = -J^2 \int \frac{d\omega_3}{2\pi} \\ \times \Big[&\partial_\Lambda G_\Lambda(\omega_3) G_\Lambda(\omega_1+\omega_2-\omega_3) + \partial_\Lambda G_\Lambda(\omega_1+\omega_2-\omega_3) G_\Lambda(\omega_3) \\ &\partial_\Lambda G_\Lambda(\omega_3) G_\Lambda(\omega_1-\omega_2+\omega_3) + \partial_\Lambda G_\Lambda(-\omega_1+\omega_2+\omega_3) G_\Lambda(\omega_3) \\ &\partial_\Lambda G_\Lambda(\omega_3) G_\Lambda(-\omega_1+\omega_2+\omega_3) + \partial_\Lambda G_\Lambda(\omega_1-\omega_2+\omega_3) G_\Lambda(\omega_3) \Big] ,\end{aligned} \tag{3.63}$$

which can be simplified with the reversed chain rule of differentiation,

$$\begin{aligned}\partial_\Lambda \Gamma^{(4)}_\Lambda(\omega_1,\omega_2) = -J^2 \int \frac{d\omega_3}{2\pi} \partial_\Lambda \Big[&G_\Lambda(\omega_3) G_\Lambda(\omega_1+\omega_2-\omega_3) \\ &+ G_\Lambda(\omega_3) G_\Lambda(\omega_1-\omega_2+\omega_3) + G_\Lambda(\omega_3) G_\Lambda(-\omega_1+\omega_2+\omega_3) \Big] .\end{aligned} \tag{3.64}$$

Interchanging the order of the integration and differentiation, the four-point vertex can then by integrated directly, giving

$$\begin{aligned}\Gamma^{(4)}_\Lambda(\omega_1,\omega_2) = -J^2 \int \frac{d\omega_3}{2\pi} G_\Lambda(\omega_3) \Big[&G_\Lambda(\omega_1+\omega_2-\omega_3) \\ &+ G_\Lambda(\omega_1-\omega_2+\omega_3) + G_\Lambda(-\omega_1+\omega_2+\omega_3) \Big] .\end{aligned} \tag{3.65}$$

The four-point vertex can then be substituted in the flow equation (3.53a) of the self energy, which, after an additional Katanin substitution, reads

$$\begin{aligned}\partial_\Lambda \Sigma_\Lambda(\omega_1) = -J^2 \int \frac{d\omega_2\, d\omega_3}{(2\pi)^2} \partial_\Lambda G_\Lambda(\omega_2)\, G_\Lambda(\omega_3) \Big[&G_\Lambda(\omega_1+\omega_2-\omega_3) \\ &+ G_\Lambda(\omega_1-\omega_2+\omega_3) + G_\Lambda(-\omega_1+\omega_2+\omega_3) \Big] .\end{aligned} \tag{3.66}$$

In order to symmetrize the frequency arguments in this expression, we swap the variable names $\omega_2 \leftrightarrow \omega_3$ in the second term and shift the integration variable $\omega_2 \to \omega_2+\omega_1-\omega_3$ in the third term, which results in

$$\begin{aligned}\partial_\Lambda \Sigma_\Lambda(\omega_1) = -J^2 \int \frac{d\omega_2\, d\omega_3}{(2\pi)^2} \Big[&\partial_\Lambda G_\Lambda(\omega_2)\, G_\Lambda(\omega_3)\, G_\Lambda(\omega_1+\omega_2-\omega_3) \\ &G_\Lambda(\omega_2)\, \partial_\Lambda G_\Lambda(\omega_3)\, G_\Lambda(\omega_1+\omega_2-\omega_3) \\ &G_\Lambda(\omega_2)\, G_\Lambda(\omega_3)\, \partial_\Lambda G_\Lambda(\omega_1+\omega_2-\omega_3) \Big] .\end{aligned} \tag{3.67}$$

Here, we identify again the reverse chain rule of differentiation. We swap the differentiation with the integral, and integrate the self energy to get

$$\Sigma_\Lambda(\omega_1) = -J^2 \int \frac{d\omega_2\, d\omega_3}{(2\pi)^2} G_\Lambda(\omega_2)\, G_\Lambda(\omega_3)\, G_\Lambda(\omega_1+\omega_2-\omega_3)\ . \tag{3.68}$$

After Fourier transformation to imaginary time, this is exactly the solution given in Eq. (3.6). Hence, it seems plausible that the Katanin substitution preserves the underlying physics. However, one of our goals is to find the anomalous dimension during the flow of the SYK model. As will become clear later, the anomalous dimension is determined by the frequency dependence of the flowing four-point vertex. Thus, in what follows, we do not apply the additional Katanin substitutions and work with the flow equation (3.61) for the four-point vertex.

3.3.6 Frequency expansion of the self energy

In summary, we have to solve the two flow equations for the self energy and the four-point vertex,

$$\partial_\Lambda \Sigma_\Lambda(\omega_1) = \int \frac{d\omega_2}{2\pi}\, \dot{G}_\Lambda(\omega_2)\, \Gamma^{(4)}_\Lambda(\omega_1,\omega_2)\ , \tag{3.69a}$$

$$\partial_\Lambda \Gamma^{(4)}_\Lambda(\omega_1,\omega_2) = -\,J^2 \left[\dot{\chi}_\Lambda(\omega_1+\omega_2) + 2\dot{\Pi}_\Lambda(\omega_1-\omega_2)\right]\ , \tag{3.69b}$$

where $\dot{\chi}_\Lambda(\omega)$ and $\dot{\Pi}_\Lambda(\omega)$ are given in Eqs. (3.60) and the single scale propagator is given in Eq. (3.48c) and depends on the self energy via the Dyson equation (3.55).

In order to further reduce the degrees of freedom, we expand the self energy for small frequencies,

$$\Sigma_\Lambda(\omega) \approx \Sigma_\Lambda(0) + \Sigma'_\Lambda(0)\, i\omega\ , \tag{3.70}$$

where we defined the prime in $\Sigma'_\Lambda(\omega)$ as derivative with respect to $i\omega$. For later convenience, we express the frequency dependence in terms of the wave function renormalization factor Z_Λ [39] as

$$\Sigma'_\Lambda(0) = 1 - \frac{1}{Z_\Lambda}\ . \tag{3.71}$$

Furthermore, we define the flowing chemical potential μ_Λ as

$$\mu_\Lambda = Z_\Lambda\, [\mu - \Sigma_\Lambda(0)]\ . \tag{3.72}$$

The motivation is that we will be able to identify μ_Λ as the effective chemical potential of the flowing action later on. Using the chain rule of differentiation, the flow equation for μ_Λ can be written as

$$\partial_\Lambda \mu_\Lambda = [\mu - \Sigma_\Lambda(0)]\, \partial_\Lambda Z_\Lambda - Z_\Lambda\, \partial_\Lambda \Sigma_\Lambda(0)\ . \tag{3.73}$$

In this expression, we identify the anomalous dimension η_Λ in the form [39]

$$\partial_\Lambda Z_\Lambda = \frac{Z_\Lambda}{\Lambda}\eta_\Lambda \,. \tag{3.74}$$

Additionally, we substitute the flow equation (3.69a) for $\partial_\Lambda \Sigma_\Lambda(0)$ and approximate $\Gamma^{(4)}_\Lambda$ to be independent of frequency, and obtain a flow equation for the effective chemical potential,

$$\partial_\Lambda \mu_\Lambda = \frac{Z_\Lambda}{\Lambda}\eta_\Lambda - Z_\Lambda \Gamma^{(4)}_\Lambda \int \frac{d\omega}{2\pi} \dot{G}_\Lambda(\omega) \,. \tag{3.75}$$

The flow equation for the static part $\Gamma^{(4)}_\Lambda$ of the flowing 4-vertex can be found by setting the frequencies in the flow equation (3.69b) to zero, so that we find

$$\partial_\Lambda \Gamma^{(4)}_\Lambda = -J^2 \left[\dot{\chi}_\Lambda(0) + 2\,\dot{\Pi}_\Lambda(0)\right] \,. \tag{3.76}$$

Note that here, we neglected the frequency dependence of the four-point vertex $\Gamma^{(4)}_\Lambda$ to obtain a flow equation for μ_Λ. As we will see later, it will be crucial to keep the frequency dependence of $\Gamma^{(4)}_\Lambda$ to find the anomalous dimension η_Λ, which then by Eq. (3.74) determines the flow of Z_Λ and hence the leading low frequency dependence of the self energy.

3.4 Sharp cutoff

To solve the remaining simplified flow equations, we need to specify the artificial scale dependence of the free propagator $G_{0,\Lambda}(\omega)$. We recall from Sec. 1.2.1 that it has to be chosen such that low frequency modes are suppressed while high frequency modes have to coincide with the free propagator of the SYK model. We employ the simplest way to define such a scale dependence, namely a sharp cutoff of the form

$$\begin{aligned} G_{0,\Lambda}(\omega) =& \frac{\Theta(|\omega| - \Lambda)}{\mu + i\omega} \\ =& \frac{\Theta(\omega - \Lambda) + \Theta(-\omega - \Lambda)}{\mu + i\omega} \,, \end{aligned} \tag{3.77}$$

which simply cuts off all modes below the energy scale Λ.

3.4.1 Propagators

With the expression (3.77) for the flowing free propagator, we can use the Dyson equation (3.55) to find an expression for the full flowing propagator,

$$\begin{aligned} G_\Lambda(\omega) = \left[G^{-1}_{0,\Lambda}(\omega) - \Sigma_\Lambda(\omega)\right]^{-1} =& \frac{G_{0,\Lambda}(\omega)}{1 - G_{0,\Lambda}(\omega)\,\Sigma_\Lambda(\omega)} \\ = \frac{\frac{\Theta(|\omega|-\Lambda)}{\mu+i\omega}}{1 - \frac{\Theta(|\omega|-\Lambda)\Sigma_\Lambda(\omega)}{\mu+i\omega}} =& \frac{\Theta(|\omega| - \Lambda)}{\mu + i\omega - \Theta(|\omega| - \Lambda)\Sigma_\Lambda(\omega)} \,. \end{aligned} \tag{3.78}$$

Inserting the low frequency expansion (3.70) for the self energy, we find

$$G_\Lambda(\omega) \approx \frac{Z_\Lambda\,\Theta(|\omega|-\Lambda)}{\mu_\Lambda + i\omega}\;, \tag{3.79}$$

where Z_Λ and μ_Λ were defined in Eqs. (3.71) and (3.72). The single scale propagator (3.40) can be written as

$$\begin{aligned}\dot{G}_\Lambda(\omega) =& -G_\Lambda^2(\omega)\,\partial_\Lambda G_{0,\Lambda}^{-1}(\omega)\\ =&\frac{\partial_\Lambda G_{0,\Lambda}(\omega)}{\left[1-G_{0,\Lambda}(\omega)\,\Sigma_\Lambda(\omega)\right]^2}\;.\end{aligned} \tag{3.80}$$

We evaluate the derivative of the free propagator (3.77) with respect to the scale Λ as

$$\partial_\Lambda G_{0,\Lambda}(\omega) \;=\; -\frac{\delta(\omega-\Lambda)+\delta(\omega+\Lambda)}{\mu+i\omega}\;, \tag{3.81}$$

where we used $\partial_\Lambda\Theta(\omega-\Lambda) = -\delta(\omega-\Lambda)$ and $\partial_\Lambda\Theta(-\omega-\Lambda) = -\delta(\omega+\Lambda)$. Substitution in Eq. (3.80) then leads to

$$\begin{aligned}\dot{G}_\Lambda(\omega) =& -\frac{\delta(\omega-\Lambda)+\delta(\omega+\Lambda)}{(\mu+i\omega)\left(1-\frac{\Theta(\omega-\Lambda)+\Theta(-\omega-\Lambda)}{\mu+i\omega}\Sigma_\Lambda(\omega)\right)^2}\\ =& -\frac{(\mu+i\omega)\,\delta(\omega-\Lambda)}{\left[\mu+i\omega-\Theta(\omega-\Lambda)\,\Sigma_\Lambda(\omega)\right]^2} - \frac{(\mu+i\omega)\,\delta(\omega+\Lambda)}{\left[\mu+i\omega-\Theta(\omega+\Lambda)\,\Sigma_\Lambda(\omega)\right]^2}\;.\end{aligned} \tag{3.82}$$

To evaluate the combinations of Dirac-deltas and Heaviside step functions, we use the Morris lemma [39, 43], which can be expressed as

$$\delta(x)\,f(\Theta(x)) = \delta(x)\int_0^1 dt\,f(t)\;. \tag{3.83}$$

Applied to Eq. (3.82), this results in

$$\dot{G}_\Lambda(\omega) = -\frac{\delta(\omega-\Lambda)+\delta(\omega+\Lambda)}{\mu+i\omega-\;\Sigma_\Lambda(\omega)}\;, \tag{3.84}$$

where we can substitute again the low frequency expansion (3.70) of the self energy to obtain

$$\dot{G}_\Lambda(\omega) \approx -\frac{Z_\Lambda}{\mu_\Lambda+i\omega}\left[\delta(\omega-\Lambda)+\delta(\omega+\Lambda)\right]\;. \tag{3.85}$$

3.4.2 Generalized susceptibilities

Next, we evaluate the generalized susceptibilities given in Eqs. (3.60). Inserting the explicit expressions for the low frequency propagator (3.79) and the single scale propagator (3.82) in Eq. (3.60a) yields

$$\begin{aligned}\dot{\chi}_\Lambda(\omega) =& -2\int \frac{d\omega_3}{2\pi} \frac{Z_\Lambda\left[\delta(\omega_3-\Lambda)+\delta(\omega_3+\Lambda)\right]}{\mu_\Lambda+i\omega_3} \frac{Z_\Lambda\,\Theta(|\omega-\omega_3|-\Lambda)}{\mu_\Lambda+i(\omega-\omega_3)} \\ =& -\frac{1}{\pi}\frac{Z_\Lambda}{\mu_\Lambda+i\Lambda}\frac{Z_\Lambda[\Theta(-\omega)+\Theta(\omega-2\Lambda)]}{\mu_\Lambda+i(\omega-\Lambda)} \\ & -\frac{1}{\pi}\frac{Z_\Lambda}{\mu_\Lambda-i\Lambda}\frac{Z_\Lambda[\Theta(\omega)+\Theta(-\omega-2\Lambda)]}{\mu_\Lambda+i(\omega+\Lambda)}\,. \end{aligned} \tag{3.86}$$

Here, we used

$$\Theta(|\omega-\Lambda|-\Lambda) = \Theta(-\omega)+\Theta(\omega-2\Lambda)\,, \tag{3.87}$$

$$\Theta(|\omega+\Lambda|-\Lambda) = \Theta(\omega)+\Theta(-\omega-2\Lambda)\,. \tag{3.88}$$

Defining $\sigma_\omega \equiv \operatorname{sign}\omega$, we simplify the expression (3.86) to

$$\begin{aligned}\dot{\chi}_\Lambda(\omega) = -\frac{Z_\Lambda^2}{\pi}\Bigg[&\frac{1}{(\mu_\Lambda-i\sigma_\omega\Lambda)(\mu_\Lambda+i\omega+i\sigma_\omega\Lambda)} \\ &+\frac{\Theta(|\omega|-2\Lambda)}{(\mu_\Lambda+i\sigma_\omega\Lambda)(\mu_\Lambda+i\omega-i\sigma_\omega\Lambda)}\Bigg]\,. \end{aligned} \tag{3.89a}$$

The other generalized susceptibility, $\dot{\Pi}_\Lambda(\omega)$ given in Eq. (3.60b), can be evaluated analogously with the result

$$\begin{aligned}\dot{\Pi}_\Lambda(\omega) = -\frac{Z_\Lambda^2}{\pi}\mathrm{Re}\Bigg\{&\frac{1}{(\mu_\Lambda+i\Lambda)(\mu_\Lambda+i\Lambda+i|\omega|)} \\ &+\frac{\Theta(|\omega|-2\Lambda)}{(\mu_\Lambda+i\Lambda)(\mu_\Lambda+i\Lambda-i|\omega|)}\Bigg\}\,. \end{aligned} \tag{3.89b}$$

3.4.3 Sharp cutoff flow equations

We wish to find the flow equations for the chemical potential μ_Λ and the static part $\Gamma^{(4)}_\Lambda$ of the two-point interaction. Therefore, we substitute the single scale propagator with sharp cutoff given in Eq. (3.85) into the flow equation (3.75) for μ_Λ. This amounts to evaluating a trivial frequency integral over two Dirac-deltas and results in

$$\begin{aligned}\partial_\Lambda\mu_\Lambda &= \frac{\mu_\Lambda}{\Lambda}\eta_\Lambda + \frac{Z_\Lambda^2}{2\pi}\left[\frac{1}{\mu_\Lambda+i\Lambda}+\frac{1}{\mu_\Lambda-i\Lambda}\right]\Gamma^{(4)}_\Lambda \\ &= \frac{\mu_\Lambda}{\Lambda}\eta_\Lambda + \frac{Z_\Lambda^2}{\pi}\frac{\mu_\Lambda}{\mu_\Lambda^2+\Lambda^2}\Gamma^{(4)}_\Lambda\,. \end{aligned} \tag{3.90}$$

To find the flow equation for $\Gamma^{(4)}_\Lambda$, we insert the generalized susceptibilities $\dot{\chi}_\Lambda(\omega)$ and $\dot{\Pi}_\Lambda(\omega)$ given in Eqs. (3.89) in the flow equation (3.76). Doing so, we need to evaluate the susceptibilities $\dot{\chi}_\Lambda(\omega)$ and $\dot{\Pi}_\Lambda(\omega)$ at zero frequency. Note that the expression (3.89a) for $\dot{\chi}_\Lambda(\omega)$ includes a sign function in the denominators, which is discontinuous at $\omega = 0$. However, the zero frequency limit of $\dot{\chi}_\Lambda(\omega)$ is the same from above and below, giving

$$\dot{\chi}_\Lambda(0) = -\frac{Z_\Lambda^2}{\pi}\frac{1}{(\mu_\Lambda - i\Lambda)(\mu_\Lambda + i\Lambda)}\,, \tag{3.91a}$$

$$\dot{\Pi}_\Lambda(0) = -\frac{Z_\Lambda^2}{\pi}\mathrm{Re}\left\{\frac{1}{(\mu_\Lambda + i\Lambda)^2}\right\}\,. \tag{3.91b}$$

This results in the flow equation

$$\begin{aligned}\partial_\Lambda \Gamma^{(4)}_\Lambda =& \frac{J^2 Z_\Lambda^2}{\pi}\left[\frac{1}{(\mu_\Lambda - i\Lambda)(\mu_\Lambda + i\Lambda)} + 2\mathrm{Re}\left\{\frac{1}{(\mu_\Lambda + i\Lambda)^2}\right\}\right] \\ =& \frac{J^2 Z_\Lambda^2}{\pi}\frac{4}{\mu_\Lambda^2 + \Lambda^2}\left[\frac{3}{4} - \frac{\Lambda^2}{\mu_\Lambda^2 + \Lambda^2}\right]\,.\end{aligned} \tag{3.92}$$

3.4.4 Rescaled flow equations

First, we perform a scaling analysis of the action to find the scaling laws for the coupling constants. The quadratic part of the action at zero temperature in the thermodynamic limit can be written as

$$S_{2,\Lambda}[\bar{\boldsymbol{c}}, \boldsymbol{c}] = -\sum_i \int \frac{d\omega}{2\pi}\left[(i\omega + \mu) - \Sigma_\Lambda(\omega)\right]\bar{c}_i(\omega)c_i(\omega)\,. \tag{3.93}$$

We approximate the self energy with the low frequency expansion introduced in Eq. (3.70),

$$\Sigma_\Lambda(\omega) \approx \Sigma_\Lambda(0) + \left(1 - \frac{1}{Z_\Lambda}\right) i\omega\,. \tag{3.94}$$

With this approximation, the quadratic action reads

$$S_{2,\Lambda}[\bar{\boldsymbol{c}}, \boldsymbol{c}] = -\sum_i \int \frac{d\omega}{2\pi}\left[\frac{i\omega}{Z_\Lambda} + (\mu - \Sigma_\Lambda(0))\right]\bar{c}_i(\omega)c_i(\omega)\,. \tag{3.95}$$

Within the FRG, the Wilsonian rescaling can be incorporated by expressing all couplings in units of the scale Λ [39]. We therfore define the dimensionless frequencies

$$\tilde{\omega} = \frac{\omega}{\Lambda}\,, \tag{3.96}$$

and rewrite the quadratic action as

$$S_{2,\Lambda}[\bar{\boldsymbol{c}}, \boldsymbol{c}] = -\sum_i \int \frac{d\tilde{\omega}}{2\pi}\left[i\tilde{\omega} + \frac{\mu_\Lambda}{\Lambda}\right]\frac{\Lambda^2}{Z_\Lambda}\bar{c}_i(\Lambda\tilde{\omega})c_i(\Lambda\tilde{\omega})\,, \tag{3.97}$$

where we identified the flowing chemical potential μ_Λ as given in Eq. (3.72). We notice that by rescaling the fields,

$$\frac{\Lambda}{\sqrt{Z_\Lambda}} c_i(\Lambda\tilde{\omega}) \equiv \tilde{c}_i(\tilde{\omega}) \,, \quad \frac{\Lambda}{\sqrt{Z_\Lambda}} \bar{c}_i(\Lambda\tilde{\omega}) \equiv \bar{\tilde{c}}_i(\tilde{\omega}) \,, \tag{3.98}$$

and the chemical potential,

$$\tilde{\mu}_\Lambda \equiv \frac{\mu_\Lambda}{\Lambda} \,, \tag{3.99}$$

we recover the bare form of the quadratic action in terms of dimensionless variables,

$$S_{2,\Lambda}[\bar{\tilde{\boldsymbol{c}}}, \tilde{\boldsymbol{c}}] = -\sum_i \int \frac{d\tilde{\omega}}{2\pi} \left(i\tilde{\omega} + \tilde{\mu}_\Lambda\right) \bar{\tilde{c}}_i(\tilde{\omega}) \tilde{c}_i(\tilde{\omega}) \,. \tag{3.100}$$

At this point, it becomes clear why Z_Λ is called the wave function renormalization factor. A simple dimensional analysis would only yield a renormalization of the fields by a factor of Λ, and Z_Λ can be understood as an additional non-trivial contribution. The presence of Z_Λ in the rescaled fields in Eq. (3.98) thus leads to an *anomalous* contribution to the overall scaling dimension of the fields. We already introduced this *anomalous dimension* η_Λ in Eq. (3.74).

To proceed, we recall that the bare vertices of the Wilsonian action for frequencies below the cutoff scale coincide with the irreducible vertices generated by the FRG. Hence, we write the $2k$-th order Wilsonian action as

$$\begin{aligned} S_{2k,\Lambda}[\bar{\boldsymbol{c}}, \boldsymbol{c}] = -\frac{1}{(k!)^2 N^k} \sum_{i_1 \dots i_k} \sum_{i'_1 \dots i'_k} \int \frac{d\omega_1 \dots d\omega_k \, d\omega'_k \dots d\omega'_1}{(2\pi)^{2k}} \\ \times 2\pi\delta(\omega_1 + \dots + \omega_k - \omega'_k \dots - \omega'_1) \\ \times \Gamma^{(2k)}_{\Lambda, i_1 \dots i_k i'_k \dots i'_1}(\omega_1 \dots \omega_n; \omega'_k \dots \omega_1) \\ \times \bar{c}_{i_1}(\omega_1) \dots \bar{c}_{i_k}(\omega_k) c_{i_k}(\omega_k) \dots c_{i_1}(\omega_1) \,. \end{aligned} \tag{3.101}$$

In order to express this in dimensionless form as

$$\begin{aligned} S_{2k,\Lambda}[\bar{\tilde{\boldsymbol{c}}}, \tilde{\boldsymbol{c}}] = -\frac{1}{(k!)^2 N^k} \sum_{i_1 \dots i_k} \sum_{i'_1 \dots i'_k} \int \frac{d\tilde{\omega}_1 \dots d\tilde{\omega}_k \, d\tilde{\omega}'_k \dots d\tilde{\omega}'_1}{(2\pi)^{2k}} \\ \times 2\pi\delta(\tilde{\omega}_1 + \dots + \tilde{\omega}_k - \tilde{\omega}'_k \dots - \tilde{\omega}'_1) \\ \times \tilde{\Gamma}^{(2k)}_{\Lambda, i_1 \dots i_k i'_k \dots i'_1}(\tilde{\omega}_1 \dots \tilde{\omega}_n; \tilde{\omega}'_k \dots \tilde{\omega}_1) \\ \times \bar{\tilde{c}}_{i_1}(\tilde{\omega}_1) \dots \bar{\tilde{c}}_{i_k}(\tilde{\omega}_k) \tilde{c}_{i_k}(\tilde{\omega}_k) \dots \tilde{c}_{i_1}(\tilde{\omega}_1) \,, \end{aligned} \tag{3.102}$$

we need to rescale the vertices as

$$\begin{aligned} &\tilde{\Gamma}^{(2k)}_{\Lambda, i_1 \dots i_k i'_k \dots i'_1}(\tilde{\omega}_1 \dots \tilde{\omega}_n; \tilde{\omega}'_k \dots \tilde{\omega}_1) \\ &\qquad \equiv \frac{Z_\Lambda^k}{\Lambda} \Gamma^{(2k)}_{\Lambda, i_1 \dots i_k i'_k \dots i'_1}(\Lambda\tilde{\omega}_1 \dots \Lambda\tilde{\omega}_n; \Lambda\tilde{\omega}'_k \dots \Lambda\tilde{\omega}_1) \,. \end{aligned} \tag{3.103}$$

To consider the limit $\Lambda \to 0$, it is practical to introduce the logarithmic flow parameter

$$l = -\ln(\Lambda/\Lambda_0) \, . \tag{3.104}$$

With the preceeding scaling analysis in mind, we thus define the rescaled chemical potential and the rescaled four-point vertex in terms of the new flow parameter l as

$$\mu_l = \frac{\mu_\Lambda}{\Lambda}\bigg|_{\Lambda=\Lambda_0 e^{-l}} \, , \tag{3.105}$$

$$u_l = \frac{Z_\Lambda^2}{\Lambda}\,\Gamma_\Lambda^{(4)}\bigg|_{\Lambda=\Lambda_0 e^{-l}} \, . \tag{3.106}$$

Note that Z_Λ and η_Λ are dimensionless and we do not rescale them. We therefore define

$$Z_l = Z_\Lambda\big|_{\Lambda=\Lambda_0 e^{-l}} \, . \tag{3.107}$$

$$\eta_l = \eta_\Lambda\big|_{\Lambda=\Lambda_0 e^{-l}} \, . \tag{3.108}$$

Using $\partial_l = -\Lambda\partial_\Lambda$ and the chain rule of differentiation, we find the flow equations

$$\begin{aligned} \partial_l \mu_l =& \mu_l - \partial_\Lambda \mu_\Lambda \\ =& (1-\eta_l)\mu_l - \frac{1}{\pi}\frac{\mu_l}{\mu_l^2+1} u_l \, , \end{aligned} \tag{3.109}$$

and

$$\begin{aligned} \partial_l u_l =& u_l - 2Z_\Lambda \Gamma_\Lambda^{(4)} \partial_\Lambda Z_\Lambda - Z_\Lambda^2 \partial_\Lambda \gamma_\Lambda^{(4)} \\ =& (1-2\eta_l)u_l + \frac{4}{\pi}\frac{J^2 Z_\Lambda^4}{\Lambda^2}\frac{1}{\mu_l^2+1}\left(\frac{1}{\mu_l^2+1}-\frac{3}{4}\right) \\ =& (1-2\eta_l)u_l + \frac{4}{\pi}\frac{g_l}{\mu_l^2+1}\left(\frac{1}{\mu_l^2+1}-\frac{3}{4}\right) \, , \end{aligned} \tag{3.110}$$

where we inserted the flow equations of the dimensionful couplings μ_Λ and $\Gamma_\Lambda^{(4)}$ given in Eqs. (3.90) and (3.92) and identified the anomalous dimension η_l as given in Eq. (3.74). In the last line of Eq. (3.110) we defined a new flowing variable

$$g_l \equiv \frac{J^2 Z_\Lambda^4}{\Lambda^2} \, , \tag{3.111}$$

which has the flow equation

$$\partial_l g_l = 2(1-2\eta_l) g_l \, . \tag{3.112}$$

This auxiliary variable encodes the leading frequency dependence of the flowing self energy by virtue of the definition of Z_Λ given in Eq. (3.71).

3.5 Discontinuity fixed point

We have not yet analyzed the flow of the anomalous dimension η_l. Nevertheless, we already notice that the flow equations (3.109), (3.110) and (3.112) for the couplings μ_l, u_l and g_l simplify in the case $\eta = 1/2$ to

$$\partial_l \mu_l = \frac{1}{2}\mu_l - \frac{1}{\pi}\frac{\mu_l u_l}{\mu_l^2 + 1} , \tag{3.113a}$$

$$\partial_l u_l = \frac{4}{\pi}\frac{g_l}{\mu_l^2 + 1}\left(\frac{1}{\mu_l^2 + 1} - \frac{3}{4}\right) , \tag{3.113b}$$

$$\partial_l g_l = 0 . \tag{3.113c}$$

This would imply a fixed point at

$$\mu_l = \mu_* \equiv \frac{1}{\sqrt{3}} , \tag{3.114a}$$

$$u_l = u_* \equiv \frac{2\pi}{3} . \tag{3.114b}$$

We will show in this section that this fixed point describes the discontinuous phase transition between the IV and the nFL phase discussed in Sec. 1.2.2. Adapting the terminology put forward in Ref. [84], we call this fixed point discontinuity fixed point (DFP). We will postpone the more technical calculations until the next section, where we show that the anomalous dimension is indeed given by $\eta = 1/2$ for the above fixed point. A more detailed analysis of the anomalous dimension is also needed to find the fixed point value of the coupling g_l, which we will determine in the next section as $g_* \approx 8.52$.

In this section, we investigate the RG flow in the vicinity of the DFP. We start by plotting the RG flow given by the flow equations (3.113) in Fig. 3.5, assuming that $\eta_l = 1/2$ and $g_l = g_*$ are fixed. This is of course an approximation because η_l and g_l are flowing themselves. However, close enough to the fixed point we expect this approximation to be sufficient for a qualitative discussion. We see that in the μ_l, u_l coupling space, the DFP has one attractive (irrelevant) and one repulsive (relevant) direction. This is indicative of a phase transition: the coupling space is divided into two regions. For initial couplings on the left side of the dashed line in Fig. 3.5 (small chemical potential), the system flows towards the top left corner during the RG flow. We will argue later that this corresponds to the nFL phase described by the exact solution (3.6). For initial couplings to the right of the dashed line in Fig. 3.5 (large chemical potential), the RG flow leads to the lower right corner, which corresponds to the IV phase. Thus, the DFP describes a phase transition between the nFL and the IV phase which is controlled by the chemical potential, and it seems likely that this is the discontinuous phase transition discussed in Sec. 1.2.2.

To verify this claim, we analyze the scaling behavior near the phase transition. Probably the most celebrated feature of the Wilsonian RG is

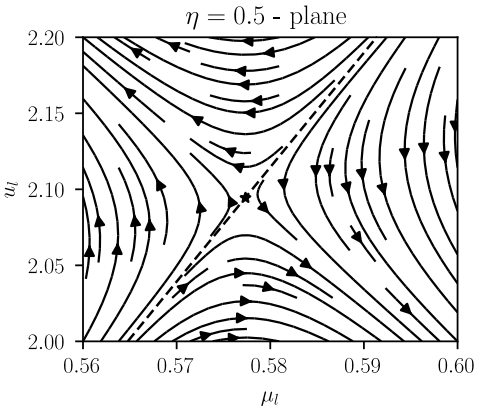

Figure 3.5: RG flow near the DFP resulting from the flow equations (3.113). The dashed line shows the separatrix wich divides the parameter space into nFL and IV phase. The star on the separatrix marks the DFP.

its capability to derive the scaling laws near phase transitions. The scaling exponents can be computed from the speed of the RG flow λ in the vicinity the corresponding fixed point [33, 39]. In our case, the scaling law for the singular part of the grand canonical potential can be written as

$$\Omega_{\text{sing}}(\mu - \mu_*) = e^{-l}\Omega_{\text{sing}}\left(e^{\lambda l}(\mu - \mu*)\right) \ . \tag{3.115}$$

We can find a power law for $\Omega_{\text{sing}}(\mu - \mu_*)$ by choosing the flow parameter l in Eq. (3.115) such that

$$e^{\lambda l_+}(\mu - \mu*) \stackrel{!}{=} \delta_+ \quad \text{if } \mu > \mu_* \ , \tag{3.116a}$$

$$e^{\lambda l_-}(\mu - \mu*) \stackrel{!}{=} \delta_- \quad \text{if } \mu < \mu_* \ , \tag{3.116b}$$

for some arbitrary energy differences $\delta_+ > 0$ above and $\delta_- < 0$ below the phase transition. Solving these conditions for e^{l_+} and e^{l_-} and substituting them in the scaling law (3.115) then leads to the power law

$$\Omega_{\text{sing}}(\mu - \mu_*) = \left(\frac{\mu - \mu_*}{\delta_\pm}\right)^{\frac{1}{\lambda}} \Omega_{\text{sing}}(\delta_\pm) \ , \tag{3.117}$$

where the $(+)$ sign has to be taken for values $\mu > \mu_*$ and the $(-)$ sign for $\mu < \mu_*$. Note that the expression in the parenthesis is always positive because the signs of $(\mu - \mu_*)$ and $\delta_\pm$ are the same. The contribution of $\Omega_{\text{sing}}(\mu - \mu_*)$ to the fermionic occupation number n is then given by

$$n_{\text{sign}} = \frac{\partial \Omega_{\text{sing}}}{\partial(\mu - \mu_*)} = \frac{1}{\lambda}\left(\frac{\mu - \mu_*}{\delta_\pm}\right)^{\frac{1}{\lambda}-1} \Omega_{\text{sing}}(\delta_\pm) \ . \tag{3.118}$$

This can be written in the more convenient form

$$n_{\text{sign}} = B_\pm |\mu - \mu_*|^{\frac{1}{\lambda}-1}, \tag{3.119}$$

where we defined the constants

$$B_\pm = \frac{1}{\lambda}\left(\frac{\pm 1}{\delta_\pm}\right)^{\frac{1}{\lambda}-1}\Omega_{\text{sing}}(\delta_\pm)\ . \tag{3.120}$$

We see from Eq. (3.119), that a scaling exponent of $\lambda = 1$ would result in a discontinuity in the occupation number of magnitude

$$\Delta n = B_+ - B_-\ . \tag{3.121}$$

Note that this is also consistent with the discussion in Refs. [84, 85], where it is argued that a scaling exponent equal to the rescaled spatial dimension results in a discontinuous phase transition. In our case, we have no spatial degrees of freedom but rescale the frequencies. Since in Euclidean field theory the conjugate to the frequencies, the complex time parameter, is effectively the same as a spatial dimension, we expect to find a scaling exponent of $\lambda = 1$ at the DFP.

To find a numerical value for our scaling exponent λ, we linearize the flow equations (3.113) in the vicinity of the DFP by introducing the small deviations

$$\delta\mu_l = \mu_l - \mu_*\ , \tag{3.122a}$$
$$\delta u_l = u_l - u_*\ . \tag{3.122b}$$

The linearized flow equations of the deviations can be found by taking variational derivatives of the flow equations (3.113), leading to

$$\partial_l\,\delta\mu_l = \frac{\delta\left(\partial_l\mu_l\right)}{\delta\mu_l}\bigg|_*\delta\mu_l + \frac{\delta\left(\partial_l\mu_l\right)}{\delta u_l}\bigg|_*\delta u_l\ , \tag{3.123a}$$
$$\partial_l\,\delta u_l = \frac{\delta\left(\partial_l u_l\right)}{\delta\mu_l}\bigg|_*\delta\mu_l + \frac{\delta\left(\partial_l u_l\right)}{\delta u_l}\bigg|_*\delta u_l\ , \tag{3.123b}$$

where the subscript $|_*$ indicates that the variational derivative is evaluated at the DFP. After evaluating the variational derivatives, we write the flow equations for the deviations (3.123) in matrix form as

$$\partial_l\begin{pmatrix}\delta\mu_l\\ \delta u_l\end{pmatrix} = \begin{pmatrix}\frac{1}{4} & -\frac{\sqrt{3}}{4\pi}\\ -\frac{9\sqrt{3}}{8\pi}g_* & 0\end{pmatrix}\begin{pmatrix}\delta\mu_l\\ \delta u_l\end{pmatrix}\ . \tag{3.124}$$

To obtain the scaling exponents, we need to find the eigenvalues and eigenvectors of the above matrix. To avoid the distinction between left and right eigenvectors, we first symmetrize the matrix by the transformation

$$\delta u_l = 3\sqrt{\frac{g_*}{2}}\delta y_l\ , \tag{3.125}$$

which leads to

$$\partial_l \begin{pmatrix} \delta\mu_l \\ \delta y_l \end{pmatrix} = \begin{pmatrix} \frac{1}{4} & -a \\ -a & 0 \end{pmatrix} \begin{pmatrix} \delta\mu_l \\ \delta y_l \end{pmatrix} , \tag{3.126}$$

with

$$a = \frac{3}{4\pi}\sqrt{\frac{3g_*}{2}} . \tag{3.127}$$

The eigenvalues $\lambda_\pm$ and eigenvectors $\boldsymbol{v}_\pm$ are then given by

$$\lambda_\pm = \frac{1}{8} \pm \sqrt{a^2 + \frac{1}{64}} , \tag{3.128a}$$

$$\boldsymbol{v}_\pm = \begin{pmatrix} -\frac{\lambda_\pm}{a} \\ 1 \end{pmatrix} . \tag{3.128b}$$

With the numerical value $g_* \approx 8.52$ evaluated in the next section, this leads to

$$\lambda_+ \approx +0.987 , \tag{3.129a}$$

$$\lambda_- \approx -0.737 . \tag{3.129b}$$

We see that the relevant direction $\boldsymbol{v}_+$ is proportional to $\delta\mu = (\mu - \mu_*)$ and hence determines the scaling behaviour of the free energy with respect to the chemical potential. Moreover, the numerical value of the scaling exponent λ_+ is reasonably close to 1, confirming that the DFP does indeed describe the discontinuous phase transition between the nFL and the IV phase. The numerical error in the scaling exponent is most likely due to the approximations used in the next section to calculate the fixed point value g_*.

3.5.1 Anomalous dimension

In this subsection, we explicitly calculate the anomalous dimension at the DFP. The anomalous dimension is determined by the linear frequency dependence $\Sigma'_\Lambda(0)$ of the self energy given in Eq. (3.71). Taking the Λ-derivative of Eq. (3.71) leads to

$$\begin{aligned} \partial_\Lambda \Sigma'_\Lambda(0) =& \frac{1}{Z_\Lambda^2} \partial_\Lambda Z_\Lambda \\ =& \frac{1}{\Lambda Z_\Lambda} \eta_\Lambda , \end{aligned} \tag{3.130}$$

where we used Eq. (3.74) to identify the anomalous dimension in the last equality. Rearranging the terms and writing $\Sigma'_\Lambda(0)$ as a frequency derivative of the self energy leads to

$$\eta_\Lambda = \Lambda Z_\Lambda \partial_\Lambda \left. \frac{\partial \Sigma_\Lambda(\omega)}{\partial(i\omega)} \right|_{\omega=0} . \tag{3.131}$$

Next, we substitute the flow equation (3.53a) for $\Sigma_\Lambda(\omega)$ and get

$$\eta_\Lambda = \Lambda Z_\Lambda \int \frac{d\omega_2}{2\pi} \dot{G}_\Lambda(\omega_2) \frac{\partial \Gamma^{(4)}_\Lambda(\omega_1, \omega_2)}{\partial(i\omega_1)}\bigg|_{\omega_1=0} . \tag{3.132}$$

The above expression shows that the frequency dependence of the four-point vertex determines the anomalous dimension. There are two possible strategies to deal with this frequency dependence:

1. The frequency derivative of the four-point vertex can be integrated using the flow equation (3.61) for the four-point vertex and the explicit expressions for $\dot{\Pi}_\Lambda(\omega)$ and $\dot{\chi}_\Lambda(\omega)$ given in Eqs. (3.91).

2. The frequency dependencies of the four-point vertex can be expressed as additional couplings with corresponding flow equations.

It turns out that the second strategy is practical for a numerical evaluation of flow trajectories, which we will do in Sec. 3.6. In this section, we want to analyze the anomalous dimension at the DFP analytically, using the first strategy. We begin by integrating the frequency derivative of the four-point vertex,

$$\begin{aligned} \frac{\partial \Gamma^{(4)}_\Lambda(\omega_1, \omega_2)}{\partial(i\omega_1)}\bigg|_{\omega_1=0} &= \frac{\partial}{\partial(i\omega_1)} \left[\int_{\Lambda_0}^{\Lambda} dx\, \partial_x \Gamma^{(4)}_x(\omega_1, \omega_2) \right]_{\omega_1=0} \\ &= \int_{\Lambda_0}^{\Lambda} dx \left[\frac{\partial}{\partial(i\omega_1)} \partial_x \Gamma^{(4)}_x(\omega_1, \omega_2) \right]_{\omega_1=0} , \end{aligned} \tag{3.133}$$

where we swapped differentiation and integration in the second equality. Inserting this and the single scale propagator (3.85) into the integral equation (3.132) for η_Λ, we get

$$\begin{aligned} \eta_\Lambda = -\frac{\Lambda Z_\Lambda^2}{2\pi} \int_{\Lambda_0}^{\Lambda} dx \Bigg[&\frac{1}{\mu_\Lambda + i\Lambda} \frac{\partial}{\partial(i\omega_1)} \partial_x \Gamma^{(4)}_x(\omega_1, \Lambda) \\ &+ \frac{1}{\mu_\Lambda - i\Lambda} \frac{\partial}{\partial(i\omega_1)} \partial_x \Gamma^{(4)}_x(\omega_1, -\Lambda) \Bigg]_{\omega_1=0} . \end{aligned} \tag{3.134}$$

Note that the ω_2 integration disappeared due to the two Dirac-deltas in the single scale propagator. Using the expression (3.61) for the flow of the momentum dependent four-point vertex, we find

$$\partial_x \Gamma^{(4)}_x(\omega_1, \pm\Lambda) = -J^2 \left[\dot{\chi}_x(\omega_1 \pm \Lambda) + 2\dot{\Pi}_x(\omega_1 \mp \Lambda) \right] . \tag{3.135}$$

Taking the derivative with respect to ω_1 yields

$$\frac{\partial}{\partial(i\omega_1)} \partial_x \Gamma^{(4)}_x(\omega_1, \pm\Lambda)\bigg|_{\omega_1=0} = -J^2 \left[\dot{\chi}'_x(\pm\Lambda) + 2\dot{\Pi}'_x(\mp\Lambda) \right] , \tag{3.136}$$

where we defined

$$\dot{\chi}'_x(\omega) \equiv \frac{\partial \dot{\chi}_x(\omega)}{\partial(i\omega)} \,, \tag{3.137a}$$

$$\dot{\Pi}'_x(\omega) \equiv \frac{\partial \dot{\Pi}_x(\omega)}{\partial(i\omega)} \,. \tag{3.137b}$$

The latter two expressions can be evaluated by taking the derivatives of the explicit sharp-cutoff expressions for $\dot{\chi}_x(\omega)$ and $\dot{\Pi}_x(\omega)$ given in Eqs. (3.89a) and (3.89b). At $\omega = \pm\Lambda$, they assume the values

$$\dot{\chi}'_x(\pm\Lambda) = \frac{Z_x^2}{\pi} \frac{1}{(\mu_x \mp ix)\left[\mu_x \pm i(\Lambda + x)\right]^2} \,, \tag{3.138a}$$

$$\dot{\Pi}'_x(\pm\Lambda) = \pm \frac{Z_x^2}{\pi}\, i\,\mathrm{Im}\left\{ \frac{1}{(\mu_x + ix)\left[\mu_x + i(\Lambda + x)\right]^2} \right\} \,. \tag{3.138b}$$

Before putting everything together, we observe that

$$\dot{\chi}'_x(-\Lambda) = \left(\dot{\chi}'_x(+\Lambda)\right)^* \,, \tag{3.139a}$$

$$\dot{\Pi}'_x(-\Lambda) = \left(\dot{\Pi}'_x(+\Lambda)\right)^* \,, \tag{3.139b}$$

which by Eq. (3.136) implies

$$\frac{\partial}{\partial(i\omega_1)} \partial_x \Gamma_x^{(4)}(\omega_1, -\Lambda)\Big|_{\omega_1=0} = \left(\frac{\partial}{\partial(i\omega_1)} \partial_x \Gamma_x^{(4)}(\omega_1, +\Lambda)\Big|_{\omega_1=0} \right)^* \,. \tag{3.140}$$

This allows us to simplify the expression for the anomalous dimension (3.134) to

$$\eta_\Lambda = -\frac{\Lambda Z_\Lambda^2}{\pi} \int_{\Lambda_0}^{\Lambda} dx\, \mathrm{Re}\left\{ \frac{1}{\mu_\Lambda + i\Lambda} \frac{\partial}{\partial(i\omega_1)} \partial_x \Gamma_x^{(4)}(\omega_1, \Lambda) \right\}_{\omega_1=0} \,. \tag{3.141}$$

Inserting the flow equation of the frequency derivative of the four-point vertex (3.136) and subsequently the explicit expressions (3.138) for $\dot{\chi}'_x(\Lambda)$ and $\dot{\Pi}'_x(-\Lambda)$ then results in

$$\begin{aligned} \eta_\Lambda = \frac{\Lambda Z_\Lambda^2 J^2}{\pi^2} \int_{\Lambda_0}^{\Lambda} dx\, Z_x^2 \Bigg[&\mathrm{Re}\left\{ \frac{1}{(\mu_\Lambda + i\Lambda)(\mu_x - ix)(\mu_x + ix + i\Lambda)^2} \right\} \\ &- 2\mathrm{Re}\left\{ \frac{i}{\mu_\Lambda + i\Lambda} \mathrm{Im}\left(\frac{1}{(\mu_x + ix)(\mu_x + ix + i\Lambda)^2} \right) \right\} \Bigg] \,. \end{aligned} \tag{3.142}$$

Next, we employ an approximation for the integral by assuming that the system has flown to the vicinity of the DFP, where the unrescaled chemical potential μ_Λ vanishes and where we set $Z_x \to Z_\Lambda$ because the integral is dominated by the region $x \approx \Lambda \ll \Lambda_0$. This results in the simpler integral

$$\eta_\Lambda = -3\frac{Z_\Lambda^4 J^2}{\pi^2} \int_{\Lambda_0}^{\Lambda} dx\, \frac{1}{x(1+x)^2} \,, \tag{3.143}$$

which can straightforwardly be integrated, giving

$$\eta_\Lambda = \frac{Z_\Lambda^4 J^2}{\Lambda^2} c \,. \tag{3.144}$$

Here, we neglected the contribution from the lower boundary Λ_0 and defined the numerical constant

$$c = \frac{3}{\pi^2}\left(\ln 2 - \frac{1}{2}\right) \approx 0.0587 \,. \tag{3.145}$$

The anomalous dimension η_Λ is related to the flow of Z_Λ by Eq. (3.74), which allows us to turn Eq. (3.144) into a differential equation for Z_Λ,

$$\partial_\Lambda Z_\Lambda = \frac{Z_\Lambda^5 J^2}{\Lambda^3}\, c \,. \tag{3.146}$$

This equation is solved by

$$Z_\Lambda = \sqrt{\frac{\Lambda}{\Lambda_c}}\left(1 + \frac{\Lambda^2}{\Lambda_c^2} - \frac{\Lambda^2}{\Lambda_0^2}\right)^{-\frac{1}{4}} \,, \tag{3.147}$$

where we chose the initial condition $Z_{\Lambda_0} = 1$ and defined the crossover scale

$$\Lambda_c = \sqrt{2c}\, J \,. \tag{3.148}$$

Differentiating the expression (3.147) with respect to Λ and using the relation (3.74) between the anomalous dimension and Z_Λ, we find

$$\eta_\Lambda = \frac{1}{2}\left(1 + \frac{\Lambda^2}{\Lambda_c^2} - \frac{\Lambda^2}{\Lambda_0^2}\right)^{-1} \,. \tag{3.149}$$

From this expression, it is evident that the anomalous dimension does indeed assume the value $\eta = 1/2$ in the limit $\Lambda \to 0$, validating our earlier analysis in Sec. 3.5, where we took this result as an assumption. We plot Z_Λ and η_Λ in Fig. 3.6.

We can now also determine the value of g_l at the DFP. In the expression (3.144) for η_Λ, we identify g_l in the form given in Eq. (3.111). Given that $\eta_\Lambda = 1/2$ at the DFP, we infer for g_l the fixed point value

$$g_* = \frac{1}{2c} \approx 8.52 \,. \tag{3.150}$$

3.6 Global flow diagram

In the previous section, we were able to solve the integral equation for the anomalous dimension η_Λ (3.142) with a crude approximation which was good only in the vicinity of the DFP. To obtain flow trajectories throughout the

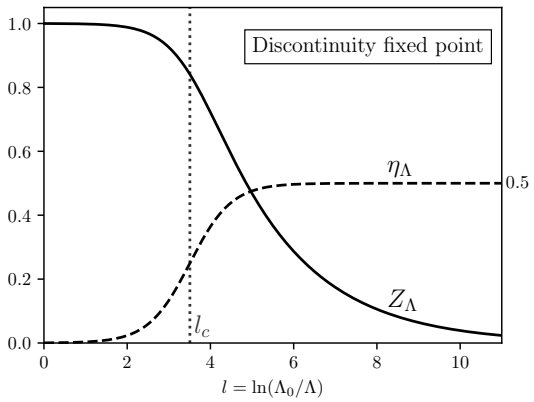

Figure 3.6: Wave function renormalization Z_Λ and anomalous dimension η_Λ at the DFP as given in Eqs. (3.147) and (3.149). Note that we plot against the flow parameter $l = \ln(\Lambda_0/\Lambda)$ defined in Eq. (3.104). The vertical dotted line marks the crossover scale $l_c = \ln(\Lambda_0/\Lambda_c)$ defined by Eq. (3.148).

coupling space and analyze the resulting phase diagram, we need to evaluate the anomalous dimension in a more general way, which necessitates a numerical approach. It turns out that numerically, there is a more convenient way than solving the integral equation (3.142). We saw in the previous section that we need to take the linear frequency dependence of the four-point vertex into account. In this section, we do this by expanding the four-point vertex as

$$\Gamma^{(4)}_\Lambda(\omega_1, \omega_2) \approx u_\Lambda(\omega_2) + \gamma_\Lambda(\omega_2) i\omega_1 \,. \tag{3.151}$$

Here, we introduced the frequency dependent expansion coefficients

$$u_\Lambda(\omega_2) = \Gamma^{(4)}_\Lambda(0, \omega_2) \tag{3.152a}$$

$$\gamma_\Lambda(\omega_2) = \frac{\partial \Gamma^{(4)}_\Lambda(\omega_1, \omega_2)}{\partial(i\omega_1)}\bigg|_{\omega_1=0} \,, \tag{3.152b}$$

which we will treat as additional couplings in the FRG flow. The general integral equation (3.132) for the anomalous dimension can then be expressed in terms of the expansion coefficient $\gamma_\Lambda(\omega_2)$ as

$$\eta_\Lambda = \Lambda Z_\Lambda \int \frac{d\omega_2}{2\pi} \dot{G}_\Lambda(\omega_2)\gamma_\Lambda(\omega_2) \,. \tag{3.153}$$

Substituting the single scale propagator (3.85), the integral is removed by the two Dirac-deltas and we get

$$\begin{aligned} \eta_\Lambda &= -\frac{\Lambda Z_\Lambda^2}{2\pi}\left(\frac{\gamma_\Lambda(\Lambda)}{\mu_\Lambda + i\Lambda} + \frac{\gamma_\Lambda(-\Lambda)}{\mu_\Lambda - i\Lambda}\right) \\ &= -\frac{\Lambda Z_\Lambda^2}{\pi} \operatorname{Re}\left\{\frac{\gamma_\Lambda(\Lambda)}{\mu_\Lambda + i\Lambda}\right\} \,, \end{aligned} \tag{3.154}$$

where in the second equality we used that $\gamma_\Lambda(\omega) = (\gamma_\Lambda(-\omega))^*$. We will show next that in order to evaluate $\gamma_\Lambda(\Lambda)$, we have to solve differential equations

for $\gamma_\Lambda(\omega)$ with $\omega < \Lambda$, i.e. the problem can be transformed from solving an integral equation to solving differential flow equations for infinitely many couplings (one for each frequency $\omega < \Lambda$). Recalling the scaling analysis presented in Sec. 3.4.4, we define the rescaled couplings

$$\gamma_l(\tilde{\omega}) \equiv Z_\Lambda^2 \gamma_\Lambda(\tilde{\omega}\Lambda)\Big|_{\Lambda=\Lambda_0 e^{-l}} , \tag{3.155}$$

where $\tilde{\omega} = \omega/\Lambda$ is the rescaled frequency defined in Eq. (3.96). In terms of rescaled quantities, the anomalous dimension (3.154) can be written as

$$\eta_l = -\frac{1}{\pi}\mathrm{Re}\left\{\frac{\gamma_l(1)}{\mu_l + i}\right\} . \tag{3.156}$$

We take the scale derivative of $\gamma_l(\tilde{\omega})$ given in Eq. (3.155) at fixed $\tilde{\omega}$ and find the flow equation

$$\begin{aligned}
\partial_l \gamma_l(\tilde{\omega}) =& -\Lambda \frac{d}{d\Lambda}\left[Z_\Lambda^2 \gamma_\Lambda(\tilde{\omega}\Lambda)\right] \\
=& -\Lambda\left(\partial_\Lambda Z_\Lambda^2\right)\gamma_\Lambda(\tilde{\omega}\Lambda) - \Lambda Z_\Lambda^2\, \partial_\Lambda \gamma_\Lambda(\tilde{\omega}\Lambda) - \Lambda Z_\Lambda^2 \frac{\partial \gamma_\Lambda(\omega)}{\partial\omega}\Big|_{\omega=\tilde{\omega}\Lambda} \frac{d(\tilde{\omega}\Lambda)}{d\Lambda} \\
=& -2Z_\Lambda^2 \eta_\Lambda \gamma_\Lambda(\tilde{\omega}\Lambda) - \Lambda Z_\Lambda^2\, \partial_\Lambda \gamma_\Lambda(\tilde{\omega}\Lambda) - \Lambda Z_\Lambda^2\, \gamma'_\Lambda(\tilde{\omega}\Lambda)\tilde{\omega} ,
\end{aligned} \tag{3.157}$$

where we defined $\gamma'_\Lambda(\omega) = d\gamma_\Lambda(\omega)/d\omega$. We discuss the three terms on the rightmost side separately:

- In the first term, we identify the rescaled coupling $\gamma_l(\tilde{\omega})$ given in Eq. (3.155) and write

$$-2Z_\Lambda^2 \eta_\Lambda \gamma_\Lambda(\tilde{\omega}\Lambda) = -2\eta_l\, \gamma_l(\tilde{\omega}) . \tag{3.158}$$

- For the second term, we need the flow equation of the unrescaled couplings $\gamma_\Lambda(\omega)$. We recall that by Eq. (3.152b), $\gamma_\Lambda(\omega)$ is a frequency derivative of the four-point vertex $\Gamma_\Lambda(\omega_1, \omega_2)$. We therefore take the frequency derivative of the flow equation of $\Gamma_\Lambda(\omega_1, \omega_2)$ given in Eq. (3.61) and find

$$\begin{aligned}
\partial\gamma_\Lambda(\omega) =& \frac{\partial}{\partial\omega_1}\left[\partial_\Lambda \Gamma_\Lambda^{(4)}(\omega_1, \omega)\right]_{\omega_1=0} \\
=& -J^2 \frac{\partial}{\partial\omega_1}\left[\dot{\chi}_\Lambda(\omega_1+\omega) + 2\dot{\Pi}_\Lambda(\omega_1-\omega)\right]_{\omega_1=0} .
\end{aligned} \tag{3.159}$$

  We have already evaluated the frequency derivatives of $\dot{\chi}_\Lambda(\omega)$ and $\dot{\Pi}_\Lambda(\omega)$ in Eqs. (3.138), and find

$$\partial\gamma_\Lambda(\omega) = -iJ^2\left[\dot{\chi}'_\Lambda(\omega) - 2\dot{\Pi}'_\Lambda(\omega)\right] . \tag{3.160}$$

The factor of i appears because $\dot{\chi}'_\Lambda(\omega)$ and $\dot{\Pi}'_\Lambda(\omega)$ are defined in Eqs. (3.137) as derivatives with respect to $i\omega$. Inserting the explicit expressions for $\dot{\chi}'_\Lambda(\omega)$ and $\dot{\Pi}'_\Lambda(\omega)$ given in Eqs. (3.138) and imposing $|\omega| \leq \Lambda$ then gives an explicit expression for the second term,

$$-\Lambda Z_\Lambda^2 \partial_\Lambda \gamma_\Lambda(\tilde{\omega}\Lambda) = \frac{J^2 Z_\Lambda^4 \Lambda}{\pi} \Bigg[\frac{1}{(\mu_\Lambda - i\sigma_\omega \Lambda)(\mu_\Lambda + i\omega + i\sigma_\omega \Lambda)^2} - 2i\sigma_\omega \mathrm{Im} \left\{ \frac{1}{(\mu_\Lambda + i\Lambda)(\mu_\Lambda + i\Lambda + i\sigma_\omega \omega)^2} \right\} \Bigg] . \tag{3.161}$$

Here, we can identify the rescaled couplings μ_l and g_l defined in Eqs. (3.106) and (3.111) and write

$$-\Lambda Z_\Lambda^2 \partial_\Lambda \gamma_\Lambda(\tilde{\omega}\Lambda) = \frac{g_l}{\pi} f(\tilde{\omega}, \mu_l) , \tag{3.162}$$

where we abbreviated

$$f(\tilde{\omega}, \mu_l) = \frac{1}{(\mu_l - i\sigma_\omega)(\mu_l + i\tilde{\omega} + i\sigma_\omega)^2} - 2i\sigma_\omega \mathrm{Im} \left\{ \frac{1}{(\mu_l + i)(\mu_l + i + i\sigma_\omega \tilde{\omega})^2} \right\} . \tag{3.163}$$

- The third term includes a frequency derivative of $\gamma_\Lambda(\omega)$. Noting that Z_Λ does not depend on frequency and that $\Lambda\, \partial/\partial\omega = \partial/\partial\tilde{\omega}$, we can identify the rescaled coupling $\gamma_l(\tilde{\omega})$ given in Eq. (3.155) and write

$$-\Lambda Z_\Lambda^2 \, \gamma'_\Lambda(\tilde{\omega}\Lambda)\tilde{\omega} = -\tilde{\omega}\, \gamma'_l(\tilde{\omega}) , \tag{3.164}$$

where we defined $\gamma'_l(\tilde{\omega}) = d\gamma_l(\tilde{\omega})/d\tilde{\omega}$.

Putting all three terms together, we get the flow equation

$$\partial_l \gamma_l(\tilde{\omega}) = -2\eta_l \gamma_l(\tilde{\omega}) + \frac{g_l}{\pi} f(\tilde{\omega}, \mu_l) - \tilde{\omega}\, \gamma'_l(\tilde{\omega}) . \tag{3.165}$$

To proceed, one could now expand the $\gamma_l(\tilde{\omega})$ around $\tilde{\omega} = 1$, treating $\gamma_l(1)$ and $\gamma'_l(1)$ as flowing couplings. The flow equation for $\gamma'_l(1)$ would then include an additional frequency derivative, and ultimately this approach would generate an infinite hierarchy of flow equations with infinitely high orders of frequency derivatives. To avoid this complication, we employ a different strategy, and take into account the full frequency dependence of $\gamma_l(\tilde{\omega})$ numerically by discretizing the frequency variable $\tilde{\omega}$. For this purpose, we rearrange the flow equation (3.165) for $\gamma_l(\tilde{\omega})$ and write

$$\left(\partial_l + \tilde{\omega} \frac{\partial}{\partial \tilde{\omega}} \right) \gamma_l(\tilde{\omega}) = -2\eta_l \gamma_l(\tilde{\omega}) + \frac{g_l}{\pi} f(\tilde{\omega}, \mu_l) . \tag{3.166}$$

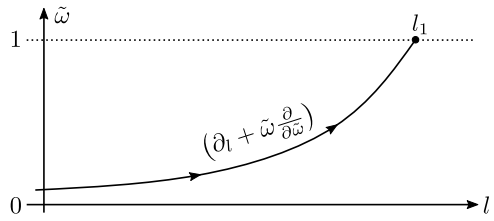

Figure 3.7: The directional derivative describing the flow of $\gamma_l(\tilde{\omega})$ given in Eq. (3.166) is tangent to the family of trajectories given in Eq. (3.167) and parameterized by the endpoints l_1.

Now, the right hand side is simply a directional derivative in the space spanned by l and $\tilde{\omega}$. As a consequence, the value $\gamma_{l_1}(1)$ for any given l_1 can be found by solving an initial value problem. First, we note that the directional derivative $\partial_l + \tilde{\omega}\partial_{\tilde{\omega}}$ is tangent to the family of trajectories given by

$$\tilde{\omega}(l) = e^{l-l_1} \,, \tag{3.167}$$

where l_1 distinguishes the trajectories and marks the point where $\tilde{\omega}(l_1) = 1$. We illustrated this in Fig. 3.7. Restricted to one of those trajectories, the directional derivative in Eq. (3.166) can be written as a one-dimensional total derivative,

$$\left(\partial_l + \tilde{\omega}\frac{\partial}{\partial\tilde{\omega}}\right)\gamma_l(\tilde{\omega})\bigg|_{\tilde{\omega}=e^{l-l_1}} = \frac{d}{dl}\gamma_l(e^{l-l_1}) \,. \tag{3.168}$$

Defining

$$\gamma_{l,l_1} \equiv \gamma_l(e^{l-l_1}) \,, \tag{3.169}$$

the flow equation (3.166) can then be written as

$$\partial_l \gamma_{l,l_1} = -2\eta_l \gamma_{l,l_1} + \frac{g_l}{\pi} f(e^{l-l_1}, \mu_l) \,. \tag{3.170}$$

Provided that we know μ_l and g_l for $0 < l < l_1$, we can simply integrate this differential equation from $l = 0$ to $l = l_1$. Because the flowing four-point vertex vanishes at the start of the RG flow, the initial value at $l = 0$ is $\gamma_{0,l_1} = 0$. After integration from this initial value, the solution for $\gamma_{l_1,l_1} = \gamma_{l_1}(1)$ can then be substituted in Eq. (3.156) to find the anomalous dimension η_l, provided that the value for the chemical potential μ_l is known.

For the readers convenience, let us reprint the flow equations for the rescaled couplings given in Eqs. (3.109), (3.110), and (3.112):

$$\partial_l \mu_l = (1-\eta_l)\mu_l - \frac{1}{\pi}\frac{\mu_l}{\mu_l^2+1}u_l \,, \tag{3.171a}$$

$$\partial_l u_l = (1-2\eta_l)u_l + \frac{4}{\pi}\frac{g_l}{\mu_l^2+1}\left(\frac{1}{\mu_l^2+1} - \frac{3}{4}\right) \,, \tag{3.171b}$$

$$\partial_l g_l = 2(1-2\eta_l)g_l \,. \tag{3.171c}$$

Using the procedure to find η_l as described previously, we can now employ a modified Runge-Kutta method to integrate the flow equations. First, we discretize the flow parameter l to the discrete set l_i where i ranges from 0 to some large number N. Suppose that we want to compute the couplings μ_l, u_l, g_l, and η_l for some $l = l_n > 0$ and that we already computed them for the previous steps $0 \leq i < n$. The couplings at $l = l_n$ can then be approximated as follows:

1. Perform one step of the Runge-Kutta method to compute $\mu_{l_n}, u_{l_n}, g_{l_n}$ from the flow equations (3.171) using the known values $\mu_{l_{n-1}}$, $u_{l_{n-1}}$, $g_{l_{n-1}}$, and $\eta_{l_{n-1}}$.

2. Numerically integrate the equation (3.170) for γ_{l,l_n} from $l = 0$ to $l = l_n$ with the initial condition $\gamma_{0,l_n} = 0$. To do so, we need the values for μ_l, u_l, and g_l for $l < l_n$. In fact, we know these values approximately even up to $l = l_n$ from the previous step.

3. Using the result for μ_{l_n} from the first step and the result for $\gamma_{l_n,l_n} = \gamma_{l_n}(1)$ from the second step, compute the anomalous dimension η_{l_n} from Eq. (3.156).

Starting at $l = 0$ with the initial conditions, we can successively apply the above algorithm to find the RG trajectories of the couplings μ_l, u_l, g_l, and η_l. We integrated the flow equations for six trajectories which pass close to the discontinuity fixed point and plotted the results in Fig. 3.8.

The flow of these trajectories confirms the physical picture worked out in the preceding sections. Depending on the initial conditions, the RG flow leads to one of the two sinks S_+ or S_-. At the sink S_+, the effective chemical potential μ_l vanishes, leading to a power-law in the propagator, while the anomalous dimension takes the value $\eta = 1/2$ and g_l assumes some finite fixed value. Recalling the discussion in Sec. 1.2.2, we conclude that S_+ describes the low energy behavior of the nFL phase. At the sink S_-, the anomalous dimension vanishes, which is consistent with the IV phase. The basins of attraction for the sinks $S_\pm$ are separated by a surface in the coupling space. The closer the initial conditions are to this separatrix, the closer the RG trajectory will approach the DFP before being deflected towards the relevant eigendirection. This confirms the RG picture discussed in Sec. 3.5 where the DFP represents the phase transition between the IV and the nFL phases. Most importantly, we confirm that the phase transition is indeed described by the DFP with anomalous dimension $\eta = 1/2$.

3.7 Physical interpretation

Our result $\eta = 1/2$ for the anomalous dimension at the discontinuous phase transition seems puzzling. Usually, one would expect a state of phase separation right at a discontinuous phase transition, where each separate phase

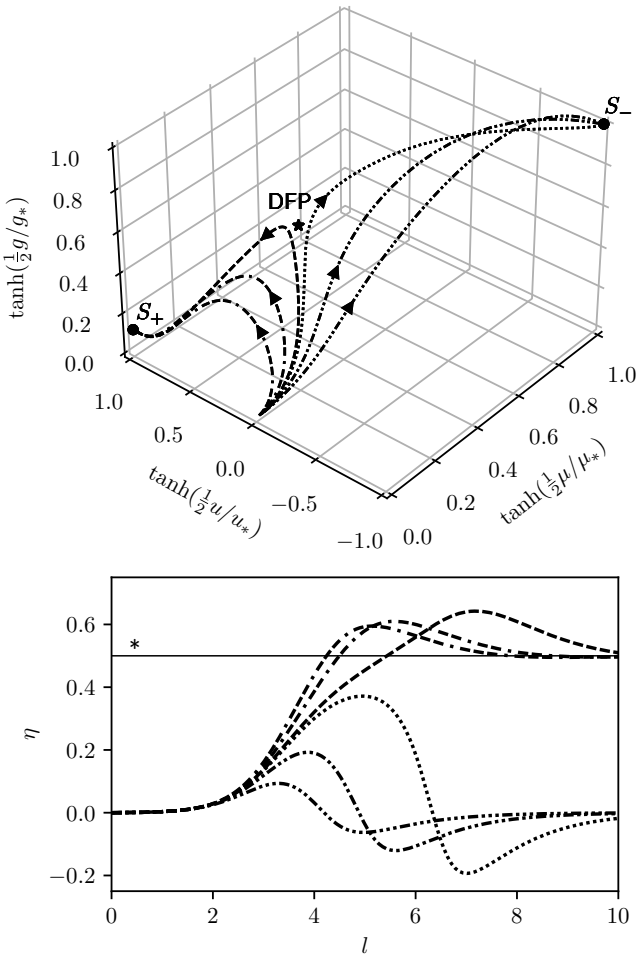

Figure 3.8: RG trajectories of the SYK model. *Top:* trajectories in the space of the couplings μ_l, u_l, and g_l, scaled by a Tangens hyperbolicus. *Bottom:* Flow of the anomalous dimension η_l. The value $\eta_l = 1/2$ is marked by the horizontal line.

is perfectly non-critical, with no diverging correlation lengths. This view seems to be contradictory to the RG description, where a consequence of the scale invariance at a fixed point is that the correlation length has to either diverge or vanish [33]. The scaling theory of discontinuous phase transitions was worked out in Refs. [84, 85], where it is concluded that while the phase transition is indeed described by the separatrix generated by the relevant directions of the fixed point, the physical meaning of the fixed point itself is somewhat elusive. Fisher and Berker [85] provide a possible interpretation, where the scale invariance is not found in the separate phases, but rather one level higher, in the spatial distribution of the phase regions.

In our case, we have a quantum phase transition at zero temperature and have no spatial degrees of freedom, and Fisher and Berker's interpretation does not apply straightforwardly. In our paper [3], we discuss the possibility that a quantum superposition of the nFL and IV phases is realized

at the transition. The analogue of the diverging length scale would then be a diverging tunneling time scale. However, this picture is far from complete, mainly because it is not clear how our frequency cutoff Λ relates to dynamical time scales. The scale Λ divides the Matsubara frequencies into infrared and ultraviolet. However, the analytic continuation to real frequencies does not preserve the cutoff and it becomes meaningless to think about the RG flow as a result of integrating out fast (real time) modes. Rather, the scale Λ manipulates the real frequency spectrum in a non-transparent way dictated by the analytical continuation. Nevertheless, the scaling laws survive the analytic continuation, because a rescaling of the imaginary frequency axis is simply a multiplication by a real number, which analytically continues to the real axis identically. Thus, we believe that the result of $\eta = 1/2$ for the anomalous dimension of the fermionic modes is robust. A finite anomalous dimension indicates strong coupling between critical fluctuations [39]. Because of the above mentioned problem with the analytic continuation however, it is not clear of which nature these fluctuations are. An interesting question would be what physical implications our findings would have. Fisher and Berker show that the scaling laws at a discontinuity fixed point can be revealed by finite size scaling, where the phase transition is rounded due to the finiteness of the system. In our derivation, the limit $N \to \infty$ was crucial to find the DFP. A generalization to finite N poses a major complication, because the large N and the zero temperature limit of the SYK model do not commute [86]. Consequently, other means of softening the transition would be necessary if one wanted to perform a similar analysis.

Appendix A

Deutsche Zusammenfassung

In dieser Arbeit befassen wir uns mit zwei Modellen, welche beide auf Alexei Kitaev zurückgehen. Im Kitaev-Heisenberg-Γ-Modell berechnen wir die Zerfallsrate magnetischer Quasiteilchen [4, 5, 6, 7, 8] und bestätigen so ein vorheriges Ergebnis [2], welches breite Spektren in Neutronenstreuexperimenten erklärt. Das zweite Modell ist das Sachdev-Ye-Kitaev Modell, welches in seiner nicht-Fermiflüssigen Phase keine Quasiteilchenartigen Anregungungen besitzt [14]. Hier untersuchen wir den Phasenübergang zu dieser exotischen Phase mithilfe der Funktionalen Renormierungsgruppe [39, 40, 41, 42].

A.1 Zerfall von Magnonen im Kitaev-Heisenberg-Γ-Modell

Mit einer wegweisenden Veröffentlichung [18] präsentierte Alexei Kitaev das später nach ihm benannte Kitaev-Modell samt seiner exakten Lösung. Dies stellt die erste bekannte rigorose Herleitung eines Quantenspinflüssigkeitszustandes [15] aus einem Magnetischen Hamiltonian dar. Das Interesse, einen solchen Zustand in realen Materialien zu finden, ist immens. Dies ist nicht nur allgemeiner akademischer Neugier geschuldet, sondern liegt auch an der konkreten Aussicht, solche Materialien zum Bau topologischer Quantencomputer zu nutzen [19, 20].

A.1.1 Die Suche nach Kitaevs Quantenspinflüssigkeit

Eine wichtige Klasse möglicher Kitaev-Materialien umfasst magnetische Isolatoren mit starker Spin-Bahn-Kopplung der exponierten Elektronen [21]. In realen Materialien treten jedoch neben den Wechselwirkungen des Kitaev-Modells noch weitere magnetische Wechselwirkungen auf, wie zum Beispiel die Heisenberg-Wechselwirkung. Dies führt dazu, dass mögliche Kitaev-Materialien durch einen Hamiltonian mit zahlreichen Wechselwirkungstermen beschrieben werden [22]. Wir betrachten hier das Kitaev-Heisenberg-

Γ-Modell, welches zur Beschreibung des Materials α-$RuCl_3$ geeignet ist [2, 49, 50, 51]. Dieses Modell ist definiert auf einem zweidimensionalen Honigwabengitter. Der Hamiltonian setzt sich aus drei verschiedenen Wechselwirkungstermen zusammen,

$$H = H_{\text{Heisenberg}} + H_{\text{Kitaev}} + H_{\Gamma} \ . \tag{A.1}$$

Der Kitaev-Term H_{Kitaev} beschreibt eine Ising-Wechselwirkung zwischen nächsten Nachbarn. Das besondere daran ist, dass die Richtung der Ising-Wechselwirkung von der räumlichen Ausrichtung der Wechselwirkungspartner zueinander abhängt, und somit zu magnetischer Frustration führt [18]. Diese Richtungsabhängigkeit kann geschrieben werden als

$$H_{\text{Kitaev}} = K \sum_{\alpha} \sum_{\langle ij \rangle_\alpha} S_i^\alpha S_j^\alpha \ , \tag{A.2}$$

wobei S_i^α die α-Komponente eines Spin-1/2 Operators an Gitterplatz i ist, α die Richtungen x, y, z aufzählt und $\langle ij \rangle_\alpha$ jene Nachbarpaare sind, welche senkrecht zur α-Achse stehen (hierfür muss das Koordinatensystem (x, y, z) natürlich passend zum Gitter gewählt werden, wie gezeigt in Fig. 2.1). Der Heisenberg-Term $H_{\text{Heisenberg}}$ beschreibt die Heisenberg-Wechselwirkung zwischen nächsten und dritt-nächsten Nachbarn und ist gegeben durch

$$H_{\text{Heisenberg}} = J \sum_{\langle ij \rangle} \boldsymbol{S}_i \cdot \boldsymbol{S_j} + J_3 \sum_{\langle\langle\langle ij \rangle\rangle\rangle} \boldsymbol{S}_i \cdot \boldsymbol{S_j} \ , \tag{A.3}$$

wobei $\langle ij \rangle$ Paare aus nächsten Nachbarn und $\langle\langle\langle ij \rangle\rangle\rangle$ Paare aus dritt-nächsten Nachbarn auflistet. Der Term H_Γ beschreibt eine weitere Wechselwirkung zwischen nächsten Nachbarn, welche von der Ausrichtung der Paare abhängt, und kann geschrieben werden als

$$H_\Gamma = \sum_{\alpha\beta\gamma} \Gamma^\alpha_{\beta\gamma} \sum_{\langle ij \rangle_\alpha} S_i^\beta S_j^\gamma \ , \tag{A.4}$$

wobei α, β, γ jeweils die Richtungen x, y, z aufzählen. $\Gamma^\alpha_{\beta\gamma}$ ist ein symmetrischer Tensor mit den nichtverschwindenden Komponenten $\Gamma^x_{yz} = \Gamma^x_{zy} = \Gamma^y_{zx} = \Gamma^y_{xz} = \Gamma^z_{xy} = \Gamma^z_{yx} \equiv \Gamma$.

Nun stellt sich heraus [23], dass das Material α-$RuCl_3$ bei tiefen Temperaturen magnetische Ordnung zeigt. Dies steht im Widerspruch zur Realisierung einer Quantenspinflüssigkeit. Üblicherweise würde man erwarten, dass die elementaren Anregungen in einem geordneten Magneten durch Spinwellen, auch Magnonen genannt, beschrieben werden [4, 8, 9]. Inkohärente Sprektren in Neutronenstreuexperimenten deuten jedoch darauf hin [29, 30], dass die elementaren Anregungszustände in α-$RuCl_3$ trotz magnetischer Ordnung gut durch Kitaevs Quantenspinflüssigkeit beschrieben werden können. Um die zugrundeliegende Physik genauer zu untersuchen, bietet sich eine Störungstheoretische Betrachtung der Magnonenspektren an.

In Ref. [2] wurde auf diese Weise gezeigt, dass die inkohärenten Streuspektren durch eine hohe Zerfallsrate der Magnonen begründet werden kann. Jedoch wurde dabei eine grobe, heuristische Näherung verwendet, deren Gültigkeit nicht offensichtlich ist. Uns ist es gelungen, einen Parameterbereich im Kitaev-Heisenberg-Γ-Modell zu finden, in welchem sich die Berechnung der Zerfallsraten vereinfacht und somit eine genauere Berechnung möglich wird. Innerhalb dieses Parameterbereichs kann dann die qualitative Gültigkeit der Näherung aus Ref. [2] bestätigt werden, wie wir in unserer Veröffentlichung [1] zeigen. Im Folgenden präsentieren wir die von uns verwendete Methode, welche auch auf andere bosonische Modelle übertragen werden kann.

A.1.2 Berechnung der magnonischen Zerfallsrate

Da α-$RuCl_3$ bei tiefen Temperaturen eine magnetische Zickzack-Ordnung ausbildet [29, 30], welche wir in Fig. 2.5 schematisch dargestellt haben, beschränken wir uns auf diese Phase des Kitaev-Heisenberg-Γ-Modells. Zunächst bestimmen wir durch Minimierung der klassischen Grundzustandsenergie die Ausrichtung der Spins in der Zickzackphase. Dann wählen wir für jeden Gitterplatz eine lokale Basis, deren dritte Komponente wir mit $\parallel$ bezeichnen und welche entlang der Magnetisierung ausgerichtet ist. Dies erlaubt es uns, die Spin-Operatoren mittels der Holstein-Primakoff-Transformation [62],

$$S_i^+ = \sqrt{2S}\left(\sqrt{1-\frac{n_i}{2S}}\right) b_i \,, \tag{A.5a}$$

$$S_i^- = b_i^\dagger \sqrt{2S}\sqrt{1-\frac{n_i}{2S}} \,, \tag{A.5b}$$

$$S_i^{\parallel} = S - n_i \,, \tag{A.5c}$$

auf die bosonischen Erzeuger $b_i^\dagger$ und Vernichter b_i abzubilden. Die bosonische Besetzungszahl n_i beschreibt dann die Abweichung der Spinquantenzahl von der vollständigen Magnetisierung. Bei hinreichend niedrigen Temperaturen sind diese Angeregten Zustände nur spärlich besetzt, was eine Entwicklung der Wurzeln in n_i/S rechtfertigt,

$$S_i^+ = \sqrt{2S}\left[1-\frac{n_i}{4S}-\frac{n_i^2}{32S^2}+\mathcal{O}\left(\frac{n_i^3}{S^3}\right)\right] b_i \,, \tag{A.6a}$$

$$S_i^- = b_i^\dagger \sqrt{2S}\left[1-\frac{n_i}{4S}-\frac{n_i^2}{32S^2}+\mathcal{O}\left(\frac{n_i^3}{S^3}\right)\right] \,, \tag{A.6b}$$

$$S_i^{\parallel} = S - n_i \,. \tag{A.6c}$$

Diese Entwicklung wird $1/S$-Entwicklung genannt, obwohl, wie zum Beispiel in unserem Fall mit $S = 1/2$, der Parameter $1/S$ nicht unbedingt klein ist.

Als nächstes können wir so den Modellhamiltonian (A.1) durch die bosonischen Erzeuger und Vernichter ausdrücken. Zur quadratischen Ordnung erhalten wir dann nach Fouriertransformation den effektiven freien Spinwellenhamiltonian

$$H_2 = \sum_{\boldsymbol{k}} \sum_{m,n} \left\{ A^{mn}_{\boldsymbol{k}} \; a^\dagger_{\boldsymbol{k}m} a_{\boldsymbol{k}n} + \frac{1}{2} \left[B^{mn}_{\boldsymbol{k}} \; a^\dagger_{\boldsymbol{k}m} a^\dagger_{-\boldsymbol{k}n} + (B^{nm}_{\boldsymbol{k}})^* \; a_{-\boldsymbol{k}m} a_{\boldsymbol{k}n} \right] \right\} . \tag{A.7}$$

Hier ist $\boldsymbol{k}$ der Kristallimpuls innerhalb der ersten Brillouin-Zone und die Bandindizes $m, n = 1, 2, 3, 4$ rühren daher, dass die magnetische Einheitszelle vier Gitterplätze umfasst. $a^\dagger_{\boldsymbol{k}n}$ ist der Erzeuger eines Magnons aus Band n mit Kristallimpuls $\boldsymbol{k}$, und $a_{\boldsymbol{k}n}$ ist der entsprechende Vernichter. Die Matrizen $A^{mn}_{\boldsymbol{k}}$ und $B^{mn}_{\boldsymbol{k}}$ sind in Gl. (2.74) gegeben. Den führenden Beitrag zur Wechselwirkung zwischen den Magnonen finden wir zu dritter Ordnung, das heißt wir erhalten analytische ausdrücke für die drei-Punkt-Wechselwirkung $\Gamma^{\mu\nu\lambda}(\boldsymbol{k}, \boldsymbol{k'}, \boldsymbol{k''})$, wobei die Indizes μ, ν, λ die vier Bandindizes und die Art, also Erzeuger oder Vernichter, aufzählen.

Es ist zu beachten, dass der freie Hamiltonian in der gegenwärtigen Form (A.7) nicht diagonal ist, wir also im eigentlichen Sinne noch nicht von Magnonenbändern sprechen können. Für die diagrammatische Störungstheorie müssen wir also den freien Hamiltonian diagonalisieren und entsprechend auch den Vertex $\Gamma^{\mu\nu\lambda}(\boldsymbol{k}, \boldsymbol{k'}, \boldsymbol{k''})$ transformieren. Dafür brauchen wir die explizite Form der Transformationsmatritzen. Dies stellt jedoch aufgrund der hohen Zahl an Bandindizes sowohl numerisch als auch analytisch eine Herausforderung dar. In Ref. [2] wird dieses Problem umgangen, indem der Wechselwirkungsvertex $\Gamma^{\mu\nu\lambda}(\boldsymbol{k}, \boldsymbol{k'}, \boldsymbol{k''})$ als Band- und Impulsunabhängig genähert wird. Diese Näherung wollen wir überprüfen. Dazu gehen wir dieses Problem anders an, nämlich indem wir die bosonischen Erzeuger und Vernichter in ihre hermiteschen und antihermiteschen Teile zerlegen,

$$b_i = \frac{1}{\sqrt{2}} \left[x_i + i p_i \right] , \tag{A.8a}$$

$$b_i^\dagger = \frac{1}{\sqrt{2}} \left[x_i - i p_i \right] . \tag{A.8b}$$

Diese Darstellung erlaubt es, einen Parameterbereich der Kopplungskonstanten $\Gamma = K > 0$ zu identifizieren, welcher die analytischen Ausdrücke stark vereinfacht. So finden wir für diesen Parameterbereich die Transformationsmatrizen und können die diagrammatische Störungstheorie anwenden, um die Zerfallsrate der Magnonen zu berechnen.

Allgemein ist die Zerfallsrate $\gamma_{\boldsymbol{k}n}$ eines Quasiteilchens zu führender Ordnung gegeben durch den Imaginärteil der Selbstenergie [8],

$$\gamma_{\boldsymbol{k}n} \equiv -\mathrm{Im}\, \Sigma^{\mathrm{ret}}_{\boldsymbol{k}n}(\omega_{\boldsymbol{k}n}) . \tag{A.9}$$

Hier ist $\omega_{\boldsymbol{k}n}$ die Energie des entsprechenden Magnons. Am absoluten Temperaturnullpunkt gibt es nur einen führenden Beitrag zum Imaginärteil der Selbstenergie, welcher durch das Diagramm

(A.10)

gegeben ist. Zur Berechnung dieses Beitrages verwenden wir unsere analytischen Ausdrücke um numerische Werte für die freien Propagatoren und Wechselwirkungsvertizes zu generieren. Anschließend führen wir dann die Integration über die innere Impulsvariable des Diagramms numerisch durch. So erhalten wir Werte für die Zerfallsrate der Magnonen, welche dann mit der gröberen Näherung aus Ref. [2] verglichen werden können.

A.2 FRG im SYK-Modell

Das Sachdev-Ye-Kitaev(SYK)-Modell wurde ursprünglich von Alexei Kitaev als einfaches Modell eingeführt [12], um das holografische Prinzip aus der Quantengravitation zu beschreiben. Doch auch in der Festkörperphysik ist das SYK-Modell interessant. Einerseits ist die Selbstenergie im thermodynamischen Limes exakt bestimmbar [46]. Desweiteren zeichnet sich das SYK-Modell durch die Existenz einer nicht-Fermiflüssigen Phase aus, in der keinerlei Quasiteilchen existieren. Dies ist eine Schlüsseleigenschaft in der bisher unzureichend verstandenen Theorie der seltsamen Metalle und der Hochtemperatursupraleitung [14, 45], und daher von fundamentalem Interesse.

A.2.1 Das SYK Modell

In seiner ursprünglichen Form beschreibt das SYK-Modell N wechselwirkende Majorana-Moden. Die Wechselwirkung ist dabei zufällig und findet zwischen allen Moden statt. In der Festkörpertheorie wird gerne eine Variante des SYK-Modells verwendet, welche durch Ersetzung der Majorana-Moden durch herkömmliche Fermionen aus dem ursprünglichen SYK-Modell hervorgeht. Der Hamiltonian ist dann gegeben durch

$$H = -\mu \sum_i c_i^\dagger c_i + \sum_{i<j,k<l} J_{ij,kl} c_i^\dagger c_j^\dagger c_k c_l. \tag{A.11}$$

Hierbei sind c_i und $c_i^\dagger$ die fermionischen Vernichter und Erzeuger, μ ist das chemische Potential, und $J_{ij,kl}$ sind die zufälligen Wechselwirkungskonstanten zwischen den Fermionen. Letztere sind Gaußsche Zufallsvariablen mit Erwartungsvert 0 und Varianz $2J^2/N^3$, wobei J eine beliebige Energieskala ist. Weiterhin erfüllen $J_{ij,kl}$ die Symmetrien $J_{ij,kl} = -J_{ji,kl} = -J_{ij,lk}$ und $J_{ij,kl} = J^*_{kl,ij}$, sind sonst jedoch statistisch unabhängig voneinander.

Bei niedrigen Temperaturen zeigt sich ein Phasenübergang erster Ordnung [46]. Dabei wird bei niedrigem chemischen Potential eine nicht-Fermiflüssigkeit realisiert, welche sich durch Skaleninvarianz und das Fehlen von Quasiteilchen auszeichnet. Bei ausreichend hohem chemischen Potential findet ein Übergang zu einem Zustand mit vollständiger fermionischer Besetzung statt (ein analoger Übergang zu einem vollständig unbesetztem Zustand findet bei negativem chemischen Potential statt). In dieser Arbeit untersuchen wir diesen Phasenübergang am absoluten Temperaturnullpunkt mittels der Funktionalen Renormierungsgruppe (FRG).

A.2.2 Die Funktionale Renormierungsgruppe

In der von Kadanoff [34] und Wilson [35, 36, 37] entwickelten Formulierung basiert die Renormierungsgruppe (RG) auf einer Vergröberung der Freiheitsgrade eines gegeben Modells. In der Regel werden dabei sukzessive Freiheitsgrade oberhalb einer stetig sinkenden Energie- oder Impulsskala ausintegriert, sodass nur noch Freiheitsgrade mit niedrigeren Energien oder Impulsen, also gröbere Freiheitsgrade, betrachtet werden. Durch das Ausintegrieren verändern sich die effektiven Wechselwirkungen zwischen den gröberen Freiheitsgraden, was zu einem Fluss im abstrakten Raum der Wechselwirkungskonstanten mit der Skala führt, dem Renormierungsgruppenfluss. Je kleiner die Energie- oder Impulsskala ist, desto größer ist die Zeit- oder Längenskala. Dies ermöglicht eine Herleitung makroskopischer Eigenschaften eines physikalischen Systems aus dessen mikroskopischer Theorie. Besonders interessant ist dies in der Theorie der Phasenübergänge: Anhand des Renormierungsgruppenflusses können das Phasendiagramm sowie die kritischen Exponenten an den Phasenübergängen bestimmt werden [33].

Wir wollen diesen Formalismus nutzen, um den im vorigen Abschnitt erwähnten Phasenübergang im SYK-Modell zu untersuchen. Dafür verwenden wir die Funktionale Renormierungsgruppe (FRG) [39, 40, 41, 42], welche häufig auch exakte Renormierungsgruppe genannt wird und eine Formulierung der Wilsonschen Renormierungsgruppe mittels Methoden aus der Funktionalanalysis darstellt. In der FRG wird die Vergröberung der Freiheitsgrade mithilfe einer künstlich eingeführten Skalenabhängigkeit im freien Propagator realisiert. Die erhaltenen Flussgleichungen für die Wechselwirkungskonstanten sind dabei äquivalent zu einer Ausintegration im Wilsonschen Sinne [43].

A.2.3 Renormierungsgruppenfluss und kritischer Fixpunkt

Wir wenden die Funktionale Renormierungsgruppe auf das SYK-Modell im thermodynamischen Limes $N \to \infty$ an. Dabei kommen uns zwei Statistische Eigenschaften zugute. Zum Einen ist das SYK-Modell im thermodynamischen Limes selbsmittelnd, das heißt, dass die Dynamik jedes ein-

zelnen Freiheitsgrades gleich der gemittelten Dynamik aller Freiheitsgrade ist [14]. Des Weiteren ist das SYK-Modell Replikadiagonal [14, 81, 82], was zur Konsequenz hat, dass alle gemittelten Korrelationsfunktionen durch die über die zufällige Wechselwirkung $J_{ij,kl}$ gemittelte Wirkung bestimmt sind. Es reicht also aus, den RG-Fluss für die gemittelte Wirkung zu betrachten. Letztere bestimmen wir, indem wir die mikroskopische Wirkung, welche aus dem Hamiltonian (A.11) resultiert, mittels des Pfadintegralformalismus über die Zufallsvariablen $J_{ij,kl}$ integrieren. Durch die Integration erhalten wir neben dem unberührten quadratischen Teil einen effektiven acht-Punkt-Wechselwirkungsvertex, welcher in Gl. (3.34) gegeben ist.

Während des RG-Flusses mit der Energieskala generiert der acht-Punkt-Vertex einen skalenabhängigen sechs-Punkt-Vertex, welcher wiederum einen vier-Punkt-Vertex generiert, welcher dann einen Beitrag zum zwei-Punkt-Vertex, also der Selbstenergie, liefert. Die Entsprechenden Flussgleichungen sind in Gln. (3.50) gegeben und eine diagrammatische Darstellung findet sich in Fig. 3.4. Um diese Flussgleichungen zu lösen, müssen diese zunächst mithilfe einiger Näherungen vereinfacht werden. Zuerst verwenden wir die sogenannte Katanin-Substitution [83], um die Flussgleichung für den sechs-Punkt-Vertex direkt zu integrieren. Wir begründen die Gültigkeit dieser Substitution damit, dass eine erneute Substitution in der Flussgleichung für den vier-Punkt-Vertex die aus der Literatur bekannte exakte Lösung für die Selbstenergie reproduziert. Als weitere Näherung entwickeln wir die Frequenzabhängigkeiten der Wechselwirkungsvertizes für kleine Frequenzen, welche die uns interessierende makroskopische Physik beschreiben. Als Nächstes wählen wir die künstliche Skalenabhängigkeit des freien Propagators so, dass Frequenzen unterhalb der Energieskala Λ vollkommen unterdrückt werden, während der Propagator für höhere Frequenzen nicht modifiziert wird („scharfer Cutoff“). Nach Reparametrisierung der Skala durch den logarithmischen Parameter l, gegeben durch $\Lambda = \Lambda_0 e^{-l}$, erhalten wir die Flussgleichungen

$$\partial_l \mu_l = (1-\eta_l)\mu_l - \frac{1}{\pi}\frac{\mu_l}{\mu_l^2+1} u_l \,, \tag{A.12a}$$

$$\partial_l u_l = (1-2\eta_l)u_l + \frac{4}{\pi}\frac{g_l}{\mu_l^2+1}\left(\frac{1}{\mu_l^2+1} - \frac{3}{4}\right) \,, \tag{A.12b}$$

$$\partial_l g_l = 2(1-2\eta_l) g_l \,. \tag{A.12c}$$

Hier ist μ_l das skalenabhängige effektive chemische Potential, u_l ist der statische Teil der vier-Punkt-Wechselwirkung, und g_l beschreibt die führende Frequenzabhängigkeit der Selbstenergie. Die Anomale Dimension η_l ist gegeben durch die Integralgleichung (3.142).

Wir lösen das obige System aus Differential- und Integralgleichungen numerisch und finden so den RG-Fluss in Fig. 3.8. Der RG-Fluss reproduziert das Bild des Phasenüberganges zwischen der nicht-Fermiflüssigkeit

und des vollständig besetzten Zustandes. Der Phasenübergang wird durch einen Fixpunkt beschrieben, welchen wir analytisch genauer untersuchen. Hier finden wir ein unerwartetes Ergebnis: Obwohl ein Phasenübergang erster Ordnung vorliegt und damit eine Phasenseparation zu erwarten ist, ist die Anomale Dimension positiv, und deutet damit auf stark korrelierte kritische Fluktuationen hin. Die Interpretation dieses Ergebnisses ist uns zum gegenwärtigen Zeitpunkt unklar. Die gute Übereinstimmung unserer Ergebnisse mit der vorhergehenden Literatur deutet jedoch auf neuartige zugrundeliegende Physik hin.

Publications

2022 — R. L. Smit:
"Hyperfunction formulation of many body Green's functions and the Matsubara formalism",
arXiv:2204.09697 (2022).

2021 — R. L. Smit, D. Valentinis, J. Schmalian, and P. Kopietz:
"Quantum discontinuity fixed point and renormalization group flow of the Sachdev-Ye-Kitaev model",
Phys. Rev. Research **3**, 033089 (2021) [3].

2020 — R. L. Smit, S. Keupert, O. Tsyplyatyev, P. A. Maksimov, A. L. Chernyshev, and P. Kopietz:
"Magnon damping in the zigzag phase of the Kitaev-Heisenberg-Γ model on a honeycomb lattice",
Phys. Rev. B **101**, 054424 (2020) [1].

2019 — R. L. Smit, P. Kopietz and O. Tsyplyatyev:
"Heat capacity of anisotropic Heisenberg antiferromagnet within the spin Hartree-Fock approach in quasi-1D regime",
Eur. Phys. J. B **92**, 252 (2019).

References

[1] R. L. Smit, S. Keupert, O. Tsyplyatyev, P. A. Maksimov, A. L. Chernyshev, and P. Kopietz, "Magnon damping in the zigzag phase of the Kitaev-Heisenberg-Γ model on a honeycomb lattice", *Phys. Rev. B* **101**, 054424 (2020).

[2] S. M. Winter, K. Riedl, P. A. Maksimov, A. L. Chernyshev, A. Honecker, and R. Valentí, "Breakdown of magnons in a strongly spin-orbital coupled magnet", *Nat. Commun.* **8**, 1152 (2017).

[3] R. L. Smit, D. Valentinis, J. Schmalian, and P. Kopietz, "Quantum discontinuity fixed point and renormalization group flow of the Sachdev-Ye-Kitaev model", *Phys. Rev. Research* **3**, 033089 (2021).

[4] N. W. Ashcroft and N. D. Mermin, *Solid State Physics* (Saunders College, Philadelphia, 1988).

[5] J. Negele and H. Orland, *Quantum Many-particle Systems* (Westview Press, Boulder, CO, 1998).

[6] A. M. Zagskin, *Quantum Theory of Many-Body Systems* (Springer, New York, 1998).

[7] A. L. Fetter and J. D. Walecka, *Quantum Theory of Many-particle Systems* (McGraw-Hill, New York, 1971).

[8] W. Nolting, *Grundkurs Theoretische Physik 7: Viel-Teilchen-Theorie* (Springer, Berlin, 2009).

[9] P. W. Anderson, *Basic Notions of Condensed Matter Physics* (Benjamin/Cummings, Menlo Park California, 1984).

[10] L. D. Landau, "The Theory of a Fermi Liquid", *Zh. Eksp. Teor. Fiz.* **30**, 1058 (1956).

[11] P. Nozieres, *Theory Of Interacting Fermi Systems* (CRC Press, Boca Raton, FL, 2018).

[12] A. Kitaev, *A simple model of quantum holography*, Talks at KITP, University of California, Santa Barbara, April 7, 2015 and May 27, 2015.

[13] A. J. Schofield, "Non-fermi liquids", *Contemporary Physics* **40**, 95–115 (1999).

[14] D. Chowdhury, A. Georges, O. Parcollet, and S. Sachdev, "Sachdev-Ye-Kitaev Models and Beyond: A Window into Non-Fermi Liquids", *arXiv:2109.05037* (2021).

[15] L. Balents, "Spin liquids in frustrated magnets", *Nature* **464**, 199–208 (2010).

[16] P. Anderson, "Resonating valence bonds: A new kind of insulator?", *Materials Research Bulletin* **8**, 153–160 (1973).

[17] C. Broholm, R. J. Cava, S. A. Kivelson, D. G. Nocera, M. R. Norman, and T. Senthil, "Quantum spin liquids", *Science* **367**, eaay0668 (2020).

[18] A. Kitaev, "Anyons in an exactly solved model and beyond", *Annals of Physics* **321**, 2–111 (2006).

[19] A. Kitaev, "Fault-tolerant quantum computation by anyons", *Annals of Physics* **303**, 2–30 (2003).

[20] C. Nayak, S. H. Simon, A. Stern, M. Freedman, and S. Das Sarma, "Non-abelian anyons and topological quantum computation", *Rev. Mod. Phys.* **80**, 1083–1159 (2008).

[21] G. Jackeli and G. Khaliullin, "Mott Insulators in the Strong Spin-Orbit Coupling Limit: From Heisenberg to a Quantum Compass and Kitaev Models", *Phys. Rev. Lett.* **102**, 017205 (2009).

[22] H. Takagi, T. Takayama, G. Jackeli, G. Khaliullin, and S. E. Nagler, "Concept and realization of Kitaev quantum spin liquids", *Nat. Rev. Phys.* **1**, 264–280 (2019).

[23] H. B. Cao, A. Banerjee, J.-Q. Yan, C. A. Bridges, M. D. Lumsden, D. G. Mandrus, D. A. Tennant, B. C. Chakoumakos, and S. E. Nagler, "Low-temperature crystal and magnetic structure of $\alpha-\mathrm{RuCl_3}$", *Phys. Rev. B* **93**, 134423 (2016).

[24] I. A. Leahy, C. A. Pocs, P. E. Siegfried, D. Graf, S.-H. Do, K.-Y. Choi, B. Normand, and M. Lee, "Anomalous Thermal Conductivity and Magnetic Torque Response in the Honeycomb Magnet $\alpha-\mathrm{RuCl_3}$", *Phys. Rev. Lett.* **118**, 187203 (2017).

[25] Y. Kasahara, T. Ohnishi, Y. Mizukami, O. Tanaka, S. Ma, K. Sugii, N. Kurita, H. Tanaka, J. Nasu, Y. Motome, T. Shibauchi, and Y. Matsuda, "Majorana quantization and half-integer thermal quantum Hall effect in a Kitaev spin liquid", *Nature* **559**, 227–231 (2018).

[26] S. Gass, P. M. Cônsoli, V. Kocsis, L. T. Corredor, P. Lampen-Kelley, D. G. Mandrus, S. E. Nagler, L. Janssen, M. Vojta, B. Büchner, and A. U. B. Wolter, "Field-induced transitions in the Kitaev material $\alpha - \mathrm{RuCl_3}$ probed by thermal expansion and magnetostriction", *Phys. Rev. B* **101**, 245158 (2020).

[27] X. Mi, X. Wang, H. Gui, M. Pi, T. Zheng, K. Yang, Y. Gan, P. Wang, A. Li, A. Wang, L. Zhang, Y. Su, Y. Chai, and M. He, "Stacking faults in $\alpha-\mathrm{RuCl_3}$ revealed by local electric polarization", *Phys. Rev. B* **103**, 174413 (2021).

[28] J. A. N. Bruin, R. R. Claus, Y. Matsumoto, N. Kurita, H. Tanaka, and H. Takagi, "Robustness of the thermal Hall effect close to half-quantization in $\alpha-\mathrm{RuCl_3}$", *Nat. Phys.* **18**, 401–405 (2022).

[29] A. Banerjee, C. A. Bridges, J.-Q. Yan, A. A. Aczel, L. Li, M. B. Stone, G. E. Granroth, M. D. Lumsden, Y. Yiu, J. Knolle, and et al., "Proximate Kitaev quantum spin liquid behaviour in a honeycomb magnet", *Nature Materials* **15**, 733–740 (2016).

[30] A. Banerjee, J.-Q. Yan, J. Knolle, C. Bridges, M. Stone, M. Lumsden, D. Mandrus, A. Tennant, R. Moessner, and S. Nagler, "Neutron scattering in the proximate quantum spin liquid $\alpha - \mathrm{RuCl_3}$", *Science* **356**, 1055–1059 (2017).

[31] A. Weiße and H. Fehske, *Computational Many-Particle Physics* (Springer, Berlin Heidelberg, 2008).

[32] P. A. Maksimov and A. L. Chernyshev, "Field-induced dynamical properties of the *XXZ* model on a honeycomb lattice", *Phys. Rev. B* **93**, 014418 (2016).

[33] N. D. Goldenfeld, *Lectures On Phase Transitions And The Renormalization Group* (CRC Press, Boca Raton, FL, 2018).

[34] L. P. Kadanoff, "Scaling laws for Ising models near T_c", *Physics Physique Fizika* **2**, 263–272 (1966).

[35] K. G. Wilson, "Renormalization Group and Critical Phenomena. I. Renormalization Group and the Kadanoff Scaling Picture", *Phys. Rev. B* **4**, 3174–3183 (1971).

[36] K. G. Wilson, "Renormalization Group and Critical Phenomena. II. Phase-Space Cell Analysis of Critical Behavior", *Phys. Rev. B* **4**, 3184–3205 (1971).

[37] K. G. Wilson, "The renormalization group: Critical phenomena and the Kondo problem", *Rev. Mod. Phys.* **47**, 773–840 (1975).

[38] B. Widom, "Surface tension and molecular correlations near the critical point", *J. Chem. Phys.* **43**, 3892–3897 (1965).

[39] P. Kopietz, L. Bartosch, and F. Schütz, *Introduction to the Functional Renormalization Group* (Springer, Berlin, 2010).

[40] C. Wetterich, "Exact evolution equation for the effective potential", *Phys. Lett. B* **301**, 90–94 (1993).

[41] W. Metzner, M. Salmhofer, C. Honerkamp, V. Meden, and K. Schönhammer, "Functional renormalization group approach to correlated fermion systems", *Rev. Mod. Phys.* **84**, 299–352 (2012).

[42] N. Dupuis, L. Canet, A. Eichhorn, W. Metzner, J. Pawlowski, M. Tissier, and N. Wschebor, "The nonperturbative functional renormalization group and its applications", *Physics Reports* **910**, 1–114 (2021).

[43] T. R. Morris, "The exact renomalization group and approximate solutions", *Int. J. Mod. Phys. A* **09**, 2411–2449 (1994).

[44] S. Sachdev and J. Ye, "Gapless spin-fluid ground state in a random quantum Heisenberg magnet", *Phys. Rev. Lett.* **70**, 3339–3342 (1993).

[45] S. Sachdev, "Bekenstein-Hawking Entropy and Strange Metals", *Phys. Rev. X* **5**, 041025 (2015).

[46] F. Ferrari and F. I. Schaposnik Massolo, "Phases of melonic quantum mechanics", *Phys. Rev. D* **100**, 026007 (2019).

[47] S. Sachdev, *Quantum Phase Transitions* (Cambridge University Press, New York, 2011).

[48] T. Azeyanagi, F. Ferrari, and F. I. S. Massolo, "Phase Diagram of Planar Matrix Quantum Mechanics, Tensor, and Sachdev-Ye-Kitaev Models", *Phys. Rev. Lett.* **120**, 061602 (2018).

[49] J. G. Rau, E. K.-H. Lee, and H.-Y. Kee, "Generic Spin Model for the Honeycomb Iridates beyond the Kitaev Limit", *Phys. Rev. Lett.* **112**, 077204 (2014).

[50] S. M. Winter, A. A. Tsirlin, M. Daghofer, J. van den Brink, Y. Singh, P. Gegenwart, and R. Valentí, "Models and materials for generalized Kitaev magnetism", *J. Phys.: Condens. Matter* **29**, 493002 (2017).

[51] S. M. Winter, Y. Li, H. O. Jeschke, and R. Valentí, "Challenges in design of Kitaev materials: Magnetic interactions from competing energy scales", *Phys. Rev. B* **93**, 214431 (2016).

[52] N. Hasselmann and P. Kopietz, "Spin-wave interactions in quantum antiferromagnets", *Europhysics Letters (EPL)* **74**, 1067–1073 (2006).

[53] A. Kreisel, N. Hasselmann, and P. Kopietz, "Probing Anomalous Longitudinal Fluctuations of the Interacting Bose Gas via Bose-Einstein Condensation of Magnons", *Phys. Rev. Lett.* **98**, 067203 (2007).

[54] A. Kreisel, F. Sauli, N. Hasselmann, and P. Kopietz, "Quantum Heisenberg antiferromagnets in a uniform magnetic field: Nonanalytic magnetic field dependence of the magnon spectrum", *Phys. Rev. B* **78**, 035127 (2008).

[55] A. Kreisel, P. Kopietz, P. T. Cong, B. Wolf, and M. Lang, "Elastic constants and ultrasonic attenuation in the cone state of the frustrated antiferromagnet Cs_2CuCl_4", *Phys. Rev. B* **84**, 024414 (2011).

[56] E. Majorana, "Teoria simmetrica dell'elettrone e del positrone", *Il Nuovo Cimento (1924-1942)* **5**, 171–184 (1937).

[57] F. Wilczek, "Majorana returns", *Nat. Phys.* **5**, 614–618 (2009).

[58] M. Leijnse and K. Flensberg, "Introduction to topological superconductivity and Majorana fermions", *Semicond. Sci. Technol.* **27**, 124003 (2012).

[59] F. Wilczek, "Majorana and Condensed Matter Physics", *arXiv:1404.0637* (2014).

[60] A. Stern, "Anyons and the quantum Hall effect—A pedagogical review", *Annals of Physics* **323**, 204–249 (2008).

[61] J. M. Luttinger and L. Tisza, "Theory of dipole interaction in crystals", *Phys. Rev.* **70**, 954–964 (1946).

[62] T. Holstein and H. Primakoff, "Field Dependence of the Intrinsic Domain Magnetization of a Ferromagnet", *Phys. Rev.* **58**, 1098–1113 (1940).

[63] J. Colpa, "Diagonalization of the quadratic boson hamiltonian", *Physica A: Statistical Mechanics and its Applications* **93**, 327–353 (1978).

[64] O. Maldonado, "On the Bogoliubov transformation for quadratic boson observables", *J. Math. Phys.* **34**, 5016–5027 (1993).

[65] A. Altland and B. Simons, *Condensed Matter Field Theory* (Cambridge University Press, New York, 2010).

[66] J. c. v. Chaloupka, G. Jackeli, and G. Khaliullin, "Kitaev-Heisenberg Model on a Honeycomb Lattice: Possible Exotic Phases in Iridium Oxides $A_2\mathrm{IrO}_3$", *Phys. Rev. Lett.* **105**, 027204 (2010).

[67] J. c. v. Chaloupka, G. Jackeli, and G. Khaliullin, "Zigzag Magnetic Order in the Iridium Oxide $\mathrm{Na}_2\mathrm{IrO}_3$", *Phys. Rev. Lett.* **110**, 097204 (2013).

[68] A. A. Vladimirov, D. Ihle, and N. M. Plakida, "Magnetic order and spin excitations in the Kitaev–Heisenberg model on a honeycomb lattice", *J. Exp. Theor. Phys.* **122**, 1060–1069 (2016).

[69] J. Hick, *A kinetic theory for spin waves in yttrium-iron garnet* (Dissertation, Frankfurt/Main, 2013).

[70] L. Van Hove, "The Occurrence of Singularities in the Elastic Frequency Distribution of a Crystal", *Phys. Rev.* **89**, 1189–1193 (1953).

[71] A. L. Chernyshev and M. E. Zhitomirsky, "Spin waves in a triangular lattice antiferromagnet: Decays, spectrum renormalization, and singularities", *Phys. Rev. B* **79**, 144416 (2009).

[72] A. L. Chernyshev and P. A. Maksimov, "Damped Topological Magnons in the Kagome-Lattice Ferromagnets", *Phys. Rev. Lett.* **117**, 187203 (2016).

[73] G. L. Squires, *Introduction to the Theory of Thermal Neutron Scattering* (Cambridge University Press, Cambridge, 2012).

[74] W. Fu, *The Sachdev-Ye-Kitaev Model and Matter Without Quasiparticles* (Dissertation, Harvard University, Graduate School of Arts & Sciences, 2013).

[75] A.N. Vasiliev, *Functional Methods in Quantum Field Theory and Statistical Physics* (Gordon and Breach Science Publishers, Amsterdam, 1998).

[76] P. Kopietz, L. Bartosch, and F. Schütz, *Introduction to the Functional Renormalization Group*, chapter 6 (Springer, Berlin, 2010).

[77] D. Sherrington and S. Kirkpatrick, "Solvable model of a spin-glass", *Phys. Rev. Lett.* **35**, 1792–1796 (1975).

[78] M. Kac, *Trondheim Theoretical Physics Seminar*, Nordita Publ. No. 286, 1968 (unpublished).

[79] T. Lin, "Problem of the Disordered Chain", *J. Math. Phys.* **11**, 1584–1590 (1970).

[80] C. De Dominicis and I. Giardina, *Random Fields and Spin Glasses: A Field Theory Approach* (Cambridge University Press, New York, 2009).

[81] W. Fu and S. Sachdev, "Numerical study of fermion and boson models with infinite-range random interactions", *Phys. Rev. B* **94**, 035135 (2016).

[82] I. Aref'eva, M. Khramtsov, M. Tikhanovskaya, and I. Volovich, "Replica-nondiagonal solutions in the SYK model", *J. High Energ. Phys.* **2019**, 113 (2019).

[83] A. A. Katanin, "Fulfillment of Ward identities in the functional renormalization group approach", *Phys. Rev. B* **70**, 115109 (2004).

[84] B. Nienhuis and M. Nauenberg, "First-Order Phase Transitions in Renormalization-Group Theory", *Phys. Rev. Lett.* **35**, 477–479 (1975).

[85] M. E. Fisher and A. N. Berker, "Scaling for first-order phase transitions in thermodynamic and finite systems", *Phys. Rev. B* **26**, 2507–2513 (1982).

[86] B. Kobrin, Z. Yang, G. D. Kahanamoku-Meyer, C. T. Olund, J. E. Moore, D. Stanford, and N. Y. Yao, "Many-Body Chaos in the Sachdev-Ye-Kitaev Model", *Phys. Rev. Lett.* **126**, 030602 (2021).